Development of a First-In-Class STAT5 PROTAC Degrader

by

Atsunori Kaneshige

A dissertation submitted in partial fulfillment
of the requirements for the degree of
Doctor of Philosophy
(Medicinal Chemistry)
in the University of Michigan
2022

Doctoral Committee:

Professor Shaomeng Wang, Chair
Professor Jolanta Grembecka
Professor Pavel Nagorny
Professor Nouri Neamati

Atsunori Kaneshige

atsunori@umich.edu

ORCID iD: 0000-0001-5956-3009

© Atsunori Kaneshige 2022

Dedication

This thesis work is dedicated to my wife, Maiko, who is truly the center of my life with her kindest heart and love, great sense of humor, and continuous encouragement. Maiko made my entire PhD journey become a reality, even though at times it was like going through a typhoon and extensive rough water in a small ship. This work is also dedicated to my parents-in-law, Hiroyasu and Kazumi, living in Osaka Japan, who have been always supportive and caring to our family, and to my parents, Satoru and Kazuyo, living in Yamaguchi Japan, who raised me to have a lot of curiosity. This work is also dedicated to my younger brothers, Takeyoshi and Akio, who live close to my parents. It is because of them I was able to do my dissertation work for 5.5 years non-stop outside Japan. Last, but not least, this work is dedicated to my lovely kids, Shima, Koitaro, and Maru, who are my everlasting source of energy. I am truly thankful that I can take this opportunity in my dissertation to express my appreciation and love to my entire family.

Acknowledgements

First and foremost, I want to thank my advisor, Prof. Shaomeng Wang, for his kindness, guidance, patience, and encouragement throughout my dissertation work. I am very fortunate to work for Prof. Wang, as a graduate student under his supervision. I was able to learn not only what is necessary to practice medicinal chemistry well and in an interdisciplinary manner, ranging from conceptualization to chemistry to biology, but also, by closely watching interactions with people, including myself, I learned how to overcome challenges associated with projects. Prof. Wang is my great role model and reference in my career and life, who I would like to resemble in the future. I also thank my committee members, Profs. Nouri Neamati, Jolanta Grembecka and Pavel Nagorny for their guidance, encouragement, patience and support. I am thankful to them for guiding me and spending time with me throughout my dissertation work.

In the Wang lab, I am very thankful to many nice colleagues. Firstly, I want to thank Longchuan Bai not only for his timely and accurate evaluation of compounds, but also for his teaching me chemical biology. I was a chemist before joining Prof. Wang's lab, but I am very fortunate to have worked with Longchuan, watching, listening and learning how biologists think in experiments. Longchuan's guidance and data made critical contributors to Chapter 2. I want to thank Mi Wang for his great kindness in testing my compounds since the very beginning of this dissertation work. This work started from almost nothing, and required intensive exploration to discover our own inhibitors. Mi tested countless idea compounds for me to make the project move forward from zero to something fruitful in the very early stage of project and later. I want

to thank Donna McEachern, Wei Jian, Yu Wang, and Hoda Metwally for all the *in vivo* testing in this dissertation work. *In vivo* tasks require much work and sensitive care in late nights for their study. I am very thankful to their critical contribution to Chapters 2 and 3. I want to thank Lijie Zhao, Liyue, Huan, Biao Hu, and Jianfeng Lu for kindly and patiently answering my very basic daily questions about experiments related to chemical biology. Their advice really helped me transform myself from one kind of chemist to rather different kind of chemist who can perform chemical biology experiments with confidence. I want to thank Chao-Yie Yang and Paul Kirchhoff for their great assistance with molecular docking. Insights they have given me really helped the quality of my molecular design in daily chemistry experiments. I want to thank so many skillful and knowledgeable chemists in the Wang lab. I want to thank Renqi Xu. His fumehood and experiment bench were located next to mine when I joined the lab. I was fortunate to watch his performance as a chemist and also how he makes each compound carefully and logically. My dissertation work would not otherwise be possible without his phosphotyrosine mimetic, which is a fruit from his intensive efforts to improve the chemical property of the original mimetic. Outside of the lab work, I am thankful for his friendship, fishing trips, exchange of all ideas on China and Japan. I want to thank so many other chemists. Particularly, I want to thank Angelo Aguilar, Haibin Zhou, Xin Han, Weiguo Xian, Jintao Hu, Ting-Rong Chern, Yangbing Li, Fuming Xu, Rohan Rej, Mingliang Wang, Meng Zhang, Zhixiang Chen, Changwei Wang, Lin Yang, Dimin Wu, Wenbin Tu, Ranjan Kumar Acharyya, and last, but not least, Junius E Thomas not only for their great advice in chemistry and medicinal chemistry in general but also for their friendship, encouragement and laughter together during each day's experiments throughout my dissertation work. I am also very thankful to Yuzhi Wang, Inna Rom, Mary Berry, and Nicholas VanDyke for their rapid assistance in ordering reagents and

goods, and much daily troubleshooting, and housekeeping. Without their concerted help, my accomplishments would have been much smaller.

I also want to thank our collaborators. I want to express my gratitude to the members of the Stuckey lab, including Dr. Stuckey, Jennifer Meagher, Elyse Petrunak, and Pryia Chinnaswamy for their huge assistance in getting our first co-crystals, which were critical in my dissertation work. I want to thank the members of the Sun lab, including Prof. Duxin Sun, Bo Wen, Krishani Rajanayake, and John Taki-Williams for evaluating the pharmacokinetics property of our compounds. I want to express my thanks to the members of the Zou lab, including Prof. Weiping Zou, Jiali Yu, Jiajia Zhou for the advice and thoughts about the evaluation of our compounds in the context of immunity. I want to also thank the members of the Wilcox lab, including Prof. Wilcox and Ashley Wolfe, for their guidance and ideas regarding the T-cell lymphoma cell lines.

Finally, I want to thank my wife, Maiko, for her great love and humor. It is unthinkable that I could have finished this dissertation work without her. My parents-in-law have been the biggest supporters with their love in our life in the US. My parents and my brothers have been in my heart and have been a great encouragement. My kids are the best and mean everything in my life. My pastor Steve Smith and his wife Linda Smith, who have been our parents in the US, and my church friends occupy an important part in my life in the US with God's great love. Finally, my friends in Japan, the US, Korea, China, Taiwan, Thailand, Brazil, and Canada have been a major source of encouragement.

Table of Contents

Dedication ii

Acknowledgements iii

List of Tables xi

List of Figures xii

Abstract xv

Chapter 1 STAT5-Targeted Therapeutics Development and Protein Degradation Strategies 1

1.1 STAT5 as an attractive therapy target in hematologic cancers 1

1.2 Current small molecule STAT5-targeted therapeutics development 2

1.3 Proteolysis-Targeting Chimera (PROTAC) and beyond 4

Chapter 2 A Potent and Selective Small-Molecule STAT5 PROTAC Degrader Capable of Achieving Tumor Regression *In Vivo* 8

2.1 Abstract 8

2.2 INTRODUCTION 9

2.3 RESULTS AND DISCUSSION 11

2.3.1 Structure-guided design of STAT5 SH2 domain inhibitors 11

2.3.2 Development of potent PROTAC STAT5 degraders. 14

2.3.3 AK-2292 is a potent and Bona Fide PROTAC degrader of both STAT5A/B proteins 17

2.3.4 AK-2292 displays a high degradation selectivity for STAT5 in whole proteome 18

2.3.5 AK-2292 induces down-regulation of STAT5 associated transcriptome in cells 20

2.3.6 AK-2292 displays potent growth-inhibitory activity in CML cells 21

2.3.7 AK-2292 effectively depletes STAT5 protein in xenograft tumors and normal tissues in mice 22

2.3.8 AK-2292 achieves tumor regression in mouse xenograft models without signs of toxicity 23

2.3.9 Discussion 24

2.4 Acknowledgements 27

2.5 Competing Interests Statement 27

2.6 Online method 28

2.6.1 Contact for Reagent and Resource Sharing 28

2.6.2 Cell Lines and Cell Culture 28

2.6.3 Animal Studies 29

2.6.4 Molecular Modeling 30

2.6.5 Expression and purification of STAT5A/STAT5B and other STAT proteins 32

2.6.6 Crystallization and Structure Determination of STAT5A with Inhibitor or Degrader 33

2.6.7 Fluorescence Polarization (FP) assay 34

2.6.8 Cereblon Binding Assay 35

2.6.9 Cell Viability Assay 36

2.6.10 Immunoblotting 36

2.6.11 Transcriptomic Profiling 38

2.6.12 Proteomic Profiling 39

2.6.13 Statistical Analysis 41

2.7 Chemistry 41

2.7.1 General Information 41

2.7.2 Synthesis 41

2.8 Main Figures 76

2.8.1 Fig. 1. Structure-guided Design of STAT5 SH2 Domain Inhibitors and PROTAC Degraders 76

2.8.2 Fig. 2. Determination of AK2292 as a Potent and Selective STAT5A/B PROTAC Degrader 78

2.8.3 Fig. 3. Transcriptomic Analysis of AK2292 in Cells 80

2.8.4 Fig. 4. Cell Growth Inhibitory Activity of AK2292 in Human CML Cell Lines..... 82

2.8.5 Fig. 5. Pharmacodynamic Effect and Antitumor Efficacy of AK2292 in Mice..... 84

2.9 Extended Data 86

2.9.1 Extended Data Fig. 1A. 86

2.9.2 Extended Data Fig. 1B. 87

2.9.3 Extended Data Fig. 1C and 1D. 88

2.9.4 Extended Data Fig. 1E. 89

2.9.5 Extended Data Fig. 1F and 1G. 90

2.9.6 Extended Data Fig. 1H. 91

2.9.7 Extended Data Fig. 1I. 92

2.9.8 Extended Data Fig. 1J and 1K. 93

2.9.9 Extended Data Fig. 2A and 2B. 94

2.9.10 Extended Data Fig. 3A, 3B, 3C, and 3D. 95

2.9.11 Extended Data Fig. 4A-4F. 96

2.9.12 Extended Data Fig. 4G and 4H. 97

2.9.13 Extended Data Fig. 4I. 98

2.9.14 Extended Data Fig. 5A-5D. 99

Chapter 3 Structure-Guided Discovery of AK-2292 as a Potent, Selective, and Efficacious STAT5 PROTAC Degrader 100

3.1 Abstract 100

3.2 INTRODUCTION 101

3.3 RESULTS AND DISCUSSION 103

3.3.1 Structure-Based Design of Small Molecule STAT5/6 SH2 Domain Inhibitors. 103

3.3.2 Investigation of residue modifications in AK-2305 for binding affinity. 107

3.3.3 Co-crystal structures of STAT5 inhibitors in complex with STAT5A. 108

3.3.4 Design of PROTAC STAT5 A/B Degraders..... 109

3.3.5 Investigation of the Optimal Linker Length and Linker Composition based on AK-2305 for STAT5 Degraders. 110

3.3.6 Investigation of the Optimal Linker Length based on AK-014 for STAT5 Degraders. 113

3.3.7 Investigation of the Optimal C-terminus Aromatic Group..... 114

3.3.8 Optimization of Hydrophobic Residue, C-terminus Aromatic Ring, and Linker in Combination. 116

3.3.9 Design and Synthesis of a Control Compound for AK2292. 118

3.3.10 AK-2292 shows a high degradation selectivity for STAT5A/B in proteome 119

3.3.11 Evaluation of STAT5 Degraders in SKNO1 Cells for Their Growth-Inhibitory Activities.121

3.3.12 AK2292 displays growth-inhibitory activities in a subset of AML cells..... 122

3.3.13 AK2292 effectively depletes STAT5A/B proteins in mouse xenograft tumors..... 124

3.3.14 AK2292 is well-tolerated in immune competent mice and achieves a significant tumor regression in mouse xenograft models..... 125

3.4 CHEMISTRY 126

3.5 CONCLUSION 132

3.6 EXPERIMENTAL SECTION 133

3.6.1 Chemistry General Information. 133

3.6.2 Synthesis Procedures and Spectrum Data 133

3.6.3 Cell Lines and Cell Culture 184

3.6.4 Mice 185

3.6.5 STAT5A Expression and Purification 186

3.6.6 STAT5A:inhibitor Crystallization and Structure Determination 187

3.6.7 Cell Viability Assay 187
3.6.8 Immunoblotting 188
3.7 Supporting Information 190
3.7.1 Figure S1. 190
3.7.2 Figure S2. 191
3.7.3 Table S3. Crystallography Data Collection and Refinement Statistics 192
3.7.4 Figure S3: 193
Chapter 4 General Discussion and Future Directions 194
4.1 Achievements and implications in this dissertation 194
4.2 Further improvement of the potency of AK-2292 both *in vitro* and *in vivo* 194
4.2.1 Binding affinities of inhibitors 194
4.2.2 Linker optimization 195
4.2.3 E3 ligase ligand optimization 195
4.2.4 PK property optimization 196
4.3 Further selectivity study over STAT6 196
4.4 Why STAT6 is not degraded by AK-2292? 197
4.5 Proteins impacted by AK-2292 and their association with STAT5 198
4.6 Genes impacted by AK-2292 and their association with STAT5 198
4.7 Cell types to be tested 200
4.8 Toxicity 201
4.9 Future directions 201
Bibliography 204

List of Tables

Table 1 Relationship of structure and binding affinity in STAT5/6 SH2 domain inhibitor development. 104

Table 2 Effect of hydrophobic residues of STAT5/6 inhibitors for binding affinity 107

Table 3 STAT5 Degraders with Various Linker Lengths and Compositions based on AK-2339. 111

Table 4 Putative Degraders with Various Linker Lengths Based on AK-014. 113

Table 5 STAT5 Degraders with Various C-terminus Aromatic Moieties. 114

Table 6 STAT5 Degrader Analogues based on AK-2305. 117

Table 7 Degradation Potencies and Cell Growth-Inhibitory Activities of STAT5 Degraders ... 121

Table 8 Table S3. Crystallography Data Collection and Refinement Statistics 192

List of Figures

Figure 1-1 Chemical structures of reported STAT5 inhibitors 3

Figure 2-1 Synthesis of 5-(Difluoro(phosphono)methyl)benzo[b]thiophene-2-carboxylic acid (39) 42

Figure 2-2 Synthesis of ((2-(((S)-1-((S)-2-((3-(Dimethylamino)-3-oxopropyl)(4-(thiazol-2-yl)phenyl)carbamoyl)-pyrrolidin-1-yl)-3,3-dimethyl-1-oxobutan-2-yl)carbamoyl)benzo[b]thiophen-5-yl)difluoro-methyl)phosphonic acid (AK305) 45

Figure 2-3 Synthesis of ((2-(((S)-3,3-dimethyl-1-oxo-1-((S)-2-(1,2,3,4-tetrahydroisoquinoline-2-carbonyl)-pyrrolidin-1-yl)butan-2-yl)carbamoyl)-1H-inden-5-yl)difluoromethyl)phosphonic acid (9) 51

Figure 2-4 Synthesis of ((2-(((2S)-1-((2S)-2-((3-((5-(2-(2,6-Dioxopiperidin-3-yl)-1-oxoisoindolin-4-yl)pent-4-yn-1-yl)(methyl)amino)-3-oxopropyl)(4-(thiazol-2-yl)phenyl)carbamoyl)pyrrolidin-1-yl)-3,3-dimethyl-1-oxobutan-2-yl)carbamoyl)benzo[b]thiophen-5-yl)difluoromethyl)phosp 58

Figure 2-5 Synthesis of ((2-(((2S)-1-((2S)-2-((9-(2-(2,6-dioxopiperidin-3-yl)-1-oxoisoindolin-4-yl)non-8-yn-1-yl)(4-(thiazol-2-yl)phenyl)carbamoyl)pyrrolidin-1-yl)-3,3-dimethyl-1-oxobutan-2-yl)carbamoyl)benzo[b]thiophen-5-yl)difluoromethyl)phosphonic acid (29) 68

Figure 2-6 Synthesis of AK-330FL 72

Figure 2-7 Fig. 1. Structure-guided Design of STAT5 SH2 Domain Inhibitors and PROTAC Degraders 76

Figure 2-8 Fig. 2. Determination of AK2292 as a Potent and Selective STAT5A/B PROTAC Degrader 78

Figure 2-9 Fig. 3. Transcriptomic Analysis of AK2292 in Cells 80

Figure 2-10 Fig. 4. Cell Growth Inhibitory Activity of AK2292 in Human CML Cell Lines 82

Figure 2-11 Fig. 5. Pharmacodynamic Effect and Antitumor Efficacy of AK2292 in Mice 84

Figure 2-12 Extended Data Fig. 1A. 86

Figure 2-13 Extended Data Fig. 1B. 87

Figure 2-14 Extended Data Fig. 1C and 1D. 88

Figure 2-15 Extended Data Fig. 1E. 89

Figure 2-16 Extended Data Fig. 1F and 1G. 90

Figure 2-17 Extended Data Fig. 1H. 91

Figure 2-18 Extended Data Fig. 1I. 92

Figure 2-19 Extended Data Fig. 1J and 1K. 93

Figure 2-20 Extended Data Fig. 2A and 2B. 94

Figure 2-21 Extended Data Fig. 3A, 3B, 3C, and 3D. 95

Figure 2-22 Extended Data Fig. 4A-4F. 96

Figure 2-23 Extended Data Fig. 4G and 4H. 97

Figure 2-24 Extended Data Fig. 4I. 98

Figure 2-25 Extended Data Fig. 5A-5D. 99

Figure 3-1 Figure 1. Key structural modifications in STAT5/6 SH2 domain inhibitors. 103

Figure 3-2 Co-crystal structures of STAT5 inhibitors in complex with STAT5A. 108

Figure 3-3 Design of putative STAT5 PROTAC degraders using AK-2339 and Cereblon ligand. 110

Figure 3-4 Design of AK-2292ME as a control compound. 118

Figure 3-5 Figure 5. Western blotting analysis of STAT proteins in SKNO1 and MV4;11 cells treated with AK-2292 or control compounds AK-2305 and AK-2292ME. 120

Figure 3-6 Figure 6. AK2292's growth-inhibitory Activity in AML Cell Lines 122

Figure 3-7 Figure 7. Pharmacodynamics study of AK-2292 in MV4;11 tumor tissues 125

Figure 3-8 Figure 8. Antitumor Activity of AK2292 in the MV4;11 Xenograft Model in Mice. 125

Figure 3-9 Scheme 1. Synthesis of 5-(Difluoro(phosphono)methyl)benzo[b]thiophene-2-carboxylic acid (95) 126

Figure 3-10 Scheme 2. Synthesis of AK256 – AK078 127

Figure 3-11 Scheme 3. Synthesis of AK2305 127

Figure 3-12 Scheme 4. Synthesis of AK014 128

Figure 3-13 Scheme 5. Synthesis of AK2292 - 128

Figure 3-14 Scheme 6. Synthesis of AK026..... 128

Figure 3-15 Scheme 7. Synthesis of AK2238..... 129

Figure 3-16 Scheme 8. Synthesis of AK330..... 129

Figure 3-17 Figure S1. The structure of STAT5/6 tracer, AK-2018330 and its Kd values for STAT5 and STAT6..... 190

Figure 3-18 Figure S2. 191

Figure 3-19 Figure S3: Maps showing the unbiased difference electron density (Fo-Fc) for the inhibitors from the initial refinement..... 193

Abstract

In the last few decades, STAT5, (signal transducer and activator of transcription 5) has become an attractive therapeutic target but targeting of STAT5 has not been successful. In this dissertation, I report the development of AK-2292 as the first, potent and selective small-molecule PROTAC degrader of both STAT5A and STAT5B isoforms. Generally, having high affinity inhibitors is necessary in a successful PROTAC degrader development. However, due to the lack of reported STAT5 inhibitors with good binding affinities and selectivity for STAT5 over other STAT family proteins, I needed to develop our own STAT5 inhibitors. A class of STAT6 inhibitors reported by the McMurray group attracted my attention and served as a potential starting point based on our hypothesis that STAT6 inhibitors could bind STAT5 because the STAT5 and STAT6 sequence identity is 44 percent. Even though our initial trial compound was a very weak STAT5 ligand with a K_i value of over10 micromolar to STAT5 and with a K_i value to STAT6 of 5 micromolar, I was able to develop a class of small molecules that bind to STAT5 with low micromolar to sub-micromolar binding affinity and better affinity to STAT6. Exploiting the selectivity for STAT5 over STAT6 turned out to be challenging and unfortunately, the best STAT5 ligand showed no cell growth-inhibitory activity in representative chronic myeloid leukemia (CML) cell lines with activated STAT5. Fortunately, we were able to obtain the first co-crystals of our STAT5 inhibitors complexed with STAT5A, revealing the detailed structures and interactions between our inhibitors and STAT5A. This success has formed a solid basis for the development of a STAT5 PROTAC degrader. Employing the PROTAC technology, I successfully transformed these non-selective and non-effective STAT5 ligands into potent and selective STAT5

degraders exemplified by AK-2292, whose selectivity has been validated by various methods. AK-2292 exerts potent cell growth inhibition in a panel of CML cell lines and a subset of acute myeloid leukemia (AML) cells, both with activated STAT5. AK-2292 effectively induces STAT5 degradation in normal mouse tissues and human CML and AML xenograft tissues and achieves tumor regression in two CML xenograft models and one AML xenograft model in mice at well-tolerated dose-schedules.

In chapter 1, the implications of STAT5 in hematologic cancers are discussed, followed by a description of current STAT5 inhibitor development and a brief description of proteolysis targeting chimera (PROTAC) technology.

Chapter 2 describes the discovery of the first-in-class selective and efficacious STAT5 PROTAC degrader, AK-2292, and its extensive testing *in vitro* and *in vivo*, using CML cells.

Chapter 3 focuses on our path to the discovery of STAT5 PROTAC degraders along with the detailed structure and activity relationship of both STAT5 inhibitors and STAT5 degraders, using AML cells.

Finally, chapter 4 is a general discussion of the major achievements described in this dissertation and potential future research directions based on lessons learned during this dissertation research.

This dissertation, taken as a whole provides intriguing insights into the first-ever selective targeting of the important transcription factor, STAT5. AK-2292, which was discovered in my research serves as an excellent compound with which to answer important biological questions raised in the study of STAT5 and importantly, it paves the way toward our ultimate goal of STAT5 targeted therapies for cancer and other diseases.

Chapter 1 STAT5-Targeted Therapeutics Development and Protein Degradation Strategies

1.1 STAT5 as an attractive therapy target in hematologic cancers

Signal transducer and activator of transcription 5 (STAT5) plays important roles in the JAK/STAT signaling pathway and regulates crucial cellular functions, such as differentiation, oncogenesis, and immune function [1-3]. STAT5 exists in two isoforms, namely STAT5A and STAT5B, which have similar but non-redundant role in human cancers. Single or double knockout and transgenic mice for STAT5A/B proteins have been generated to understand the roles of these proteins in cells [4]. Past studies indicate that the constitutive activation of STAT5A/B assists the generation, progression, and survival of tumor cells [5]. In particular, a number of publications and several review articles focus on STAT5A/B as attractive therapeutic targets of hematologic cancers [4, 6-14].

Interest in STAT5 is high because, mechanistically, hyperactivated growth-factor receptors, cytokine receptors, and non-receptor tyrosine kinases lead to the persistent activation of STAT5A/B in cancer cells [15]. For instance, activated ABL (Abelson leukemia protein), a non-receptor cytoplasmic tyrosine kinase, is often detected in chronic myeloid leukemia (CML). Similarly, FMS-like tyrosine kinase 3 (FLT3), a cytokine receptor, has been found mutated in acute myeloid leukemia (AML) [16]. Furthermore, even though the detailed mechanism has been elusive, other cell types such as peripheral T-cell lymphoma (PTCL) and relapsed T cell acute lymphoblastic leukemia (T-ALL) have been reported to have constitutively activated STAT5A/B [10, 17-21].

This understanding of STAT5A/B has led to tremendous efforts to develop therapeutics. Imatinib, for example, targets BCR-ABL1. This discovery has revolutionized the treatment of leukemia particularly for CML patients [22]. One of the major sources of its therapeutic effect is silencing aberrant STAT5A/B signaling, a BCR-ABL1 downstream effector. Another notable example is the emergence of JAK2 inhibitors, which inhibit the phosphorylation of STAT5A/B. Despite the success in indirectly targeting STAT5A/B, the emergence of resistance to Bcr-Abl inhibitors and adverse effects due to the lack of specificity of Jak inhibitors [23, 24] has led to considerable clinical interest to directly target vital downstream genes such as STAT5A/B.

1.2 Current small molecule STAT5-targeted therapeutics development

Despite the pressing need to directly target STAT5A/B, current direct STAT5 inhibitor development has lagged [25]. To the best of our knowledge, only a handful of STAT5 inhibitors have been reported [26-30] and target selectivity as well as *in vitro* and *in vivo* efficacy have yet to be achieved. No clinical candidates have directly and selectively targeted STAT5A/B, underscoring the challenge of STAT5A/B as targets [25]. Among the steps in which STAT5 works as a transcriptional factor, it is well documented that the STAT5 dimerization step is critical for its transcriptional activity where p-Y^{694}-STAT5A and p-Y^{699}-STAT5B proteins homo- or heterodimerize through a reciprocal SH2 domain-phosphotyrosine interaction [31-33]. Therefore, targeting the SH2 domain of STAT5 has been a major focus of STAT5 inhibitor development. Thus far, all reported STAT5 inhibitors that have a known mode of action target the SH2 domain of STAT5.

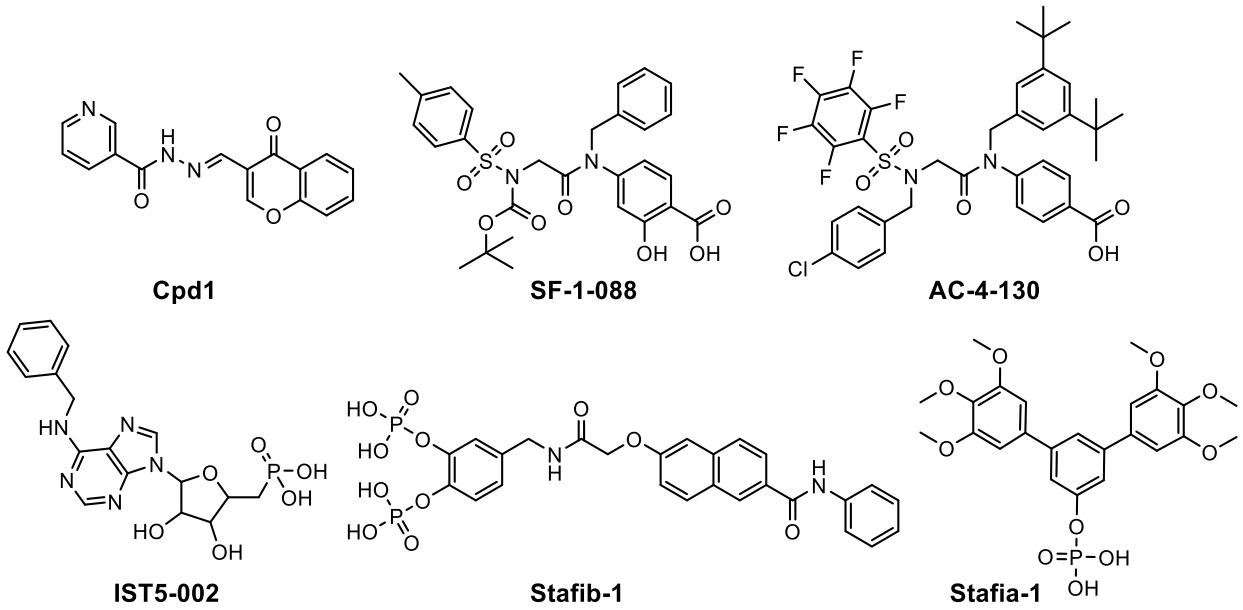

Figure 1-1 Chemical structures of reported STAT5 inhibitors

In 2008, Muller et al. reported a chromone-based STAT5 SH2 domain inhibitor, Cpd1 (Figure 1-1) [34]. Cpd1 has an IC_{50} value of 47 μM for STAT5B's SH2 domain in a fluorescence polarization (FP) assay.

In 2012, Page et al reported a set of salicylic acid-containing STAT5 SH2 domain inhibitors with SF-1-088 (K_i = 8.3 μM) being the best in binding among tested [26]. SF-1-088 showed ~3-fold higher binding affinity to STAT5 compared with STAT1 and STAT3. SF-1-088 was followed by AC-4-130 developed by Wingelhofer et al. in 2018. AC-4-130 shows cell growth-inhibitory activities (IC_{50} = 2-5 μM) in a panel of AML cell lines and also shows some efficacy in an MV4;11 mouse? xenograft model at 25 mg/kg per day with reduced tumor? levels of pSTAT5 and STAT5 [29].

In 2015, Liao et al. reported IST5002 [28]. Even though Liao et al. indicated that IST5-002 was developed to disrupt phosphorylated STAT5 dimerization by mimicking peptides with phosphorylated tyrosine residues, there is no direct evidence of direct binding of IST5-002 to STAT5. The cell growth inhibitory and *in vivo* activities seem to be minimal.

Also in 2015, Elumalai et al. reported Stafib-1 as a selective STAT5B SH2 domain inhibitor with a K_i value of 44 nM [30]. Stafib-1 demonstrates that selective targeting of STAT5B is possible even though the sequence identity between STAT5A and STAT5B is over 95%. However, the selectivity compared with other STAT proteins as well as *in vitro* and *vivo* effects of Stafib-1 have not been reported.

In 2020, Natarajan et al. reported Stafia-1 as STAT5A inhibitor with a preferential binding to STAT5A over STAT5B [35]. Similar to Stafib-1, characterization of Stafia-1 with respect to selectivity over other STAT family proteins and its effects *in vitro* and *in vivo* have been elusive.

As demonstrated in previous investigations of targeting STAT5, achieving selectivity, cellular potency, and *in vivo* efficacy has proven very challenging. This is largely due to the structural similarity among STAT proteins, the shallow binding site on the STAT5 SH2 domain, and the lack of high-resolution co-crystal structures with STAT5 inhibitors. Importantly, traditional occupation-driven inhibition of STAT proteins has proven surprisingly ineffective even with high affinity inhibitors, as demonstrated by the previous intensive inhibitor development efforts to target STAT3 [36]. Lessons learned from STAT3 inhibitor development led our lab to investigate an alternative STAT3 targeting strategy and has resulted in a successful STAT3 degrader [37, 38]. We hypothesized that we may be able to apply proteolysis-targeting chimera (PROTAC) technology to STAT5A/B. We sought to develop the first-in-class STAT5 degrader using novel in-house STAT5 inhibitors to form PROTACs in this dissertation work.

1.3 Proteolysis-Targeting Chimera (PROTAC) and beyond

Recently, PROTAC technology has significantly stimulated the drug discovery arena given its ability to target proteins once considered undruggable [39-43]. PROTACs are

heterobifunctional molecules in which an E3 binding ligand and a target protein binding ligand are connected by a linker. By inducing the proximity between a target protein and an E3 ubiquitin ligase, a resulting ternary complex consisting of a target protein, PROTAC molecule, and target-ubiquitinating machinery initiates the ubiquitination and subsequent proteasomal degradation of the target protein. Because PROTACs work through an event-driven mechanism, unlike a traditional small molecule with an occupation-driven mechanism, PROTACs work as a catalyst to remove a protein of interest, contributing to improving potency and safety. Importantly, PROTACs have the potential to target "undruggable" proteins. By targeting any domain or binding site on the protein of interest, PROTACs can induce the depletion of the protein. This results in the inhibition of the functions of the protein of interest, which is not possible using traditional inhibitors [44, 45]. The introduction of PROTAC technology roughly twenty years ago has led to publications and excellent review articles on PROTAC technology and its applications.

Sakamoto et al. (2001) reported the first PROTACs targeting degradation of the methionine aminopeptidase-2 protein (MetAP-2) [46], followed by, in 2003, the further expansion of the PROTAC application to androgen receptor (AR) and estrogen receptor (ER) [47]. These initial peptide-based PROTACs contained a long phosphopeptide to recruit SCFβ-TrCP E3 ubiquitin ligase.

Soon after, in 2004, Schneekloth et al. reported the first cell permeable PROTAC [48]. The length of peptide-based E3 ligase ligand that recruit VHL protein was shortened to heptamers.

In 2008, Schneekloth et al. reported the first non-peptide AR-targeted PROTACs [49], which contain nutlin-3a, a small molecule E3 ligase ligand, in the PROTACs to recruit the E3

ubiquitin ligase protein MDM2. Another class of PROTACs, called specific and non-genetic inhibitors of apoptosis protein dependent protein erasers (SNIPER), was reported by Itoh et al. in 2010, which was also expanded to several target proteins in later years [50-52].

In 2010, Ito et al. discovered that CRBN, which is the substrate acceptor of the CRL4CRBN E3 ubiquitin ligase, is the target of thalidomide [53]. Based on this discovery, in 2015, Lu et al. and Winter et al. both published new thalidomide-based or thalidomide analogue-based PROTACs targeting either BRD4, BET, or FKBP12 proteins [54, 55].

Since then, several dozens of small molecule PROTAC degraders targeting "undruggable" or "difficult-to-drug" proteins have been reported by many groups, underscoring the great potential of the PROTAC strategy in the field of drug discovery [56].

Beyond identifying PROTACs, the pioneering PROTAC technology has created and facilitated the field of targeted protein degradation (TPD). Some of the major classes of modalities are, for example, molecular glues, lysosomal-targeting chimeras (LYTACs), and macroautophagy degradation targeting chimeras (MADTACS) [57]. Briefly, molecular glues are monomeric degraders that bind an E3 ligase and change its substrate recognition site to recruit a neosubstrate for degradation. Thalidomide is known as the first molecular glue molecule, which was introduced in 1950s without knowledge of its mode of action as a molecular glue [53, 58]. While PROTACs and molecular glues exploit the ubiquitin-proteasome system (UPS), LYTACs take advantage of lysosome system to direct secreted or membrane proteins for lysosomal degradation [59]. MADTACS include autophagy-targeting chimera (AUTACs) and autophagosome-tethering compounds (ATTECs) and uses the macroautophagy system. Unlike the UPS, macroautophagy can remove not only proteins, but also larger objects such as

intracellular pathogens and dysfunctional organelles [60]. Takahashi et al. reported the first AUTAC molecule [61], followed by Li et al. reporting ATTEC molecule soon after [62].

Chapter 2 A Potent and Selective Small-Molecule STAT5 PROTAC Degrader Capable of Achieving Tumor Regression *In Vivo*

2.1 Abstract

STAT5, (signal transducer and activator of transcription 5) is an attractive therapeutic target but successful targeting of STAT5 has proved to be difficult. We report herein the development of AK-2292 as a first, potent and selective small-molecule degrader of both STAT5A and STAT5B isoforms. We designed a class of small molecules that bind to STAT5 with micromolar binding affinity and better affinity to STAT6. Using the PROTAC technology, we successfully transformed these STAT5 ligands into potent and selective STAT5 degraders exemplified with AK-2292. It induces degradation of STAT5 proteins in a dose- and time-dependent manner and demonstrates an outstanding selectivity over all other STAT proteins and >6,000 non-STAT proteins. RNA-seq analysis revealed that AK-2292 downregulates the transcriptome associated with STAT5A/STAT5B. AK-2292 displays potent cell growth inhibition in a panel of human chronic myeloid leukemia (CML) cell lines with activated STAT5. It effectively induces STAT5 degradation in normal mouse tissues and human CML xenograft tissues and achieves tumor regression in two CML xenograft models in mice at well-tolerated dose-schedules. Determination of co-crystals of AK-2292 and its corresponding inhibitor in complex with STAT5A provides their detailed interactions and a structural basis for further optimization. AK-2292 is a powerful research tool compound with which to investigate the biology and therapeutic potential through selective depletion of STAT5 *in vitro* and *in vivo* and represents a promising lead compound toward ultimate development of a STAT5-targeted cancer therapy.

2.2 INTRODUCTION

STAT5 (signal transducer and activator of transcription 5) is a gene transcriptional factor and plays a key role in numerous cellular processes [1, 2]. It has two isoforms, namely STAT5A and STAT5B, which have similar but non-redundant roles in human cancers.

Upon phosphorylation by upstream JAK and other kinases, STAT5 forms homo- or hetero-dimers through its SH2 domain [31, 32]. This STAT5 dimerization has been demonstrated to be essential for its gene transcriptional activity [31, 32]. It has been hypothesized that small-molecule inhibitors designed to bind to the SH2 domain of STAT5 can effectively block its dimerization and gene transcriptional activity [33]. Unfortunately, despite extensive efforts in the last 20 years, successful targeting STAT5 by small-molecule inhibitors remains elusive. STAT5 inhibitors that have been reported to date generally lack desirable potency and selectivity and/or a clear mechanism of action at the cellular level [25].

In recent years, targeted protein degradation (TPD) has gained a major momentum as a promising approach for the discovery of high-quality research compounds for target validation and importantly for the development of new therapeutic agents [39]. TPD is particularly attractive for its ability to target undruggable or difficult-to-drug protein targets. For example, employing the powerful proteolysis targeting chimera (PROTAC) technology, we have achieved the successful development of SD-36 as a potent, selective, and efficacious degrader of STAT3 [37]. Because STAT5 and STAT3 have similar SH2 domains, we reasoned that a potent and selective STAT5 degrader may be developed with the PROTAC technology. We discovered however that design of high-affinity and selective ligands for the STAT5 SH2 domain is particularly challenging, and all of our designed inhibitors were found to bind to STAT6 with higher affinities than to STAT5. Determination of co-crystal structures of our STAT5 inhibitors

in complexes with the STAT5 SH2 domain revealed that STAT5 has a shallower binding pocket than STAT3 and STAT6, providing a possible explanation for the difficulty associated with the design of high affinity inhibitors for STAT5. Gratifyingly, using inhibitors with moderate affinities to STAT5 and higher affinities to STAT6, we successfully obtained PROTAC molecules that potently and effectively induce degradation of STAT5 but fail to degrade STAT6 protein. This led to the development of AK-2292 as a first, potent, highly selective, and efficacious STAT5 degrader.

Constitutive activation of STAT5 plays a role in initiation, progression and/or maintenance of certain hematological malignancies, such as chronic myeloid leukemia (CML) [4, 7, 8]. The central pathogenesis of CML is the fusion of the Ableson murine leukemia 1 (ABL1) gene with the breakpoint cluster region (BCR) gene, which generates the BCR-ABL1 oncoprotein. This oncoprotein acts as a constitutively active non-receptor cytosolic tyrosine kinase and promotes tumor progression *via* a set of well-characterized downstream mediators [63], including STAT5A and STAT5B [64]. Indeed, constitutively activated STAT5A/STAT5B is a signaling hallmark of CML [6, 24, 65-67], and plays a critical role in the induction and maintenance of CML. Therefore, in addition to BCR-ABL1, STAT5A and STAT5B are potentially attractive therapeutic targets for CML. Despite the tremendous success of multiple generations of BCR-ABL1 inhibitors, some CML patients ultimately developed drug resistance or were intolerant to these otherwise highly effective drugs. Consequently, there is still a need to develop new therapeutic approaches for CML [13, 68].

As a proof-of-concept, we explored in the present study the therapeutic potential of AK-2292 in a panel of human CML cell lines *in vitro* and *in vivo*. Our data show that AK-2292 effectively and potently induces degradation of STAT5 in all cell lines tested. Furthermore, AK-

2292 demonstrates an exceptional degradation selectivity for STAT5 over other STAT members, and >6,000 other non-STAT proteins. AK-2292 exerted potent growth-inhibitory activities in human CML cell lines with activated STAT5, while its corresponding STAT5 inhibitor showed no effect. AK-2292 effectively depleted STAT5 protein in CML xenograft tumor tissues and achieved tumor regression in two xenograft mouse models of CML at well tolerated dose-schedules. Determination of co-crystal structures of AK-2292 and its inhibitor in complex with STAT5A provides a solid structural basis for further structure-based optimization. AK-2292 provides a powerful chemical biology research tool compound with which to investigate the role of STAT5 in different biological processes and human diseases and is a promising lead compound for further optimization towards ultimate development of a new class of therapies through selective degradation of STAT5.

2.3 RESULTS AND DISCUSSION

2.3.1 Structure-guided design of STAT5 SH2 domain inhibitors

Our laboratory has reported the design of high-affinity and cell-permeable small-molecule inhibitors targeting the STAT3 SH2 domain and our subsequent successful development of a first-in-class, potent, selective, and highly efficacious STAT3 degrader [37, 38, 69]. STAT5 and STAT3 share homologous SH2 domains, and accordingly, we first pursued structure-guided design of STAT5 SH2 inhibitors towards development of STAT5 degraders.

Previously, McMurray et al. reported their development of cell-permeable prodrug peptidomimetic STAT6 inhibitors [70, 71]. Because STAT5 and STAT6 proteins share homologous SH2 domains with 44.8% sequence identity (Extended Data Fig. 1A), we reasoned that the STAT6 inhibitors reported by the McMurray group may possess useful affinities to STAT5. We therefore synthesized compound **1** (Fig. 1A) and determined its binding affinities to

recombinant human STAT5A and STAT6 SH2 domain proteins in biochemical binding assays. Compound **1** binds to STAT6 with a moderate affinity (K_i = 2.7 μM), but has a very weak affinity for STAT5A and STAT5B (K_i >10 μM) (Extended Data Fig. 1E).

Previously, we employed an indole-based phosphotyrosine mimetic for the successful development of potent and cell-permeable STAT3 degraders [37]. However, this indole-based phosphotyrosine mimetic was found to have chemical stability issues [69]. Extensive modification of the indole-based phosphotyrosine mimetic led to the identification of a chemically stable benzothiophene-based phosphotyrosine mimetic [72]. Replacing the phosphotyrosine mimetic in compound **1** with this novel benzothiophene-based phosphotyrosine mimetic yielded compound **2**, which binds to STAT5A, STAT5B and STAT6 with K_i values of 3.9, 4.9 and 1.8 μM, respectively. Hence, use of this benzothiophene-based phosphotyrosine mimetic led to a marked improvement in binding affinities of the resulting inhibitor to STAT5A/5B.

For the design of bifunctional PROTAC degraders, an exit vector is needed from the inhibitor of the protein of interest to tether to a ligand for an E3 ligase complex. For this purpose, the fused tetrahydroquinoline ring in compound **2** was opened, producing compounds **3** and **4**. While compound **3** displays a weak affinity to STAT5A and STAT5B, compound **4** binds to STAT5A, STAT5B and STAT6 with K_i values of 5.8, 7.3 and 3.0 μM, respectively, slightly weaker than compound **2** to these three proteins.

To guide our subsequent optimization efforts, we predicted the binding models of compound **4** in complex with STAT5A. The predicted binding models showed that the compound **4** binds to STAT5A in a manner similar to that of SD-36 in its complex with STAT3. In particular, the phenyl group in compound **4** occupies a large binding pocket in STAT5A (Extended Data Fig. 1B), suggesting that further modifications of the phenyl group in compound **4** may improve its

binding affinities to STAT5. Furthermore, the *N*-methyl group in compound **4**, which is exposed to solvent can serve as a tethering site to link to a ligand for an E3 ligase complex for PROTAC degrader development.

We replaced the phenyl group in compound **4** with a benzyl or 4-bromobenzyl group leading to compound **11** or compound **12**, respectively (Extended Data Fig. 1E). Both **11** and **12** bind to STAT5A or 5B with an affinity weaker than that of compound **4** but both have an affinity to STAT6 similar to that of compound **4**.

To further facilitate the development of degrader molecules, we replaced the *N*-methyl group with *N*,*N*-dimethylpropanamide, yielding compound **15**, which has affinities to STAT5A, STAT5B and STAT6 that are similar to those of compound **4**. Compound **15** provides a convenient tethering site, which was used as the template molecule for further modifications.

Our predicted model for compound **15** bound to STAT5A suggested that the phenyl group in **15** occupies a large and shallow pocket, formed by residues Phe646, Arg659 and Asp650 and Lys644. We performed extensive modification of the phenyl group in compound **15** and identified a number of analogues with STAT5A binding affinities better than that of compound **15**. For examples, compounds **5**, **18** and AK-305 bind to STAT5A with K_i values of 2.2, 0.7 and 1.2 μM, respectively, and bind to STAT5B with K_i values of 1.9, 0.6 and 0.6 μM, respectively (Extended Data Fig. 1). For STAT6, compounds **5**, **18** and AK-305 have K_i values of 0.19, 0.08 and 0.6 μM, respectively. Thus, while AK-305 has similar affinities to STAT5A, STAT5B and STAT6 proteins, compounds **5** and **18** have higher affinities to STAT6 than to STAT5A and STAT5B proteins.

We successfully determined the co-crystal structure of AK-305 (PDB: 7TVB) in complex with STAT5A at 2.65 Å resolution (Fig. 1C). This co-crystal structure showed that the phosphate

in the phosphorylated peptide binding site is placed in a location similar to that in the SD-36-STAT3 complex [37]. This phosphate is stabilized through hydrogen bonding with the sidechains of Ser620, Ser622 and the backbone amide nitrogens of Asp621 and Ser622 as well as electrostatic interactions with the sidechains of Arg618 and Lys600. The difluoromethyl group in the AK-305-STAT5A complex enjoys van der Waals interactions with the sidechains of Thr628 and Pro645 and the pro-(*S*)-F atom hydrogen bonds with the NH_2 group of Arg618. Residues Pro645 and Lys644 on STAT5A are sandwiched between the indole and the benzothiazole groups which, together with the sidechains of Leu643, Phe646, Asp650 and Arg656 line a pocket in which the benzothiazole inserts allow the thiazole to establish an edge-on π-π stacking with the sidechain of Phe646. The amides on either side of the neopentyl group in AK-305 form hydrogen bonds with the backbone amides of Asn642 and Lys644, while the trimethyl sidechain in AK-305 is positioned in a hydrophobic environment produced by the sidechains of Leu643, Trp641 and Trp631. The proline residue in STAT5A forms a rigid kink which helps to position the benzothiazole and forms van der Waals interactions with the aliphatic sidechain of Lys644. The dimethylacetamide in STAT5A entertains hydrophobic interactions with Leu663 and forms a hydrogen bond with the hydroxyl of Tyr665.

2.3.2 Development of potent PROTAC STAT5 degraders.

We next investigated if PROTAC degraders for either STAT5 or STAT6 could be developed using these inhibitors with moderate binding affinities to STAT5A and STAT5B and higher affinities to STAT6.

The co-crystal structure of AK-305 in the complex with STAT5A suggested that the dimethylacetamide in AK-305 is a suitable tethering site for the design of potential PROTAC

degraders (Fig. 1C). We initially tested our design ideas using compound **5** as the inhibitor and lenalidomide as the ligand for cereblon/cullin 4A which were tethered together through an alkynyl group with a spacer of different lengths to generate potential degraders (Fig. 1B). These compounds were evaluated for their ability to reduce the levels of STAT5 or STAT6 protein in the KU812 human chronic myeloid leukemia (CML) cell line, which has a high expression of STAT5A, STAT5B and STAT6 proteins. Compound **23** (Extended Data Fig. 1F) with a 2-methylene spacer was found to have no effect on the levels of both STAT5 and STAT6 proteins. Increasing the length of the spacer in compound **23** by one methylene group yielded compound **6**, which also failed to reduce the levels of STAT6 but effectively reduced the levels of STAT5 protein, giving a DC_{50} value of 0.5 μM. Significantly, compound **6** also achieved a maximum degradation (Dmax) of 95% at 5 μM. Encouraged with the promising degradation activity achieved by compound **6**, we further explored the linker in compound **6**. Extending the spacer by two more methylenes generated compound **25** (Extended Data Fig. 1F), which effectively reduced the level of STAT5 but is less potent than compound **6**. Similar to compound **6**, compound **25** has no effect on the levels of STAT6 protein. We placed a methyl group onto the amino group in the linker in compound **6**, yielding compound **7**, which had no effect on STAT6, but is slightly more potent than compound **6** in reducing STAT5 protein, with a DC_{50} value of 0.38 μM and a Dmax of >95%.

We next investigated the effect on the STAT5 degradation activity of conformational restriction in the linker of the degrader molecule. Compounds **26**, **27** and **28** with a restricted linker were found to be completely ineffective in reducing the levels of both STAT5 and STAT6 proteins (Extended Fig. 1F).

Because the 4-bromophenyl group in compounds **6** and **7** is potentially chemically reactive, we replaced the inhibitor portion in degraders **6** and **7** with AK-305, which generated degraders **8** and AK-2292, respectively. Compound **8** and AK-2292 effectively reduce the levels of STAT5 protein with DC_{50} values of 0.3 μM and 0.1 μM and Dmax >95%, respectively. Similar to compounds **6** and **7**, compound **8** and AK-2292 failed to reduce the levels of STAT6 protein (Extended Fig. 1G).

We successfully determined a co-crystal structure of AK-2292 in complex with STAT5A (PDB: 7TVA) at 2.85 Å resolution (Fig. 1D). Comparison of the co-crystal structures of AK-305 and AK-2292 in their complexes with STAT5A showed that the inhibitor portion in AK-2292 binds to STAT5A with essentially an identical binding mode as AK-305.

In the co-crystal structure of AK-2292 with STAT5A, the carbonyl group of the dimethylacetamide in AK-2292 forms a hydrogen bond with the hydroxyl group of Tyr665 of STAT5A. To investigate the importance of this hydrogen bond, we synthesized compound **29** (Extended Data Fig. 1G), by replacing the amide group in AK-2292 with two methylenes. Compound **29** failed to reduce the levels of STAT5 and STAT6 up to 15 μM, indicating that the hydrogen bond in these PROTAC degrader molecules plays a critical role for the formation of a productive complex with STAT5/cereblon/Cullin 4A for degradation of STAT5.

We synthesized AK-2292Me (Fig. 1B) by installation of a methyl group onto the amino group of the piperidine-2,6-dione moiety in the cereblon ligand portion of AK-2292. While AK-2292 binds to cereblon with a K_i value of 27 nM, AK-2292Me has a K_i value of 3.9 μM (Extended Data Fig. 1I). Thus, AK-2292Me binds to cereblon with >100-times weaker affinity than AK-2292. Consistently, AK-2292Me was found to be completely ineffective in reducing the levels of

STAT5 proteins (Figs. 2A-2B), highlighting the importance of strong cereblon binding for the degrader molecules to achieve effective STAT5 degradation.

2.3.3 AK-2292 is a potent and Bona Fide PROTAC degrader of both STAT5A/B proteins

We further evaluated the degradation potency and selectivity of AK-2292, together with its corresponding inhibitor AK-305 and the degrader control AK-2292Me in the KU812 CML cell line with constitutively activated STAT5.

AK-2292 achieved an DC_{50} value of 150 nM and a Dmax >95% against both STAT5A and STAT5B with 18 h treatment time in the KU812 cell line (Figs. 2A-2C). Activation of STAT5 leads to STAT5 phosphorylated at the Tyr694 residue ($pSTAT5^{Y694}$). AK-2292 effectively reduces the levels of $pSTAT5^{Y694}$ protein in the KU812 cell line with a similar potency as in its degradation of the total STAT5A and STATB proteins.

To investigate if AK-2292 is a *bona fide* PROTAC degrader, we performed blocking experiments using the cereblon ligand lenalidomide, a proteasome inhibitor MG-132 and the STAT5 inhibitor, AK-305 (Extended Data Fig. 2A). Consistent with its design, the AK-2292 induced degradation of the total STAT5A/STAT5B and $pSTAT5^{Y694}$ proteins was effectively blocked by AK-305, lenalidomide and MG-132. These data clearly demonstrate that AK-2292 is a *bona fide* PROTAC STAT5 degrader.

AK-2292 was further investigated for its ability to reduce total STAT5A/STAT5B and $pSTAT5^{Y694}$ proteins in several additional human CML cell lines (Fig. 4B and Extended Data Figs. 4A-4H). AK-2292 effectively reduced the total STAT5A/B and $pSTAT5^{Y694}$ proteins in each of these CML cell lines with DC_{50} values ranging between 0.1 and 0.8 μM and Dmax values of >90%.

2.3.4 AK-2292 displays a high degradation selectivity for STAT5 in whole proteome

Because STAT proteins share a high sequence homology, particularly in their SH2 domains, it has been very challenging to design selective SH2 domain inhibitors for a particular STAT member. We next investigated the degradation selectivity of AK-2292.

Western blot analysis showed that AK-2292 selectively depleted STAT5A/STAT5B over other STAT family members in both KU812 CML cell line and human peripheral blood mononuclear cells (PBMC) that express all STAT family proteins (Figs. 2A-2B). While AK-2292 reduced STAT5A/STAT5B by >90% at 1 μM with 18 h treatment time in KU812 and PBMCs, it showed no obvious effect up to 5 μM on other STAT family proteins with the same treatment time. In comparison, both AK-305 and AK-2292Me failed to reduce the levels of STAT5A/STAT5B and $pSTAT5^{Y694}$ proteins in KU812 cells and PBMCs at 5 μM. We further investigated the selectivity of AK-2292 in KU812 cells at higher concentrations with a shorter treatment time (7 h), and found that while AK-2292 effectively reduces the levels of STAT5 and $pSTAT5^{Y694}$ proteins in a dose-dependent manner and by >50% at 6.3 μM, it has no effect on other STAT proteins at concentrations as high as 100 μM (Extended Data Fig. 2B).

We probed STAT5A and STAT5B individually, as well as the $pSTAT5^{Y694}$ protein in KU812 cells and PBMCs. In the KU812 cells, AK-2292 demonstrated very similar potencies in reducing the levels of STAT5A and STAT5B isoforms, as well as $pSTAT5^{Y694}$ protein with DC_{50} values of 0.11-0.16 μM and Dmax values of >90% (Figs. 2A-2C) at the 18 h time point. Both AK-305 and AK-2292Me had no effect on these proteins at 5 μM. In PBMCs, AK-2292 effectively degraded STAT5A and STAT5B proteins in a dose-dependent manner with very similar potencies and achieved DC_{50} values of ~0.2 μM and Dmax values of >90%. Of note,

PBMCs have undetectable levels of pSTAT5^{Y694} protein, indicating a low level of STAT5 activation.

We examined the kinetics of STAT5 degradation by AK-2292 in KU812 cells (Fig. 2D) and found that AK-2292 effectively reduced the levels of both total STAT5 and pSTAT5^{Y694} in a time-dependent manner. While 10 μM of AK-2292 is needed to reduce STAT5 proteins by >90% with a 4 h treatment time, 1 μM of AK-2292 has the same effect with a 24 h treatment time.

To further investigate the degradation selectivity of AK-2292 beyond STAT family proteins, we performed unbiased proteomics analyses in KU812 cells and PBMCs (Fig. 2E). In KU812 cells, AK-2292 at 1 μM with a 24 h treatment time profoundly reduced the levels of STAT5A and STAT5B proteins with PIM1 being the only other protein whose level is reduced significantly. PIM1 is a known targeted gene regulated by STAT5 [73]. We performed a further proteomics analysis by treating KU812 cells with 10 μM of AK-2292 for 8 h. AK-2292 at 10 μM effectively and profoundly reduced the levels of STAT5A and STAT5B proteins with SMTN (Smoothelin) being the only other protein whose level was reduced by >2-fold.

In PBMCs, AK-2292 at 5 μM with 18 h treatment time reduced the levels of STAT5A and STAT5B proteins by >85% and has no significant effect on any other of the >6,000 proteins analyzed.

To further assess the selective degradation in tumor cells with highly activated STAT5 protein, we performed a proteomic analysis in the NCO2 CML cell line carrying the BCR-ABL1 fusion (Fig. 2E). AK-2292 at 1 μM with 24 h treatment time reduced the levels of STAT5A and STAT5B proteins by >85% in NCO2 cells. In this case, the levels of three other proteins, PIM1,

MYC and FAM18B2, were also reduced significantly. Similar to PIM1, MYC is a known STAT5-targeted gene product [74].

We also performed a proteomics analysis of AK-2292Me, a control compound for AK-2292, in KU812 cells (Fig. 2F). AK-2292Me at 5 μM with 24 h treatment had no effect on the levels of STAT5A and STAT5B, or any other STAT family protein. Interestingly, AK-2292Me was found to reduce the level of MSANTD2 (Myb/SANT DNA Binding Domain Containing 2) protein while increasing the level of the PPFIBP2 protein.

Collectively therefore, AK-2292 is a highly selective degrader of STAT5A and STAT5B proteins over all other STAT family members and >6,000 other proteins.

2.3.5 AK-2292 induces down-regulation of STAT5 associated transcriptome in cells

To investigate the effect of STAT5A/STAT5B depletion on transcriptome, we treated KU812 and NCO2 cells with AK-2292 at 1 μM for 8 h and performed RNA-seq analysis (Fig. 3A and Extended Data Fig. 3A). As a control, we treated KU812 and NCO2 cells with AK-2292Me at 5 μM for 24 h for RNA-seq analysis (Fig. 3D and Extended Data Fig. 3D). In both cell lines, only 7 - 8 genes were significantly downregulated by ≥ 2-fold ($p \leq 0.05$) with AK-2292 treatment and no gene was downregulated by more than 2-fold with AK-2292Me treatment. Five genes (PIM1, OSM, SOCS3, APOL4, CISH), all known to be regulated by STAT5, were significantly downregulated in both KU812 and NCO2 cell lines [19, 73, 75, 76]. These data confirm that selective degradation of STAT5A/B only down-regulates a very small set of genes in these two CML cell lines.

Gene set enrichment analysis (GSEA) revealed that STAT5 depletion has a major effect on several pathways with IL2/STAT5 signaling and c-Myc targets being the top two pathways affected (Figs. 3B-3C, Extended Data Figs. 3B-3C).

2.3.6 AK-2292 displays potent growth-inhibitory activity in CML cells

Because BCR-ABL fusion in CML cells leads to activation of STAT5, we evaluated AK-2292 in a panel of 8 human CML cell lines all carrying a BCR-ABL1 fusion.

All these 8 human CML cell lines expressed marked levels of total STAT5 protein with NALM1 having the lowest levels and KYO-1 and LAMA-84 having the highest levels (Fig. 4A). Isoform specific antibodies revealed that the expression levels of STAT5A and STATB are correlated with in each of these cell lines. In addition, the levels of $pSTAT5^{Y694}$ protein correlate well with the levels of total STAT5 protein.

We evaluated AK-2292 for its ability to reduce both the total STAT5 and $pSTAT5^{Y694}$ proteins in each of these 8 CML cell lines (Extended Data Figs. 4A-4H). Western blotting analysis showed that AK-2292 effectively reduces the levels of both the total STAT5 and $pSTAT5^{Y694}$ proteins in each of these CML cell lines in a concentration-dependent manner.

We evaluated AK-2292 for its anti-proliferative activity in these CML cell lines with AK-305 and AK-2292Me included as the controls (Figs. 4B-4C and Extended Data Fig. 4I). While the inhibitor AK-305 and the degrader control AK-2292Me at up to 15 μM have no effect on cell viability in each of these 8 CML cell lines, AK-2292 effectively inhibits cell growth in 6 out of the 8 CML cell lines with IC_{50} values of 0.2-2.2 μM. AK-2292 has partial inhibition in the K562 cell line but is completely ineffective in the NALM1 up to 15 μM. Of note, although the NALM1 cell line carries a BCR-ABL1 fusion, it has the lowest level of total STAT5 protein, as well as $pSTAT5^{Y694}$ protein among these 8 cell lines examined (Fig. 4A and Extended Data Fig. 4E).

SU-DHL-1 has a high level of pSTAT3 but a very low level of pSTAT5Y^{694} (Extended Data Fig. 4F) and our selective STAT3 degrader SD-36 effectively inhibits cell growth in the SU-DHL-1 cell line, indicating the cell line's dependence on STAT3 for its proliferation [37]. Consistent with its lack of degradation on STAT3, AK-2292 has no effect on the viability of the SU-DHL-1 cell line up to 15 μM. The data also indicated that both STAT5A and STAT5B have no significant role in the survival of the SU-DHL-1 cell line.

2.3.7 AK-2292 effectively depletes STAT5 protein in xenograft tumors and normal tissues in mice

We investigated if AK-2292 is capable of depleting STAT5 proteins in KU812 and NCO2 xenograft tumors in mice (Figs. 5A-5B).

Western blotting analysis revealed that a single intraperitoneal (i.p.) dose of AK-2292 at 100 mg/kg reduced STAT5A/STAT5B protein level at the 1 h time-point and achieved near complete depletion of STAT5A/STAT5B protein at the 6 h time-point in both KU812 and NCO2 tumor tissues. AK-2292 was still very effective in reducing the levels of STAT5A/STATB proteins by >70% at the 24 h time point. Importantly, AK-2292 was equally effective in reducing both the total STAT5 and pSTAT5^{Y694} proteins at all the time points examined. We evaluated AK-305, the inhibitor control in the NCO2 tumor tissue and found that AK-305 has no effect on the levels of STAT5 and pSTAT5^{Y694} levels (Fig. 5B).

We investigated the degradation of STAT5 in normal mouse tissue. Our data showed that a single dose of AK-2292 at both 100 mg and 200 mg/kg effectively reduced the level of STAT5 protein in mouse liver and spleen tissues (Extended Data Fig. 5A). We further tested the effect of AK-2292 on STAT5 protein in mouse liver and spleen tissues with daily dosing for 3

consecutive days at 100 and 200 mg/kg (Fig. 5C). Our data showed that AK-2292 is very effective in reducing the levels of STAT5 protein in liver and spleen tissues at both doses at 3 and 24 h time-points examined. AK-2292 at 200 mg/kg reduced the STAT5 protein levels by >90% and >80% in the liver and spleen tissues with the effect persisting for >24 h. Furthermore, AK-2292 has no significant effect on the levels of STAT6 protein.

Taken together, these pharmacodynamic (PD) data demonstrate that a single dose of AK-2292 is effective in reducing the levels of STAT5A/STAT5B and $pSTAT5^{Y694}$ proteins in human xenograft tumor tissues with a strong effect persisting for at least 24 hr.

2.3.8 AK-2292 achieves tumor regression in mouse xenograft models without signs of toxicity

Based upon the strong PD effect of AK-2292 in tumor tissues, we evaluated AK-2292 for its antitumor efficacy in both the KU812 and NCO2 xenograft models in severe combined immunodeficient (SCID) mice (Fig 5D).

In the KU812 model, AK-2292 was dosed at 200 mg/kg daily or at 100 mg/kg twice daily (or BID) to assess its antitumor activity, with the corresponding inhibitor AK-305 included as a control. At 200 mg/kg daily or 100 mg/kg, twice daily for 2 weeks, AK-2292 induced tumor regression by a maximum of 70%. In comparison, the corresponding inhibitor AK-305 at 200 mg/kg, daily had no significant effect on tumor growth compared to the vehicle control.

In the NCO2 xenograft model, AK-2292 inhibited tumor growth in a dose-dependent manner by 61, 96 and 103% at the end of the 2-week treatment after being treated with 50, 100 and 200 mg/kg daily, respectively. AK-2292 at 200 mg/kg reduced the average tumor size from 123 mm^3 at the beginning to 31 mm^3, a regression of 75% during the treatment time.

Significantly, AK-2292 did not induce significant weight changes or other signs of toxicity during all the three efficacy experiments in SCID mice (Fig. 5D and Extended Data Fig. 5B).

We investigated the potential toxicity of STAT5 degradation in immune competent mice. Our data showed that AK-2292 administered at 100 mg/kg daily for 2 weeks by I.P. injection had a minimal effect on animal weights (Extended Data Fig. 5C) and did not have significant adverse effects on blood chemistry parameters. (Extended Data Fig. 5D). Therefore, AK-2292 is well tolerated in both immune competent and immune-compromised mice.

2.3.9 Discussion

Induced protein degradation using the hetero-bifunctional PROTAC technology has become a powerful approach with which to target those traditionally undruggable or difficult-to-drug targets. In the present study, we have aimed at development of PROTAC degraders against the STAT5 protein, an attractive therapeutic target which has been pursued for 20 years but remains elusive to date.

For the successful design of a potent PROTAC degrader for a specific protein, a high affinity ligand is typically a pre-requisite. We therefore attempted first to design high-affinity small-molecule inhibitors for the STAT5 SH2 domain starting from a previously reported peptidomimetic prodrug for STAT6 [70, 71]. Because the initial lead compound displays only a minimal affinity to STAT5 (K_i >10 μM), we performed structure-guided design with the objective of improving the binding affinity to STAT5 protein but, despite our extensive efforts, we were only able to identify small-molecule ligands that bind to the STAT5 SH2 domain with moderate binding affinities (K_i = 0.7-1.7 μM). Determination of the co-crystal structure of one

such ligand (AK-305) in complex with STAT5 revealed that STAT5 domain has a shallower binding pocket, than the STAT3 SH2 domain, providing an explanation why design of high-affinity ligands for STAT5 is more challenging than for STAT3. Furthermore, the most potent STAT5 ligands we identified also show higher affinities to STAT6 than to STAT5.

Employing these moderately potent ligands to STAT5 and reasonably potent ligands to STAT6, we designed a series of PROTAC degraders using a lenalidomide derivative to recruit the cereblon/cullin 4A E3 ligase complex for targeted degradation. While none of our designed PROTAC degraders reduced the levels of the STAT6 protein in cells, a number of them potently and effectively reduced the levels of STAT5 protein, and AK-2292 was the most potent degrader. STAT5 protein has two isoforms, STAT5A and STAT5B. AK-2292 reduced both STAT5A and STAT5B with similar degradation potencies and kinetics. Importantly, AK-2292 is equally potent and effective in reducing the levels of the phosphorylated, active form STAT5 protein ($pSTAT5^{Y694}$) in cells. Proteomics analysis in two human CML cell lines and in PBMCs further demonstrated that AK-2292 only reduces the levels of STAT5 protein and does not induce degradation of all other STAT members and >6,000 other non-STAT proteins, thus displaying an exceptional degradation selectivity for STAT5.

We next sought to investigate the therapeutic potential of AK-2292 *in vitro* and *in vivo*. STAT5 has been implicated in several hematological malignancies, including T-cell lymphoma [10], acute leukemia [9, 29] and CML [6, 7, 24, 67]. It is well established that BCR-ABL1 fusion in CML cells leads to activation of STAT5, which contributes to initiation and progression of CML. In the present study, we focused our investigation on CML using a panel of human CML cell lines for a proof-of-concept study. Our data showed that AK-2292 is equally potent and effective in reducing the levels of total STAT5 protein (both STAT5A and STAT5B isoforms)

and importantly, of the phosphorylated, active form STAT5 protein (pSTAT5^{Y694}). AK-2292 also effectively inhibits cell growth in 6 out of 8 human CML cell lines evaluated, with K562 and NALM1 cell lines being the exceptions. Since the NALM1 cell line has very low levels of total STAT5 and pSTAT5^{Y694} proteins, it is perhaps unsurprising that degradation of STAT5 had no effect on the viability of the NALM1 cells. Although the K562 cell line has marked levels of total STAT5 and pSTAT5^{Y694} proteins and AK-2292 effectively degrades total STAT5 and pSTAT5^{Y694} proteins, AK-2292 was only marginally effective in inhibition of cell growth in this CML cell line. RNAseq analysis revealed that degradation of total STAT5 and pSTAT5^{Y694} proteins induces down-regulation only on 7-8 genes, all of which are known to be regulated by STAT5, including MYC and PIM1, further indicating that AK-2292 specifically and effectively targets STAT5 through selective degradation of STAT5 protein.

In vivo, a single dose of AK-2292 rapidly and efficiently reduces the levels of total STAT5 and pSTAT5^{Y694} proteins in KU812 and NCO2 xenograft tumors, with a Dmax value of >90% and the effect lasting for at least 24 h. Impressively, AK-2292 is capable of achieving tumor regression of >70% with daily administration in both models. AK-2292 is well tolerated in mice in the efficacy experiments and does not induce significant weight loss or other signs of toxicity. AK-2292 is also highly effective in reducing STAT5 protein in mouse spleen and liver tissues and is well tolerated in immune-competent mice. Furthermore, daily administration of AK-2292 in immune-competent mice does not induce significant weight loss or other signs of toxicity. Therefore, our data suggested that selective degradation of STAT5 in normal mouse tissues does not induce overt toxicity in both immune-comprised and immune-competent mice.

We have previously reported our successful development of a potent, selective, and efficacious PROTAC degrader of STAT3 [37]. This current study provides another powerful

example that the PROTAC technology can be employed to successfully target STAT5, a difficult therapeutic target that has been elusive for the last 20 years. In particular, our study demonstrates that a potent, selective, and highly efficacious degrader can be successfully developed even in cases where the design of selective and high-affinity small-molecule inhibitors for the protein of interest has proven to be very challenging. The exceptional STAT5 degradation selectivity achieved by AK-2292 over all other STAT members and >6,000 non-STAT proteins makes it an ideal chemical biology tool compound with which to investigate the role of STAT5 in different biological processes and human diseases. Importantly, AK-2292 is a promising lead compound for further optimization toward development of a new therapy for the treatment of human cancers and other diseases in which either STAT5A or STAT5B plays a pivotal role.

2.4 Acknowledgements

We are grateful for the financial support from Oncopia Therapeutics, Inc, Proteovant Therapeutics Inc. and Roivant Sciences Inc. This study is also supported in part by the Cancer Center Support Grant (P30CA046592) from the National Cancer Institute, NIH to Rogel Cancer Center of the University of Michigan. We thank G.W.A. Milne for proof-reading of the manuscript.

2.5 Competing Interests Statement

The University of Michigan has filed patent applications on STAT5 inhibitors and degraders described in this study, which have been licensed to Oncopia Therapeutics Inc., Proteovant Therapeutics Inc. and Roivant Sciences Inc. S. Wang, A. Kaneshige, L. Bai, M. Wang, D. McEachern and J. Stuckey are co-inventors on one or more of these patent applications

and receive royalties from the University of Michigan. The University of Michigan has received a research contract from Oncopia/Proteovant/Roivant, for which S. Wang serves as the principal investigator. S. Wang was a paid consultant to Oncopia Therapeutics and owned equity in Oncopia. S. Wang is a paid consultant to Proteovant and Roivant and owns equity in Roivant.

2.6 Online method

2.6.1 Contact for Reagent and Resource Sharing

Please contact the corresponding author Shaomeng Wang at shaomeng@umich.edu regarding reagents and resource sharing.

2.6.2 Cell Lines and Cell Culture

AR230 (cat. no. CRL-3345), K562 (cat. no. CRL-3343), KU812 (cat. no. CRL-2099), and NALM1 (cat. no. 1567) cells were purchased from American Type Culture Collection (ATCC). KYO-1(cat. no. ACC 601) and SU-DHL-1 (cat. no. ACC 356) cells were purchased from German Collection of Microorganisms and Cell Culture GmbH (DSMZ). NCO2 (cat. no. IFO50525) cells were purchased from Japanese Collection of Research Bioresources Cell Bank (JCRB Cell Bank). MEG01 (cat. no. 94012401-1VL) and LAMA-84 (cat. no. SCC140) cells were purchased from Sigma-Aldrich. AR230 (ATCC CRL-3345), K562 (ATCC CRL-3343), KU812 (ATCC CRL-2099), LAMA-84 (EMD Millipore SCC140), MEG01 (Sigma Aldrich 94012401-1VL), NCO2 (XenoTech IFO50525), and SU-DHL-1 (DSMZ ACC 356) cells were cultured in RPMI 1640 medium (cat. no. 22400-089, Thermo Fisher Scientific) supplemented with 10% (v/v) heat-inactivated fetal bovine serum (FBS, cat. no. S11150H, Atlanta Biologicals, Flowery Branch, GA, USA), 100 U/ml penicillin and 100 µg/ml streptomycin (penicillin-streptomycin, cat. no. 15140122, Thermo Fisher Scientific). NALM1 (ATCC 1567) cells were

cultured in RPMI 1640 medium supplemented with 15% (v/v) heat-inactivated FBS, 100 U/ml penicillin,100 µg/ml streptomycin. KYO-1 (DSMZ ACC 601), cells were cultured in RPMI 1640 medium supplemented with 20% (v/v) heat-inactivated FBS, 100 U/ml penicillin,100 µg/ml streptomycin. All the cell lines were maintained in a humidified incubator at 37 ºC and 5% CO_2.

2.6.3 Animal Studies

All the *in vivo* studies were performed under an animal protocol (PRO00009463) approved by the Institutional Animal Care & Use Committee of the University of Michigan, in accordance with the recommendations in the Guide for the Care and Use of Laboratory Animals of the National Institutes of Health.

In PD and efficacy studies, SCID female mice were injected subcutaneously with 3×10^6 KU812 cells or 1×10^6 NCO2 cells in 5 mg/ml Matrigel (Corning) for tumor growth. After the tumors grew by an average volume of 150 mm^3, mice with similar size tumors were grouped and assigned to different experimental groups for experiments. In PD study, mice were treated as indicated in Results. At the indicated time points, mice were euthanized and blood and tissue samples were collected for analyses.

In toxicity studies, Balb/c female mice, mice were treated with AK-2292 or vehicle control (10% PEG400 + 90% PBS) as indicated in Results. Mouse body weights were measured every 2 to 3 days. At the end of experiments, mice were euthanized, and blood and organs were collected for analyses. The toxicity studies, including hematology and chemistry analyses, were performed by the University of Michigan Unit for Laboratory Animal Medicine *In Vivo* Animal Core.

In efficacy studies, drugs or vehicle control (10% PEG400 + 90% PBS) were administered at the dose schedules described in the Figures. Tumor sizes and animal weights were measured every 2 to 3 days. Tumor volume (mm^3) = (length×$width^2$)/2. Tumor growth inhibition (TGI) was calculated as TGI (%) = $(V_c-V_t)/(V_c-V_o) \times 100$, where V_c and V_t are the medians of the control and treated groups at the end of the study respectively, and V_o at the start of the study.

2.6.4 Molecular Modeling

All modeling was conducted using the software package MOE [77]. The crystal structure of STAT3 in complex with SD36 (PDB ID: 6NJS) was used as the template for the homology modeling. The complex structure was retrieved from the RCSB, imported into MOE, and prepared for modeling in a standard fashion. Briefly, bond orders for the ligand were corrected if necessary and crystallographic water molecules were removed. Since this structure is being used as a template for homology modeling, the three chain breaks present due to unresolved residues, and the N- and C-termini were not built in or capped. Missing sidechains were built in using MOE utilities. Hydrogen atoms were added, and the system parameterized with AMBER 10. All heavy atoms were fixed, and the positions of the hydrogen atoms allowed to relax using energy minimization. All constraints such as the fixed positions of the heavy atoms were turned off prior to using the structure as the homology modeling template.

Whole sequences for the human proteins STAT3 (P40736), STAT5A (P42229), STAT5B (P51692), and STAT6 (P42226) were downloaded from UniProtKB. STAT5A, STAT5B, and STAT6 sequences were separately aligned to the STAT3 sequence using the default settings in the UniProtKB alignment tools.

Each STAT sequence to be modeled was separately imported into MOE in FASTA format along with the prepared template structure for STAT3. In turn each STAT sequence to be modeled was aligned to the template sequence as obtained from the UniProtKB alignments. Residues which are not part of the SH2 domain were deleted [78]. Leading and ending residues without associated template structure were also deleted. MOE's homology modeling tool was used for the modeling with a maximum number of mainchain models set to 100 and a refinement level of 0.5 (fine). Models were scored and ranked with the GB/VI scoring function.

The SD36 ligand present in the STAT3 template structure was defined as an environment object. This allows the ligand to be present when generating the homology models and in the refinement steps to prevent clashes between the ligand and modeled protein with the goal of generating a more holo like binding site. Default settings were used for all other variables in the homology modeling tool.

Once completed, the overlap of the best ranked models with the STAT3 template were examined. The best ranked homology model for STAT5A and STAT6 and the second-best ranked homology model for STAT5B were chosen as the structures for further modeling. Structures for these homology models are provided in the supplemental materials in PDB format. They are named as: STAT5A_Homology_SH2.pdb, STAT5B_Homology_SH2.pdb, and STAT6_Homology_SH2.pdb.

The crystal structure of the STAT3 core in complex with compound SD36 (PDB id: 6NJS) and the generated homology models for STAT5A, STAT5B, and STAT6 were used to help guide the design of new inhibitors. As described in the creation of the homology models, the SD36 ligand was also present during the generation and refinement of the models which were saved as protein-ligand complexes. Potential inhibitors were designed by simple visualization of the complexes to

look for lipophilic regions and hydrogen bond donors and acceptors in the proteins that could be accessed by analogs of SD36.

Proposed analogs were then docked into the proteins for further visualization. Docking was conducted using MOE's template docking method with substructure matching. The SD36 ligand was used to define the binding site. The maximum common substructure between the SD36 and the ligand to be docked was used for the substructure matching. (To create larger common substructures for proposed analogs with a benzothiophene ring in place of the indole ring of SD36, the nitrogen atom of the indole ring was mutated to a sulfur atom.) This method takes conformations for the ligand to be docked and superimposes them into the protein binding site by aligning it to the substructure of the SD36 ligand. Once aligned, the SD36 ligand is removed, and additional conformational sampling is conducted by rotating bonds of the docked ligand. That sampling is followed by energy minimization of the docked ligand keeping the protein rigid to create a refined pose which is then scored for ranking.

Default settings for MOE were used except that sampling was increased by increasing the number of placements for refinement from 10 to 100 and the number of refined poses output from a max of 5 to 10. Also, the level of refinement was increased by changing the energy minimization termination criterion to a minimum value for the gradient and a maximum value for the number of iterations. Examples of several inhibitors docked to the homology models are presented in **Extended Data Fig. 1B.**

2.6.5 Expression and purification of STAT5A/STAT5B and other STAT proteins

The gene for human STAT5A corresponding to residues 136 – 705 was cloned into the pMCSG9 vector and expressed as a fusion protein bearing a cleavable N-terminal 6x-His-MBP tag in *Escherichia coli* Rosetta 2 (DE3) cells. The gene for human STAT5A, corresponding to

residues 138 – 710 was cloned similarly. Transformed cells were grown at 37 °C to an OD_{600} of 1.0 in Terrific Broth supplemented with 100 µg/mL ampicillin. Expression was induced by addition of isopropyl β-d-1-thiogalactopyranoside to a concentration of 0.4 mM and cells were incubated at 20 °C overnight then pelleted by centrifugation. The harvested pellet was frozen at -80 °C. Protein was purified from a thawed pellet resuspended in lysis buffer containing 25 mM HEPES pH 7.5, 150 mM NaCl, 10 mM $MgCl_2$, 10 µg/mL aprotinin, 1 µg/mL leupeptin, 0.1% β-mercaptoethanol, and ~200 U benzonase (Millipore-Sigma) and lysed by sonication. Insoluble debris was removed by centrifugation at 40000g for 35 min and the cleared lysate was incubated with 5 mL Ni-NTA Agarose (QIAGEN) for 1 h at 4 °C. Resin was washed with lysis buffer containing 10 mM imidazole, followed by wash buffer containing 25 mM HEPES pH 7.5 and 1 M NaCl. The protein was eluted in buffer containing 25 mM HEPES pH 7.5, 150 mM NaCl, and 300 mM imidazole. Eluate was dialyzed into buffer containing 25 mM HEPES pH 7.0, 150 mM NaCl, and 0.1% β-mercaptoethanol and cleaved with Tobacco Etch Virus protease overnight at 4 °C. Cleaved STAT5A was treated with additional Ni-NTA resin to remove the His-tag and then was further purified on a 5 mL HiTrap Heparin HP (GE Healthcare) column followed by size exclusion chromatography on a HiLoad 16/60 Superdex 200 column (GE Healthcare) in buffer containing 20 mM HEPES pH 7.0, 200 mM NaCl, and 5 mM DTT. Other STAT proteins, STAT1, STAT2, STAT3 and STAT4 proteins were prepared as previously described [37].

2.6.6 Crystallization and Structure Determination of STAT5A with Inhibitor or Degrader

AK-305 or AK2292 was added to concentrated STAT5A (7.2 mg/mL in 20 mM HEPES pH 7.0, 200 mM NaCl, and 5 mM DTT) in a 2:1 molar ratio and incubated at 4 °C for 2 h. The STAT5a-inhibitor complexes were crystallized by sitting drop vapor diffusion at 20 °C in a 2:1 protein to well drop ratio. The STAT5A-inhibitor complexes crystallized in the well solution

containing 0.9 – 1.0 M sodium malonate pH 7.0, 1% Jeffamine pH 7.0 and 5 – 10 % polyethylene glycol 400. Crystals were cryoprotected in well solution with 20% polyethylene glycol 400 and flash-cooled in liquid nitrogen prior to data collection. Diffraction data (Extended Data Fig. 1K) were collected on the Advanced Photon Source LS-CAT beamlines 21-ID-F (AK-305) and 21-ID-D (AK-2292) and processed in HKL2000 [79].

The structures of the complexes were solved by molecular replacement in Phaser[2] using a STAT5A structure previously developed in this lab as a search model. The structure of STAT5A: AK-305 was solved to 2.65 Å, in the R32 space group with 1 molecule in the asymmetric unit. The structure of STAT5A:AK2292 was solved to 2.85 Å in the R3 space group with 2 molecules in the asymmetric unit. Electron density corresponding to the inhibitors was observed in the phosphotyrosine binding site of STAT5A after molecular replacement (Extended Data Fig. 1L-A and 1L-B). Iterative model-building and refinement were performed in COOT [80] and BUSTER [81], respectively. Ligand restraints were generated in Grade [82]. All residues were found to be ordered in electron density maps with the exception of residues 136, 428–433, 701-705 in STAT5A:AK-305 and residues 136-137, 428–433, 700-705 in both chains of STAT5A:AK2292. Refinement statistics for the structures can be found in Extended Data Fig. 1K.

2.6.7 Fluorescence Polarization (FP) assay

FP experiments were performed in 96-well, black round-bottom plates (Microfluor 2, Fisher Scientific) using the CLARIOstar microplate reader (BMG Labtech). To each well, 5 nM of fluorescein-labeled tracer (AK2018330) and 200 nM of STAT5/6 protein were added to a final volume of 100 µl in the assay buffer (PBS pH 7.4 + 0.01%BGG + 0.01% Tween-20, 2 mM DTT). The plate was mixed on a shaker for 15 min and incubated at rt for 1 h to reach equilibrium. The polarization values in millipolarization (mP) units were measured at an

excitation wavelength of 485 nm and an emission wavelength of 530 nm. All experimental data were analyzed using Prism 8.0 software (GraphPad Software), and the inhibition constants were determined by nonlinear curve fitting as the concentration of the STAT5/6 at which 50% of the ligand is bound.

K_i values of competitive inhibitors were calculated based upon the measured IC_{50} values, the K_d values of the tracer to the protein, and the concentrations of the proteins and tracers in the competitive assays as described previously [83]. The same procedures were used with STAT1, STAT3, and STAT4 proteins. Tracer AK-1153FL was used for STAT1 (tracer concentration: 2 nM, protein concentration: 40 nM) and STAT4 (tracer concentration: 2 nM, protein concentration: 75 nM) (Extended Data Fig. 1H). The tracer for STAT3 was described previously [37].

2.6.8 Cereblon Binding Assay

The binding to cereblon (CRBN) was determined using the Cereblon Binding Kit (Cisbio, #64BDCRBNPEG) following the manufacturer's instruction. Briefly, serially diluted compounds were incubated with GST-tagged wild-type human CRBN protein, XL665-labelled Thalidomide and Europium Cryptate labelled GST antibody at room temperature for 2-3 hours. Time Resolved Fluorescence Resonance Energy Transfer (TR-FRET) measurements were acquired on a TECAN SPARK plate reader, with the following settings: 320 nm excitation; 665 nm and 620 nm emission, 100 μs delay and 400 μs integration. The TR-FRET ratio was taken as the 665/620 nm intensity ratio. The readings were normalized to the control (0.5% DMSO) and the IC_{50} was calculated by nonlinear regression (four parameters sigmoid fitted with variable slope) analysis using the GraphPad Prism 8 software. The K_i values of competitive inhibitors were calculated based upon

the measured IC_{50} values, the K_d values of the tracer to the protein, and the concentrations of the proteins and tracers in the competitive assays as described previously [83]

2.6.9 Cell Viability Assay

5 mM stock solutions in DMSO of AK-2292 and other compounds were diluted with cell culture medium. The prepared compound solution was added to 96-well Microplates (Corning cat 3610) in triplicate and serial 1/3 dilution was performed. Wells in one column were left with no compounds as control wells. The volume of each well at this point was set to 50 µl. Cell culture medium containing approximately 100,000 cells per ml was prepared in a reagent reservoir and 50 µl of the prepared cell containing medium was added to each well to seed approximately 5,000 cells per well. After 3-4 days in an incubator at 37 °C and 5% CO_2, the cell viability was measured by CellTiter-Glo (CTG) Luminescent Cell Viability Assay. 50 µl of CTG reagent (Promega cat G7573) was added to each well and the plate was gently vortexed for 5 minutes. The luminescence was recorded using plate reader. The average cell viability values were calculated by setting the average luminescence value in control wells at 100%.

2.6.10 Immunoblotting

About 1 million cells per each data point were treated with AK-2292 and other compounds at indicated concentrations and durations. Untreated and treated cells in cell culture medium were transferred into tubes, followed by centrifugation at 3,000 rpm and 4 ºC for 6 min. Supernatants were removed from the tubes and radioimmunoprecipitation assay (RIPA) lysis buffer supplemented with 1% protease inhibitor cocktail (Fisher Scientific cat. PI87786) and phosphatase inhibitor (Roche cat. 04906837001) were added to tubes containing the remaining cell pellets. The tubes were then left on ice for 30 min and put in a -80 ºC freezer. Afterwards

they were thawed out in 37 ºC water, centrifuged at 14,000 rpm for 15 min and the cell lysates were transferred to new tubes. The concentration of total proteins in each tube was calculated using the Pierce BCA protein Assay kit (cat. 23225). Based on the calculated protein concentration, cell lysates containing approximately the same amount of protein were transferred to new tubes, then distilled water and 4X Protein Sample Loading Buffer for Western Blots (LI-COR cat. 928-40004) supplemented with 20% of mercaptoethanol (Sigma Aldrich, M6250) were added on ice. The cell lysates were then reduced and denatured at 95 ºC for 5 min. From the tubes containing cell lysates an equal amount of protein samples (20-40 µg) was pipetted and loaded into precast 8%, 10%, 4%-12%, or 4%-20% Tris-glycine gels (Novex) filled with Tris-glycine SDS running buffer. After the proteins were resolved, they were transferred onto Immobile-FL PVDF Membrane (Millipore Sigma cat. IPFL00010), using Mini Trans-Blot Electrophoretic Transfer Cell (Bio-Rad 1703930). The membranes were blocked with Intercept Blocking Buffer (LI-COR cat. 927-70001) in LI-COR Western Blot boxes for 1 h at rt. The membranes were washed with 1X Tris-buffered saline-Tween-20 (TBST, 1X solution was made from 20X TBST solution, ThermoFisher Scientific cat. 28360) 4 times for 5 min each. The membranes were incubated overnight at 4 ºC in Intercept Blocking Buffer supplemented with primary antibodies (normally antibody:buffer 1:1000) and Tween-20. The membranes were washed with TBST 4 times for 5 min and were incubated with Intercept Blocking Buffer supplemented with IRDye 800CE Secondary Antibodies, IRDye 680RD Secondary Antibodies (LI-COR biosciences), Tween-20, and 10% SDS solution, for 1 h at rt. The membranes were then washed with TBST 4 times for 5 min then rinsed with deionized water before drying and scanning with Odyssey Dlx Amazing System (LI-COR). The immunoblots were finally quantified by the software.

2.6.11 Transcriptomic Profiling

Procedures of transcriptomic profiling are the same procedures described previously [37]. Total RNA was purified by RNeasy Mini Kit (Qiagen, #74104) following the manufacturer's instructions. RNA quality was checked using the TapeStation (Agilent). Samples with RINs (RNA Integrity Numbers) ≥8 were ribosomal RNA depleted by Ribo-Zero rRNA Removal Kit (Human/Mouse/Rat) (cat# MRZH11124, Illumina). The rRNA-depleted samples were then prepared by the TruSeq mRNA Sample Prep v2 kit (Catalog #s RS-122–2001, RS-122–2002, Illumina). The entire fraction of 0.1–3 μg of rRNA-depleted total RNA was fragmented and copied into first strand cDNA using reverse transcriptase and random primers. The 3 prime ends of the cDNA were then adenylated and adapters were ligated. One of the adapters that was ligated had a 6 nucleotide barcode that was unique for each sample and this allowed sequencing of more than one sample in each lane of a HiSeq flow cell (Illumina). The products were purified and enriched by PCR to create the final cDNA library. Final libraries were checked for quality and quantity by TapeStation (Agilent) and qPCR using Kapa's library quantification kit for Illumina Sequencing platforms (catalog # KK4835, Kapa Biosystems). They were clustered on the cBot (Illumina) and sequenced with 16 samples per lane in a 50 cycle single end High Output mode using version 4 reagents and HiSeq Control Software version 2.2.68 according to manufacturer's protocols. Demultiplexing and Fastq file generation was done using bcl2fastq version 2.17.1.14. RNA-seq data are deposited at Gene Expression Omnibus (GEO). Raw data were normalized into reads per kilobase per million (RPKM) values. Genes with the average RPKM values less than 1.00 were removed from the analysis. All the RPKM values were then added to one before the analysis to avoid singularity in the fold change calculations. The MultiplotPreprocess module from the GenePattern [84] website were used to calculate the

overall fold changes and the corresponding p-values in paired comparison. The data were plotted using the R program.

GSEA was performed using the GSEA program [85] and the Molecular Signature Database (v6.1) [86, 87] (http://www.broad.mit.edu/gsea/) using the GSEA preranked function. Differential expression of SD-36 versus DMSO treatment was used to generate the ranked list file. In the analysis, 1000 permutations were applied to determine the significance of the enrichment for the gene sets.

2.6.12 Proteomic Profiling

Procedures of proteomic profiling are the procedures described previously [37]. Cultured cell lines and xenograft tumors samples were lysed in RIPA buffer (Sigma, #R0278). Cell lysis samples (75 μg/condition) were proteolysed and labeled with TMT 10-plex Isobaric Label Reagent (Thermo Fisher Scientific, #90110) essentially following manufacturer's protocol. Briefly, upon reduction and alkylation of cysteines, the proteins were precipitated by adding 6 volumes of ice-cold acetone followed by overnight incubation at -20° C. The precipitate was spun down, and the pellet was allowed to air dry. The pellet was resuspended in 0.1M TEAB and digested overnight with trypsin (1:50; enzyme:protein) at 37 °C with constant mixing using a thermomixer. The TMT 10-plex reagents were dissolved in 41 μl of anhydrous CH_3CN and labeling was performed by transferring the entire digest to the TMT reagent vial and incubating it at rt for 1 h. Reaction was quenched by adding 8 μl of 5% hydroxylamine and further 15 min incubation. Labeled samples were mixed together, and dried using a vacufuge. An offline fractionation of the combined sample (~200 μg) into 10 fractions was performed using high pH reversed-phase peptide fractionation kit according to the manufacturer's protocol (Pierce; Cat

#84868). Fractions were dried and reconstituted in 12 µl of 0.1% formic acid/2% acetonitrile in preparation for LC-MS/MS analysis.

In order to obtain high accuracy in quantitation, we employed multinotch-MS3 [88] which minimizes the reporter ion ratio distortion resulting from fragmentation of co-isolated peptides during MS analysis. Orbitrap Fusion (Thermo Fisher Scientific) and RSLC Ultimate 3000 nano-UPLC (Dionex) was used to acquire the data. The sample (2 µl) was resolved on a PepMap RSLC C18 column (75 µm i.d. × 50 cm; Thermo Fisher Scientific) at the flow-rate of 300 nl/min using 0.1% HCOOH/CH_3CN gradient system (2–22% CH_3CN in 150 min; 22–32% CH_3CN in 40 min; 20 min wash at 90% followed by 50 min re-equilibration) and direct spray into the mass spectrometer using EasySpray source (Thermo Fisher Scientific). The mass spectrometer was set to collect one MS1 scan (Orbitrap; 60K resolution; AGC target 2×10^5; max IT 100 ms) followed by data-dependent, "Top Speed" (3 sec) MS2 scans (collision induced dissociation; ion trap; NCD 35; AGC 5×10^3; max IT 100 ms). For multinotch-MS3, top 10 precursors from each MS2 were fragmented by HCD followed by Orbitrap analysis (NCE 55; 60K resolution; AGC 5×10^4; max IT 120 ms, 100–500 m/z scan range).

Proteome Discoverer (v2.1; Thermo Fisher Scientific) was used for data analysis. MS2 spectra were searched against SwissProt human protein database (release 2015–11-11; 42084 sequences) using the following search parameters: MS1 and MS2 tolerances were set to 10 ppm and 0.6 Da, respectively; carbamidomethylation of cysteines (57.02146 Da) and TMT labeling of lysine and N-termini of peptides (229.16293 Da) were considered static modifications; oxidation of methionine (15.9949 Da) and deamidation of asparagine and glutamine (0.98401 Da) were considered variable. Identified proteins and peptides were filtered to retain only those that passed

≤1% FDR threshold. Quantitation was performed using high-quality MS3 spectra (Average signal-to-noise ratio of 20 and <30% isolation interference).

2.6.13 Statistical Analysis

For tumor growth kinetics, data are presented as mean ± SEM. For concentration-response cell viability, data were plotted as mean ± SD and fitted to a sigmoidal curve by nonlinear regression. Differences in mean values between groups were analyzed by two-sided Student's *t* test. All statistical analyses were performed using GraphPad Prism 7.

2.7 Chemistry

2.7.1 General Information

Unless otherwise indicated, all purchased reagents were used as received without further purification. ^{1}H NMR and ^{13}C NMR spectra were measured on a Bruker Advance 400 MHz spectrometer. ^{1}H NMR spectra were described in parts per million (ppm) downfield from tetramethylsilane (TMS). All ^{13}C NMR spectra were given in ppm and were obtained with ^{1}H decoupling. In reported spectral data, the format (δ) chemical shift (multiplicity, J values in Hz, integration) was used with the following abbreviations: s = singlet, d = doublet, t = triplet, q = quartet, m = multiplet. Mass spectral (MS) analysis was performed with a Waters UPLC mass spectrometer. Flash column chromatography was performed using silica gel (type H) from TM Chemicals, Inc. The final compounds were purified by C18 reverse phase preparative HPLC column with solvent A (0.1% TFA in H_2O) and solvent B (0.1% TFA in CH_3CN) as eluents. The purity of all the final compounds was confirmed to be >95% by UPLC−MS or UPLC.

2.7.2 Synthesis

Synthesis of 5-(Difluoro(phosphono)methyl)benzo[b]thiophene-2-carboxylic acid (39)

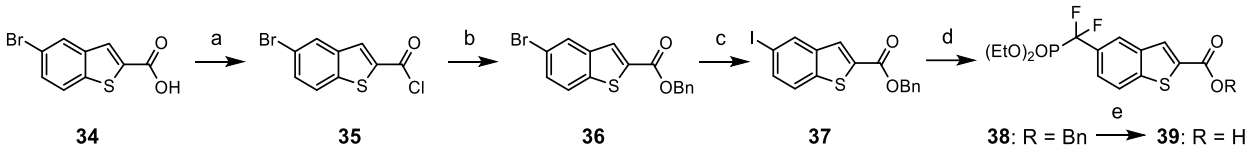

Figure 2-1 Synthesis of 5-(Difluoro(phosphono)methyl)benzo[b]thiophene-2-carboxylic acid (39)

Reaction conditions: (a) Oxalyl Chloride, DMF, DCM, 0 °C to rt; (b) BnOH, TEA, DCM, rt; (c) CuI, KI, Dioxane, DMEDA, 110 °C, sealed; (d) $BrCdCF_2PO_3Et_2$, CuI, DMF, rt; (e) Pd/C, H_2, MeOH, rt

The procedures for the preparation of **39** have also been described in our STAT3 degrader patent [72]. 5-Bromobenzo[b]thiophene-2-carboxylic acid **34** (1.0 g, 3.9 mmol, 1.0 equiv) and anhydrous DCM (50 mL) were added to a 100 mL round bottom flask equipped with a magnetic stirring bar . The suspension was cooled with ice/water bath before addition of oxalyl chloride (1.5 g, 11.7 mmol, 3.0 equiv) and DMF (0.3 mL). The solution was stirred at the same temperature for 30 min then returned to room temperature (rt). The suspension became a clear solution after 1.5 h. All of the solvent and excess oxalyl chloride was removed in vacuum. The residual crude product (**35**) was used directly for the next step without further purification.

The previously prepared crude acyl chloride (**35**) and anhydrous DCM (50 mL) were added to a 100 mL round bottom flask equipped with a magnetic stirring bar . The solution was cooled in an ice water bath before adding benzyl alcohol (0.8 g, 0.8 mL, 7.8 mmol, 2.0 equiv) and triethylamine (1.2 g, 1.6 mL, 11.7 mmol, 3.0 equiv). The solution was returned to rt and stirred for 1 h before being quenched with ammonium chloride aqueous solution. The reaction was extracted with DCM (50 mL x 3), dried with anhydrous sodium sulfate, filtered and concentrated under vacuum. The residual crude product was purified by flash column chromatography (PE:EA = 10:1) to afford the desired benzylic ester (**36**) as a white solid (1.1 g, 85% yield).

A 50 mL sealed bottle equipped with a magnetic stirring bar was filled with argon before adding benzyl 5-bromobenzo[b]thiophene-2-carboxylate (**36**) (1.0 g, 2.9 mmol, 1.0 equiv), CuI (110 mg, 0.58 mmol, 0.2 equiv), KI (1.0 g, 5.8 mmol, 2.0 equiv), N,N'-dimethylethane-1,2-diamine (51 mg, 62 L, 0.58 mmol, 0.2 equiv) and anhydrous 1,4-dioxane (20 mL). The reaction atmosphere was changed to argon another three times before the reaction at 110 °C for 24 h. The reaction system was cooled to rt and quenched with ammonium chloride aqueous solution. The reaction mixture was extracted with EtOAc (50 mL x 3), washed with brine, dried with anhydrous sodium sulfate, then filtered and concentrated under vacuum. The residual crude product was purified by flash column chromatography (PE:EA = 10:1) to afford a mixture of the desired iodide (**4**) and the starting material (**3**) as a white solid (0.85 g, 4:3 = 3:1 monitored by LC-MS). This mixture can be used directly for the next step without further purification.

A 100 mL round bottom bottle equipped with a magnetic stirring bar was filled with argon before adding anhydrous DMF (50 mL), cadmium powder (2.7 g), and diethyl (bromodifluoromethyl)phosphonate (3.3 g). The mixture was stirred overnight (cadmium reagent DMF solution A) and stopped stirring to let all the insoluble matter fall to the bottom of the bottle. A 50 mL round bottom bottle equipped with a magnetic stirring bar was filled with argon before adding the previously prepared mixture of **37** and **36** (0.85 g, 4:3 = 3:1, 2.1 mmol, 1.0 equiv), CuI (0.8 g, 4.2 m mol, 2.0 equiv) and cadmium reagent DMF solution A (13 mL, 0.33M, 4.2 mmol, 2.0 equiv). The atmosphere of the reaction system was changed to argon another three times before stirring at rt for 24 h. The reaction mixture was quenched with ammonium chloride aqueous solution, extracted with EtOAc (50 mL x 3), washed with brine for three times, dried with anhydrous sodium sulfate, filtered, and concentrated under vacuum. The residual crude

product was purified by flash column chromatography (PE:EA = 1:1) to generate the desired phosphate (**38**) as a colorless oil (0.5 g, 70% yield).

Benzyl 5-((diethoxyphosphoryl)difluoromethyl) benzo[b]thiophene-2-carboxylate (**38**) (130 mg, 0.28 mmol, 1.0 equiv), MeOH (5 mL) and 10% Pd/C (150 mg) were added to a 50 mL round bottom bottle equipped with a magnetic stirring bar and filled with argon. The reaction system atmosphere was changed to hydrogen three times before stirring at rt for 5 min (a longer reaction time can reduce the yield of this reaction). The reaction mixture was filtered to remove Pd/C and the solvent was removed under vacuum. The residual crude product was purified by HPLC (MeCN/H_2O 35%-100%, 65min, 60 mL/min, the product started coming out when MeCN was 46%) to afford the desired carboxylic acid (**39**) as a white solid (43 mg, 42% yield). NMR (400 MHz, CD_3OD) δ 8.20 (s, 1H), 8.17 (s, 1H), 8.09 (d, = 8.4 Hz, 1H), 7.67 (d, = 8.4 Hz, 1H), 4.29-4.17 (m, 4H), 1.31 (td, = 7.1, 0.7 Hz, 6H). UPLC-MS calculated for $C_{14}H_{16}F_2O_5PS^+$ 365.03, found $[M + H]^+$ 365.24.

((2-(((S)-1-((S)-2-((3-(Dimethylamino)-3-oxopropyl)(4-(thiazol-2-yl)phenyl)carbamoyl)-pyrrolidin-1-yl)-3,3-dimethyl-1-oxobutan-2-yl)carbamoyl)benzo[b]thiophen-5-yl)difluoro-methyl)phosphonic acid (AK305)

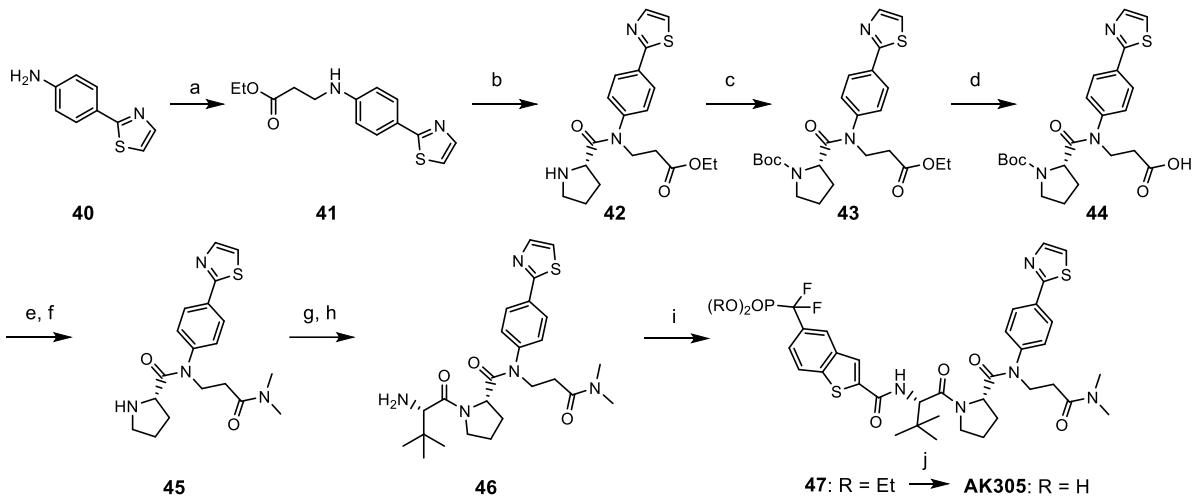

Figure 2-2 Synthesis of ((2-(((S)-1-((S)-2-((3-(Dimethylamino)-3-oxopropyl)(4-(thiazol-2-yl)phenyl)carbamoyl)-pyrrolidin-1-yl)-3,3-dimethyl-1-oxobutan-2-yl)carbamoyl)benzo[b]thiophen-5-yl)difluoro-methyl)phosphonic acid (AK305)

Reaction conditions: (a) Ethyl acrylate, AcOH, 90 °C; (b) PCl_5, $CHCl_3$, 50 °C; (c) Boc_2O, TEA, CH_3CN, rt; (d) LiOH, MeOH, water, rt; (e) HATU, DIPEA, DMF, rt; (f) TFA, DCM, rt; (g) HATU, DIPEA, DMF, rt; (h) TFA, DCM, rt; (i) HATU, DIPEA, DMF, rt; (j) TMSI, BSTFA, DCM, rt, 0 °C

4-(Thiazol-2-yl)aniline **40** (2.5 g, 14.2 mmol), AcOH (8 ml), and ethylacrylate (1.3 ml, 0.9 equiv.) were added to a round bottom flask equipped with a magnetic stirring bar . The suspension was stirred at 90 °C for 5 h. The reaction mixture was cooled to rt and the solvent was removed on a rotary evaporator. The residual crude product was purified by flash column chromatography to yield **41** in 52% yield (2.0 g). ^{1}H NMR (400 MHz, DMSO) δ 7.79 (d, *J* = 3.4 Hz, 1H), 7.70 (d, *J* = 8.7 Hz, 2H), 7.56 (d, *J* = 3.4 Hz, 1H), 7.32 (s, 1H), 6.66 (d, *J* = 8.7 Hz, 2H), 4.08 (q, *J* = 7.1 Hz, 2H), 3.35 (t, *J* = 6.7 Hz, 2H), 2.59 (t, *J* = 6.7 Hz, 2H), 1.18 (t, *J* = 7.1 Hz, 3H). ^{13}C NMR (400 MHz, DMSO) δ 171.46, 168.52, 150.44, 142.03, 127.77, 120.35, 117.74, 112.06, 60.00, 38.43, 33.51, 14.07. ESI−MS calculated for $C_9H_8N_2S^+$ 276.35, found $[M + H]^+$ 276.89.

Boc-L-proline (5.8 g, 5 equiv.) was dissolved in $CHCl_3$ (50 ml). PCl_5 (5.6 g, 5 equiv.) was slowly added at rt over a period of 10 min. After the addition, the mixture was stirred for 10 min at rt. The thazole (**41**) (1.5 g, 5.4 mmol) was added to this mixture which was then stirred at 50°C for 20 min. The volatile components were removed on a rotary evaporator. The obtained crude oil was purified by reverse phase semi-preparative HPLC. The resulting colorless oil (**42**) was dissolved in CH_3CN (20 ml). To the solution was added triethylamine (3 ml, 3.8 equiv.), followed by Boc_2O (1.75 g, 1.5 equiv.). The colorless mixture was stirred for 2 h at rt. The volatile components were then removed in vacuum and the crude was purified by flash column chromatography to yield **43** in 39% (1.0 g, 2 steps yield). ^{1}H NMR (400 MHz, DMSO) δ 8.05 (d, *J* = 8.5 Hz, 2H), 7.94 (d, *J* = 3.3 Hz, 1H), 7.77 (d, *J* = 3.3 Hz, 1H), 7.58 – 7.08 (m, 2H), 4.12 (m, 1H), 4.10 – 3.75 (m, 4H), 3.43 – 3.23 (m, 2H), 2.55 (m, 2H), 1.86 (s, 3H), 1.70 (m, 1H), 1.42 (s, 9H), 1.14 (t, *J* = 7.1 Hz, 3H). ^{13}C NMR (400 MHz, DMSO) δ 171.34, 170.35, 165.75, 153.27, 143.64, 132.39, 128.88, 127.10, 120.49, 77.07, 59.61, 56.69, 46.48, 44.92, 32.39, 30.55, 29.63, 27.93, 22.42, 13.52. ESI−MS calculated for $C_{24}H_{31}N_3O_5S^+$ 473.59, found $[M + H]^+$ 374.06.
43 (450 mg, 0.95 mmol) was dissolved in MeOH (5 ml) and H_2O (1 ml) and the mixture was placed in an ice bath. LiOH monohydrate (200 mg, 5 equiv.) was added to the mixture and then it was stirred for 30 min at rt. The mixture was placed in an ice bath again and neutralized by slowly adding TFA. The volatile components were removed on a rotary evaporator and the residue was purified by flash column chromatography to yield **44** in 73% (310 mg). ^{1}H NMR (400 MHz, DMSO) δ 12.00 (s, 1H), 8.05 (d, *J* = 8.0 Hz, 3H), 7.95 (d, *J* = 3.3 Hz, 1H), 7.78 (d, *J* = 3.3 Hz, 1H), 7.44 (s, 2H), 4.11 (m, 1H), 3.99 – 3.69 (m, 2H), 3.39 – 3.26 (m, 2H), 3.13 (s, 2H), 1.85 (m, 4H). ^{13}C NMR (400 MHz, DMSO) δ 171.78, 171.30, 165.79, 143.65, 132.34, 128.87,

127.10, 120.47, 78.39, 56.69, 46.50, 45.01, 32.31, 30.56, 29.38, 27.96, 23.04, 22.57. ESI−MS calculated for $C_{22}H_{77}N_3O_5S^+$ 445.53, found $[M + H]^+$ 346.20.

HATU (140 mg, 0.37 mmol, 1.1 equiv.) was added to a solution of **44** (150 mg, 0.33 mmol, 1 equiv.), Me_2NH (330 µl, 0.67 mmol, 2 equiv.) in 2M THF solution, and Et_3N (0.23 ml, 1.65 mmol, 5 equiv.) in CH_3CN (5 ml). The mixture was stirred at rt for 30 min. The yellow solution was concentrated in vacuum and the crude was purified by flash column chromatography to yield Boc-protected **45**. Boc protection was removed by DCM/TFA at rt for 30 min. The volatile components were removed in vacuum to yield **45** as a TFA salt in 80% (128 mg). ^{1}H NMR (400 MHz, $CDCl_3$) δ 8.11 – 8.03 (m, 2H), 7.75 – 7.71 (m, 1H), 7.59 (d, *J* = 3.2 Hz, 1H), 7.45 (d, *J* = 7.9 Hz, 2H), 4.42 – 4.38 (m, 1H), 4.28 – 4.24 (m, 1H), 3.89 (d, *J* = 6.6 Hz, 1H), 3.46 – 3.42 (m, 2H), 3.02 (s, 3H), 2.91 (s, 3H), 2.75 (d, *J* = 7.5 Hz, 1H), 2.69 – 2.50 (m, 1H), 2.02 – 1.96 (m, 1H), 1.93 – 1.85 (m, 3H). ESI−MS calculated for $C_{19}H_{24}N_4O_2S^+$ 372.49, found $[M + H]^+$ 372.99. CH_3CN (5 ml), Et_3N (0.18 ml, 2.5 mmol, 5 equiv.), Boc-L-*tert*-leucine (90 mg, 0.39 mmol, 1.5 equiv.) and HATU (118 mg, 0.31 mmol, 1.2 equiv.) were added to **45** (128 mg, 0.26 mmol) and the mixture was stirred at rt for 30 min. The yellow solution was concentrated in vacuum and the crude was purified by flash column chromatography to yield Boc-protected **46**. Boc protection was removed by DCM/TFA at rt for 30 min. The volatile components were removed in vacuum to yield **46** as a TFA salt in 85% (107 mg). ^{1}H NMR (400 MHz, MeOD) δ 8.00 (d, *J* = 8.2 Hz, 2H), 7.90 (d, *J* = 3.3 Hz, 1H), 7.64 (d, *J* = 3.3 Hz, 1H), 7.57 (d, *J* = 8.1 Hz, 2H), 4.33 (t, *J* = 7.7 Hz, 1H), 3.96 – 3.90 (m, 3H), 3.75 – 3.68 (m=, 1H), 3.60 – 3.55 (m, 1H), 3.00 (s, 3H), 2.83 (s, 3H), 2.69 (t, *J* = 7.4 Hz, 2H), 2.10 – 1.80 (m, 3H), 1.80 – 1.60 (m, 1H), 1.13 (s, 9H). ESI−MS calculated for $C_{25}H_{35}N_5O_3S^+$ 485.65, found $[M + H]^+$ 486.21.

CH_3CN (5 ml), Et_3N (0.15 ml, 1.1 mmol, 5 equiv.), benzothiophene **39** (97 mg, 0.26 mmol, 1.2 equiv.), and HATU (100 mg, 0.26 mmol, 1.2 equiv.) were added to **46** (107 mg, 0.22 mmol),. The mixture was stirred at rt for 30 min. The yellow solution was concentrated in vacuum and the crude was purified by flash column chromatography to yield **47** in 68% yield (147 mg). ^{1}H NMR (400 MHz, $CDCl_3$) δ 8.09 (s, 1H), 8.00 (d, *J* = 1.4 Hz, 1H), 7.98 (d, *J* = 1.5 Hz, 1H), 7.94 – 7.88 (m, 3H), 7.66 – 7.60 (m, 1H), 7.51 – 7.44 (m, 2H), 7.38 (d, *J* = 3.3 Hz, 1H), 7.24 (d, *J* = 9.4 Hz, 1H), 4.92 (d, *J* = 9.4 Hz, 1H), 4.35 (t, *J* = 7.6 Hz, 1H), 4.25 – 4.13 (m, 5H), 4.04 – 3.93 (m, 1H), 3.91 – 3.70 (m, 2H), 3.07 (s, 3H), 2.92 (s, 3H), 2.85 – 2.70 (m, 2H), 2.12 – 2.08 (m, 1H), 1.98 – 1.87 (m, 2H), 1.87 – 1.74 (m, 1H), 1.34 – 1.30 (m, 6H), 1.17 (s, 9H). ESI−MS calculated for $C_{39}H_{48}F_2N_5O_7PS_2^+$ 831.93, found $[M + H]^+$ 832.12.

47 (150 mg, 0.17 mmol, 1 equiv.), DCM (2 ml) and $CF_3CON(TMS)_2$ (0.27 ml, 1.0 mmol, 6 equiv.) were added to a round bottom flask. The solution was cooled in an ice bath. 1M of TMS-I in DCM (0.9 ml, 0.9 mmol, 5 equiv.) was added dropwise to the ice cooled reaction mixture, and the mixture was stirred for 10 min in an ice bath. The volatile components were removed under vacuum at below 5 °C. The residue was dissolved in a mixed solvent of CH_3CN (3 ml) and water (1 ml). The resulting solution was purified by HPLC to yield AK-305 in 80% (150 mg). ^{1}H NMR (400 MHz, DMSO) δ 8.54 (s, 1H), 8.43 (d, *J* = 9.0 Hz, 1H), 8.11 (m, 1H), 8.06 – 7.95 (m, 3H), 7.92 (m, *J* = 3.2 Hz, 1H), 7.79 (d, *J* = 3.2 Hz, 1H), 7.55 (m, 2H), 4.77 (d, *J* = 9.0 Hz, 1H), 4.19 (m, 1H), 3.93 – 3.70 (m, 3H), 3.70 – 3.57 (m, 1H), 2.94 (m, 4H), 2.77 (m, 4H), 2.66 – 2.53 (m, 2H), 2.06 – 1.92 (m, 1H), 1.85 (m, 3H), 1.10 (s, 9H). ESI−MS calculated for $C_{30}H_{40}F_2N_5O_7PS_2^+$ 775.82, found $[M + H]^+$ 775.89.

((4-((E)-4-(((S)-3,3-Dimethyl-1-oxo-1-((S)-2-(1,2,3,4-tetrahydroquinoline-1-carbonyl)-pyrrolidin-1-yl)butan-2-yl)amino)-4-oxobut-2-en-2-yl)phenyl)difluoromethyl)phosphonic acid (1).

Similar synthetic methods have been previously reported [70]. ^{1}H NMR (400 MHz, DMSO) δ 10.34 (s, 1H), 8.05 (d, J = 9.1 Hz, 1H), 7.65 – 7.51 (m, 4H), 7.16 (m, 3H), 6.57 (s, 1H), 4.78 (m, 1H), 4.62 (d, J = 9.0 Hz, 1H), 4.05 – 3.76 (m, 2H), 3.76 – 3.61 (m, 1H), 3.46 (m, 1H), 2.75 (m, 2H), 2.47 (s, 3H), 2.28 – 1.98 (m, 3H), 1.89 (m, 5H), 1.00 (s, 9H). ^{13}C NMR (400 MHz, DMSO) δ 171.83, 169.11, 165.72, 158.54, 158.17, 147.67, 144.06, 139.15, 133.93, 128.63, 126.30, 126.24, 126.17, 125.87, 124.60, 121.30, 119.86, 117.83, 56.96, 56.23, 48.12, 35.07, 29.38, 26.50, 26.02, 24.98, 23.38, 16.52. ESI−MS calculated for $C_{31}H_{38}F_2N_3O_9PS^+$ 617.63, found $[M + H]^+$ 617.98.

((2-(((S)-3,3-Dimethyl-1-oxo-1-((S)-2-(1,2,3,4-tetrahydroquinoline-1-carbonyl)pyrrolidin-1-yl)butan-2-yl)carbamoyl)benzo[b]thiophen-5-yl)difluoromethyl)phosphonic acid (2).

Compound **2** was synthesized using a procedure similar to that used for AK-305. ^{1}H NMR (400 MHz, DMSO) δ 8.53 (s, 1H), 8.39 (d, *J* = 8.9 Hz, 1H), 8.12 (d, *J* = 8.5 Hz, 1H), 8.04 (s, 1H), 7.58 (m, 1H), 7.22 – 7.04 (m, 3H), 5.14 – 4.43 (m, 3H), 4.00 – 3.76 (m, 2H), 3.76 – 3.62 (m, 1H), 3.50 (m, 1H), 2.88 – 2.56 (m, 2H), 2.50 (s, 1H), 2.05 (m, 2H), 1.88 (m, 4H), 1.07 (s, 9H). ^{13}C NMR (400 MHz, DMSO) δ 171.74, 168.48, 161.49, 141.89, 140.38, 139.02, 138.76, 131.17, 130.95, 130.83, 130.61, 128.62, 126.11, 125.86, 125.22, 124.55, 123.71, 123.64, 122.93, 122.79, 57.42, 57.07, 48.19, 35.36, 29.34, 26.56, 26.01, 24.95, 23.39. ESI−MS calculated for $C_{30}H_{34}F_2N_3O_6PS^+$ 633.65, found $[M + H]^+$ 634.01.

((2-(((S)-3,3-Dimethyl-1-oxo-1-((S)-2-(phenylcarbamoyl)pyrrolidin-1-yl)butan-2-yl)carbamoyl)benzo[b]thiophen-5-yl)difluoromethyl)phosphonic acid (3).

Compound **3** was synthesized using a procedure similar to that used for AK-305. ^{1}H NMR (400 MHz, DMSO) δ 10.03 (s, 1H), 8.53 (s, 1H), 8.35 (d, *J* = 8.7 Hz, 1H), 8.14 (d, *J* = 8.6 Hz, 1H), 8.05 (s, 1H), 7.64 – 7.52 (m, 3H), 7.38 – 7.24 (m, 2H), 7.11 – 6.96 (m, 1H), 4.77 (d, *J* = 8.7 Hz, 1H), 4.49 (dd, *J* = 8.1, 5.3 Hz, 1H), 3.90 – 3.85 (m, 1H), 3.76 – 3.70 (m, 1H), 2.23 – 2.16 (m, 1H), 2.06 – 2.00 (m, 1H), 1.98 – 1.82 (m, 2H), 1.09 (s, 9H). ESI−MS calculated for $C_{27}H_{30}F_2N_3O_6PS^+$ 593.58, found $[M + H]^+$ 594.12.

((2-(((S)-3,3-Dimethyl-1-((S)-2-(methyl(phenyl)carbamoyl)pyrrolidin-1-yl)-1-oxobutan-2-yl)carbamoyl)benzo[b]thiophen-5-yl)difluoromethyl)phosphonic acid (4).

Compound **4** was synthesized using a procedure similar to that used for AK-305. ^{1}H NMR (400 MHz, DMSO) δ 11.51 (s, 1H), 8.53 (s, 1H), 8.39 (d, *J* = 8.9 Hz, 1H), 8.19 – 7.94 (m, 2H), 7.62 – 7.54 (m, 1H), 7.46 – 7.32 (m, 4H), 4.76 (d, *J* = 8.9 Hz, 1H), 4.23 (s, 1H), 3.85 – 3.71 (m, 1H), 3.71 – 3.47 (m, 1H), 3.16 (s, 3H), 2.15 – 1.87 (m, 2H), 1.76 (d, *J* = 5.5 Hz, 3H), 1.09 (s, 9H). ^{13}C NMR (400 MHz, DMSO) δ 171.11, 168.45, 161.47, 143.39, 141.93, 140.46, 138.81, 129.67, 127.75, 127.61, 126.11, 125.97, 123.76, 122.83, 57.47, 57.11, 48.19, 37.18, 36.07, 35.42, 29.11, 26.63, 26.20, 24.79. ESI−MS calculated for $C_{28}H_{32}F_2N_3O_6PS^+$ 607.61, found $[M + H]^+$ 607.96.

((2-(((S)-1-((S)-2-((4-Bromophenyl)(3-(dimethylamino)-3-oxopropyl)carbamoyl)pyrrolidin-1-yl)-3,3-dimethyl-1-oxobutan-2-yl)carbamoyl)benzo[b]thiophen-5-yl)difluoromethyl)-phosphonic acid (5).

Compound **5** was synthesized by a procedure similar to that used for **AK305**. ^{1}H NMR (400 MHz, DMSO) δ 8.54 (s, 1H), 8.41 (d, *J* = 8.9 Hz, 1H), 8.12 (d, *J* = 8.2 Hz, 1H), 8.04 (s, 1H), 7.66 – 7.54 (m, 3H), 7.44 – 7.32 (m, 2H), 4.75 (d, *J* = 9.0 Hz, 1H), 4.15 – 4.10 (m, 1H), 3.84 – 3.57 (m, 4H), 2.93 (s, 3H), 2.77 (s, 3H), 2.60 – 2.50 (m, 2H), 2.03 – 1.92 (m, 1H), 1.87 – 1.62

(m, 3H), 1.08 (s, 9H). ESI−MS calculated for $C_{32}H_{38}BrF_2N_4O_7PS^+$ 771.61, found $[M + H]^+$ 771.00, 772.93.

((2-(((S)-3,3-dimethyl-1-oxo-1-((S)-2-(1,2,3,4-tetrahydroisoquinoline-2-carbonyl)-pyrrolidin-1-yl)butan-2-yl)carbamoyl)-1H-inden-5-yl)difluoromethyl)phosphonic acid (9)

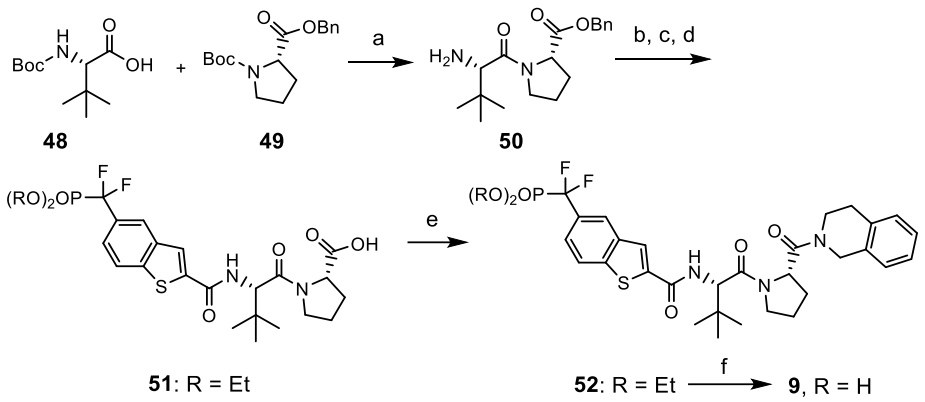

Figure 2-3 Synthesis of ((2-(((S)-3,3-dimethyl-1-oxo-1-((S)-2-(1,2,3,4-tetrahydroisoquinoline-2-carbonyl)-pyrrolidin-1-yl)butan-2-yl)carbamoyl)-1H-inden-5-yl)difluoromethyl)phosphonic acid (9)

Reaction conditions: (a) HATU, DIPEA, DMF, rt; (b) TFA, DCM, rt; (c) HATU, TEA, DMF, rt; (d) Pd/C, H_2, EtOH, rt; (e) HATU, DIPEA, DMF, rt; (f) TMSI, BSTFA, DCM, 0 °C.

CH_3CN (10 ml), Et3N (0.74 ml, 1.5 equiv.) and HATU (1.5 g, 1.2 equiv.) were added to **48** (840 mg, 3.6 mmol) and **49** (740 mg, 3.6 mmol),. The mixture was stirred at rt for 30 min. The yellow solution was concentrated in vacuum and the crude was purified by flash column chromatography to yield Boc-protected **9**. Boc protection was removed by DCM/TFA at rt for 30 min. The volatile components were removed in vacuum to yield **50** as a TFA salt in 80% (1.2 g). CH_3CN (10 ml), Et_3N (2 ml, 5 equiv.), benzothiophene **39** (1 g, 3.1 mmol, 1.1 equiv.), and HATU (1.3 g, 1.2 equiv.) were added to compound **50 (**1.2 g**)**. The mixture was stirred at rt for 30 min. The yellow solution was concentrated in vacuum and the crude was purified by flash column chromatography. The obtained compound was treated with 10% Pd/C and hydrogen in EtOH (10 ml) at rt for 1 h, followed by the filtration and concentration, to yield **51** in 75% (1.2

g) over 2 steps. ^{1}H NMR (400 MHz, DMSO) δ 12.44 (s, 1H), 8.63 – 8.36 (m, 2H), 8.21 (d, *J* = 8.6 Hz, 1H), 8.11 (d, *J* = 1.7 Hz, 1H), 7.63 – 7.57 (m1H), 4.77 (d, *J* = 8.9 Hz, 1H), 4.30 – 4.25 (m, 1H), 4.18 – 4.05 (m, 4H), 4.00 – 3.85 (m, 1H), 3.73 – 3.66 (m, 1H), 2.25 – 2.11 (m, 1H), 2.01 – 1.76 (m, 3H), 1.25 – 1.15 (m, 6H), 1.08 (s, 9H). ESI−MS calculated for $C_{25}H_{33}F_2N_2O_7PS^+$ 574.58, found $[M + H]^+$ 575.51.

CH_3CN (1 ml), DIPEA (20 µl, 3 equiv.), 1,2,3,4-tetrahydroisoquinoline (10 µg, 1.5 equiv.), and HATU (15 mg, 1.1 equiv.) were added to **51** (20 mg, 0.035 mmol). The mixture was stirred at rt for 30 min. The yellow solution was purified by HPLC to yield **52** in 85% (20 mg). ^{1}H NMR (400 MHz, DMSO) δ 8.53 – 8.50 (m, 1H), 8.44 – 8.32 (m, 1H), 8.21 (d, *J* = 8.6 Hz, 1H), 8.10 (s, 1H), 7.62 – 7.58 (m, 1H), 7.20 – 7.15 (m, 4H), 5.03 – 4.87 (m, 1H), 4.84 – 4.66 (m, 2H), 4.20 – 4.05 (m, 5H), 3.95 – 3.85 (m, 2H), 3.72 – 3.62 (m, 3H), 3.00 – 2.93 (m, 1H), 2.89 – 2.71 (m, 1H), 2.33 – 2.13 (m, 1H), 2.02 – 1.83 (m, 2H), 1.82 – 1.55 (m, 1H), 1.25 – 1.15 (m, 6H), 1.07 (s, 9H). ESI−MS calculated for $C_{34}H_{42}F_2N_3O_6PS^+$ 689.76, found $[M + H]^+$ 690.12.

52 (15 mg, 0.02 mmol, 1 equiv.), DCM (2 ml) and $CF_3CON(TMS)_2$ (32 µl, 6 equiv.) were added to a round bottom flask. The solution was cooled in an ice bath. To the ice cooled reaction mixture, 1M of TMS-I in DCM (0.1 ml, 5 equiv.) was added dropwise and the mixture was stirred for 10 min in an ice bath. The volatile components were removed under vacuum at <5° C. The residue was dissolved in a mixed solvent of CH_3CN (3 ml) and H_2O (1 ml). The resulting solution was purified by HPLC to yield **9** in 83% (11 mg). ^{1}H NMR (400 MHz, DMSO) δ 8.51 (d, *J* = 4.3 Hz, 1H), 8.34 – 8.24 (m, 1H), 8.11 (d, *J* = 8.5 Hz, 1H), 8.03 (s, 1H), 7.58 (d, *J* = 8.6 Hz, 1H), 7.19-7.21 (m, 3H), 4.98-4.92 (m, 1H), 4.84 – 4.63 (m, 2H), 4.51-4.97 (m, 1H), 3.98 – 3.79 (m, 2H), 3.73 – 3.61 (m, 2H), 3.00 – 2.89 (m, 1H), 2.88 – 2.67 (m, 1H), 2.31 – 2.07 (m,

1H), 2.06 – 1.81 (m, 2H), 1.73 – 1.67 (m, 1H), 1.07 (s, 9H). ESI−MS calculated for $C_{30}H_{34}F_2N_3O_6PS^+$ 633.65, found $[M + H]^+$ 634.25.

((2-(((S)-3,3-Dimethyl-1-oxo-1-((S)-2-(2,3,4,5-tetrahydro-1H-benzo[d]azepine-3-carbonyl)pyrrolidin-1-yl)butan-2-yl)carbamoyl)-1H-inden-5-yl)difluoromethyl)phosphonic acid (10)

Compound **10** was synthesized by a procedure similar to that used for Compound **9**.

^{1}H NMR (400 MHz, DMSO) δ 8.50 (s, 1H), 8.31 (d, *J* = 8.9 Hz, 1H), 8.07 (d, *J* = 8.5 Hz, 1H), 8.01 (s, 1H), 7.65 – 7.50 (m, 1H), 7.25 – 7.02 (m, 4H), 4.94 (dd, *J* = 8.2, 6.4 Hz, 1H), 4.79 (d, *J* = 8.9 Hz, 1H), 3.95 – 3.88 (m, 3H), 3.69 – 3.59 (m, 2H), 3.20 – 3.10 (m, 2H), 2.90 – 2.76 (m, 3H), 2.24 – 2.15 (m, 1H), 2.06 – 1.94 (m, 1H), 1.92 – 1.77 (m, 1H), 1.69 – 1.65 (m, 1H), 1.09 (s, 9H). ESI−MS calculated for $C_{32}H_{38}F_2N_3O_6PS^+$ 647.67, found $[M + H]^+$: 648.40.

((2-(((S)-1-((S)-2-(Benzyl(methyl)carbamoyl)pyrrolidin-1-yl)-3,3-dimethyl-1-oxobutan-2-yl)carbamoyl)benzo[b]thiophen-5-yl)difluoromethyl)phosphonic acid (11).

Compound **11** was synthesized by a procedure similar to that used for Compound **9**. ^{1}H NMR (400 MHz, DMSO) δ 8.55 (d, *J* = 2.0 Hz, 1H), 8.40 (d, *J* = 8.4 Hz, 1H), 8.09 (d, *J* = 8.6 Hz, 1H), 8.04 (s, 1H), 7.58 (d, *J* = 8.6 Hz, 1H), 7.40 – 7.21 (m, 5H), 4.87 – 4.81 (m, 3H), 4.27 – 4.23 (m, 1H), 3.93 – 3.88 (m, 1H), 3.72 – 3.64 (m, 1H), 3.01 (s, 3H), 2.26 – 2.20 (m, 1H), 2.15 – 1.99 (m, 1H), 1.97 – 1.84 (m, 1H), 1.77 – 1.73 (m, 1H), 1.10 (s, 9H). ESI−MS calculated for $C_{29}H_{34}F_2N_3O_6PS^+$ 621.67, found $[M + H]^+$ 622.17.

((2-(((S)-1-((S)-2-((4-Bromobenzyl)(methyl)carbamoyl)pyrrolidin-1-yl)-3,3-dimethyl-1-oxobutan-2-yl)carbamoyl)benzo[b]thiophen-5-yl)difluoromethyl)phosphonic acid (12).

Compound **12** was synthesized using a procedure similar to that used for compound **9**. ^{1}H NMR (400 MHz, DMSO) δ 8.54 (d, *J* = 3.4 Hz, 1H), 8.43 – 8.34 (m, 1H), 8.11 (d, *J* = 8.5 Hz, 1H), 8.04

(s, 1H), 7.58 – 7.52 (m2H), 7.50 – 7.43 (m, 1H), 7.39 – 7.29 (m, 1H), 7.27 – 7.21 (m, 1H), 4.90 – 4.66 (m, 3H), 4.24 – 4.20 (m, 1H), 3.97 – 3.84 (m, 1H), 3.73 – 3.64 (m, 1H), 3.02 (s, 3H), 2.31 – 2.16 (m, 1H), 2.15 – 1.99 (m, 1H), 1.96 – 1.83 (m, 1H), 1.76 – 1.72 (m, 1H), 1.09 (s, 9H). ESI−MS calculated for $C_{29}H_{33}BrF_2N_3O_6PS^+$ 700.53, found $[M + H]^+$ 700.16, 701.98.

((2-(((S)-1-((S)-2-(1,4-Oxazepane-4-carbonyl)pyrrolidin-1-yl)-3,3-dimethyl-1-oxobutan-2-yl)carbamoyl)benzo[b]thiophen-5-yl)difluoromethyl)phosphonic acid (13).

Compound **13** was synthesized using a procedure similar to that used for Compound **9**. ^{1}H NMR (400 MHz, DMSO) δ 8.54 (s, 1H), 8.37 (dd, *J* = 8.9, 3.4 Hz, 1H), 8.12 (d, *J* = 8.5 Hz, 1H), 8.04 (s, 1H), 7.66 – 7.46 (m, 1H), 4.82 – 4.76 (m, 2H), 3.94 – 3.84 (m, 1H), 3.80 – 3.60 (m, 6H), 3.52 – 3.42 (m, 2H), 3.29 – 3.20 (m, 1H), 2.28 – 2.13 (m, 1H), 2.04 – 1.97 (m, 1H), 1.94 – 1.62 (m, 4H), 1.08 (s, 9H). ESI−MS calculated for $C_{26}H_{34}F_2N_3O_7PS^+$ 601.60, found $[M + H]^+$ 602.26.

((2-(((S)-1-((S)-2-(6-Azaspiro[3.4]octane-6-carbonyl)pyrrolidin-1-yl)-3,3-dimethyl-1-oxobutan-2-yl)carbamoyl)benzo[b]thiophen-5-yl)difluoromethyl)phosphonic acid (14).

Compound **14** was synthesized by a procedure similar to that used for Compound **9**. ^{1}H NMR (400 MHz, DMSO) δ 8.52 (d, *J* = 4.7 Hz, 1H), 8.35 – 8.29 (m, 1H), 8.08 (d, *J* = 8.6 Hz, 1H), 8.03 (s, 1H), 7.58 (d, *J* = 8.5 Hz, 1H), 4.75 (dd, *J* = 8.8, 2.0 Hz, 1H), 4.57 – 4.50 (m, 1H), 3.96 – 3.80 (m, 1H), 3.76 – 3.72 (m, 1H), 3.65 – 3.60 (m, 1H), 3.51 – 3.43 (m, 1H), 3.37 – 3.33 (m, 1H), 3.26 – 3.20 (m, 1H), 2.23 – 2.10 (m, 1H), 2.08 – 1.94 (m, 1H), 1.93 – 1.82 (m, 1H), 1.76 – 1.72 (m, 2H), 1.53 – 1.48 (m, 7H), 1.05 (s, 9H). ESI−MS calculated for $C_{28}H_{36}F_2N_3O_6PS^+$ 611.64, found $[M + H]^+$ 612.37.

((2-(((S)-1-((S)-2-((3-(Dimethylamino)-3-oxopropyl)(phenyl)carbamoyl)pyrrolidin-1-yl)-3,3-dimethyl-1-oxobutan-2-yl)carbamoyl)benzo[b]thiophen-5-yl)difluoromethyl)phosphonic acid (15).

Compound **15** was synthesized by a procedure similar to that for **AK305**.

^{1}H NMR (400 MHz, DMSO) δ 8.53 (s, 1H), 8.41 (d, *J* = 9.0 Hz, 1H), 8.14 – 8.02 (m, 2H), 7.60 – 7.55 (m, 1H), 7.43 (m, 4H), 7.37 – 3.33 (m, 1H), 4.76 (d, *J* = 9.0 Hz, 1H), 4.11 (t, *J* = 7.1 Hz, 1H), 3.79 – 3.75 (m, 3H), 3.70 – 3.58 (m, 1H), 2.93 (s, 3H), 2.76 (s, 3H), 2.60 – 2.51 (m, 2H), 2.02 – 1.87 (m, 1H), 1.84 – 1.69 (m, 3H), 1.09 (s, 9H). ESI−MS calculated for $C_{32}H_{39}F_2N_4O_7PS^+$ 692.72, found $[M + H]^+$ 693.13.

((2-(((S)-1-((S)-2-((4-chlorophenyl)(3-(dimethylamino)-3-oxopropyl)carbamoyl)pyrrolidin-1-yl)-3,3-dimethyl-1-oxobutan-2-yl)carbamoyl)benzo[b]thiophen-5-yl)difluoromethyl)-phosphonic acid (16).

Compound **16** was synthesized by a procedure similar to that used for AK-0305. ^{1}H NMR (400 MHz, DMSO) δ 8.54 (s, 1H), 8.41 (d, *J* = 9.0 Hz, 1H), 8.12 (d, *J* = 8.4 Hz, 1H), 8.04 (s, 1H), 7.62 – 7.55 (m, 1H), 7.52 – 7.35 (m, 4H), 4.75 (d, *J* = 9.0 Hz, 1H), 4.15 – 4.05 (m, 1H), 3.84 – 3.69 (m, 3H), 3.69 – 3.61 (m, 1H), 2.93 (s, 3H), 2.77 (s, 3H), 2.60 – 2.52 (m, 2H), 2.02 – 1.90 (m, 1H), 1.89 – 1.67 (m, 3H), 1.08 (s, 9H). ESI−MS calculated for $C_{32}H_{38}ClF_2N_4O_7PS^+$ 727.16, found $[M + H]^+$ 727.08.

((2-(((S)-1-((S)-2-((3-Bromophenyl)(3-(dimethylamino)-3-oxopropyl)carbamoyl)pyrrolidin-1-yl)-3,3-dimethyl-1-oxobutan-2-yl)carbamoyl)benzo[b]thiophen-5-yl)difluoromethyl)-phosphonic acid (17).

Compound **17** was synthesized by a procedure similar to that used for AK-305. ^{1}H NMR (400 MHz, DMSO) δ 8.55 (s, 1H), 8.48 (d, *J* = 9.0 Hz, 1H), 8.12 (d, *J* = 8.8 Hz, 1H), 8.04 (s, 1H), 7.69 – 7.65 (m, 1H), 7.62 – 7.55 (m, 2H), 7.47 – 7.38 (m, 2H), 4.77 (d, *J* = 9.0 Hz, 1H), 4.15 – 4.05 (m, 1H), 3.85 – 3.75 (m, 3H), 3.69 – 3.59 (m, 1H), 2.94 (s, 3H), 2.77 (s, 3H), 2.62 – 2.54

(m, 2H), 2.00 – 1.90 (m, 1H), 1.85 – 1.75 (m, 3H), 1.09 (s, 9H). ESI−MS calculated for $C_{32}H_{38}BrF_2N_4O_7PS^+$ 771.61, found $[M + H]^+$ 770.99, 772.13.

((2-(((S)-1-((S)-2-((3-(Dimethylamino)-3-oxopropyl)(naphthalen-2-yl)carbamoyl)-pyrrolidin-1-yl)-3,3-dimethyl-1-oxobutan-2-yl)carbamoyl)benzo[b]thiophen-5-yl)difluoromethyl)phosphonic acid (18).

Compound **18** was synthesized by a procedure similar to that used for AK-305. ^{1}H NMR (400 MHz, DMSO) δ 8.53 (s, 1H), 8.43 (d, *J* = 9.0 Hz, 1H), 8.10 (d, *J* = 8.5 Hz, 1H), 8.04 (s, 1H), 7.99 (d, *J* = 8.7 Hz, 1H), 7.96 – 7.86 (m, 3H), 7.60 – 7.48 (m, 4H), 4.76 (d, *J* = 9.0 Hz, 1H), 4.18 – 4.12 (m, 1H), 3.90 – 3.84 (m, 2H), 3.79 – 3.70 (m, 1H), 3.68 – 3.57 (m, 1H), 2.94 (s, 3H), 2.76 (s, 3H), 2.70 – 2.60 (m, 2H), 2.01 – 1.90 (m, 1H), 1.88 – 1.82 (m, 2H), 1.77 – 1.66 (m, 1H), 1.11 (s, 9H). ESI−MS calculated for $C_{36}H_{41}F_2N_4O_7PS^+$ 742.78, found $[M + H]^+$ 743.15.

((2-(((S)-1-((S)-2-([1,1'-Biphenyl]-4-yl(3-(dimethylamino)-3-oxopropyl)carbamoyl)-pyrrolidin-1-yl)-3,3-dimethyl-1-oxobutan-2-yl)carbamoyl)benzo[b]thiophen-5-yl)difluoromethyl)phosphonic acid (19).

Compound **19** was synthesized by a procedure similar to that used for AK-305. ^{1}H NMR (400 MHz, DMSO) δ 8.55 (s, 1H), 8.43 (d, *J* = 9.0 Hz, 1H), 8.13 – 8.08 (m, 1H), 8.04 (s, 1H), 7.73 (d, *J* = 8.5 Hz, 2H), 7.70 – 7.63 (m, 2H), 7.61 – 7.55 (m, 1H), 7.53 – 7.48 (m, 2H), 7.47 – 7.43 (m, 2H), 7.37 – 7.32 (m, 1H), 4.76 (d, *J* = 9.0 Hz, 1H), 4.21 (t, *J* = 7.1 Hz, 1H), 3.82 – 3.78 (m, 3H), 3.70 – 3.62 (m, 1H), 2.95 (s, 3H), 2.78 (s, 3H), 2.63 – 2.55 (m, 2H), 2.04 – 1.93 (m, 1H), 1.90 – 1.69 (m, 3H), 1.10 (s, 9H). ESI−MS calculated for $C_{38}H_{43}F_2N_4O_7PS^+$ 768.81, found $[M + H]^+$ 769.16.

((2-(((S)-1-((S)-2-(Benzofuran-5-yl(3-(dimethylamino)-3-oxopropyl)carbamoyl)pyrrolidin-1-yl)-3,3-dimethyl-1-oxobutan-2-yl)carbamoyl)benzo[b]thiophen-5-yl)difluoromethyl)-phosphonic acid (20).

Compound **20** was synthesized by a procedure similar to that used for AK-305. ^{1}H NMR (400 MHz, DMSO) δ 8.54 (s, 1H), 8.42 (d, *J* = 9.0 Hz, 1H), 8.17 – 8.10 (m, 1H), 8.10 – 8.00 (m, 2H), 7.70 (d, *J* = 2.1 Hz, 1H), 7.65 (d, *J* = 8.7 Hz, 1H), 7.60 – 7.54 (m, 1H), 7.43 – 7.32 (m, 1H), 6.98 (s, 1H), 4.75 (d, *J* = 9.0 Hz, 1H), 4.15 – 4.10 (m, 1H), 3.90 – 3.70 (m, 3H), 3.69 – 3.55 (m, 1H), 2.94 (s, 3H), 2.76 (s, 3H), 2.66 – 2.54 (m, 2H), 2.00 – 1.90 (m, 1H), 1.86 – 1.65 (m, 3H), 1.10 (s, 9H). ESI−MS calculated for $C_{34}H_{39}F_2N_4O_8PS^+$ 732.74, found $[M + H]^+$ 733.11.

((2-(((S)-1-((S)-2-(Benzo[d]thiazol-5-yl(3-(dimethylamino)-3-oxopropyl)carbamoyl)-pyrrolidin-1-yl)-3,3-dimethyl-1-oxobutan-2-yl)carbamoyl)benzo[b]thiophen-5-yl)difluoromethyl)phosphonic acid (21).

Compound **21** was synthesized by a procedure similar to that used for **AK305**. ^{1}H NMR (400 MHz, DMSO) δ 9.44 (s, 1H), 8.57 – 8.41 (m, 2H), 8.22 – 8.03 (m, 4H), 7.60 – 7.52 (m, 2H), 4.76 (d, *J* = 9.0 Hz, 1H), 4.15 (m, 1H), 3.98 – 3.46 (m, 5H), 2.97 (d, *J* = 14.2 Hz, 3H), 2.75 (d, *J* = 10.9 Hz, 3H), 2.63 (m, 2H), 2.03 – 1.66 (m, 5H), 1.11 (s, 9H). ^{13}C NMR (400 MHz, DMSO) δ 171.29, 168.50, 168.10, 161.45, 158.02, 153.68, 141.90, 140.47, 140.44, 139.90, 138.79, 134.02, 133.25, 126.11, 125.85, 123.36, 122.80, 57.42, 57.38, 48.19, 46.50, 36.70, 36.08, 35.45, 34.69, 30.77, 29.01, 26.62, 26.21, 24.85. ESI−MS calculated for $C_{33}H_{38}F_2N_5O_7PS^+$ 749.79, found $[M + H]^+$ 750.10.

((2-(((S)-1-((S)-2-((3-(Dimethylamino)-3-oxopropyl)(3-(thiazol-2-yl)phenyl)carbamoyl)-pyrrolidin-1-yl)-3,3-dimethyl-1-oxobutan-2-yl)carbamoyl)benzo[b]thiophen-5-yl)difluoromethyl)phosphonic acid (22).

Compound **22** was synthesized by a procedure similar to that used for AK-305. ^{1}H NMR (400 MHz, DMSO) δ 8.52 (s, 1H), 8.43 (d, *J* = 8.9 Hz, 1H), 8.17 – 8.05 (m, 2H), 8.03 (s, 1H), 7.97 (d, *J* = 2.0 Hz, 1H), 7.95 – 7.89 (m, 2H), 7.78 (d, *J* = 3.3 Hz, 1H), 7.60 – 7.50 (m, 3H), 4.76 (d, *J* = 8.9 Hz, 1H), 4.17 (t, *J* = 7.2 Hz, 1H), 3.91 – 3.73 (m, 3H), 3.70 – 3.58 (m, 1H), 2.95 (s, 3H), 2.77 (s, 3H), 2.64 – 2.55 (m, 2H), 2.02 – 1.92 (m, 1H), 1.90 – 1.80 (m, 2H), 1.78 – 1.70 (m, 1H), 1.10 (s, 9H). ESI−MS calculated for $C_{35}H_{40}F_2N_5O_7PS^+$ 775.82, found $[M + H]^+$ 775.95.

((2-(((2S)-1-((2S)-2-((3-((5-(2-(2,6-Dioxopiperidin-3-yl)-1-oxoisoindolin-4-yl)pent-4-yn-1-yl)(methyl)amino)-3-oxopropyl)(4-(thiazol-2-yl)phenyl)carbamoyl)pyrrolidin-1-yl)-3,3-dimethyl-1-oxobutan-2-yl)carbamoyl)benzo[b]thiophen-5-yl)difluoromethyl)phosphonic acid (AK-2292)

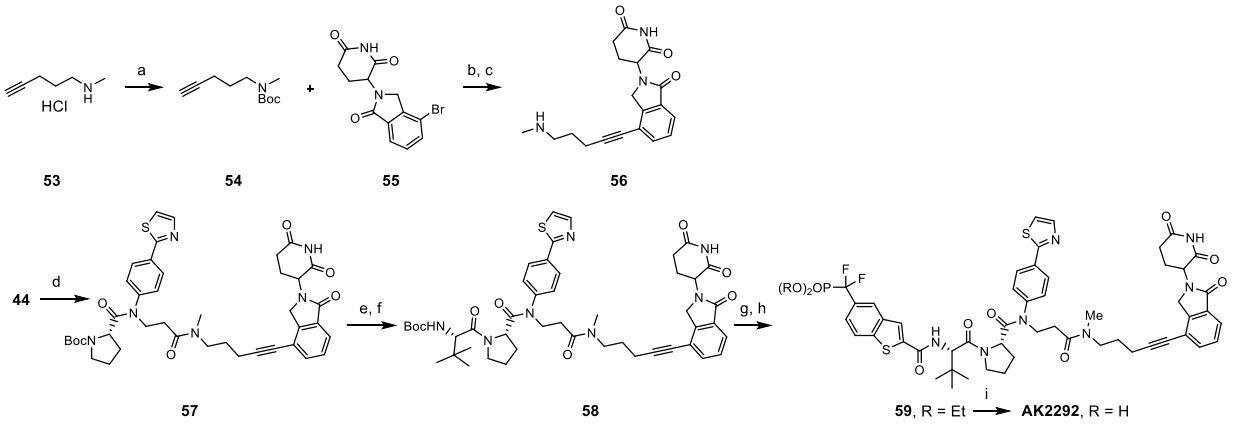

Figure 2-4 Synthesis of ((2-(((2S)-1-((2S)-2-((3-((5-(2-(2,6-Dioxopiperidin-3-yl)-1-oxoisoindolin-4-yl)pent-4-yn-1-yl)(methyl)amino)-3-oxopropyl)(4-(thiazol-2-yl)phenyl)carbamoyl)pyrrolidin-1-yl)-3,3-dimethyl-1-oxobutan-2-yl)carbamoyl)benzo[b]thiophen-5-yl)difluoromethyl)phosp

Reaction conditions: (a) Boc_2O, TEA, CH_3CN, rt; (b) $PdCl_2(PPh_3)_2$, CuI, TEA/DMF, 90 °C; (c) TFA, DCM, rt; (d) HATU, DIPEA, DMF, rt; (e) TFA, DCM, rt; (f) HATU, DIPEA, DMF, rt; (g) TFA, DCM, rt; (h) HATU, DIPEA, DMF, rt; (i) TMSI, BSTFA, DCM, rt, 0 °C

N-Methylpent-4-yn-1-amine hydrochloride **53** (1 g, 7.5 mmol, 1 equiv.), CH_3CN (10 ml), Et3N (3 ml, 22.5 mmol, 3 equiv.), and Boc_2O (2.45 g, 11.3 mmol, 1.5 eq) were added to a round bottom flask equipped with a magnetic stirring bar. The mixture was stirred at rt for 1 h. The

volatile components were removed in vacuum. The residue was purified by flash column chromatography to yield **54** in 90% yield. ^{1}H NMR (400 MHz, DMSO) δ 3.21 (s, *J* = 7.1 Hz, 3H), 2.76 (m, 3H), 2.13 (m, 2H), 1.62 (m, 2H), 1.39 (s, 9H). ^{13}C NMR (400 MHz, DMSO) δ 154.71, 83.80, 78.32, 71.22, 47.15, 33.79, 28.03, 26.42, 15.17. ESI−MS calculated for $C_{11}H_{19}NO_2^+$ 197.28, found $[M + H]^+$ 97.86, 141.76.

Et_3N (1.5 ml) was added to a mixture of **55** (323 mg, 1 mmol, 1 equiv.), **54** (300 mg, 1.5 mmol, 1.5 eq), CuI (40 mg, 0.2 mmol, 0.2 equiv.), and $Pd(PPh_3)_2Cl_2$ (70 mg, 0.1 mmol, 0.1 equiv.) in DMF (1.5 ml). The resulting mixture was purged and refilled with argon three times and stirred at 90 °C for 1.5 hours under argon. The reaction mixture was cooled to rt. The mixture was filtered through celite and evaporated to remove most of the solvent. The residue was purified by HPLC to yield Boc-protected **56** which was dissolved in DCM (5 ml). TFA (2 ml) was added to remove the Boc protection. The mixture was stirred at rt for 10 min. Most of the volatile components were removed in vacuum and the residue was purified by HPLC. The sample was dried in a lyophilizer, yielding 270 mg of **56** (60%). ^{1}H NMR (400 MHz, DMSO) δ 11.00 (s, 1H), 8.73 (s, 2H), 7.73 (dd, *J* = 7.6, 1.1 Hz, 1H), 7.66 (dd, *J* = 7.6, 1.1 Hz, 1H), 7.53 (t, *J* = 7.6 Hz, 1H), 5.15 (dd, *J* = 13.3, 5.1 Hz, 1H), 4.48 (d, *J* = 17.7 Hz, 1H), 4.33 (d, *J* = 17.7 Hz, 1H), 3.81 (s, 3H), 2.93 (m, 1H), 2.42 (m, 1H), 2.03 (m, 1H), 1.89 (m, 2H). ^{13}C NMR (400 MHz, DMSO) δ 172.88, 170.99, 167.65, 143.86, 134.18, 132.00, 128.62, 122.87, 118.49, 94.53, 77.12, 51.65, 47.39, 46.93, 32.52, 31.21, 24.53, 22.42, 16.16. ESI−MS calculated for $C_{19}H_{21}N_3O_3^+$ 339.40, found $[M + H]^+$ 340.26.

HATU (280 mg, 0.74 mmol, 1.1 equiv.) was added to a solution of **44** (300 mg, 0.67 mmol, 1 equiv.), **56** (300mg, 0.67 mmol, 1 equiv.), and Et3N (0.46 ml, 3.35 mmol, 5 equiv.) in CH_3CN (5 ml). The mixture was stirred at rt for 30 min. The yellow solution was concentrated in vacuum

and the crude was purified by flash column chromatography to yield **57** in 74% yield (385 mg). ^{1}H NMR (400 MHz, DMSO) δ 10.76 (s, 1H), 8.03 (s, 2H), 7.93 (d, *J* = 3.3 Hz, 1H), 7.76 (d, *J* = 3.3 Hz, 1H), 7.69 (d, *J* = 7.6 Hz, 1H), 7.60 (d, *J* = 7.6 Hz, 1H), 7.53 – 7.43 (m, 2H), 5.10 (m, 1H), 4.48 (m, 1H), 4.36 (m, 1H), 4.10 (m, 1H), 3.87 (m, 2H), 3.46 – 3.27 (m, 4H), 3.11 (s, 3H), 2.98 – 2.79 (m, 4H), 2.62 (m, 3H), 2.46 (m, 2H), 2.05 (m, 1H), 1.78 (m, 5H), 1.41 (s, 9H). ^{13}C NMR (400 MHz, DMSO) δ 172.82, 171.56, 170.93, 170.00, 167.65, 153.70, 152.48, 150.94, 144.03, 133.85, 132.57, 131.92, 129.32, 128.53, 127.45, 122.59, 121.07, 120.71, 118.71, 95.74, 78.69, 78.49, 77.24, 74.25, 56.92, 51.57, 46.79, 45.77, 38.21, 35.71, 31.18, 28.21, 25.81, 22.82, 22.30, 16.39, 8.61. ESI−MS calculated for $C_{41}H_{46}N_6O_7S^+$ 766.91, found $[M + H]^+$ 767.19.

57 (380 mg, 0.5 mmol, 1 equiv.) was dissolved in DCM (5 ml), and TFA (2 ml) was added to remove Boc protection. The mixture was stirred at rt for 10 min. Most of the volatile components were removed in vacuum. To the residue, CH_3CN (5 ml), Et_3N (0.35 ml, 2.5 mmol, 5 equiv.), Boc-L-*tert*-leucine (175 mg, 0.75 mmol, 1.5 equiv.), and HATU (230 mg, 0.6 mmol, 1.2 equiv.) were added. The mixture was stirred at rt for 30 min. The yellow solution was concentrated in vacuum and the crude was purified by flash column chromatography to yield **58** in 70% (354 mg). ^{1}H NMR (400 MHz, DMSO) δ 10.99 (m, 1H), 8.07 – 7.88 (m, 3H), 7.86 – 7.77 (m, 1H), 7.77 – 7.63 (m, 2H), 7.62 – 7.47 (m, 3H), 5.14 (m, 1H), 4.47 (m, 1H), 4.39 – 4.23 (m, 1H), 4.15 (m, 2H), 3.93 – 3.74 (m, 2H), 3.43 – 3.25 (m, 2H), 2.99 – 2.85 (m, 3H), 2.79 (m, 1H), 2.67 – 2.41 (m, 7H), 2.13 – 1.60 (m, 8H), 1.36 (s, 9H), 0.97 (s, 9H). ^{13}C NMR (400 MHz, DMSO) δ 172.84, 170.95, 169.95, 169.67, 169.29, 167.67, 166.10, 155.39, 144.01, 133.86, 132.45, 131.94, 129.22, 128.53, 127.28, 122.60, 120.94, 118.74, 95.76, 95.13, 78.04, 76.69, 76.53, 58.44, 57.29, 51.59, 48.00, 46.99, 45.93, 45.74, 35.10, 34.91, 31.21, 28.93, 28.11, 26.33, 25.88, 24.88, 22.33, 16.41, 8.59. ESI−MS calculated for $C_{47}H_{57}N_7O_8S^+$ 880.07, found $[M + H]^+$ 880.24.

58 (230 mg, 0.26 mmol, 1 equiv.) was dissolved in DCM (3 ml), and TFA (1.5 ml) was added to remove Boc protection. The mixture was stirred at rt for 10 min. Most of the volatile components were removed in vacuum. CH_3CN (5 ml), Et3N (0.18 ml, 1.3 mmol, 5 equiv.), benzothiophene **39** (115 mg, 0.31 mmol, 1.2 equiv.), and HATU (118 mg, 0.31 mmol, 1.2 equiv.) were added to the residue and the mixture was stirred at rt for 30 min. The yellow solution was concentrated in vacuum and the crude was purified by flash column chromatography to yield **59** in 68% yield (200 mg).

^{1}H NMR (400 MHz, DMSO) δ 11.08 – 10.86 (m, 1H), 8.60 – 8.39 (m, 2H), 8.18 (m, 1H), 8.09 (s, 1H), 8.04 – 7.92 (m, 2H), 7.91 (m, 1H), 7.78 (d, *J* = 3.3 Hz, 1H), 7.74 – 7.64 (m, 1H), 7.63 – 7.40 (m, 5H), 5.15 (m, 1H), 4.75 (m, 1H), 4.48 (m, 1H), 4.33 (m, 1H), 4.23 – 4.00 (m, 5H), 3.87 – 3.73 (m, 3H), 3.46 – 3.35 (m, 2H), 2.99 – 2.83 (m, 3H), 2.72 – 2.53 (m, 3H), 2.47 (m, 3H), 2.44 (m, 2H), 2.04 – 1.93 (m, 2H), 1.89 – 1.57 (m, 5H), 1.22 (m, 6H), 1.09 (m, 9H). ^{13}C NMR (400 MHz, DMSO) δ 172.85, 170.97, 169.92, 168.44, 167.68, 167.64, 166.06, 161.36, 143.98, 142.63, 140.92, 138.90, 133.87, 132.48, 131.95, 129.15, 128.54, 127.31, 126.04, 123.40, 122.62, 120.94, 118.74, 118.62, 117.05, 95.76, 95.12, 76.72, 76.56, 64.76, 64.69, 57.46, 51.59, 48.19, 47.00, 45.96, 45.78, 35.42, 35.36, 34.89, 33.13, 31.22, 29.01, 26.57, 26.27, 25.87, 24.87, 22.33, 16.42, 16.20, 16.15, 8.62. ESI−MS calculated for $C_{56}H_{62}F_2N_7O_{10}PS_2^+$ 1126.24, found $[M + H]^+$ 1126.31.

59 (200 mg, 0.17 mmol, 1 equiv.), DCM (2 ml) and $CF_3CON(TMS)_2$ (0.27 ml, 1.0 mmol, 6 equiv.) were added to a round bottom flask. The solution was cooled in an ice bath. 1 M of trimethylsilyl iodide in DCM (0.85 ml, 0.85 mmol, 5 equiv.) was added dropwise to the ice cooled reaction mixture, and the mixture was stirred for 10 min in an ice bath. The volatile components were removed under vacuum at below 5 °C. The residue was dissolved in a mixed

solvent of CH_3CN (3 ml) and H_2O (1 ml). The resulting solution was purified by HPLC to yield AK-2292 in 82% yield (150 mg). ^{1}H NMR (400 MHz, DMSO) δ 10.99 (s, 1H), 8.53 (m, 1H), 8.40 (m, 1H), 8.12 – 8.04 (m, 2H), 8.00 (m, 2H), 7.90 (m, 1H), 7.75 (m, 1H), 7.70 (m, 1H), 7.59 (m, 3H), 7.49 (m, 2H), 5.23 – 5.05 (m, 1H), 4.77 (m, 1H), 4.46 (m, 1H), 4.40 – 4.25 (m, 1H), 4.20 (m, 1H), 4.00 – 3.70 (m, 3H), 3.64 (m, 1H), 3.50 – 3.28 (m, 2H), 2.95 (m, 3H), 2.80 (m, 1H), 2.61 (m, 3H), 2.43 (m, 2H), 2.00 (m, 2H), 1.77 (m, 5H), 1.10 (s, 9H). ^{13}C NMR (400 MHz, DMSO) δ 172.97, 171.09, 170.08, 169.80, 168.63, 167.84, 166.22, 161.57, 159.11, 158.72, 158.34, 157.96, 144.03, 142.03, 140.54, 138.89, 133.97, 132.59, 132.12, 132.08, 129.26, 128.62, 127.45, 126.19, 123.84, 122.87, 121.01, 119.47, 118.89, 116.60, 113.74, 110.87, 95.86, 95.21, 76.68, 57.59, 51.74, 48.33, 47.14, 46.09, 35.54, 35.01, 34.98, 32.97, 31.35, 29.14, 26.68, 25.98, 25.00, 22.48, 16.54. ESI−MS calculated for $C_{52}H_{54}F_2N_7O_{10}PS_2^+$ 1070.13, found $[M + H]^+$ 1070.40.

((2-(((2S)-3,3-Dimethyl-1-((2S)-2-((3-(methyl(5-(2-(1-methyl-2,6-dioxopiperidin-3-yl)-1-oxoisoindolin-4-yl)pent-4-yn-1-yl)amino)-3-oxopropyl)(4-(thiazol-2-yl)phenyl)-carbamoyl)pyrrolidin-1-yl)-1-oxobutan-2-yl)carbamoyl)benzo[b]thiophen-5-yl)difluoro-methyl)phosphonic acid (AK-2292Me)

AK-2292Me was synthesized using a similar procedure to that used for AK-2292. ^{1}H NMR (400 MHz, DMSO) δ 8.53 (s, 1H), 8.41 (m, 1H), 8.19 – 8.04 (m, 2H), 8.00 (m, 1H), 7.98 – 7.93 (m, 1H), 7.90 (m, 1H), 7.77 (m, 1H), 7.71 (m, 1H), 7.68 – 7.40 (m, 5H), 5.21 (m, 1H), 4.76 (m, 1H), 4.46 (m, 1H), 4.37 (m, 1H), 4.18 (m, 1H), 4.01 – 3.69 (m, 3H), 3.65 (m, 1H), 3.40 (m, 2H), 3.05 – 2.92 (m, 6H), 2.80 (m, 2H), 2.59 (m, 3H), 2.44 (m, 2H), 2.01 (m, 2H), 1.76 (m, 5H), 1.10 (s, 9H). ^{13}C NMR (400 MHz, DMSO) δ 171.91, 171.17, 171.06, 170.64, 169.98, 169.71, 168.53, 167.79, 166.13, 161.49, 159.02, 158.64, 158.26, 157.87, 144.01, 141.95, 140.46, 138.81, 133.94,

132.56, 132.03, 132.00, 129.18, 128.58, 127.39, 126.13, 123.76, 122.83, 120.98, 119.46, 118.82, 116.59, 113.72, 110.86, 95.78, 95.13, 76.65, 57.51, 52.14, 48.25, 47.04, 45.97, 35.47, 35.41, 34.90, 32.90, 31.44, 29.08, 26.62, 25.92, 24.94, 21.67, 16.47. ESI−MS calculated for $C_{53}H_{56}F_2N_7O_{10}PS^+$ 1087.16, found $[M + H]^+$ 1084.08.

((2-(((2S)-1-((2S)-2-((4-Bromophenyl)(3-((5-(2-(2,6-dioxopiperidin-3-yl)-1-oxoisoindolin-4-yl)pent-4-yn-1-yl)amino)-3-oxopropyl)carbamoyl)pyrrolidin-1-yl)-3,3-dimethyl-1-oxobutan-2-yl)carbamoyl)benzo[b]thiophen-5-yl)difluoromethyl)phosphonic acid (6).

Compound **6** was synthesized by using a procedure similar to that used for AK-2292. ^{1}H NMR (400 MHz, DMSO) δ 10.98 (s, 1H), 8.49 (s, 1H), 8.32 (m, 1H), 8.02 (m, 2H), 7.95 (s, 1H), 7.72 – 7.47 (m, 5H), 7.35 (m, 2H), 5.14 (m, 2H), 4.74 (m, 2H), 4.46 (m, 2H), 4.31 (m, 2H), 4.10 (m, 2H), 3.76 (m, *J* = 8.5 Hz, 2H), 2.95 – 2.83 (m, 2H), 2.35 – 2.18 (m, 3H), 1.98 (m, 3H), 1.87 – 1.57 (m, 6H), 1.08 (s, 9H). ESI−MS calculated for $C_{48}H_{50}BrF_2N_6O_{10}PS^+$ 1051.89, found $[M + H]^+$ 1051.23.

((2-(((2S)-1-((2S)-2-((4-Bromophenyl)(3-((5-(2-(2,6-dioxopiperidin-3-yl)-1-oxoisoindolin-4-yl)pent-4-yn-1-yl)(methyl)amino)-3-oxopropyl)carbamoyl)pyrrolidin-1-yl)-3,3-dimethyl-1-oxobutan-2-yl)carbamoyl)benzo[b]thiophen-5-yl)difluoromethyl)phosphonic acid (7).

Compound **7** was synthesized by using a procedure similar to that used for AK-2292. ^{1}H NMR (400 MHz, DMSO) δ 10.98 (s, 1H), 8.52 (m, 1H), 8.40 (m, 1H), 8.12 (m, 1H), 8.04 (m, 1H), 7.75 – 7.49 (m, 6H), 7.44 – 7.30 (m, 2H), 5.15 (m, 1H), 4.79 – 4.68 (m, 1H), 4.47 (m, 2H), 4.39 – 4.24 (m, 1H), 4.09 (m, 1H), 3.77 (m, 2H), 3.64 (m, 1H), 3.38 (m, 2H), 2.95 (s, 3H), 2.79 (m, 1H), 2.65 – 2.53 (m, 2H), 2.26 (m, 2H), 1.99 (m, 2H), 1.87 – 1.57 (m, 6H), 1.08 (s, 9H). ESI−MS calculated for $C_{49}H_{52}BrF_2N_6O_{10}PS^+$ 1065.92, found $[M + H]^+$ 1064.94, 1066.79.

((2-(((2S)-1-((2S)-2-((3-((5-(2-(2,6-Dioxopiperidin-3-yl)-1-oxoisoindolin-4-yl)pent-4-yn-1-yl)amino)-3-oxopropyl)(4-(thiazol-2-yl)phenyl)carbamoyl)pyrrolidin-1-yl)-3,3-dimethyl-1-oxobutan-2-yl)carbamoyl)benzo[b]thiophen-5-yl)difluoromethyl)phosphonic acid (8).

Compound **8** was synthesized by using a procedure similar to that used for AK-2292. ^{1}H NMR (400 MHz, DMSO) δ 10.97 (s, 1H), 8.52 (s, 1H), 8.37 (m, 2H), 8.11 (m, 2H), 8.05 – 7.96 (m, 3H), 7.91 (m, 1H), 7.78 (m, 1H), 7.69 (m, 1H), 7.62 – 7.54 (m, 2H), 7.50 (m, 2H), 5.13 (m, 1H), 4.75 (m, 1H), 4.45 (m, 2H), 4.30 (m, 2H), 4.18 (m, 1H), 3.77 (m, 4H), 3.15 (m, 2H), 2.92 – 2.86 (m, 1H), 1.98 (m, 3H), 1.81 (m, 4H), 1.66 (m, 3H), 1.09 (s, 9H). ESI−MS calculated for $C_{51}H_{52}F_2N_7O_{10}PS_2^+$ 1056.11, found $[M + H]^+$ 1056.88.

((2-(((2S)-1-((2S)-2-((4-Bromophenyl)(3-((4-(2-(2,6-dioxopiperidin-3-yl)-1-oxoisoindolin-4-yl)but-3-yn-1-yl)amino)-3-oxopropyl)carbamoyl)pyrrolidin-1-yl)-3,3-dimethyl-1-oxobutan-2-yl)carbamoyl)benzo[b]thiophen-5-yl)difluoromethyl)phosphonic acid (23).

Compound **23** was synthesized using a procedure similar to that used for AK-2292. ^{1}H NMR (400 MHz, DMSO) δ 11.00 (s, 1H), 8.48 (s, 1H), 8.33 (m, 1H), 8.17 (m, 1H), 8.02 (m, 1H), 7.75 – 7.46 (m, 7H), 7.34 (m, 2H), 5.14 (m, 1H), 4.74 (m, 1H), 4.45 (m, 2H), 4.31 (m, 1H), 4.08 (m, 1H), 3.77 (m, 2H), 2.89 (m, 2H), 2.60 – 2.53 (m, 3H), 2.36 – 2.22 (m, 2H), 2.12 – 1.88 (m, 3H), 1.75 (m, 4H), 1.07 (s, 9H). ESI−MS calculated for $C_{47}H_{48}BrF_2N_6O_{10}PS^+$ 1037.87, found $[M + H]^+$ 1037.00, 1039.43.

((2-(((2S)-1-((2S)-2-((4-Bromophenyl)(3-((6-(2-(2,6-dioxopiperidin-3-yl)-1-oxoisoindolin-4-yl)hex-5-yn-1-yl)amino)-3-oxopropyl)carbamoyl)pyrrolidin-1-yl)-3,3-dimethyl-1-oxobutan-2-yl)carbamoyl)benzo[b]thiophen-5-yl)difluoromethyl)phosphonic acid (24).

Compound **24** was synthesized using a procedure similar to that used for AK-2292. ^{1}H NMR (400 MHz, DMSO) δ 10.98 (s, 1H), 8.52 (s, 1H), 8.36 (d, *J* = 8.9 Hz, 1H), 8.12 (d, *J* = 8.4 Hz,

1H), 8.04 (s, 1H), 7.927.88 (m, 1H), 7.69 – 7.55 (m, 5H), 7.34 (d, *J* = 8.5 Hz, 2H), 5.14 (dd, *J* = 13.2, 5.2 Hz, 1H), 4.74 (d, *J* = 8.9 Hz, 1H), 4.47 – 4.42 (m, 1H), 4.33 – 4.28 (m, 1H), 4.09 (dd, *J* = 8.0, 5.8 Hz, 1H), 3.93 – 3.46 (m, 4H), 3.05 – 3.00 (m, 2H), 2.98 – 2.85 (m, 1H), 2.69 – 2.52 (m, 2H), 2.44 – 2.16 (m, 3H), 2.10 – 1.89 (m, 3H), 1.88 – 1.67 (m, 3H), 1.63 – 1.41 (m, 5H), 1.08 (s, 9H). ESI−MS calculated for $C_{49}H_{52}BrF_2N_6O_{10}PS^+$ 1065.92, found $[M + H]^+$ 1065.21, 1067.31.

((2-(((2S)-1-((2S)-2-((4-Bromophenyl)(3-((7-(2-(2,6-dioxopiperidin-3-yl)-1-oxoisoindolin-4-yl)hept-6-yn-1-yl)amino)-3-oxopropyl)carbamoyl)pyrrolidin-1-yl)-3,3-dimethyl-1-oxobutan-2-yl)carbamoyl)benzo[b]thiophen-5-yl)difluoromethyl)phosphonic acid (25).

Compound **25** was synthesized using a procedure similar to that used for AK-2292. ^{1}H NMR (400 MHz, DMSO) δ 10.97 (s, 1H), 8.52 (s, 1H), 8.36 (m, 1H), 8.12 (m, 1H), 8.04 (s, 1H), 7.87 (m, 1H), 7.72 – 7.49 (m, 5H), 7.34 (m, 2H), 5.14 (m, 1H), 4.74 (d, *J* = 8.9 Hz, 1H), 4.44 (m, 2H), 4.31 (m, 1H), 4.09 (m, 1H), 3.86 – 3.75 (m, 2H), 3.64 (m, 2H), 2.95 – 2.79 (m, 2H), 2.36 – 2.15 (m, 3H), 2.07 – 1.91 (m, 3H), 1.76 (m, 3H), 1.56 (m, 3H), 1.39 (m, 4H), 1.08 (s, 9H). ESI−MS calculated for $C_{50}H_{54}BrF_2N_6O_{10}PS^+$ 1079.95, found $[M + H]^+$ 1079.01, 1081.13.

((2-(((2S)-1-((2S)-2-((4-Bromophenyl)(3-(4-((2-(2,6-dioxopiperidin-3-yl)-1-oxoisoindolin-4-yl)ethynyl)piperidin-1-yl)-3-oxopropyl)carbamoyl)pyrrolidin-1-yl)-3,3-dimethyl-1-oxobutan-2-yl)carbamoyl)benzo[b]thiophen-5-yl)difluoromethyl)phosphonic acid (26).

Compound **26** was synthesized using a procedure similar to that used for AK-2292. ^{1}H NMR (400 MHz, DMSO) δ 11.00 (s, 1H), 8.48 (m, 1H), 8.37 (m, 1H), 8.02 (m, 2H), 7.74 – 7.52 (m, 6H), 7.40 (m, 2H), 5.13 (m, 1H), 4.75 (m, 1H), 4.52 – 4.38 (m, 2H), 4.32 (m, 2H), 4.10 (m, 1H), 3.76 (m, 4H), 2.97 (m, 2H), 2.13 – 1.91 (m, 5H), 1.81 (m, 5H), 1.57 (m, 4H), 1.08 (s, 9H). ESI−MS calculated for $C_{50}H_{52}BrF_2N_6O_{10}PS^+$ 1077.93, found $[M + H]^+$ 1077.24, 1077.15.

((2-(((2S)-1-((2S)-2-((4-Bromophenyl)(3-(3-(3-(2-(2,6-dioxopiperidin-3-yl)-1-oxoisoindolin-4-yl)prop-2-yn-1-yl)azetidin-1-yl)-3-oxopropyl)carbamoyl)pyrrolidin-1-yl)-3,3-dimethyl-1-oxobutan-2-yl)carbamoyl)benzo[b]thiophen-5-yl)difluoromethyl)phosphonic acid (27).

Compound **27** was synthesized using a procedure similar to that used for AK-2292. ^{1}H NMR (400 MHz, DMSO) δ 11.00 (s, 1H), 8.52 (d, *J* = 7.0 Hz, 1H), 8.39 (d, *J* = 8.6 Hz, 1H), 8.15 – 8.00 (m, 2H), 7.73 – 7.53 (m, 6H), 7.38 – 7.32 (m, 2H), 5.15 – 5.10 (m, 1H), 4.74 (dd, *J* = 8.9, 5.2 Hz, 1H), 4.51 – 4.37 (m, 2H), 4.30 – 4.17 (m, 2H), 4.13 – 4.05 (m, 2H), 3.80 – 3.75 (m, 3H), 3.68 – 3.60 (m, 2H), 2.85 – 2.70 (m, 3H), 2.38 – 2.19 (m, 3H), 2.12 – 1.92 (m, 3H), 1.77 – 1.72 (m, 4H), 1.06 (s, 9H). ESI−MS calculated for $C_{49}H_{50}BrF_2N_6O_{10}PS^+$ 1063.91, found $[M + H]^+$ 1062.93, 1064.34.

((2-(((2S)-1-((2S)-2-((4-Bromophenyl)(3-(3-(4-(2-(2,6-dioxopiperidin-3-yl)-1-oxoisoindolin-4-yl)but-3-yn-1-yl)azetidin-1-yl)-3-oxopropyl)carbamoyl)pyrrolidin-1-yl)-3,3-dimethyl-1-oxobutan-2-yl)carbamoyl)benzo[b]thiophen-5-yl)difluoromethyl)phosphonic acid (28).

Compound **28** was synthesized using a procedure similar to that used for AK-2292. ^{1}H NMR (400 MHz, DMSO) δ 10.99 (s, 1H), 8.52 (m, 1H), 8.37 (m, 1H), 8.14 – 7.99 (m, 2H), 7.72 – 7.51 (m, 6H), 7.37 (m, 2H), 5.22 – 5.09 (m, 1H), 4.73 (m, 1H), 4.45 (m, 2H), 4.31 (m, 1H), 4.21 – 4.04 (m, 2H), 3.90 (m, 2H), 3.64 (m, 2H), 3.00 – 2.84 (m, 2H), 2.73 – 2.53 (m, 4H), 2.28 (m, 2H), 2.10 – 1.93 (m, 3H), 1.91 – 1.65 (m, 5H), 1.07 (s, 9H). ESI−MS calculated for $C_{50}H_{52}BrF_2N_6O_{10}PS^+$ 1077.93, found $[M + H]^+$ 1076.97, 1078.83.

((2-(((2S)-1-((2S)-2-(Benzo[d]thiazol-5-yl(3-((5-(2-(2,6-dioxopiperidin-3-yl)-1-oxoisoindolin-4-yl)pent-4-yn-1-yl)amino)-3-oxopropyl)carbamoyl)pyrrolidin-1-yl)-3,3-dimethyl-1-oxobutan-2-yl)carbamoyl)benzo[b]thiophen-5-yl)difluoromethyl)phosphonic acid (30).

Compound **30** was synthesized using a procedure similar to that used for AK-2292. ^{1}H NMR

(400 MHz, DMSO) δ 10.97 (s, 1H), 9.43 (d, *J* = 2.4 Hz, 1H), 8.52 (d, *J* = 2.4 Hz, 1H), 8.41 (m, 1H), 8.23 (d, *J* = 8.4 Hz, 1H), 8.15 – 7.93 (m, 4H), 7.78 – 7.41 (m, 6H), 5.19 – 5.06 (m, 1H), 4.75 (m, 1H), 4.45 (m, 2H), 4.30 (m, 2H), 4.20 – 4.10 (m, 2H), 3.20 – 3.10 (m, 3H), 2.95 – 2.85 (s, 3H), 2.00 – 1.90 (m, 3H), 1.85 – 1.60 (m, 7H), 1.10 (s, 9H). ESI−MS calculated for $C_{49}H_{50}F_2N_7O_{10}PS_2^+$ 1030.07, found $[M + H]^+$ 1030.07.

((2-(((2S)-1-((2S)-2-(Benzo[d]thiazol-5-yl(3-((5-(2-(2,6-dioxopiperidin-3-yl)-1-oxoisoindolin-4-yl)pent-4-yn-1-yl)(methyl)amino)-3-oxopropyl)carbamoyl)pyrrolidin-1-yl)-3,3-dimethyl-1-oxobutan-2-yl)carbamoyl)benzo[b]thiophen-5-yl)difluoromethyl)phosphonic acid (31). Compound **31** was synthesized using a procedure similar to that used for **AK-2292**. ^{1}H NMR (400 MHz, DMSO) δ 10.98 (s, 1H), 9.43 (s, 1H), 8.53 (m, 1H), 8.44 (d, *J* = 8.3 Hz, 1H), 8.25 – 8.16 (m, 2H), 8.11 (d, *J* = 8.6 Hz, 1H), 8.03 (s, 1H), 7.75 – 7.65 (m, 2H), 7.58 – 7.49 (m, 3H), 5.18 – 5.05 (m, 1H), 4.75 (m, 1H), 4.53 – 4.43 (m, 1H), 4.36 – 4.29 (m, 1H), 4.13 (m, 1H), 3.85 (m, 2H), 3.78 – 3.72 (m, 1H), 3.65 (d, *J* = 8.1 Hz, 1H), 3.47 – 3.32 (m, 3H), 3.03 – 2.91 (m, 3H), 2.80 – 2.61 (m, 4H), 1.22 – 1.95 (d, *J* = 5.4 Hz, 3H), 1.87 – 1.60 (m, 6H), 1.10 (s, 9H). ESI−MS calculated for $C_{50}H_{52}F_2N_7O_{10}PS_2^+$ 1044.10, found $[M + H]^+$ 1044.32.

Synthesis of ((2-(((2S)-1-((2S)-2-((3-((5-(2-(2,6-dioxopiperidin-3-yl)-1-oxoisoindolin-4-yl)pent-4-yn-1-yl)amino)-3-oxopropyl)(naphthalen-2-yl)carbamoyl)pyrrolidin-1-yl)-3,3-dimethyl-1-oxobutan-2-yl)carbamoyl)benzo[b]thiophen-5-yl)difluoromethyl)phosphonic acid (32). Compound **32** was synthesized by employing a similar procedure for AK-2292. ^{1}H NMR (400 MHz, DMSO) δ 10.97 (s, 1H), 8.51 (s, 1H), 8.38 (d, *J* = 9.0 Hz, 1H), 8.10 (dd, *J* = 9.2, 5.2 Hz, 1H), 8.03 (s, 1H), 8.00 – 7.85 (m, 5H), 7.72 – 7.65 (m, 1H), 7.63 – 7.48 (m, 6H), 5.12 (dd, *J* = 13.3, 5.3 Hz, 1H), 4.74 (d, *J* = 9.0 Hz, 1H), 4.44 (dd, *J* = 17.9, 4.1 Hz, 2H), 4.29 (d, *J* = 17.8 Hz, 1H), 4.17 – 4.12 (m, 1H), 3.99 – 3.92 (m, 1H), 3.76 – 3.70 (m, 3H), 3.66 – 3.60 (m,

1H), 2.92 – 2.87 (m, 2H), 2.40 – 2.17 (m, 3H), 2.03 – 1.76 (m, 5H), 1.76 – 1.54 (m, 4H), 1.10 (s, 9H). ESI−MS calculated for $C_{52}H_{53}F_2N_6O_{10}PS^+$ 1023.06, found $[M + H]^+$ 1023.00.

((2-(((2S)-1-((2S)-2-((3-((5-(2-(2,6-Dioxopiperidin-3-yl)-1-oxoisoindolin-4-yl)pent-4-yn-1-yl)(methyl)amino)-3-oxopropyl)(naphthalen-2-yl)carbamoyl)pyrrolidin-1-yl)-3,3-dimethyl-1-oxobutan-2-yl)carbamoyl)benzo[b]thiophen-5-yl)difluoromethyl)phosphonic acid (33).

Compound **33** was synthesized using a procedure similar to that used for AK-2292. ^{1}H NMR (400 MHz, DMSO) δ 10.98 (s, 1H), 8.52 (d, *J* = 5.0 Hz, 1H), 8.42 (d, *J* = 8.5 Hz, 1H), 8.10 (d, *J* = 8.4 Hz, 1H), 8.03 (s, 1H), 8.00 – 7.84 (m, 4H), 7.72 – 7.66 (m, 1H), 7.64 – 7.46 (m, 7H), 5.19 – 5.08 (m, 1H), 4.77 – 4.72 (m, 1H), 4.50 – 4.41 (m, 1H), 4.34 – 4.30 (m, 1H), 4.16 – 4.10 (m, 1H), 3.98 – 3.72 (m, 4H), 3.66 – 3.62 (m, 1H), 3.48 – 3.32 (m, 3H), 2.97 (s, 3H), 2.43 – 2.38 (m, 2H), 2.07 – 1.50 (m, 10H), 1.10 (s, 9H). ESI−MS calculated for $C_{53}H_{55}F_2N_6O_{10}PS^+$ 1037.09, found $[M + H]^+$ 1037.40.

((2-(((2S)-1-((2S)-2-((9-(2-(2,6-dioxopiperidin-3-yl)-1-oxoisoindolin-4-yl)non-8-yn-1-yl)(4-(thiazol-2-yl)phenyl)carbamoyl)pyrrolidin-1-yl)-3,3-dimethyl-1-oxobutan-2-yl)carbamoyl)benzo[b]thiophen-5-yl)difluoromethyl)phosphonic acid (29)

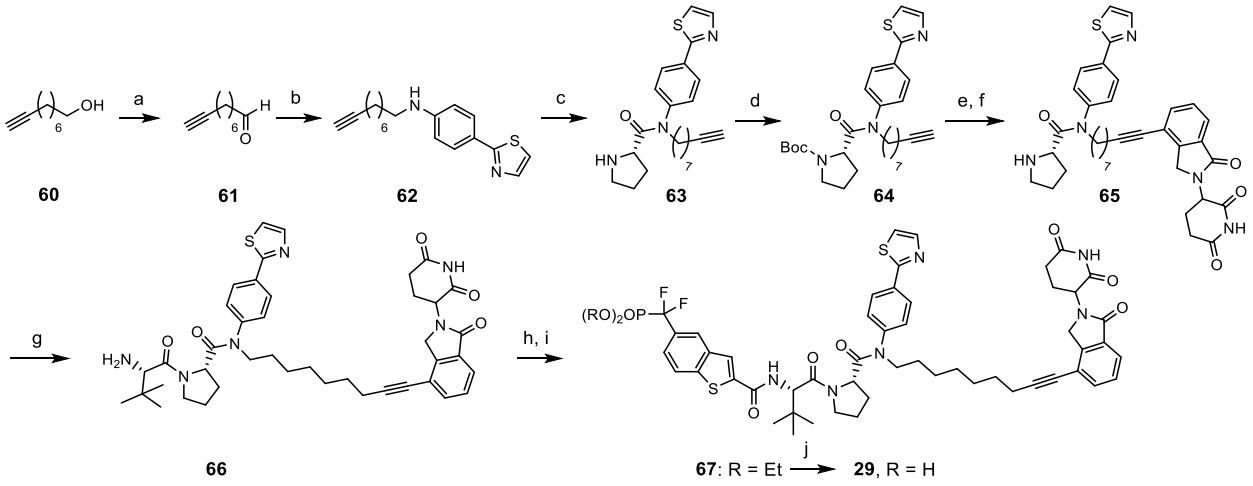

Figure 2-5 Synthesis of ((2-(((2S)-1-((2S)-2-((9-(2-(2,6-dioxopiperidin-3-yl)-1-oxoisoindolin-4-yl)non-8-yn-1-yl)(4-(thiazol-2-yl)phenyl)carbamoyl)pyrrolidin-1-yl)-3,3-dimethyl-1-oxobutan-2-yl)carbamoyl)benzo[b]thiophen-5-yl)difluoromethyl)phosphonic acid (29)

Reaction conditions: (a) IBX, DCM, rt; (b) $NaB(OAc)_3$, AcOH, DCM, rt; (c) PCl_5, $CHCl_3$, 50 °C; (d) Boc_2O, TEA, CH3CN, rt; (e) $PdCl_2(PPh_3)_2$, CuI, TEA/DMF, 90 °C; (f) TFA, DCM, rt; (g) HATU, DIPEA, DMF, rt; (h) TFA, DCM, rt; (i) HATU, DIPEA, DMF, rt; (j) TMSI, BSTFA, DCM, rt, 0 °C

To **60** (1 g, 7.13 mmol) in DCM (20 ml), Dess-martin periodinane (3 g, 1 equiv.) was added. The mixture was stirred at room temperature for 30 min. White precipitates were formed. Celite was added to the reaction mixture and the mixture was concentrated in vacuum. Then, after the purification by flash column chromatography, **61** was obtained as colorless oil in 70% yield (700 mg). ^{1}H NMR (400 MHz, DMSO) δ 9.66 (s, 1H), 2.76 – 2.69 (m, 1H), 2.24 – 2.05 (m, 4H), 1.52 – 1.21 (m, 8H). ESI−MS calculated for $C_9H_{14}O^+$ 138.21, found $[M + H]^+$ 139.31.

To **61** (200 mg, 1.4 mmol) in DCM (5 ml), 4-(thiazol-2-yl)aniline (1 equiv.), NaB(OAc)3 (2 equiv.), and AcOH (1 equiv.) were added and the mixture was stirred for 30 minutes at room temperature. Water and ethanol were added to the mixture and the mixture was concentrated in vacuum. The purification by HPLC gave **62** in 92% (400 mg). ^{1}H NMR (400 MHz, DMSO) δ 7.75 (d, *J* = 3.3 Hz, 1H), 7.70 – 7.61 (m, 2H), 7.53 (d, *J* = 3.3 Hz, 1H), 6.64 (d, *J* = 8.8 Hz, 2H), 3.06 (t, *J* = 7.0 Hz, 2H), 2.73 (t, *J* = 2.7 Hz, 1H), 2.15 (td, *J* = 6.9, 2.7 Hz, 2H), 1.55 (t, *J* = 6.9 Hz, 2H), 1.48 – 1.10 (m, 8H). ESI−MS calculated for $C_{18}H_{22}N_2S^+$ 298.45, found $[M + H]^+$ 299.01.

Boc-L-proline (1.8 g, 5 equiv.) was dissolved in $CHCl_3$ (20 ml). At room temperature, PCl_5 (1.7 g, 5 equiv.) was slowly added over a period of 10 min. After the addition, the mixture was stirred for 10 min at room temperature. To this mixture was added **62** (400 mg, 1.3 mmol) and the mixture was stirred at 50°C for 20 min. The volatile components were removed on a rotary evaporator. The obtained crude oil was purified by reverse phase semi-preparative HPLC

to give **63** as TFA salt in 60% (420 mg). ^{1}H NMR (400 MHz, DMSO) δ 8.10 (d, *J* = 8.5 Hz, 2H), 7.99 (d, *J* = 3.2 Hz, 1H), 7.87 (d, *J* = 3.2 Hz, 1H), 7.53 (d, *J* = 8.5 Hz, 2H), 4.06 (t, *J* = 7.6 Hz, 1H), 3.86 – 3.80 (m, 1H), 3.66 – 3.58 (m, 1H), 3.23 – 3.18 (m, 2H), 3.13 – 3.02 (m, 1H), 2.15 – 2.07 (m, 2H), 1.98 – 1.93 (m, 1H), 1.87 – 1.61 (m, 4H), 1.57 – 1.37 (m, 4H), 1.35 – 1.20 (d, *J* = 18.1 Hz, 5H). ESI−MS calculated for $C_{23}H_{29}N_3OS^+$ 395.57, found $[M + H]^+$ 396.25.

63 (420 mg, 0.82 mmol) was dissolved in CH_3CN (8 ml). To the solution was added triethylamine (350 µl, 3 equiv.), followed by Boc_2O (260 mg, 1.5 equiv.). The colorless mixture was stirred for 2 hours at room temperature. The volatile components were then removed by vacuum and the crude was purified by flash column chromatography to yield **64** in 56% (230 mg). ^{1}H NMR (400 MHz, DMSO) δ 8.08 (d, *J* = 8.5 Hz, 2H), 7.98 – 7.94 (m, 1H), 7.86 – 7.82 (m, 1H), 7.41 (d, *J* = 8.5 Hz, 2H), 4.04 (dd, *J* = 7.3, 5.1 Hz, 1H), 3.86 – 3.72 (m, 1H), 3.72 – 3.62 (m, 1H), 3.61 – 3.46 (m, 1H), 3.38 – 3.34 (m, 1H), 2.71 – 2.69 (m, 1H), 2.14 – 2.10 (m, 2H), 1.91 – 1.71 (m, 3H), 1.66 – 1.62 (m, 1H), 1.45 – 1.39 (m, 13H), 1.30 – 1.08 (m, 6H).). ESI−MS calculated for $C_{28}H_{37}N_3O_3S^+$ 495.68, found $[M + H]^+$ 396.10.

Triethylamine (1.5 ml) was added to a mixture of **16** (323 mg, 1 mmol, 1 equiv.), **64** (230 mg, 0.46 mmol, 1 equiv.), CuI (35 mg, 0.4 equiv.), and $Pd(PPh_3)_2Cl_2$ (65 mg, 0.2 equiv.) in DMF (1.5 ml). The resulting mixture was purged and refilled with argon three times and stirred at 90°C for 1.5 hours under argon. The reaction mixture was cooled to room temperature. The mixture was filtered through celite and evaporated to remove most of the solvent. The residue was purified by HPLC to yield Boc-protected **65**. The Boc-protected **65** was dissolved in DCM (5 ml), and TFA (5 ml) was added to remove Boc protection. The mixture was stirred at room temperature for 10 min. Most of the volatile components were removed in vacuum and the residue was purified by HPLC to yield **65** as TFA salt in 43% (150 mg). ^{1}H NMR (400 MHz,

DMSO) δ 10.98 (s, 1H), 8.19 – 8.04 (m, 2H), 8.56 – 8.49 (m, 1H), 8.11 – 8.04 (m, 1H), 7.98 (d, *J* = 3.2 Hz, 1H), 7.87 (d, *J* = 3.2 Hz, 1H), 7.70 (d, *J* = 7.6 Hz, 1H), 7.61 (d, *J* = 7.6 Hz, 1H), 7.55 – 7.36 (m, 3H), 5.18 – 5.12 (m, 1H), 4.43 (d, *J* = 17.6 Hz, 1H), 4.29 (d, *J* = 17.7 Hz, 1H), 4.08 – 4.04 (m, 1H), 3.90 – 3.71 (m, 2H), 3.65 – 3.58 (m, 1H), 3.23 – 3.17 (m, 2H), 3.11 – 3.07 (m, 1H), 2.95 – 2.78 (m, 1H), 2.45 – 2.36 (m, 2H), 2.11 – 1.90 (m, 2H), 1.86 – 1.62 (m, 4H), 1.60 – 0.95 (m, 10H). ESI−MS calculated for $C_{36}H_{39}N_5O_4S^+$ 637.80, found $[M + H]^+$ 638.25.

To **65** (75 mg, 0.1 mmol, 1 equiv.), CH_3CN (5 ml), triethylamine (70 µl, 5 equiv.), Boc-L-*tert*-leucine (45 mg, 2 equiv.), and HATU (80 mg, 2 equiv.) were added. The mixture was stirred at room temperature for 30 min. The yellow solution was concentrated in vacuum and the crude was purified by flash column chromatography to yield Boc-protected **66**. Boc protection was removed by DCM/TFA at room temperature for 30 min. The volatile components were removed in vacuum to yield **66** as a TFA salt in 57% (50 mg).

To **66** (25 mg, 0.03 mmol), DMF (3 ml), triethylamine (70 µl), benzothiophene **39** (13 mg, 1.2 equiv.), and HATU (15 mg, 1.2 equiv.) were added. The mixture was stirred at room temperature for 30 min. The yellow solution was purified by HPLC to yield **67** in 93% (30 mg) To a round bottom flask were added **67** (30 mg, 0.027 mmol, 1 equiv.), DCM (2 ml) and $CF_3CON(TMS)_2$ (45 µl, 6 equiv.). The solution was cooled in an ice bath. To the ice cooled reaction mixture, 1M of TMS-I in DCM (0.14 ml, 5 equiv.) was added dropwise and the mixture was stirred for 10 min in an ice bath. The volatile components were removed under vacuum at below 5°C. The residue was dissolved in a mixed solvent of CH_3CN (3 ml) and water (1 ml). The resulting solution was purified by HPLC to yield **29** in 83% (23 mg). ^{1}H NMR (400 MHz, DMSO) δ 10.99 (s, 1H), 8.53 (s, 1H), 8.41 (d, *J* = 9.0 Hz, 1H), 8.11 (d, *J* = 8.5 Hz, 1H), 8.06 – 7.97 (m, 3H), 7.92 (d, *J* = 3.2 Hz, 1H), 7.79 (d, *J* = 3.2 Hz, 1H), 7.70 – 7.48 (m, 6H), 5.14 (m,

1H), 4.75 (m, 1H), 4.51 – 4.36 (m, 2H), 4.30 (m, 1H), 4.20 (m, 1H), 3.94 – 3.72 (m, 2H), 3.64 (m, 1H), 3.48 (m, 1H), 2.90 (m, 1H), 2.59 (m, 1H), 2.26 (m, 1H), 2.09 – 1.92 (m, 2H), 1.86 (m, 1H), 1.81 – 1.64 (m, 2H), 1.70 – 1.50 (m, 2H), 1.40 – 1.25 (m, 8H), 1.08 (s, 9H). ESI−MS calculated for $C_{52}H_{55}F_2N_6O_9PS_2^+$ 1041.14, found $[M + H]^+$ 1041.33.

((2-(((S)-1-((S)-2-((4-bromophenyl)(3-((8-(3-(3',6'-dihydroxy-3-oxo-3H-spiro[isobenzo-furan-1,9'-xanthen]-5-yl)thioureido)octyl)amino)-3-oxopropyl)carbamoyl)pyrrolidin-1-yl)-3,3-dimethyl-1-oxobutan-2-yl)carbamoyl)benzo[b]thiophen-5-yl)difluoromethyl)-phosphonic acid (AK-330FL).

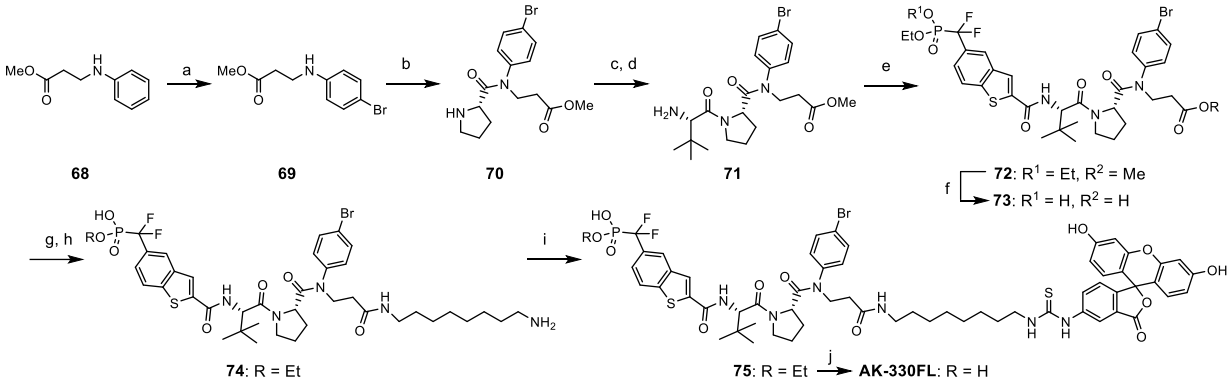

Figure 2-6 Synthesis of AK-330FL

Reaction conditions: (a) NBS, CH_3CN, rt; (b) PCl_5, $CHCl_3$, 50 °C; (c) HATU, DIPEA, DMF, rt; (d) TFA, DCM, rt; (e) HATU, DIPEA, DMF, rt; (f) LiOH, MeOH, water, rt; (g) HATU, DIPEA, DMF, rt; (h) TFA, DCM, rt; (i) DIPEA, DMF, rt; (j) TMSI, BSTFA, DCM, rt, 0 °C

68 (520 mg, 2.9 mmol, 1 equiv.), CH_3CN (5 ml) and NBS (520 mg, 1 equiv.) were added to a round bottom flask. The solution was stirred at rt for 10 min. then the volatile components were removed under vacuum. H_2O and EtOAc were added to the residue and a normal workup was performed. After the volatile components were removed under vacuum, **69** was obtained as white solid in 80% (598 mg). ^{1}H NMR (400 MHz, DMSO) δ 7.19 (d, *J* = 8.8 Hz, 2H), 6.52 (d, *J*

= 8.9 Hz, 2H), 5.86 (t, *J* = 5.8 Hz, 1H), 3.60 (s, 3H), 3.28 – 3.23 (m, 2H), 2.56 (t, *J* = 6.7 Hz, 2H). ESI−MS calculated for $C_{10}H_{12}BrNO_2^+$ 258.12, found $[M + H]^+$ 258.21, 260.12.

Boc-L-proline (1.6 g, 5 equiv.) was dissolved in $CHCl_3$ (10 ml). PCl_5 (1.5 g, 5 equiv.) was slowly added at rt over a period of 10 min. After the addition, the mixture was stirred for 10 min at rt. **69** (390 mg, 1.5 mmol) was added to this mixture and the mixture was stirred at 50 °C for 20 min. The volatile components were removed on a rotary evaporator. The obtained crude oil was purified by HPLC to yield **70** as TFA salt in 60% yield (420 mg). ^{1}H NMR (400 MHz, DMSO) δ 7.81 – 7.68 (m, 2H), 7.41 – 7.35 (m, 2H), 4.02 – 3.78 (m, 3H), 3.53 (s, 3H), 3.22 – 3.13 (m, 1H), 3.08 – 3.02 (m, 1H), 2.56 – 2.53 (m, 1H), 2.45 – 2.40 (m, 1H), 1.80 – 1.70 (m, 5H). ESI−MS calculated for $C_{15}H_{19}BrN_2O_3^+$ 355.23, found $[M + H]^+$ 355.17, 357.17.

CH_3CN (5 ml), Et3N (0.45 ml, 5 equiv.), Boc-L-*tert*-leucine (170 mg, 1.5 equiv.), and HATU (230 mg, 1.2 equiv.) were added to this TFA salt (**70)** (230 mg, 0.49 mmol). The mixture was stirred at rt for 30 min. The yellow solution was concentrated in vacuum and the crude was purified by flash column chromatography to yield Boc-protected **71**. Boc protection was removed by DCM/TFA at rt for 30 min. The volatile components were removed in vacuum to yield **63** as a TFA salt in 85% (240 mg). ^{1}H NMR (400 MHz, DMSO) δ 7.98 (s, 2H), 7.80 – 7.59 (m, 2H), 7.48 – 7.26 (m, 2H), 4.09 – 4.03 (m, 1H), 4.00 – 3.88 (m, 1H), 3.80 – 3.60 (m, 5H), 3.57 – 3.37 (m, 2H), 2.45 – 2.40 (m, 2H), 2.02 – 1.47 (m, 4H), 1.05 (s, 9H). ESI−MS calculated for $C_{21}H_{30}BrN_3O_4^+$ 468.39, found $[M + H]^+$ 468.32, 470.31.

CH_3CN (5 ml), Et_3N (0.13 ml, 5 equiv.), **39** (70 mg, 1.1 equiv.), and HATU (75 mg, 1.1 equiv.) were added to the TFA salt (**71**) salt (110 mg, 0.19 mmol). The mixture was stirred at rt for 30 min. The yellow solution was concentrated in vacuum and the crude was purified by flash column chromatography to yield **72** in 75% (116 mg). ^{1}H NMR (400 MHz, DMSO) δ 8.54 (s,

1H), 8.47 (dd, *J* = 9.0, 2.1 Hz, 1H), 8.19 (d, *J* = 8.5 Hz, 1H), 8.10 (s, 1H), 7.75 – 7.57 (m, 3H), 7.37 (dd, *J* = 8.6, 2.2 Hz, 2H), 4.75 (d, *J* = 8.9 Hz, 1H), 4.29 – 4.06 (m, 6H), 3.91 – 3.71 (m, 3H), 3.66 – 3.62 (m, 1H), 3.52 (s,32H), 2.46 – 2.33 (m, 1H), 2.00 – 1.95 (m, 1H), 1.91 – 1.62 (m, 3H), 1.25 – 1.20 (m, 6H), 1.08 (s, 9H). ESI−MS calculated for $C_{35}H_{43}BrF_2N_3O_8PS^+$ 814.68, found $[M + H]^+$ 814.19, 816.16.

72 (150 mg, 0.18 mmol) was dissolved in MeOH (5 ml) and water (1 ml) and the mixture was placed in an ice bath. LiOH monohydrate (60 mg, 8 equiv.) was added to the mixture which was then stirred for 1 h at rt. The mixture was placed in an ice bath again and neutralized by slowly adding TFA. The volatile components were removed on a rotary evaporator and the residue was purified by flash column chromatography to yield **73** in 70% yield (100 mg). ^{1}H NMR (400 MHz, DMSO) δ 8.52 (s, 1H), 8.42 (d, *J* = 8.9 Hz, 1H), 8.12 (d, *J* = 8.5 Hz, 1H), 8.05 (s, 1H), 7.76 – 7.55 (m, 3H), 7.44 – 7.30 (m, 2H), 4.75 (d, *J* = 9.0 Hz, 1H), 4.09 (t, *J* = 7.1 Hz, 1H), 4.02 – 3.97 (m, 2H), 3.78 (t, *J* = 7.4 Hz, 3H), 3.66 – 3.62 (m, 1H), 2.46 – 2.35 (m, 2H), 1.99 – 1.95 (m, 1H), 1.89 – 1.67 (m, 3H), 1.18 (t, *J* = 7.1 Hz, 3H), 1.08 (s, 9H). ESI−MS calculated for $C_{32}H_{37}BrF_2N_3O_8PS^+$ 772.60, found $[M + H]^+$ 771.32, 773.53.

DMF (2 ml), DIPEA (30 µl, 6 equiv.), 1-Boc-1,8-diaminooctane (10 mg, 1.5 equiv.), and HATU (12 mg, 1.1 equiv.) were added to **73** (20 mg, 0.026 mmol). The mixture was stirred at rt for 30 min. The yellow solution was purified by HPLC to yield Boc-protected **74**. Boc protection was removed by DCM/TFA at rt for 30 min. The volatile components were removed in vacuum to yield **74** as a TFA salt in 80% yield (20 mg). **74** (10 mg), DMF (1 ml), fluorescein 5-isothiocyanate (5 mg), and DIPEA (10 µl) were mixed at rt for 30 min. The mixture was purified by HPLC to yield **75** in 75% yield (10 mg). To a round bottom flask were added **75** (10 mg, 8 µmol, 1 equiv.), DCM (2 ml), and $CF_3CON(TMS)_2$ (12 µl, 6 equiv.). The solution was cooled in

an ice bath. To the ice cooled reaction mixture, 1M of trimethylsilyl iodide in DCM (40 µl, 5 equiv.) was added dropwise and the mixture was stirred for 10 min in an ice bath. The volatile components were removed under vacuum at below 5°C. The residue was dissolved in a mixed solvent of CH_3CN (3 ml) and H_2O (1 ml). The resulting solution was purified by HPLC to yield **AK-330FL** in 83% yield (8 mg). ^{1}H NMR (400 MHz, DMSO-d_6) δ 10.11 (s, 2H), 8.49 – 8.45 (m, 2H), 8.16 – 8.12 (m, 2H), 7.95 (s, 1H), 7.83 – 7.73 (m, 2H), 7.65 – 7.58 (m, 2H), 7.38 – 7.30 (m, 2H), 6.65 – 6.49 (m, 9H), 4.75 (s, 1H), 4.11 – 4.03 (m, 2H), 3.78 – 3.60 (d, J = 50.5 Hz, 6H), 2.98 – 2.92 (m, 2H), 2.40 – 2.30 (m, 2H), 1.99 – 1.87 (m, 2H), 1.80 – 1.70 (m, 2H), 1.50 – 0.93 (m, 21H). ESI−MS calculated for $C_{59}H_{62}BrF_2N_6O_{12}PS_2^+$ 1260.17, found $[M + H]^+$ 630.31.

((2-(((5S,8S,10aR)-8-(((S)-5-Amino-1-(((S)-1-cyclohexyl-2-(4-((12-(3',6'-dihydroxy-3-oxo-3H-spiro[isobenzofuran-1,9'-xanthene]-5-carboxamido)dodecyl)carbamoyl)piperidin-1-yl)-2-oxoethyl)amino)-1,5-dioxopentan-2-yl)carbamoyl)-3-(methoxycarbonyl)-6-oxodecahydropyrrolo[1,2-a][1,5]diazocin-5-yl)carbamoyl)benzo[b]thiophen-5-yl)difluoromethyl)phosphonic acid (AK-1153FL).

AK-1153FL was synthesized using a previously described procedure [37]. ^{1}H NMR (400 MHz, DMSO) δ 10.14 (s, 2H), 8.96 – 8.90 (m, 2H), 8.78 (s, 1H), 8.44 (s, 1H), 8.25 – 8.17 (m, 2H), 7.77 (s, 2H), 7.43 – 7.33 (m, 2H), 7.21 – 7.16 (m, 2H), 6.70 – 6.65 (m, 2H), 6.60 – 6.47 (m, 6H), 4.88 (s, 1H), 4.62 – 4.56 (m, 1H), 4.41 – 4.32 (m, 2H), 4.25 – 4.11 (m, 4H), 4.06 (s, 3H), 3.84 – 3.80 (m, 2H), 3.68 – 3.62 (m, 3H), 3.05 – 2.98 (m, 2H), 2.78 – 2.70 (m, 1H), 2.72 – 2.67 (m, 2H), 2.10 – 2.00 (m, 10H), 1.76 – 1.44 (m, 13H), 1.26 – 1.18 (m, 14H), 1.15 – 1.08 (m, 7H). ESI−MS calculated for $C_{74}H_{90}F_2N_9O_{18}PS^+$ 1494.61, found $[M + H]^+$ 748.23.

2.8 Main Figures

2.8.1 Fig. 1. Structure-guided Design of STAT5 SH2 Domain Inhibitors and PROTAC Degraders

A. Design of STAT5 inhibitors.

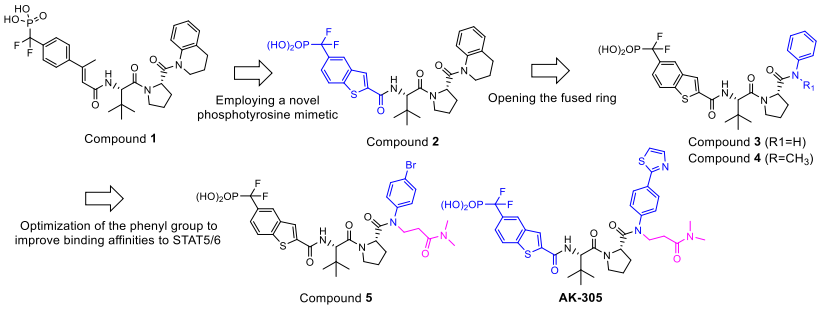

B. Design of PROTAC STAT5 degraders.

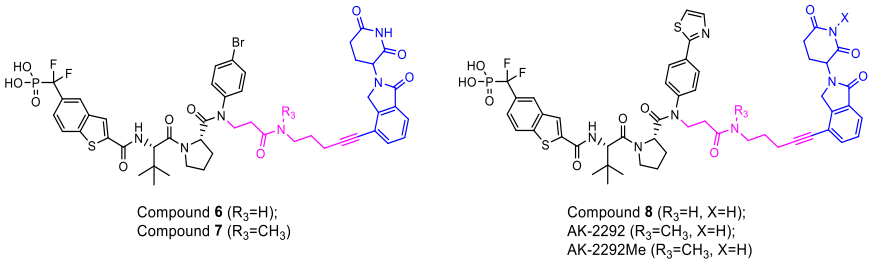

C. and D. Co-crystal structures of AK-305 (PDB: 7TVB) and AK-2292 (PDB: 7TVA) in complex with STAT5A

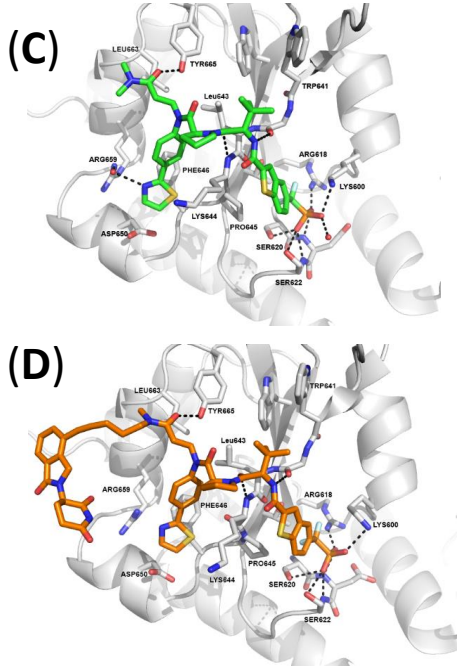

Figure 2-7 Fig. 1. Structure-guided Design of STAT5 SH2 Domain Inhibitors and PROTAC Degraders

Fig. 1. Structure-guided Design of STAT5 SH2 Domain Inhibitors and PROTAC Degraders

(A) Design of STAT5 SH2 domain inhibitors. (B) Design of PROTAC STAT5 degraders. (C) Co-crystal structure of AK-305, a STAT5/6 SH2 domain inhibitor, in complex with STAT5A. (D) Co-crystal structures of AK-2292, a STAT5 PROTAC degrader, in complex with STAT5A.

See also Extended Data Fig. 1.

2.8.2 Fig. 2. Determination of AK2292 as a Potent and Selective STAT5A/B PROTAC Degrader

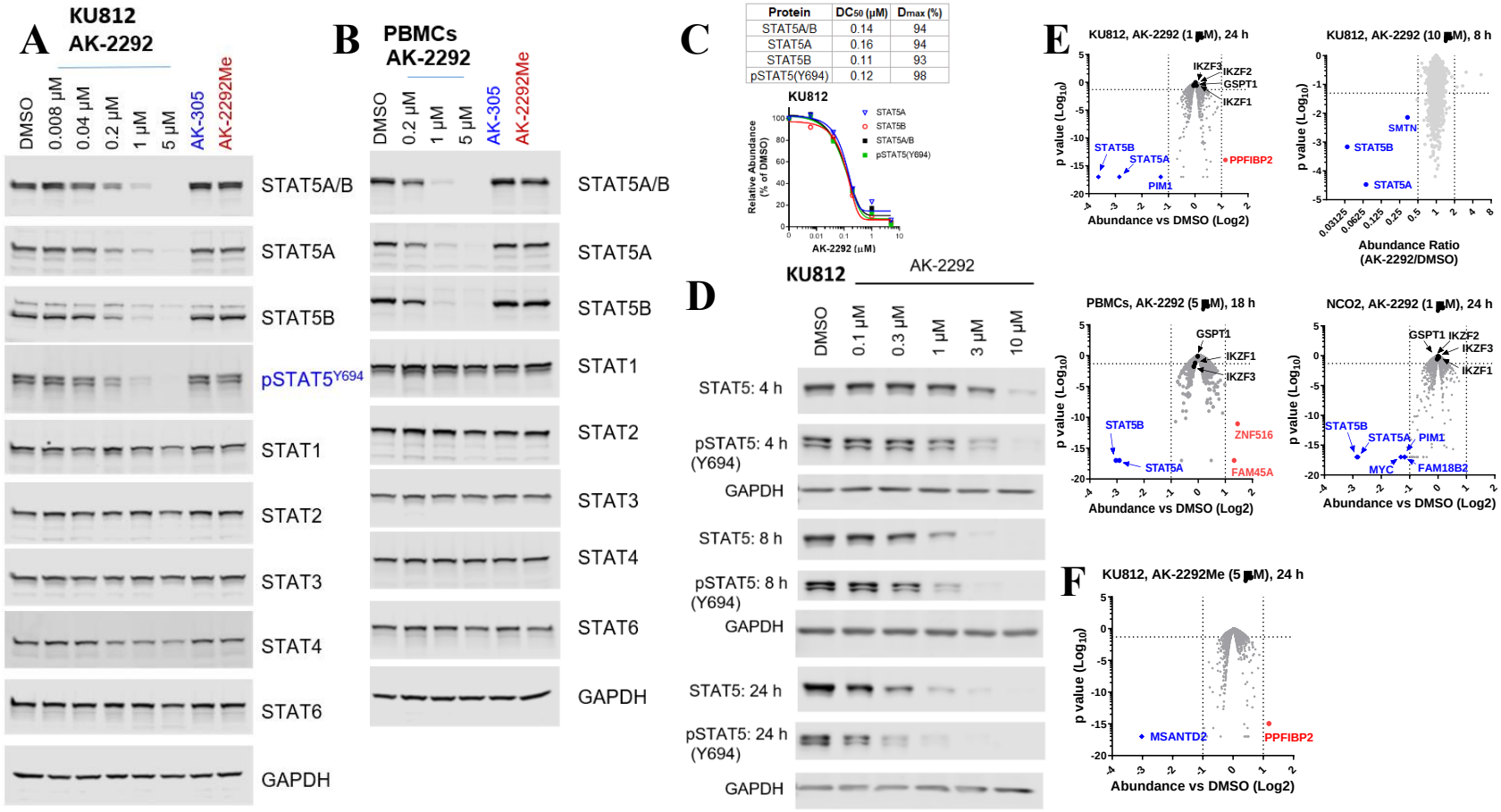

Figure 2-8 Fig. 2. Determination of AK2292 as a Potent and Selective STAT5A/B PROTAC Degrader

Fig. 2. Determination of AK2292 as a Potent and Selective STAT5A/B PROTAC Degrader

(A) Immunoblot analysis of KU812 cells treated with AK-2292, 5 μM of AK-305 or AK-2292Me for 18 hr. Data represent *n* = 3 independent experiments. (B) Immunoblot analysis of PBMC cells treated with AK-2292, 5 μM of AK-305 or AK-2292Me for 18 hr. Data represent *n* = 3 independent experiments. (C) DC_{50} values of AK-2292 for STAT5, STAT5A, STAT5B, and $pSTAT5^{Y694}$ treated with AK-2292 for 18 hr with 5 μM as the highest concentration. Data represent *n* = 3 independent experiments. (D) Immunoblot analysis of KU812 cells treated with AK-2292 under indicated concentrations and treatment durations. Data represent *n* = 2 independent experiments. (E) Cells were treated with AK-2292 under indicated concentrations and treatment durations for multiplexed quantitative proteomics analysis. P-value: Student's t-test. KU812 (>6,800 quantified proteins), PBMCs (>6,640 quantified proteins), NCO2 (>6,800 quantified proteins). Each experiment was performed in triplicate. (F) KU812 cells were treated with AK2292Me under indicated concentrations and treatment durations for multiplexed quantitative proteomics analysis. P-value: Student's t-test. KU812 (>6,800 quantified proteins). The experiment was performed in triplicate.

See also Extended Data Fig. 2.

2.8.3 Fig. 3. Transcriptomic Analysis of AK2292 in Cells

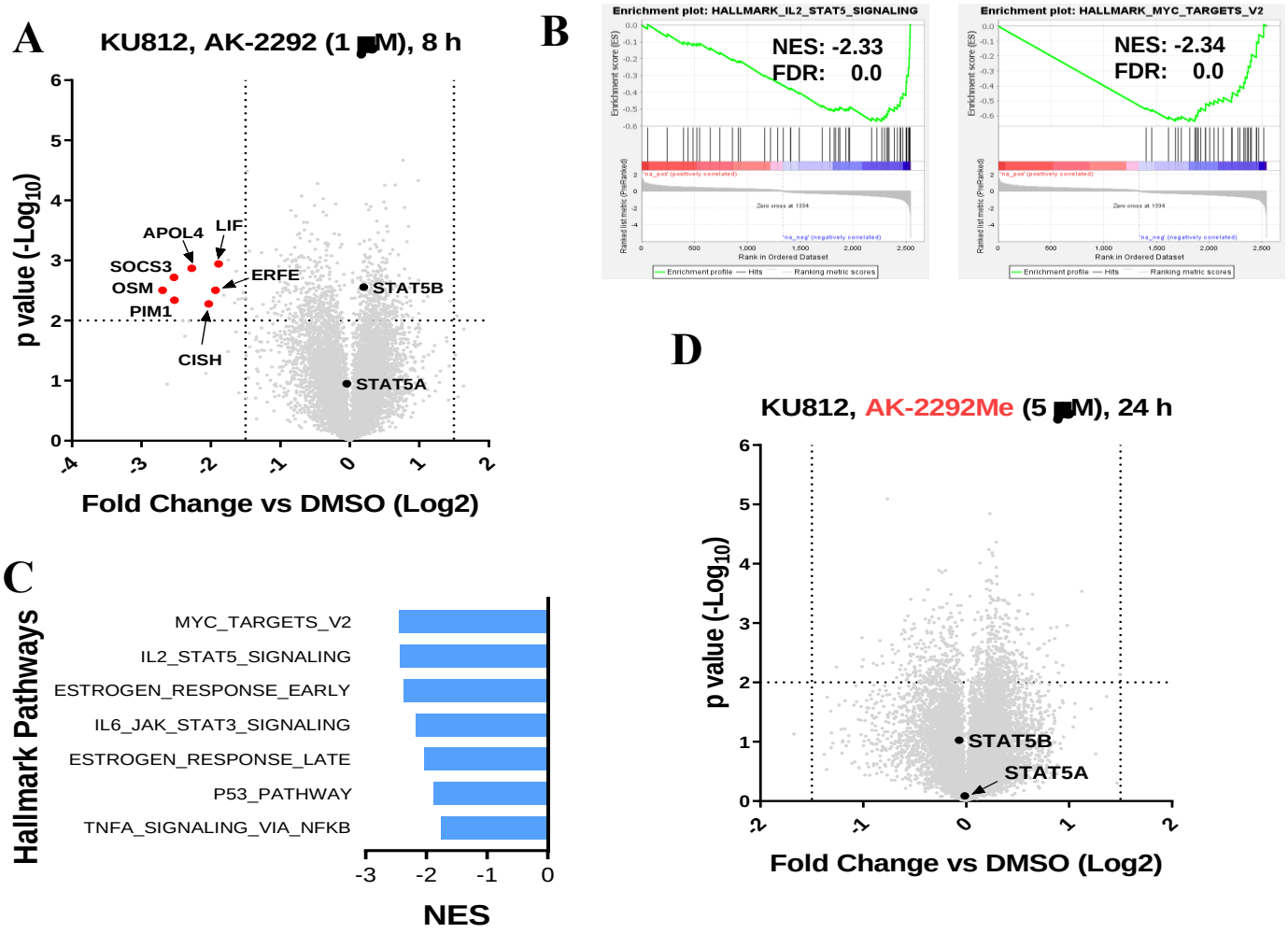

Figure 2-9 Fig. 3. Transcriptomic Analysis of AK2292 in Cells

Fig. 3. Transcriptomic Analysis of AK2292 in Cells

(A) KU812 cells were treated with 1 μM of AK-2292 for 8 hr for RNA-seq analysis. The experiment was performed in triplicate. (B) GSEA indicated that genes that are up-regulated by STAT5 upon IL2 stimulation and a subset of genes regulated by Myc are the two most down-regulated in KU812 cells treated with 1 μM of AK-2292 for 8 hr . NES: normalized enrichment score. (C) Down-regulated hallmark pathways in KU812 cells treated with 1 μM of AK-2292 for 8 hr in GSEA. (D) KU812 cells were treated with 5 μM of AK2292Me for 24 hr for RNA-seq analysis. The experiment was performed in triplicate.

See also Extended Data Fig. 3.

2.8.4 Fig. 4. Cell Growth Inhibitory Activity of AK2292 in Human CML Cell Lines

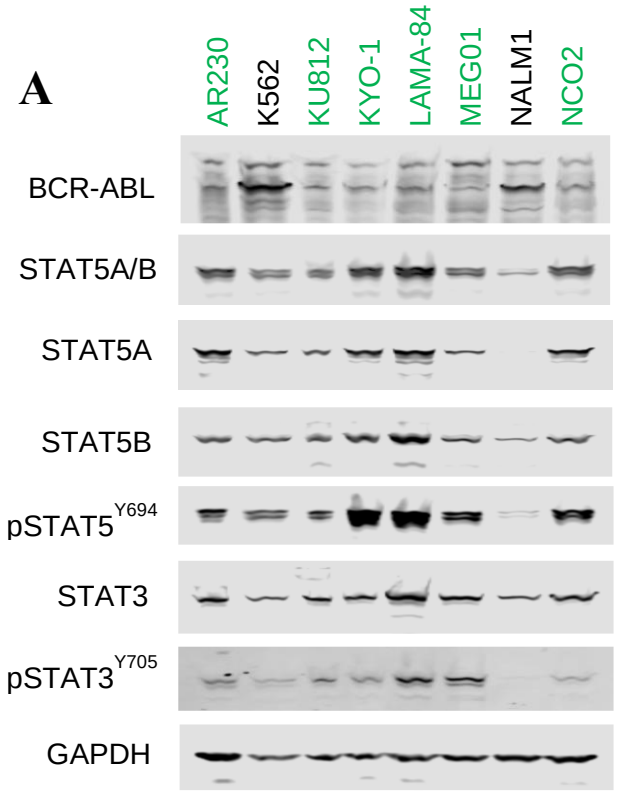

B

Cell Line	Type	IC_{50} (uM)	Imax (%)	DC_{50} (μM)		Dmax (%)	
				STAT5A/B	pSTAT5	STAT5A/B	pSTAT5
AR230	CML	0.60	>95	0.11	0.15	>95	>95
K562	CML	~15	50%	0.33	0.39	>95	>95
KU812	CML	0.30	>95	0.15	0.15	>95	>95
KYO-1	CML	2.18	>95	0.61	0.82	>95	>95
LAMA-84	CML	1.36	>95	0.45	0.35	>95	>95
MEG01	CML	1.80	>95	0.13	0.20	>95	93
NALM1	CML	>15	Inactive	0.53	low pSTAT5	98	N/A
NCO2	CML	0.20	>95	0.27	0.23	>95	>95

C

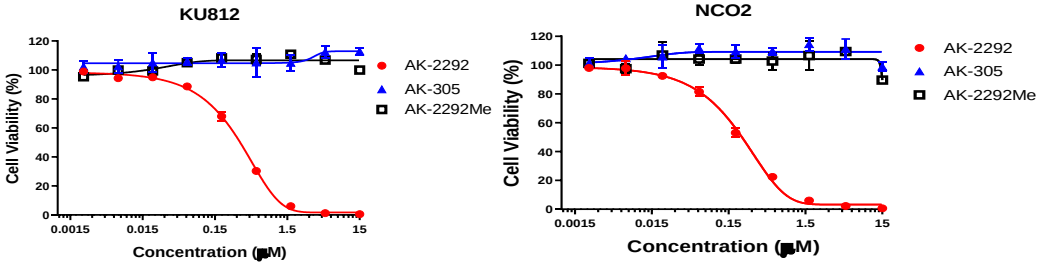

Figure 2-10 Fig. 4. Cell Growth Inhibitory Activity of AK2292 in Human CML Cell Lines

Fig. 4. Cell Growth Inhibitory Activity of AK2292 in Human CML Cell Lines

(A) Immunoblot analysis of CML cell lines to profile the expression levels of indicated proteins. AK-2292 responding cell lines are colored in green. Data represent $n = 2$ independent experiments. (B) AK-2292's growth-inhibitory activities were determined as IC_{50} by Cell Titer Glo (CTG) assay (3 to 4 days). IC_{50} data with KU812, NCO2, AR230, KYO-1, and LAMA-84 represent $n = 3$ independent experiments. Data with K562, MEG01, and NALM1 represent $n = 2$ individual experiments. AK-2292's STAT5 degradation efficiency was calculated as DC_{50} by immunoblot analysis. DC_{50} data with KU812 and NCO2 represent $n = 3$ independent experiments. DC_{50} data with AR230, KYO-1, LAMA-84, NALM-1, and MEG01 represent $n = 2$ independent experiments. AK-2292 responding cell lines are colored in green. (C) Representative concentration-viability curves of Cell Titer Glo assay. Data represent $n = 3$ independent experiments.

See also Extended Data Fig. 4.

2.8.5 Fig. 5. Pharmacodynamic Effect and Antitumor Efficacy of AK2292 in Mice

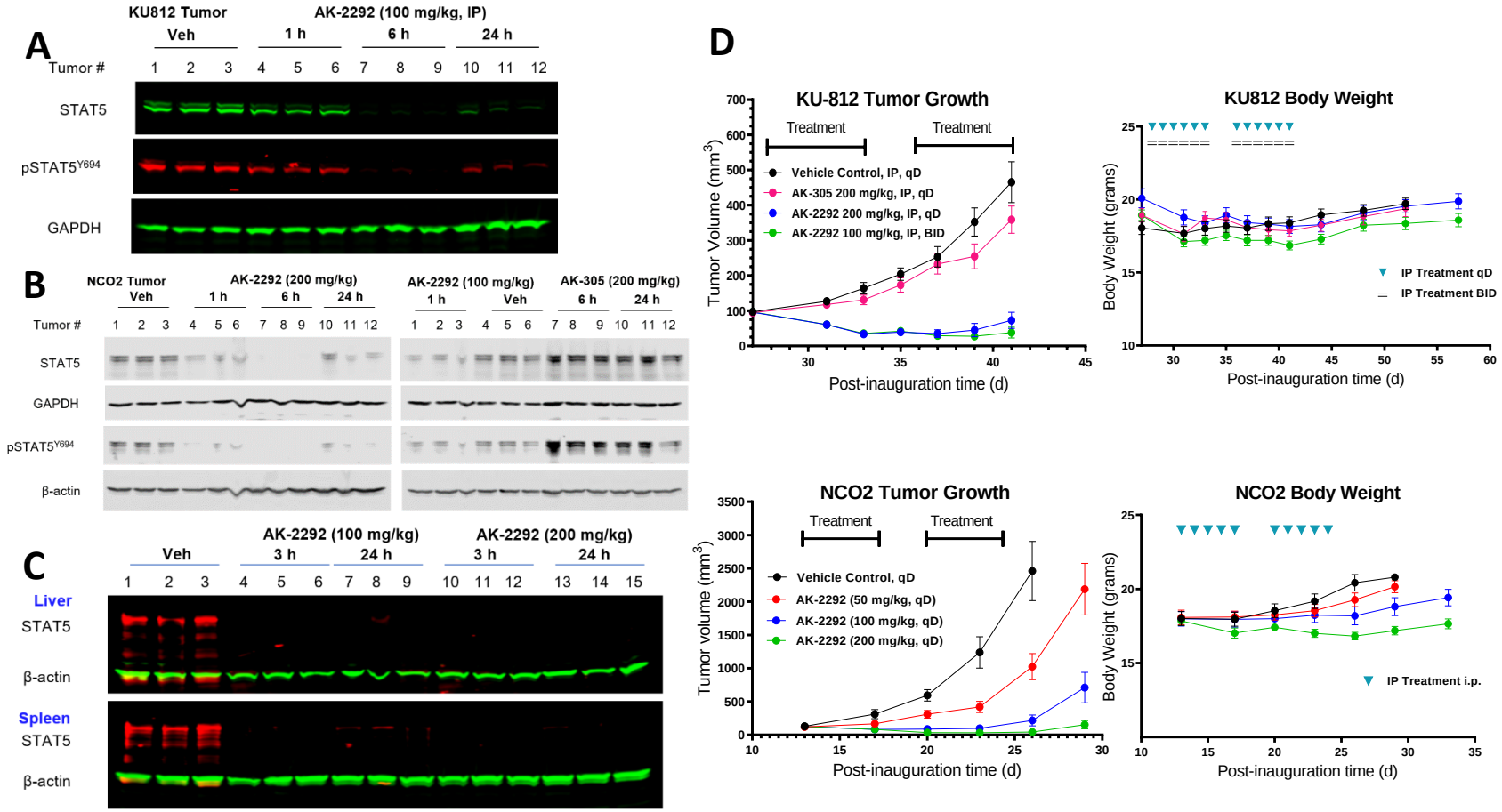

Figure 2-11 Fig. 5. Pharmacodynamic Effect and Antitumor Efficacy of AK2292 in Mice

Fig. 5. Pharmacodynamic Effect and Antitumor Efficacy of AK2292 in Mice

(A) SCID mice bearing KU812 tumors were treated i.p. as indicated and tumor cell lysates were analyzed by immunoblotting. (B) SCID mice bearing NCO2 tumors were treated i.p. as indicated and tumor cell lysates were analyzed by immunoblotting. (C) Female CD-1 mice were treated daily with AK-2292 at 200 mg/kg i.p. for 3 days and tissues were analyzed by immunoblotting. (D) Tumor-bearing SCID mice were treated under the indicated treatment schedules. Tumor volumes were measured every 2-3 days (mean ±SEM; n = 8) and the body weights of mice were measured every 2-3 days (mean ± SEM; n = 8). qD: daily,

See also Extended Data Fig. 5.

2.9 Extended Data

2.9.1 Extended Data Fig. 1A.

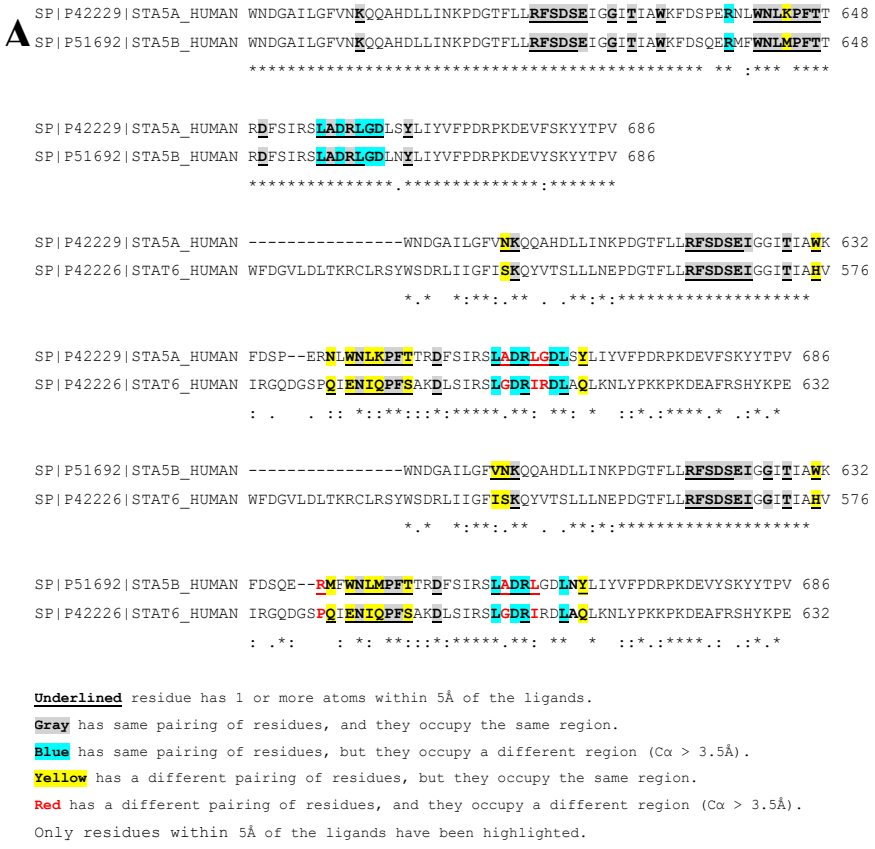

	SH2 Domain Sequence Identity (%)
STAT5A vs STAT5B	93.9
STAT5A vs STAT6	44.8
STAT5B vs STAT56	44.8

Figure 2-12 Extended Data Fig. 1A.

Extended Data Fig. 1A. Sequence alignment of STAT5A, STAT5B vs STAT6 SH2 domains and percentage of sequence identity of STAT5A vs STAT5B, STAT5A vs STAT6, STAT5B vs STAT6 SH2 domains. Sequence alignments were performed using UniProtKB.

2.9.2 Extended Data Fig. 1B.

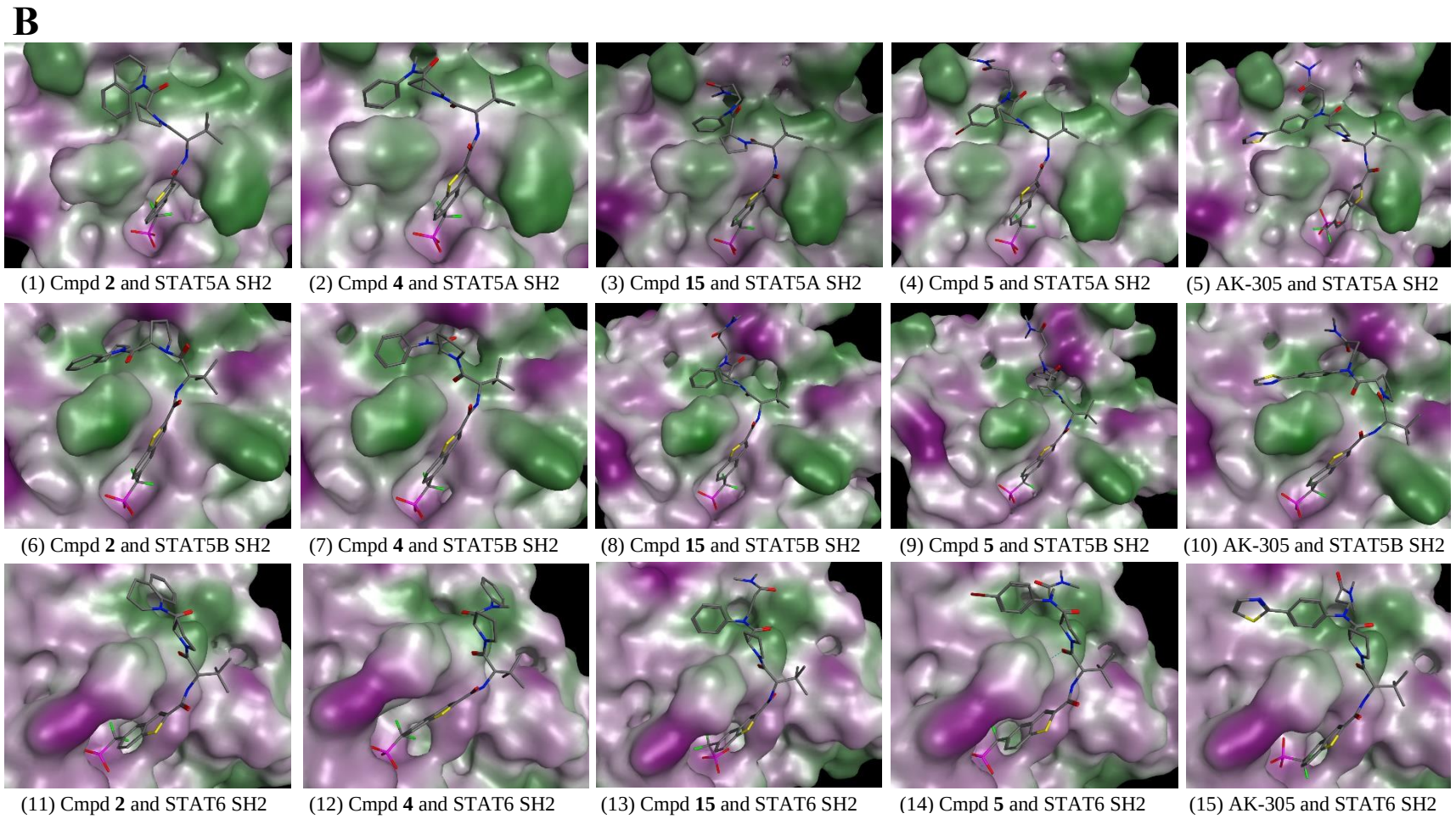

Figure 2-13 Extended Data Fig. 1B.

Extended Data Fig. 1B. Predicted binding mode of compound **2**, **4**, **15**, **5**, and AK-305 in complex with STAT5A, STAT5B, and STAT6 homology models. The surfacing color of pink indicates hydrophilic regions, and green indicates lipophilic regions.

2.9.3 Extended Data Fig. 1C and 1D.

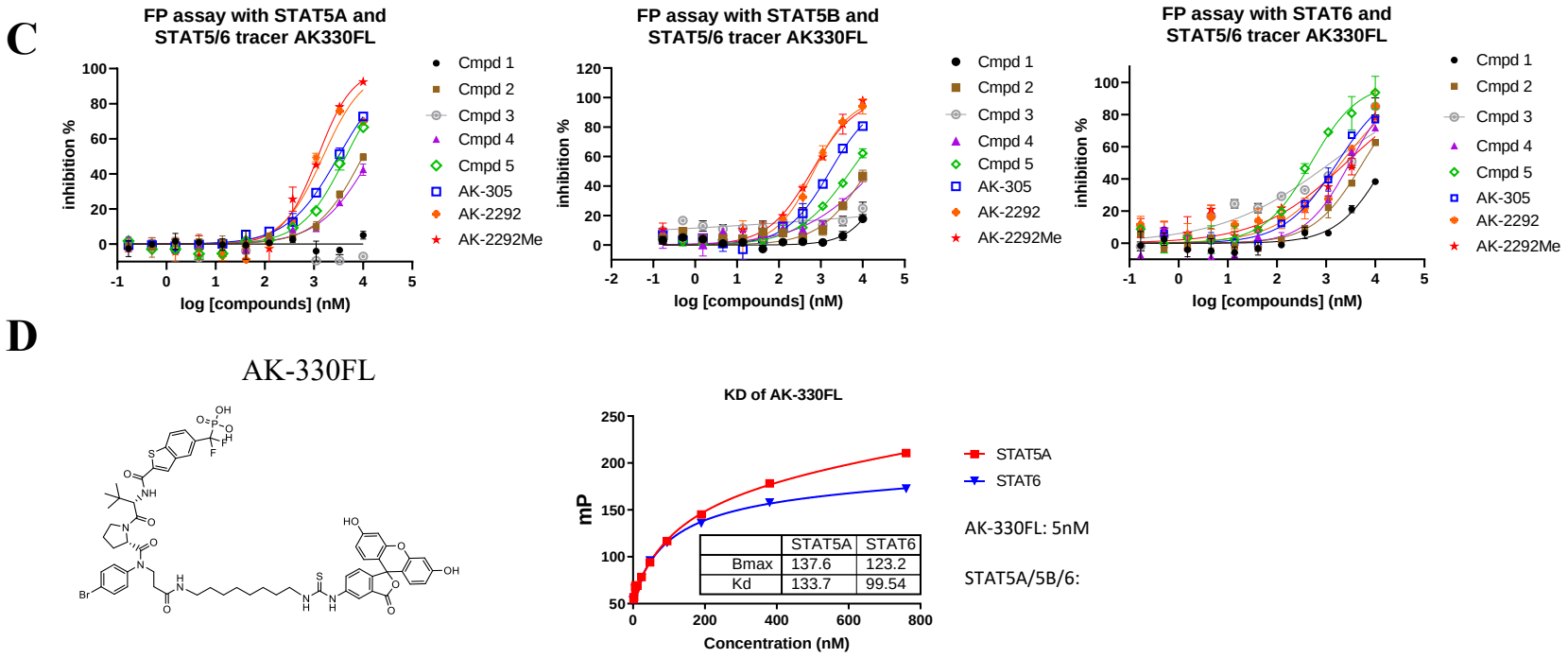

Figure 2-14 Extended Data Fig. 1C and 1D.

Extended Data Fig. 1.

(C) Representative FP assay data with STAT5A, STAT5B, and STAT6. See also the method section for the calculation of *Ki* values from IC50 values. Data represent *n* = 2 independent experiments.

(D) Structure of STAT5/6 tracer, AK-330FL and its Kd values with STAT5A and STAT6. See also the method section for the FP assay condition. Data represent *n* = 2 independent experiments.

2.9.4 Extended Data Fig. 1E.

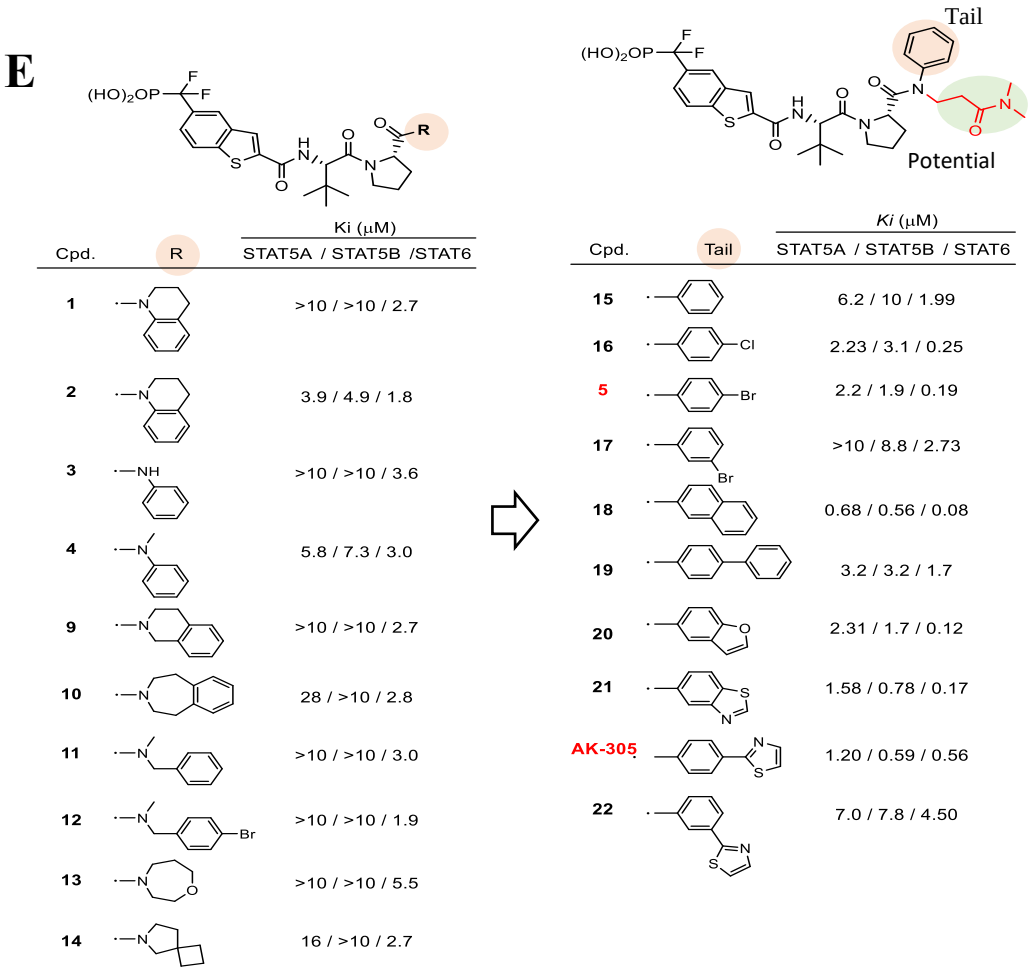

Figure 2-15 Extended Data Fig. 1E.

Extended Data Fig. 1E. Chemical structure and binding data of key representative ligands to STAT5A, STAT5B and STAT6. Data represent $n = 2$ independent experiments.

2.9.5 Extended Data Fig. 1F and 1G.

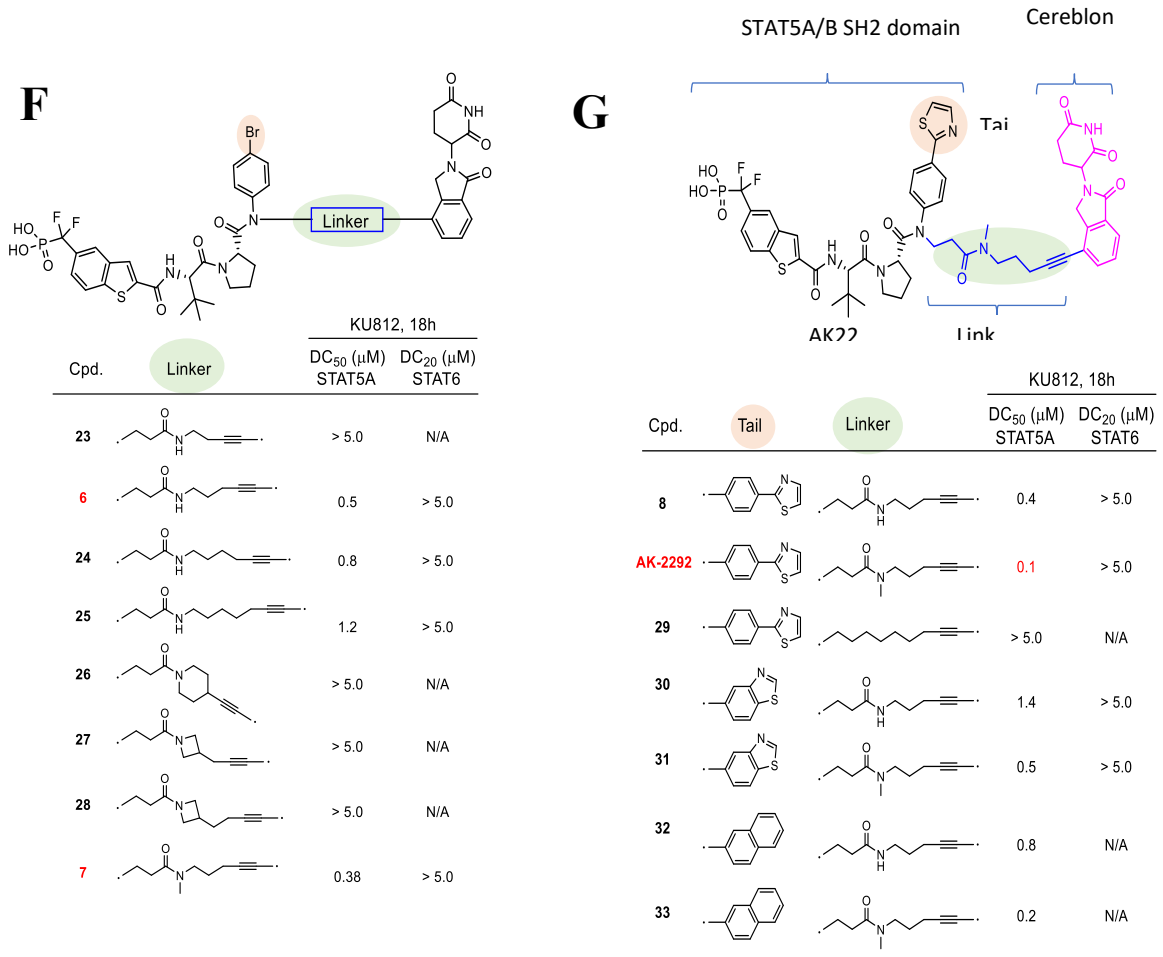

Figure 2-16 Extended Data Fig. 1F and 1G.

Extended Data Fig. 1. (F) Structure and DC_{50} relationship of key degraders based on Compound 5. (G) Structure and DC_{50} relationship of key degraders based on AK-305 and structurally similar analogues. Data represent $n = 2$ independent experiments.

2.9.6 Extended Data Fig. 1H.

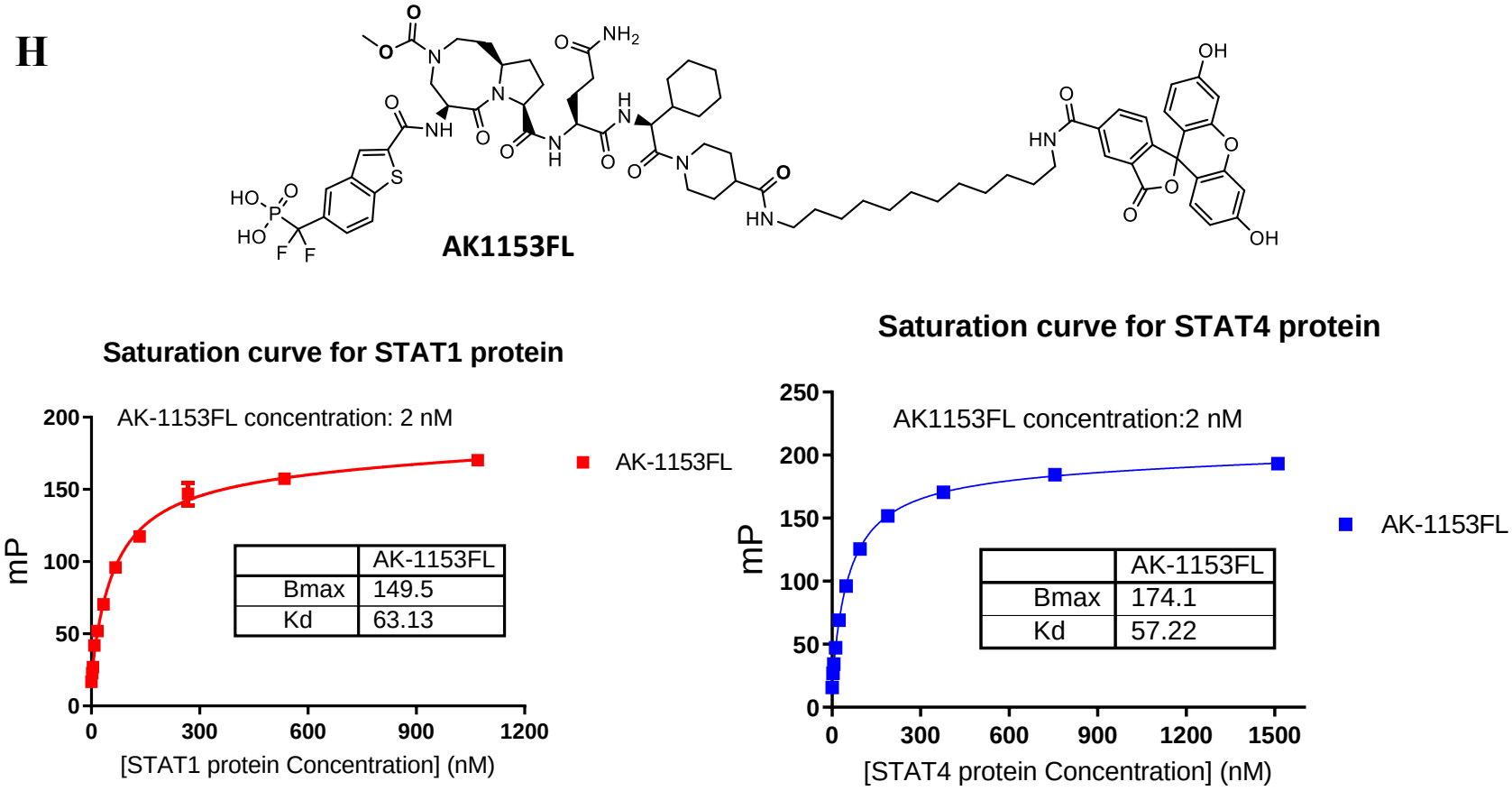

Figure 2-17 Extended Data Fig. 1H.

Extended Data Fig. 1H. Chemical structures of AK-1153FL, a fluorescence tracer for STAT1 and STAT4 proteins and its saturation curves for STAT1 and STAT4. Data represent $n = 2$ independent experiments.

2.9.7 Extended Data Fig. 1I.

I

Compound	STAT1	STAT3	STAT4	STAT6	STAT5A	STAT5B	Cereblon
	Ki(μM)	Ki(μM)	Ki(μM)	Ki(μM)	Ki(μM)	Ki(μM)	Ki (μM)
5	14.9	4.3	>10	0.2	1.7	1.9	N/A
AK-305	6.8	3.5	>10	0.5	1.2	0.6	N/A
AK-2292	>10	4.6	>10	1.5	0.5	0.2	0.027
AK-2292Me	9.1	7.9	>10	2.2	0.4	0.2	3.9

Figure 2-18 Extended Data Fig. 1I.

Extended Data Fig. 1I. Summary of K_i values of compound 5, AK-305, AK-2292, and AK-2292Me with STAT1, STAT3, STAT4, STAT5A, STAT5B, STAT6 and Cereblon. Data represent $n = 2$ independent experiments.

2.9.8 Extended Data Fig. 1J and 1K.

J

Data Collection	STAT5a:AK-305	STAT5a:AK-2292
PDBID	7TVB	7TVA
Space Group	R32	R3
Unit Cell (Å)	239.9 239.9 113.2 90 90 120	232.4 232.4 112.5 90 90 120
Wavelength (Å)	1.1271	1.1271
Resolution (Å)[1]	2.65 (2.70 – 2.65)	2.85 (2.80 – 2.90)
Rsym[2]	0.095 (0.976)	0.077 (1.246)
<I/sI>[3]	34 (2.0)	19 (1.6)
Completeness (%)[4]	99.9 (99.9)	99.7 (100)
Redundancy	20.6 (17.2)	5.1 (5.1)
Refinement		
Resolution (Å)	2.65	2.85
R-Factor [5]	0.2088	0.2211
R-Free [6]	0.2484	0.2734
Protein atoms	4446	8786
Ligands	1	2
Water Molecules	390	232
Unique Reflections	34349	49797
R.m.s.d.[7]		
Bonds	0. 008	0.008
Angles	0.96	0.99
MolProbity Score[8]	1.80	2.44
Clash Score[8]	2.91	5.68
RSCC[9]	0.97	0.91/0.92
RSR[9]	0.11	0.33/0.27

Statistics for highest resolution bin of reflections in parentheses.

[2] $R_{sym} = \Sigma_h \Sigma_j | I_{hj} - \langle I_h \rangle | / \Sigma_h \Sigma_j I_{hj}$, where I_{hj} is the intensity of observation j of reflection h and $\langle I_h \rangle$ is the mean intensity for multiply recorded reflections.

[3] Intensity signal-to-noise ratio.

[4] Completeness of the unique diffraction data.

[5] R-factor = $\Sigma_h | IF_o I - IF_c I | / \Sigma_h |F_o|$, where F_o and F_c are the observed and calculated structure factor amplitudes for reflection h.

[6] R_{free} is calculated against a 5% random sampling of the reflections that were removed before structure refinement.

[7] Root mean square deviation of bond lengths and bond angles.

[8] Chen et al. (2010) MolProbity: all-atom structure validation for macromolecular crystallography. Acta Crystallographica D66:12-21.

[9] wwPDB Validation Server.

K

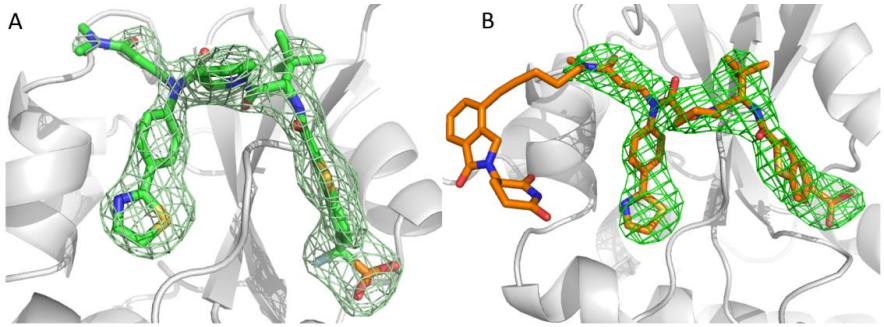

Figure 2-19 Extended Data Fig. 1J and 1K..

Extended Data Fig. 1.

(J) Summary of crystallography data collection and refinement statistics. (K) Unbiased difference (Fo-Fc) electron density maps of (A) AK-305 and (B) AK-2292 placement in Stat5a. The maps are represented as green grids contoured at 3s. Density for the degrader portion of AK-2292 is weak for both molecules of AK2292 found in the asymmetric unit.

2.9.9 Extended Data Fig. 2A and 2B.

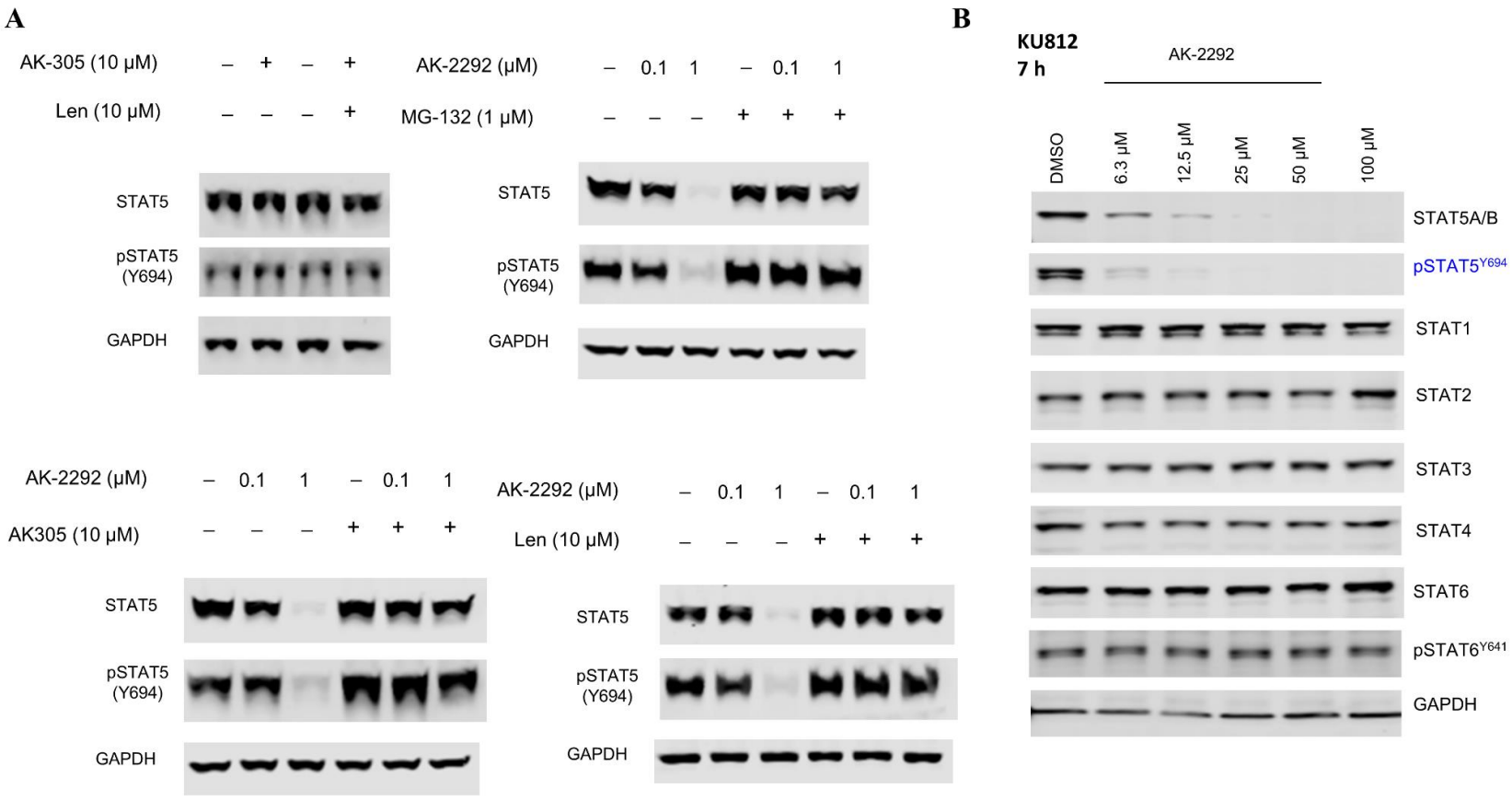

Figure 2-20 Extended Data Fig. 2A and 2B.

Extended Data Fig. 2. (A) Immunoblot analysis of KU812 cells treated with indicated compounds under indicated concentrations for 24 hr. AK305: STAT5/6 inhibitor; Len: Lenalidomide; MG-132: proteasome inhibitor.(B) Immunoblot analysis of KU812 cells treated with AK2292 at high concentrations for 7 hr. Data represent $n = 2$ independent experiments.

2.9.10 Extended Data Fig. 3A, 3B, 3C, and 3D.

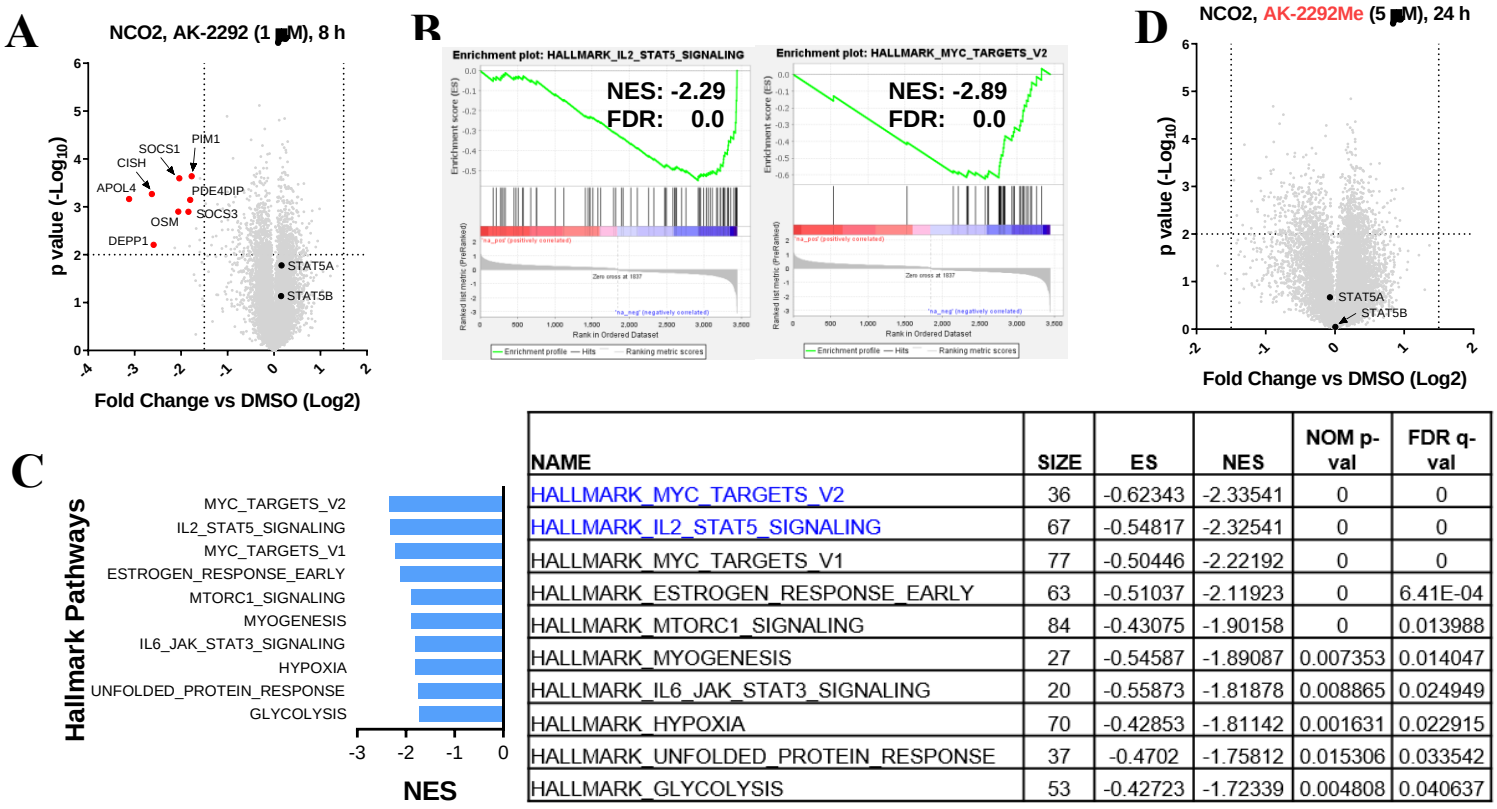

NAME	SIZE	ES	NES	NOM p-val	FDR q-val
HALLMARK_MYC_TARGETS_V2	36	-0.62343	-2.33541	0	0
HALLMARK_IL2_STAT5_SIGNALING	67	-0.54817	-2.32541	0	0
HALLMARK_MYC_TARGETS_V1	77	-0.50446	-2.22192	0	0
HALLMARK_ESTROGEN_RESPONSE_EARLY	63	-0.51037	-2.11923	0	6.41E-04
HALLMARK_MTORC1_SIGNALING	84	-0.43075	-1.90158	0	0.013988
HALLMARK_MYOGENESIS	27	-0.54587	-1.89087	0.007353	0.014047
HALLMARK_IL6_JAK_STAT3_SIGNALING	20	-0.55873	-1.81878	0.008865	0.024949
HALLMARK_HYPOXIA	70	-0.42853	-1.81142	0.001631	0.022915
HALLMARK_UNFOLDED_PROTEIN_RESPONSE	37	-0.4702	-1.75812	0.015306	0.033542
HALLMARK_GLYCOLYSIS	53	-0.42723	-1.72339	0.004808	0.040637

Figure 2-21 Extended Data Fig. 3A, 3B, 3C, and 3D.

Extended Data Fig. 3. (A). RNA-seq analysis of NCO2 cells treated with 1 μM of AK-2292 for 8 hr. The experiment was performed in triplicate. (B). GSEA indicated that genes that are up-regulated by STAT5 upon IL2 stimulation and a subset of genes regulated by Myc are the two most down-regulated by AK-2292 in NCO2 cells (1 μM for 8 hr). NES: normalized enrichment score. (C). Top Hallmark gene sets enriched by AK-2292 (1 μM for 8 hr) in KU812 cells. ES: enrichment score; NES: normalized enrichment score; NOM p-value: Nominal p value; FDR q-val: False Discovery Rate q-value. (D). RNA-seq analysis of NCO2 cells treated with 5 μM of AK-2292Me for 24 hr. The experiment was performed in triplicate.

2.9.11 Extended Data Fig. 4A-4F.

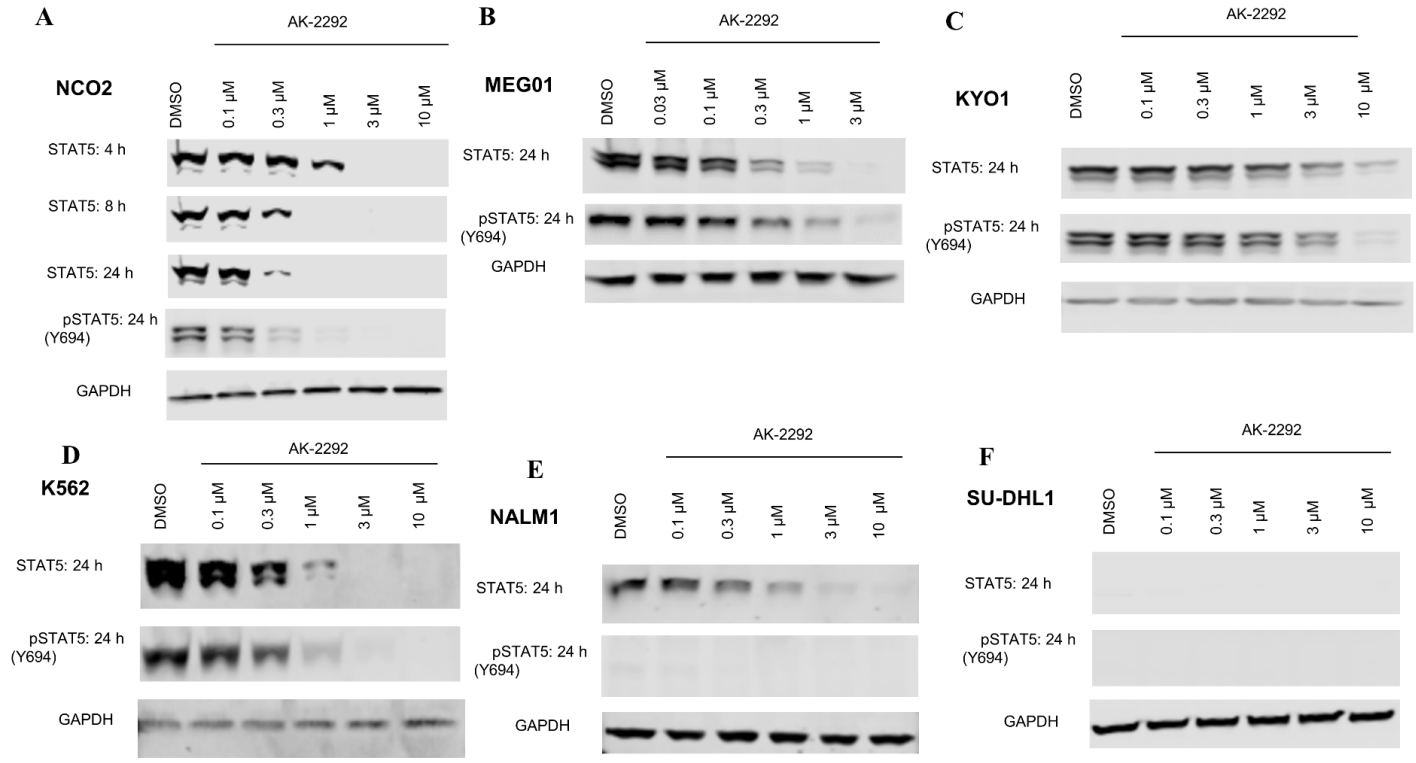

Figure 2-22 Extended Data Fig. 4A-4F.

Extended Data Fig. 4. (A). Immunoblot analysis of NCO2 cells treated with AK-2292 at indicated concentrations and treatment time. (B). Immunoblot analysis of MEG01 cells treated with AK-2292 at indicated concentrations and treatment time. (C).Immunoblot analysis of KYO1 cells treated with AK-2292 at indicated concentrations and treatment time. (D). Immunoblot analysis of K562 cells treated with AK-2292 at indicated concentrations and treatment time. (E). Immunoblot analysis of NALM1 cells treated with AK-2292 at indicated concentrations and treatment time. (F). Immunoblot analysis of SU-DHL1 cells treated at indicated concentrations and treatment time. Data with NCO2 represent *n* = 3independent experiments. Data with MEG01, KYO-1, K562, NALM1, and SU-DHL1 represent *n* = 2 individual experiments.

2.9.12 Extended Data Fig. 4G and 4H.

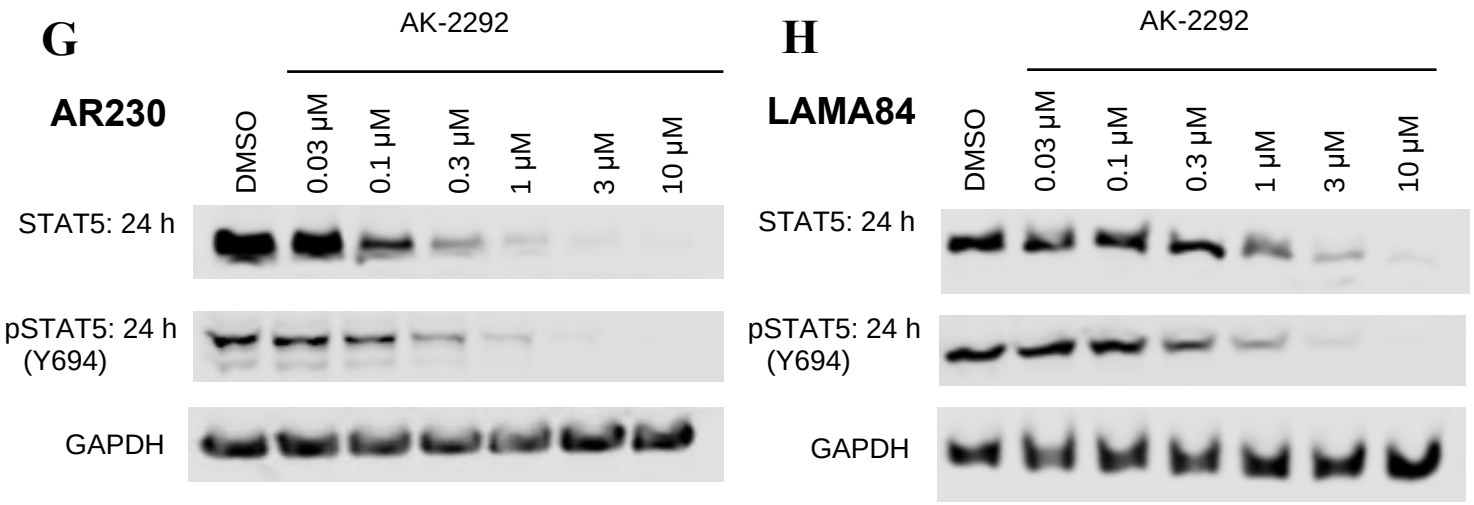

Figure 2-23 Extended Data Fig. 4G and 4H.

Extended Data Fig. 4. (G). Immunoblot analysis of AR230 cell line treated with AK-2292 at indicated concentrations and treatment time. (H) Immunoblot analysis of LAMA84 cell line treated with AK-2292 at indicated concentrations and treatment time. Data represent $n = 2$ independent experiments.

2.9.13 Extended Data Fig. 4I.

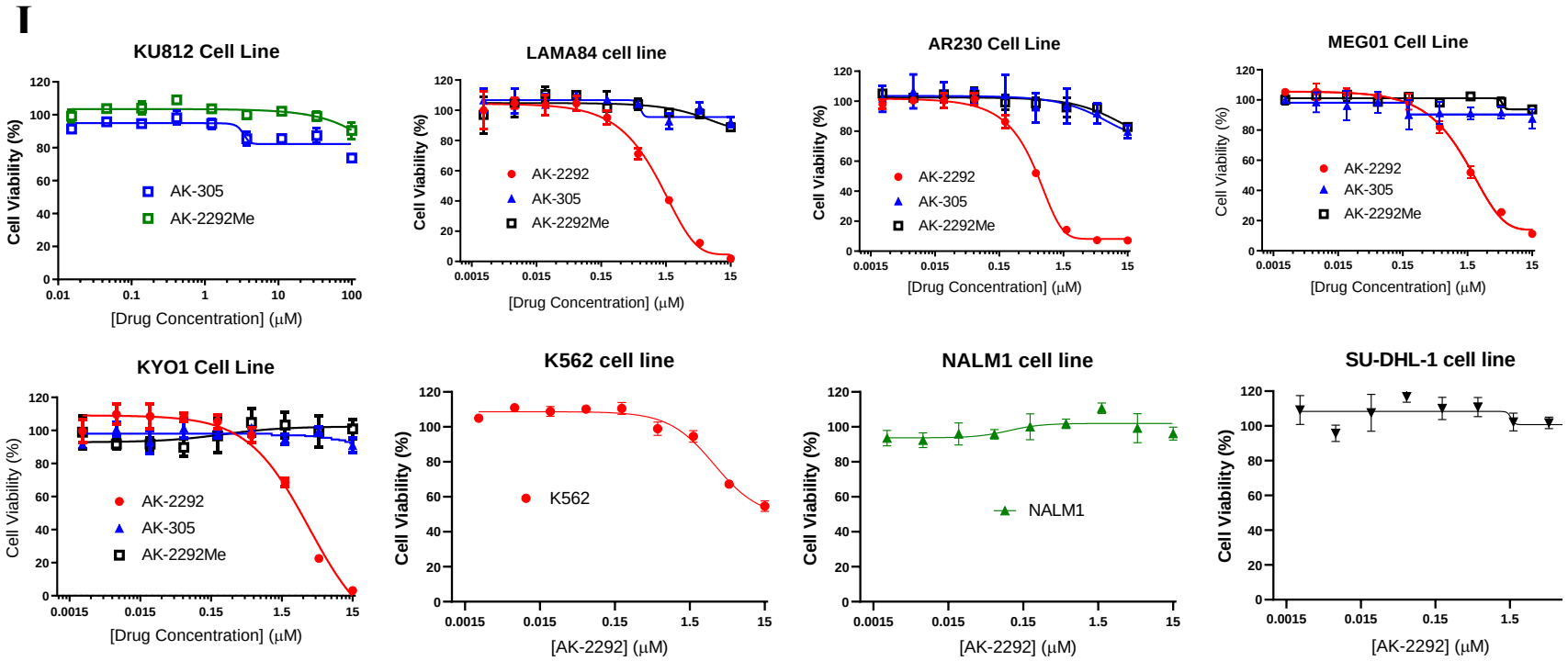

Figure 2-24 Extended Data Fig. 4I.

Extended Data Fig. 4I. Representative cell growth inhibition curves of several CML cell lines and SU-DHL-1 control cell line by AK-2292 (degrader), AK-2292Me (degrader control), and AK-305 (inhibitor). Data with LAMA84, AR230, and KYO-1 represent *n* = 3 independent experiments. Data with KU812, K562, NALM1, and SU-DHL1 represent *n* = 2 independent experiments.

2.9.14 Extended Data Fig. 5A-5D.

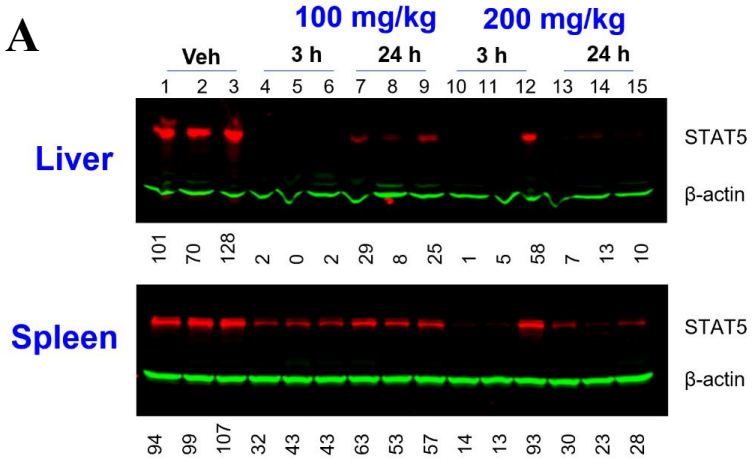

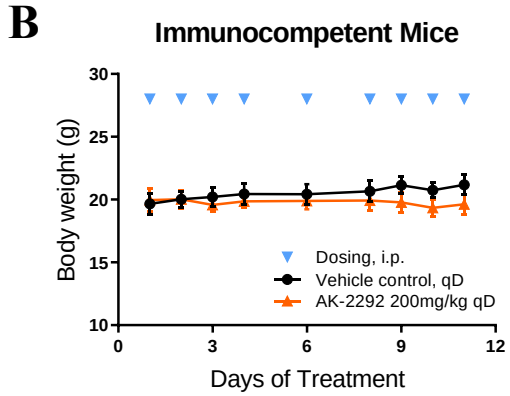

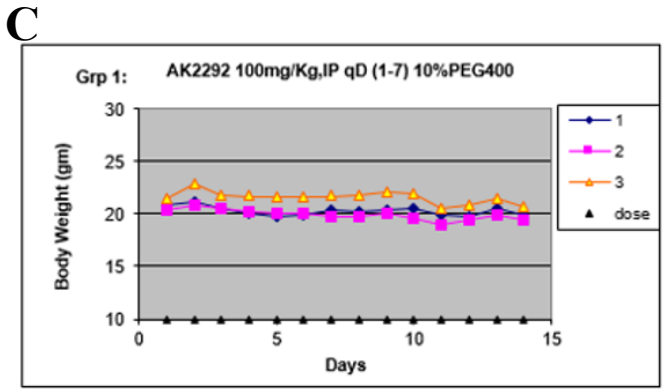

D

Markers (mg/dL)	Control ± SD	AK-2292 IP, 100mg/kg, qD(1-14)
CREA (mg/dL)	0.23 ± 0.02	0.19 ± 0.03
GLUC (mg/dL)	219 ± 27	237 ± 32
TPRO (g/dL)	6.3 ± 0.29	6.3 ± 0.09
CA (mg/dL)	10 ± 0.66	10 ± 0.29
ALT (U/L)	52 ± 14	87 ± 58
TBIL (mg/dL)	0.07 ± 0.02	0.05 ± 0.01
BUN (mg/dL)	24 ± 3	22 ± 4
ALKP (U/L)	75 ± 5	76 ± 5
ALB2 (g/dL)	4.4 ± 0.29	4.6 ± 0.09

Figure 2-25 Extended Data Fig. 5A-5D.

Extended Data Fig. 5. (A) Female CD-1 mice were treated with AK-2292 at 100 mg/kg or 200 mg/kg i.p. and tissues were analyzed by immunoblotting. (B) Female immunocompetent mice were treated with AK-2292 at 200 mg/kg i.p. and the body weights of mice were measured on every dosing day (mean ± SEM; n = 5). (C) CD-1 mice were treated daily with 100mg/kg of AK-2292 through I.P. for 2 weeks and the body weights of mice were measured every dosing day (n = 3). (D) CD-1 mice were treated daily with 100mg/kg of AK-2292 through I.P. for 2 weeks (n = 3) and the blood was analyzed.

Chapter 3 Structure-Guided Discovery of AK-2292 as a Potent, Selective, and Efficacious STAT5 PROTAC Degrader

3.1 Abstract

Signal Transducer and Activator of Transcription 5 has been an active pursuit in the drug discovery community for >20 years, yet remained in a category of "difficult-to-target" protein. We report herein our structure-guided discovery of AK2292 as a potent STAT5 PROTAC degrader. Starting from a STAT6 inhibitor with a very weak affinity to STAT5, we first developed a set of non-selective STAT5 inhibitors with low μM affinity to STAT5 and much higher affinity to STAT6. By deploying PROTAC technology, we developed a series of STAT5 degraders with AK2292 as among the best, here evaluated in AML cells. AK2292 shows an excellent degradation selectivity toward STAT5 over other STAT family proteins and exerts anti-growth activity in cells while the corresponding inhibitor shows no effect. AK2292 achieves a strong anti-tumor effect in the MV4;11 xenograft mouse model with minimal weight loss. AK2292 is a potent, selective, and efficacious STAT5 PROTAC degrader.

3.2 INTRODUCTION

Signal Transducer and Activator of Transcription 5 (STAT5) is a pivotal downstream player in JAK/STAT signaling pathway and regulates crucial cellular functions [1, 2]. It is now clearly established that the constitutive activation of STAT5A/B greatly assists the generation, progression and survival of tumor cells, pointing to STAT5A/B as attractive therapeutic targets of hematopoietic cancers [4, 6-11].

It is well documented that the dimerization step is critical for its transcriptional activity where, upon phosphorylation by JAK or other kinases, STAT5A/B homo- or hetero- dimerizes through its SH2 domain [31-33]. Therefore, blocking the dimerization by occupying the SH2 domain on STAT5 has been proposed as a promising strategy for STAT5 inhibitor development [33]. After >20 years of persistent research effort, two pioneering STAT5 inhibitors, Stafib-1 by Berg group and AC-4-130 by Gunning group, have been reported as the major progress in the direct targeting of STAT5 [26-30]. Unfortunately, achieving desirable potency in cells and selectivity with clear cellular mechanism of action was found very challenging task, leaving STAT5 as an undruggable or “difficult-to-target” protein.

Recently, proteolysis targeting chimera (PROTAC) technology has significantly stimulated the drug discovery arena by its ability to target proteins once considered undruggable or difficult-to-target proteins [42, 43]. Together with accumulated knowledge in PROTAC field, lessons learnt from our past intensive research on the development of STAT3 inhibitor and STAT3 PROTAC degrader (SD-36) [37] guided us to develop the first-in-class STAT5 PROTAC degrader, AK2292 [ref]. We previously reported AK2292’s excellent selectivity and low nM potency in CML cells as well as strong *in vivo* effects in CML xenograft mouse models.

In addition to the effect of STAT5 knockdown by AK2292 in CML cells, there are considerable interests about the effect in AML cells. FMS-like tyrosine kinase 3 (FLT3), a cytokine receptor, has been found mutated in a subset of acute myeloid leukemia (AML) cells. STAT5 is one of major downstream effector proteins of FLT3 and therefore it is expected that the pharmacological inhibition of STAT5 may have anti-growth effect in AML cells where the aberrant STAT5 is driving the cell growth [17, 29].

Here, we report our structure-guided development of STAT5/6 inhibitors and 3 co-crystal structures of our noble STAT5/6 inhibitors in complex with STAT5A, having facilitated the discovery of PROTAC degraders with AK2292 as among the best. We evaluate a series of STAT5 degraders in the context of AML. Our best STAT5 degrader, AK2292, shows anti-growth activities in a subset of AML cells, namely SKNO1, MV4;11, and Kasumi-3, displays an excellent selectivity among structurally similar STAT family proteins in multiple AML cell lines, and exerts *in vivo* efficacy in MV4;11 xenograft mouse model.

3.3 RESULTS AND DISCUSSION

3.3.1 Structure-Based Design of Small Molecule STAT5/6 SH2 Domain Inhibitors.

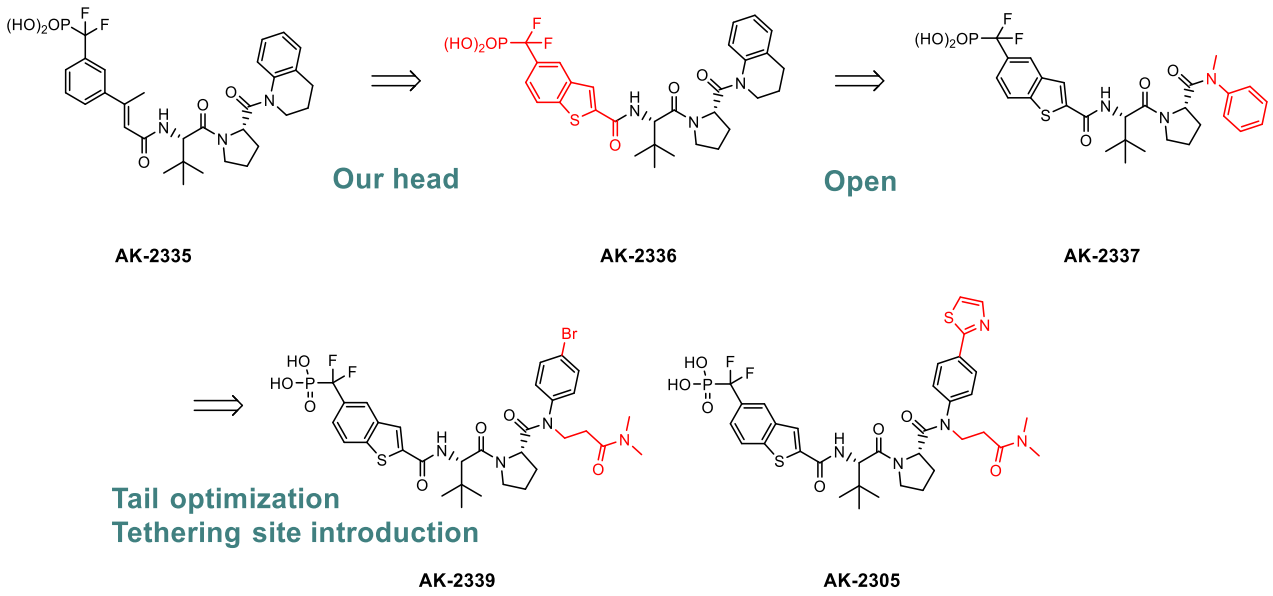

Figure 3-1 Figure 1. Key structural modifications in STAT5/6 SH2 domain inhibitors.

Figure 1. Key structural modifications in STAT5/6 SH2 domain inhibitors.

Starting from a very weak STAT5/6 inhibitor, we were able to develop a series of STAT5/6 inhibitors with moderate binding affinity to STAT5 and better binding affinity to STAT6, exemplified by AK-2339 and AK2305 (Figure 1). Our laboratory has previously reported STAT3 SH2 domain inhibitors with single digit nanomolar binding affinities, followed by STAT3 PROTAC degraders [37]. Encouraged by our group's earlier success in targeting STAT3, we decided to target STAT5A/B. We were especially intrigued by the pioneering work done by the McMurray group in prodrug peptidomimetic STAT6 inhibitor development [70, 71, 89]. Because of the structural similarity between STAT6 and STAT5A/B, we reasoned that McMurray group's peptidomimetics may show some meaningful affinity to STAT5A/B.

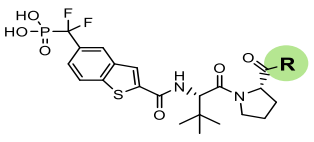

(a)

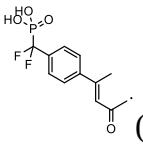

(b)

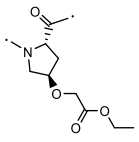

Cmpds	R	Ki (μM) STAT5A/5B/6	Cmpds	R	Ki (μM) STAT5A/5B/6	Cmpds	R	Ki (μM) STAT5A/5B/6
AK233[a]		>10 / > 10 / 5.4	**AK075**	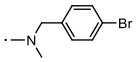	>10 / >10 / 1.7	**AK2367**	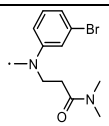	>10 / 8.9 / 2.7
AK2336		3.9 / 4.9 / 1.8	**AK064**		>10 / >10 / 4.8	**AK2342**	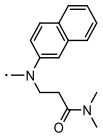	0.7 / 0.6 / 0.1
AK2452		>10 / > 10 / 3.6	**AK078**		>10 / >10 / 5.3	**AK2343**	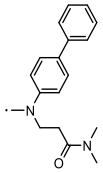	3.2 / 3.3 / 1.7
AK2337		5.8 / 7.3 / 1.0	**AK014**[b]		0.8 / 1.6 / 0.1	**AK2305**	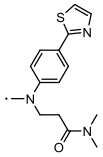	1.2 / 0.6 / 0.5
AK256		>10 / >10 / 2.6	**AK2446**	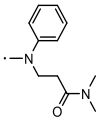	6.2 / 10 / 2.0	**AK2368**	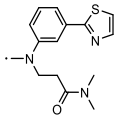	7.0 / 7.8 / 4.5
AK070	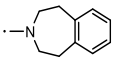	>10 / >10 / 5.4	**AK2338**	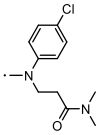	2.2 / 3.1 / 0.3	**AK2340**	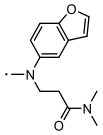	2.3 / 1.7 / 0.1
AK073		>10 / >10 / 4.9	**AK2339**	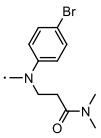	1.7 / 1.9 / 0.3	**AK2341**	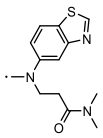	1.6 / 0.8 / 0.2

Table 1 Relationship of structure and binding affinity in STAT5/6 SH2 domain inhibitor development.

Table 1. Relationship of structure and binding affinity in STAT5/6 SH2 domain inhibitor development.

To test our idea, we synthesized AK-2335, which showed reasonable affinity (5.4 μM) to STAT6 and very weak affinity to STAT5A (>10 μM) (Table 1). Aiming at improving the binding affinity to STAT5A/B, we replaced the cinnamic acid based phosphotyrosine mimetics moiety with the benzothiophene based phosphotyrosine mimetics to generate AK-2336 with an improved binding both to STAT5 (3.9 μM) and to STAT6 (1.8 μM). In our previous reports, we used indole based phosphotyrosine mimetic, but due to its chemical stability issue [69], we developed a chemically stable benzothiophene based mimetics with equivalent binding capability to SH2 domain [72]. We, then, opened the ring of tetrahydroquinoline moiety at C-terminus to make AK2337, retaining the binding affinity, which gave us an easier access to further modification around C-terminus aromatic ring and potential tethering site originating from methyl group on nitrogen for degrader development. Our docking study suggested that tethering site could be introduced at the methyl group or proline, and also binding affinity can be improved by introducing hydrophobic group at the aromatic ring (supplement, or our ref), demonstrated by AK-014 and AK-2446. AK-014 demonstrates that an introduction of tethering group in proline retained the binding to STAT5 (0.8 – 1.6 μM) and STAT6 (0.1 μM), giving us an option to tether E3 ligase ligand from proline. Furthermore, AK-2446 indicated that tethering from C-terminus is also possible since the introduction of tethering group at C-terminus maintained the binding to STAT5 and STAT6. To investigate the chemical space around C-terminus, we synthesized AK-256 to AK-078, confirming that aniline type aromatic ring is necessary at C-terminus to retain the binding to STAT5 and STAT6. Compared with AK2446, the introduction of hydrophobic halogen groups or another aromatic 5 membered ring at para position of the C-terminus ring, but not meta position,

improved the binding to STAT5 and STAT6 shown as AK2338, AK2339, AK2367, AK2305, and AK2368. The introduction of 6 membered ring at para position was detrimental for STAT5 and STAT6 binding shown as AK2343. Further, fused aromatic ring systems also show better binding shown as AK-2342, AK2340, and AK2341, compared to AK2446 with a simple phenyl ring at C-terminus.

Taken together, with our concerted efforts in finding a starting compound to target STAT5, in exploring the chemical space in N-terminus and C-terminus of the initial peptidomimetic compound with very week binding affinities to STAT5 and STAT6, and in docking study for affinity improvement, we were able to achieve a reasonable binding to STAT5 (0.7 ~ 1.2 μM) and a much higher binding to STAT6 (0.1 ~ 0.5 μM). We also found two potential tethering sites, one from proline shown in AK014, the other from C-terminus exemplified in AK2305 for our degrader development.

3.3.2 Investigation of residue modifications in AK-2305 for binding affinity.

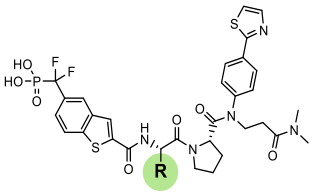

Cmpds	R	Ki (STAT5A/5B/6, μM)
AK2305		1.2 / 0.6 / 0.5
AK2415		2.6 / 2.9 / 0.6
AK2417		0.7 / 0.7 / 0.7
AK2418		3.4 / 3.7 / 1.5
AK2419		0.7 / 1.3 / 1.7
AK2420		0.7 / 1.3 / 1.5
AK2421		1.9 / 2.1 / 2.4
AK2422		1.1 / 1.3 / 0.7

Table 2 Effect of hydrophobic residues of STAT5/6 inhibitors for binding affinity

Table 2. Effect of hydrophobic residues of STAT5/6 inhibitors for binding affinity

Our predicted binding models (SI) of AK-2339 and AK-2305 in complex with STAT5A (SI) suggested that tertiary-butyl residue of our inhibitors is surrounded by hydrophobic residues of STAT5 proteins such as Trp631 and Trp641. We synthesized a set of inhibitors by replacing tertiary-butyl residue with other hydrophobic residues with different size (Table 2). Structurally larger hydrophobic residues tend to improve the binding to STAT5 while cyclopropane, a smaller

residue, was detrimental. The effect of replacing tertiary-butyl with other hydrophobic residues seemed rather minimal.

3.3.3 Co-crystal structures of STAT5 inhibitors in complex with STAT5A.

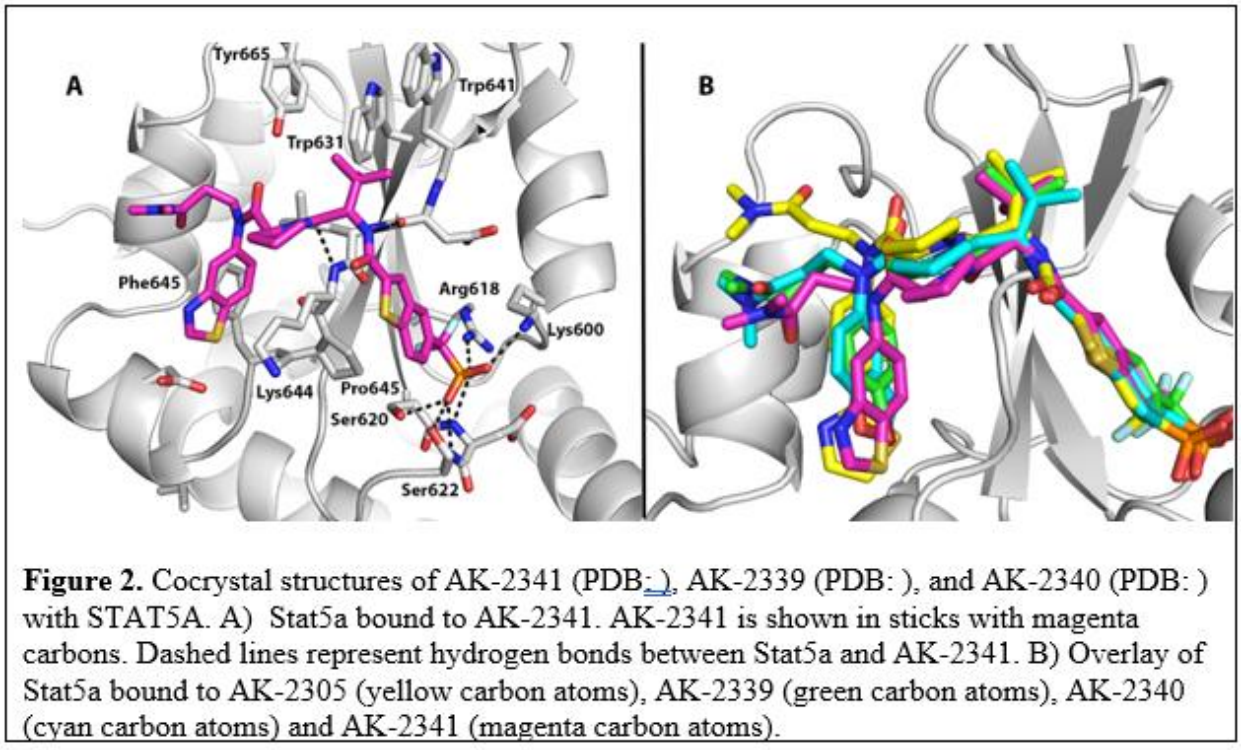

Figure 2. Cocrystal structures of AK-2341 (PDB:), AK-2339 (PDB:), and AK-2340 (PDB:) with STAT5A. A) Stat5a bound to AK-2341. AK-2341 is shown in sticks with magenta carbons. Dashed lines represent hydrogen bonds between Stat5a and AK-2341. B) Overlay of Stat5a bound to AK-2305 (yellow carbon atoms), AK-2339 (green carbon atoms), AK-2340 (cyan carbon atoms) and AK-2341 (magenta carbon atoms).

Figure 3-2 Co-crystal structures of STAT5 inhibitors in complex with STAT5A.

In this study, the co-crystal structures of STAT5A bound to the inhibitors AK-2339 and AK-2340 were solved to 3.1 Å (Figure 2B), while the structure of STAT5A-AK-2341 (Figure 2A and 2B) was solved to 2.35 Å. The structures are very similar to the previously reported structure of STAT5A -AK-305 (PDB: 7TVB), with a RMSD of 0.516 – 0.685 Å between the STAT5A protein. The core components of the inhibitors, AK-2339, AK-2340 and AK-2341, bind to the phosphopeptide binding pocket in the same manner as AK-305 (PDB ID: 7TVB) forming the same noncovalent interactions with STAT5A (Figure 2B). In all three inhibitors, the oxygen atoms of the phosphonic acid moiety are hydrogen bonded to the sidechains of Ser620

and Ser622 and to the backbone amides of Asp621 and Ser622 and interact electrostatically with the sidechains of Arg618 and Lys600. The difluoromethyl moiety of the inhibitors interacts with residues Thr628 and Lys600 via van der waals interactions, in addition to a hydrogen bond with Arg618. The inhibitors differ in the C-terminal group, with AK-2339 having a bromophenyl group, AK-2340 having a benzofuran group and AK-2341 having a benzothiazole group (Table 1). The C-terminal group of the inhibitors all bind in with same pocket, lined by residues Pro645, Lys644, Leu643, Phe646, Asp650 and Arg656. The aromatic rings form a π-π interaction Phe646 and a π-cation interaction with Lys644. In contrast to the structure of Stat5a-AK-2305, the structures of AK-2339, AK-2340 and AK-2341 are pulled deeper into the binding pocket, shifting the inhibitor and preventing the formation of a hydrogen bond to Tyr665 as was seen in the AK-2305 structure.

3.3.4 Design of PROTAC STAT5 A/B Degraders.

We were able to develop a set of inhibitors that have reasonable binding affinity to STAT5 and better affinity to STAT6 (Table 1) and our corrective knowledge from structure-binding relationship investigation, co-crystal structures, and predicted models gave us a solid structural foundation to develop a degrader of either STAT5 or STAT6 and we reasoned that we could tether lenalidomide either from C-terminus and synthesized a series of putative STAT5 or STAT6 degraders.. We decided to use AK-2339 and AK-014 as the inhibitors and lenalidomide as the ligand for cereblon/cullin 4A to see if we could degrade either STAT5 or STAT6 (Figure 3).

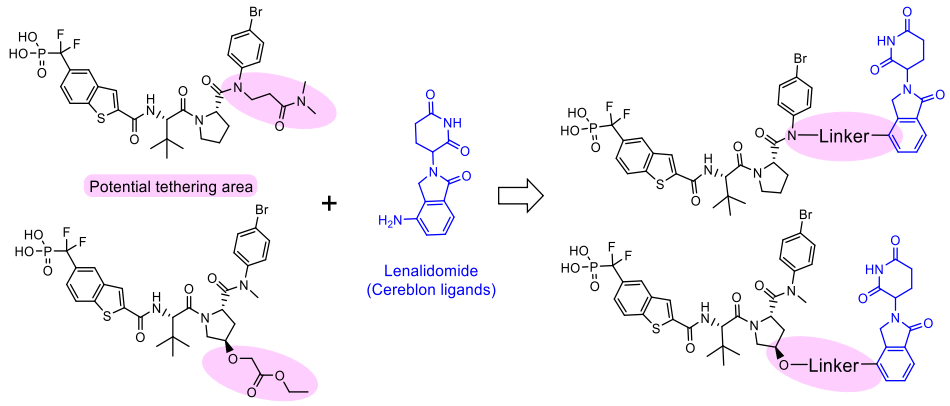

Figure 3-3 Design of putative STAT5 PROTAC degraders using AK-2339 and Cereblon ligand.

Figure 3. Design of putative STAT5 PROTAC degraders using AK-2339 and Cereblon ligand.

3.3.5 Investigation of the Optimal Linker Length and Linker Composition based on AK-2305 for STAT5 Degraders.

We first synthesized a set of putative STAT5 or STAT6 degraders using AK-2339 as the inhibitor and lenalidomide as the E3 ligase ligand both linked by linkers with various lengths (Table 3). AK-1930 was synthesized with the shortest linker. We used SKNO1 cell line for our degrader screening due to its high level of STAT5 expression among AML cell lines. We treated SKNO1 with AK-1930 for 18 h, but AK-1930 did not show any sign of both STAT5 and STAT6 degradation up to 5 μM. Surprisingly, AK-318 that has a longer linker by one carbon compared to AK-1930 degraded STAT5 very efficiently with about 200 nM IC_{50} while AK-318 failed to degrade STAT6 at least up to 5 μM. To investigate the optimal linker length, we synthesized putative STAT5 degraders with longer linkers, finding that the linker length of AK-318 is optimal to induce STAT5 degradation.

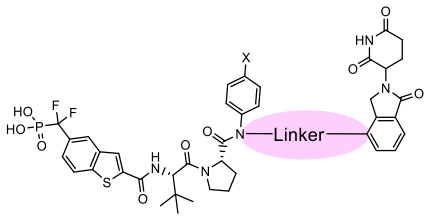

Cmpds	X	Linker	DC_{50} (STAT5/6, μM) SKNO1, 18 h
AK1930	Br	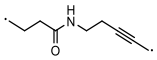	>5 / >5
AK318	Br	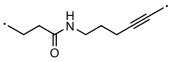	0.23 / >5
AK2450	Br	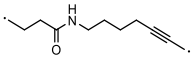	0.50 / >5
AK317	Br	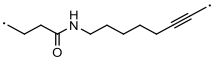	1.1 / >5
AK316	Br	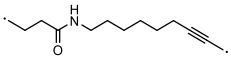	1.4 / >5
AK1931	Br	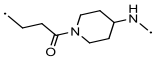	>5 / NA
AK1929	Br	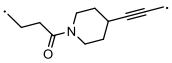	>5 / NA
AK2221	Br	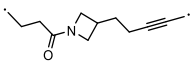	4.2 / NA
AK2222	Br	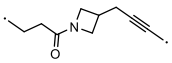	>5 / NA
AK2220	Br	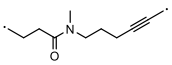	0.19 / >5
AK1994	Cl	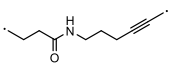	2.1 / >5
AK2000	Cl	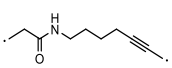	>5 / >5

Table 3 STAT5 Degraders with Various Linker Lengths and Compositions based on AK-2339.

Table 3. STAT5 Degraders with Various Linker Lengths and Compositions based on AK-2339.

We, then, constrained the linker while keeping the linker length about the same as AK-318. All our attempts to rigidify linkers failed to improve the STAT5 degradation efficiency demonstrated by AK-1931, AK-1929, AK-2221, and AK-2222, while a simple methyl introduction at amide nitrogen slightly improved DC_{50} with AK-2220. Based on AK-318, we replaced bromide with chloride shown as AK-1994 and kept all the other component the same, finding that the DC_{50} significantly decreased about 10 times. Further, we moved the position of the amide bond within the linker by one atom closer to the inhibitor side shown as AK-2000, and it completely lost the ability to degrade STAT5, indicating that the position of the amide group is likely important for the induction of STAT5 degradation.

3.3.6 Investigation of the Optimal Linker Length based on AK-014 for STAT5 Degraders.

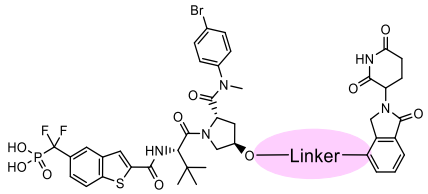

Cmpds	Linker	DC_{50} (STAT5/6, μM) SKNO1, 18 h
AK2019026	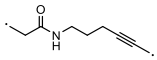	>5 / >5
AK2019027	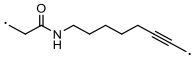	>5 / >5
AK2019028	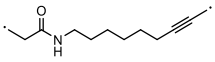	>5 / >5
AK2019029	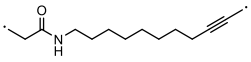	>5 / >5
AK2019030	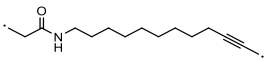	>5 / >5

Table 4 Putative Degraders with Various Linker Lengths Based on AK-014.

Table 4. Putative Degraders with Various Linker Lengths Based on AK-014.

AK-014 also binds to STAT5 and STAT6 to the same extent as AK-318 binds (Table 4) and it seemed reasonable for us to tether lenalidomide from the proline of AK-014 based on our predicted binding model (SI), co-crystals (Figure 2), and FP assay (Table 1). We synthesized a set of putative STAT5 or STAT6 degraders with various linker lengths (Table 4). As opposed to AK-2339 with which we tethered lenalidomide from C-terminus to obtain successful STAT5 degraders represented by AK-318, AK-014-based degraders did not show any sign of both STAT5 and STAT6 degradation. This is likely because AK-014-based degraders would not form a productive ternary complex with Cereblon, STAT5, and STAT6.

3.3.7 Investigation of the Optimal C-terminus Aromatic Group.

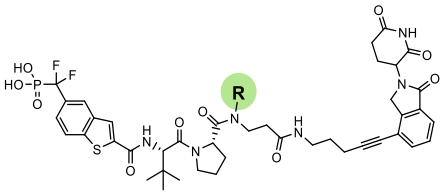

Cmpds	R	DC_{50} (STAT5μM) SKNO1, 18h	Cmpds	R	DC_{50} (STAT5μM) SKNO1, 18h
AK1992		>5	**AK2224**	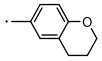	>5
AK1993		>5	**AK2145**	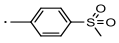	>5
AK1995	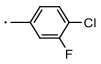	>5	**AK2100**	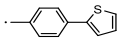	0.21
AK1996		0.53	**AK2146**	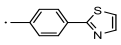	0.13
AK2094	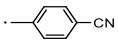	>5	**AK2102**	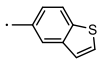	0.18
AK2095		>5	**AK2215**		>5
AK2096	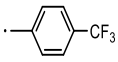	2.0	**AK2223**	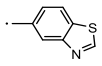	0.45
AK2097	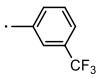	>5	**AK2217**	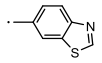	>5
AK2098	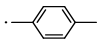	0.31	**AK2216**	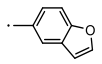	0.33
AK2099	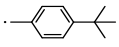	>5	**AK2147**	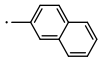	0.21
AK2103	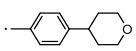	>5			

Table 5 STAT5 Degraders with Various C-terminus Aromatic Moieties.

Table 5. STAT5 Degraders with Various C-terminus Aromatic Moieties.

With AK-318 in our hand, we synthesized a series of STAT5 degraders with different C-terminus aromatic groups to improve the potency in inducing STAT5 degradation (Table 5). We paid more attention to the chemical space around the para-position of the C-terminus aromatic ring since our predicted modeling and co-crystals indicated that further introductions of hydrophobic groups around the para-position of the ring could confer the inhibitors and degraders more interactions with the surface of STAT5 protein. AK-1992 does not have any substitutions at the para-position of the benzene ring lost DC_{50} by 20 times compared to AK-318. AK-1993 and AK-1995 both having smaller size halogens than bromide also lost DC_{50} values to the similar extent as AK-1992. AK-1992 with iodide at the para-position retained the degradation efficiency but still DC_{50} was 2-fold worse than DC_{50} of AK-318. Cyan group shown in AK-2094 indicated no improvement in the STAT5 degradation efficiency. Trifluoromethyl group at the para-position indicated in AK-2096 but not at the ortho-position retained the STAT5 degradation capability to some extent. AK-2098 with methyl group at the para-position showed an equivalent STAT5 degradation efficiency as AK-318 while AK-2099, AK-2103, AK-2224, and AK-2145 with bulkier groups completely lost the STAT5 degradation. The introduction of another aromatic ring system at the para-position of the C-terminus benzene ring shown as AK-2146 and AK-2100 showed a better or equivalent DC_{50} values compared to AK-318. This improvement is consistent with the binding enhancement from AK-318's STAT5 inhibitor portion, AK-2339, to AK-2146's STAT5 inhibitor portion, AK-2305. The further extension of aromatic ring system shown in AK-2102, AK-2223, AK-2216, and AK-2147 also showed similar DC_{50} values as expected from the binding affinities of corresponding inhibitors. Overall, degraders with better binding affinities of corresponding inhibitors tend to show better STAT5 degradation efficiency and AK-2146 showed the best DC_{50} value among tested.

3.3.8 Optimization of Hydrophobic Residue, C-terminus Aromatic Ring, and Linker in Combination.

Further, we attempted to improve the STAT5 degradation efficiency. The corrective lessons leant from our STAT5 inhibitor and degradation optimization campaign suggested possible combinations of components (Table 6). In our linker length and component optimization trial, our data pointed the optimal linker length and composition as well as the position of amide group within the linker. In our C-terminus aromatic ring optimization attempts, extended aromatic ring systems showed better outcomes. In the hydrophobic residue optimization, improvement in STAT5 binding was rather minimal while replacement of tertiary butyl with other hydrophobic residue seemed possible, such as homophenylalanine residue with a similar binding affinity to STAT5, but with occupying larger chemical space than tertiary butyl.

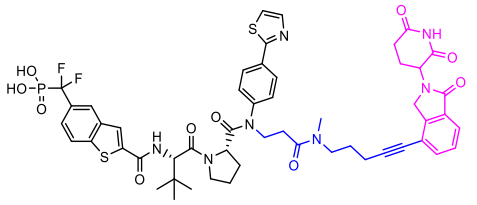

Cmpds	Hydrophobic residue	C-terminus ring	Linker	DC_{50} (STAT5, μM) SKNO1, 18 h
AK2146		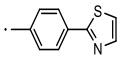	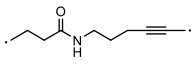	0.13
AK2292		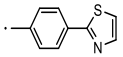	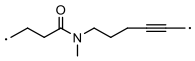	0.10
AK2435	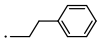	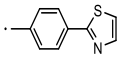	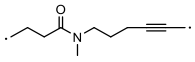	0.10
AK2238		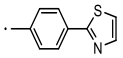	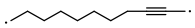	>5
AK2102			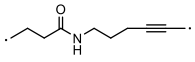	0.21
AK2438			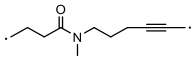	0.13
AK2147			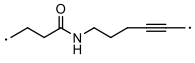	0.21
AK2291			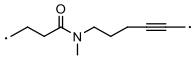	0.13
AK2216			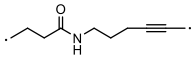	0.3
AK2236			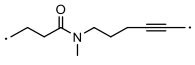	0.2
AK2223			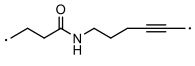	0.45
AK2437			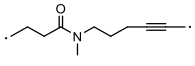	0.33

Table 6 STAT5 Degrader Analogues based on AK-2305.

Table 6. STAT5 Degrader Analogues based on AK-2305.

The observations were combined to synthesize a set of STAT5 degraders. As expected, in all cases, the linker with a N-methylated amide showed superior inductions of STAT5 degradation shown as AK-2292, AK-2438, AK-2291, AK-2236, and AK-2437, compared to the linker with a normal amide shown as AK-2146, AK-2102, AK-2147, AK-2216, and AK-2223. Interestingly, a removal of an amide boned from the linker while the length was kept about the same completely took the STAT5 degradation capability away demonstrated by AK-2238. Although AK-2435's inhibitor AK-2422 has a significantly large homophenylalanine residue as the hydrophobic residue, AK-2422 showed an equivalent binding affinity to STAT5 compared to AK-2305. Consistent with having a similar binding to STAT5, AK-2146 and AK-2435 showed a similar DC_{50}. Based on abovementioned observations, we chose AK-2292 as our best STAT5 degrader among tested and decided to evaluate AK-2292 in further biological studies.

3.3.9 Design and Synthesis of a Control Compound for AK2292.

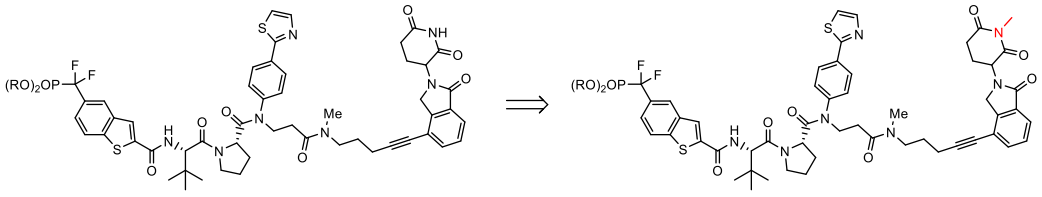

Figure 3-4 Design of AK-2292ME as a control compound.

Figure 4. Design of AK-2292ME as a control compound.

To check if cereblon/cullin 4A is involved and AK-2292 works under PROTAC mechanism, we synthesized a control compound, AK-2292ME in which a methyl group was installed in lenalidomide moiety to remove the binding affinity to cereblon/cullin 4A (Figure 4) [37]. Indeed, AK-2292ME failed to induce STAT5 degradation in SKNO1 and MV4;11 cell

lines (Fig), indicating that AK-2292 works under PROTAC mechanism. We used our STAT5 inhibitor, AK-2305, and AK-2292ME, an inactive STAT5 degrader, as control compounds.

3.3.10 AK-2292 shows a high degradation selectivity for STAT5A/B in proteome

Selectivity has been a challenge in STAT inhibitor development and indeed our STAT5 inhibitors do bind STAT6 with higher affinity than STAT5 (Table1), which prompted us to evaluate AK2292's degradation selectivity toward STAT5 over other STAT family proteins. Our western blot analysis displayed AK2292 as selectively depleting STAT5A/B and pSTAT5^{Y694} among STAT family proteins in SKNO1 and in MV4:11 (Figure 5). Our control compounds, AK-2305 and AK-2292ME failed to reduce the level of STAT5A/B as well as other STAT family proteins in both cell lines. Importantly, pSTAT5^{Y694} and pSTAT6^{Y691} are critical for the functions of STAT5 and STAT6 [33]. Our control compounds, AK-2305 and AK-2292ME cannot reduce the level of pSTAT5^{Y694} and pSTAT6^{Y691} at all at least up to 5 μM even though AK-2305 and AK-2292ME (SI for Ki value, Table 1) bind to SH2 domains of STAT5A/B and STAT6 with much higher affinities (Ki values: 0.5 to 1.2 μM), pointing to the tremendous challenge to develop inhibitors that are effective to modulate the functions of STAT5 and STAT6 and necessitating a non-traditional targeting technology such as PROTAC.

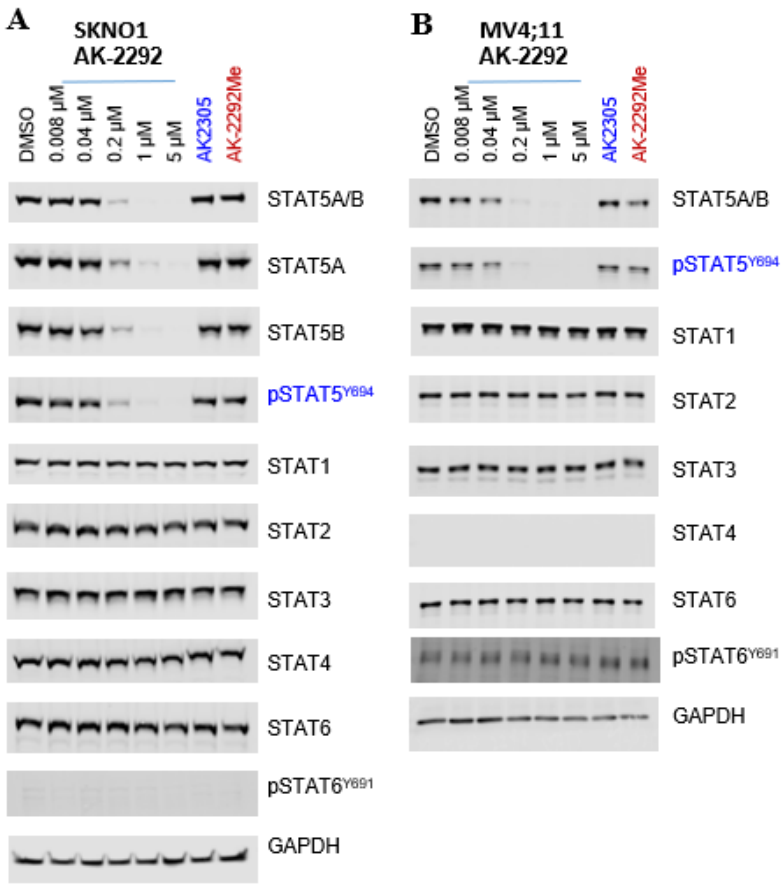

Figure 3-5 Figure 5. Western blotting analysis of STAT proteins in SKNO1 and MV4;11 cells treated with AK-2292 or control compounds AK-2305 and AK-2292ME.

Figure 5. Western blotting analysis of STAT proteins in SKNO1 and MV4;11 cells treated with AK-2292 or control compounds AK-2305 and AK-2292ME.

(A) SKNO1 cells were treated with AK-2292 at 0.008 − 5 µM or AK-2305 and AK-2292ME at 5 µM for 18 h. (B) MV4;11 cells were treated with AK-2292 at 0.008 − 5 µM or AK-2305 and AK-2292ME at 5 µM for 6 h.

3.3.11 Evaluation of STAT5 Degraders in SKNO1 Cells for Their Growth-Inhibitory Activities.

	SKNO1		
Cmpds	**DC_{50} (μM), 18 h**	**IC_{50} ± SD (μM) 3 days**	**IMAX ± SD (%) at 15 μM**
1992	>5	a	7 ± 1
1995	>5	a	11 ± 2
2097	>5	a	10 ± 1
2221	4.2	a	35 ± 4
1994	2.1	a	43 ± 2
2096	2.0	a	47 ± 4
316	1.4	a	35 ± 1
317	1.1	a	37 ± 2
2223	0.5	2.6 ± 0.1	54 ± 1
1996	0.5	a	51 ± 1
2216	0.3	5.6 ± 0.3	61 ± 2
2437	0.3	1.0 ± 0.4	61 ± 2
2098	0.3	a	42 ± 1
318	0.2	2.7 ± 0.4	58 ± 1
2436	0.2	1.0 ± 0.2	55 ± 3
2100	0.2	2.7 ± 0.2	55 ± 1
2147	0.2	2.9 ± 0.3	53 ± 1
2220	0.2	2.8 ± 0.4	61 ± 1
2102	0.2	1.7 ± 0.1	55 ± 1
2146	0.1	0.7 ± 0.1	53 ± 2
2291	0.1	1.8 ± 0.2	55 ± 3
2438	0.1	1.6 ± 0.4	57 ± 1
2292	0.1	0.4 ± 0.1	65 ± 1
2435	0.1	1.9 ± 0.1	69 ± 1
2305	>5	a	11 ± 1
2292ME	>5	a	6 ± 2

[a]Not tested.

Table 7 Degradation Potencies and Cell Growth-Inhibitory Activities of STAT5 Degraders

Table 7. Degradation Potencies and Cell Growth-Inhibitory Activities of STAT5 Degraders

AK-2292 efficiently depleted STAT5 as well as $pSTAT5^{Y694}$ and showed an excellent selectivity to STAT5 over other STAT family proteins (Figure 5). We then treated SKNO1 cells with a series of our STAT5 degraders together with control compounds to see if there are any

relationships among DC_{50}, IC_{50}, and Imax (Table 7). Control compounds, AK-2305 and AK-2292ME, and degraders with >5 µM DC_{50} values exemplified as AK-1992, AK-1995, and AK-2097 showed minimal impact on cell viability. On the contrary, degraders with lower DC_{50} values tend to decrease cell viability more significantly. All degraders with DC_{50} values below 0.5 µM seemed to reach roughly 60% viability reduction as the maximum effect of STAT5 degraders in SKNO1 cell line. Overall, we observed a good co-relation where STAT5 degraders with more efficient STAT5 degradation capability, namely better DC_{50} values, exerted superior growth-inhibitory activities shown in IC_{50} and Imax values together.

3.3.12 AK2292 displays growth-inhibitory activities in a subset of AML cells

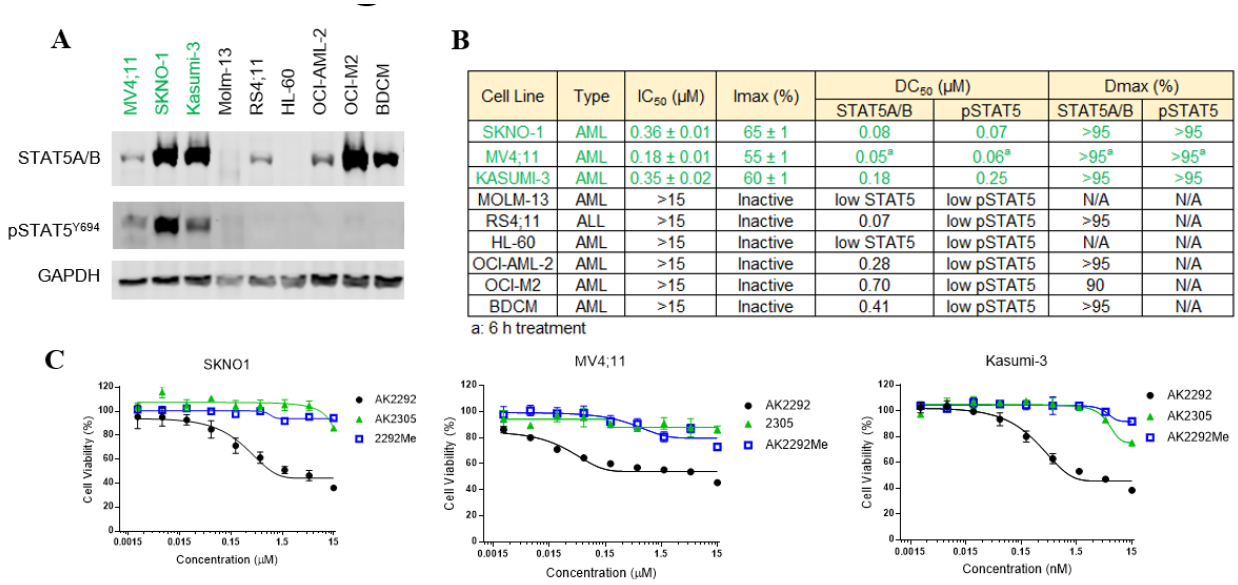

Cell Line	Type	IC_{50} (µM)	Imax (%)	DC_{50} (µM)		Dmax (%)	
				STAT5A/B	pSTAT5	STAT5A/B	pSTAT5
SKNO-1	AML	0.36 ± 0.01	65 ± 1	0.08	0.07	>95	>95
MV4;11	AML	0.18 ± 0.01	55 ± 1	0.05[a]	0.06[a]	>95[a]	>95[a]
KASUMI-3	AML	0.35 ± 0.02	60 ± 1	0.18	0.25	>95	>95
MOLM-13	AML	>15	Inactive	low STAT5	low pSTAT5	N/A	N/A
RS4;11	ALL	>15	Inactive	0.07	low pSTAT5	>95	N/A
HL-60	AML	>15	Inactive	low STAT5	low pSTAT5	N/A	N/A
OCI-AML-2	AML	>15	Inactive	0.28	low pSTAT5	>95	N/A
OCI-M2	AML	>15	Inactive	0.70	low pSTAT5	90	N/A
BDCM	AML	>15	Inactive	0.41	low pSTAT5	>95	N/A

a: 6 h treatment

Figure 3-6 Figure 6. AK2292's growth-inhibitory Activity in AML Cell Lines

Figure 6. AK2292's growth-inhibitory Activity in AML Cell Lines

(A) Immunoblot analysis of AML cell lines to profile the expression levels of indicated proteins. AK2292 responding cell lines are colored in green. (B) AK2292's growth-inhibitory activities were determined by CellTiter Glo assay (3 to 4 days). DC_{50} values of AK-2292 were calculated based on immunoblotting analysis of cells treated with AK-2292 for 18 hr. IC_{50} values are the means of three independent experiments. ALL: Acute lymphoblastic leukemia. AK2292

responding cell lines are colored in green. (C) Representative concentration-viability curves of CellTiter Glo assay.

We then investigated the growth-inhibitory effect of AK-2292 with various AML cell types [17]. We first analyzed 9 cell lines for a relative basal level of STAT5 and pSTAT5^{Y694} (Figure 6A) and found that there was a significant difference in the basal expression level among tested cell lines. Regarding the STAT5 expression level, SKNO1, Kasumi-3, OCI-M2, and BDCM express STAT5 at a high level whereas MV4;11, RS4;11, and OCI-AML2 have lower level of STAT5. Further contrastingly, MOLM-13 and HL-60 seemed to have very low level of STAT5. Regarding pSTAT5^{Y694} expression level, pSTAT5^{Y694} expression was high in only 3 cell lines, MV4;11 being the lowest, Kasumi-3, and SKNO1 being the highest. The rest of 6 cell lines showed a very low level of pSTAT5^{Y694}.

We next treated cells with AK-2292 and performed western blotting analysis to evaluate AK-2292's degradation capability for STAT5 and pSTAT5^{Y694} (Figure 6B). AK-2292 efficiently depleted STAT5 and pSTAT5Y^{694} with Dmax values >95% in cases where cells express detectable level of either STAT5 or pSTAT5^{Y694}. In MV4;11 cells, AK-2292 induced the degradation of STAT5 and pSTAT5^{Y694} with DC_{50} values being as low as 0.05 µM and 0.06 µM respectively at 6 h treatment time point (SI). AK-2292 also efficiently depleted STAT5 and pSTAT5^{Y694} in SKNO1 cells with DC_{50} values of 0.08 µM and 0.07 µM after 18 h treatment. In Kasumi-3 cells, AK-2292 showed DC_{50} values of 0.18 µM and 0.25 µM at 18 h time point for STAT5 and pSTAT5^{Y694} respectively (SI). RS4;11, OCI-AML2, OCI-M2, and BDCM cells do not have detectable level of pSTAT5^{Y694}, but have STAT5 expression. DC_{50} values for STAT5 were 0.07 µM, 0.28 µM, 0.70 µM, and 0.41 µM respectively. Molm-13 and HL-60 showed very low level of both STAT5 and pSTAT5^{Y694}.

We treated all 9 cells with AK-2292 for 3 days to see the effect of AK-2292 in the growth-inhibitory activity (Figure 6C). 3 cell lines, namely SKNO1, MV4;11, and Kasumi-3, out of 9 cells responded to AK-2292 with Imax values being 65%, 55%, and 60% respectively, while 6 cells did not decrease the viability up to 15 μM. We observed that 3 responding cell lines express pSTAT5^{Y694}, which is the active form of STAT5, and rest of 6 cell lines do not, indicative of pSTAT5^{Y694} being an indicator of cellular response to AK-2292 in AML cells. Importantly, the response of SKNO1, MV4;11, and Kasumi-3 is not complete, but rather partial, which warrants further study to investigate the reason of their partial response instead of complete response.

3.3.13 AK2292 effectively depletes STAT5A/B proteins in mouse xenograft tumors

We examined AK2292's pharmacodynamics (PD) effect in MV4;11 tumor bearing mice (Figure). Our western blotting analysis displayed that a single intraperitoneal (i.p.) dose of AK2292 at 150 mg/kg effectively decreased STAT5A/B protein level at 1 h, and nearly completely depleted STAT5A/B protein at 6 h in MV4;11 tumor tissues. At 24 h time point, however, STAT5A/B protein started to rise again in all of three tumor tissues. Our PD data thus demonstrated that a single dose of AK2292 is effective in inducing STAT5A/B and pSTAT5^{Y694} proteins in mouse tissues with the effect persisting for around 24 h.

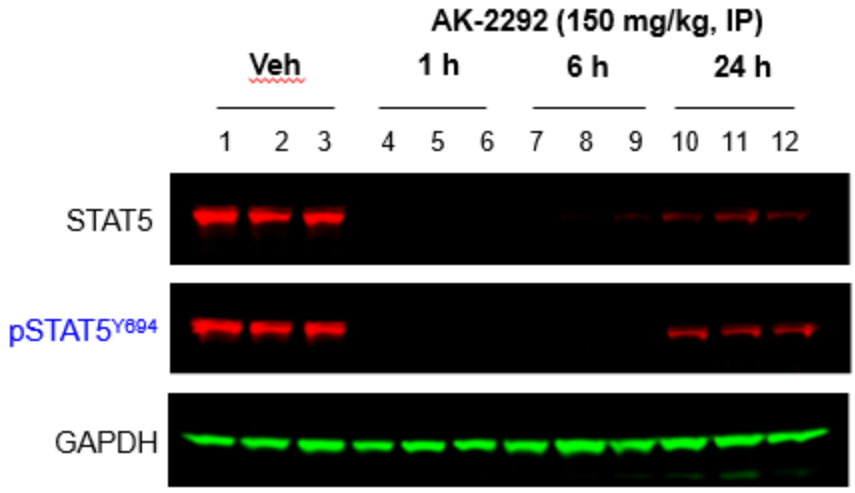

Figure 3-7 Figure 7. Pharmacodynamics study of AK-2292 in MV4;11 tumor tissues

Figure 7. Pharmacodynamics study of AK-2292 in MV4;11 tumor tissues

SCID mice bearing MV4;11 were treated i.p. as indicated and tumor cell lysates were analyzed by immunoblotting.

3.3.14 AK2292 is well-tolerated in immune competent mice and achieves a significant tumor regression in mouse xenograft models

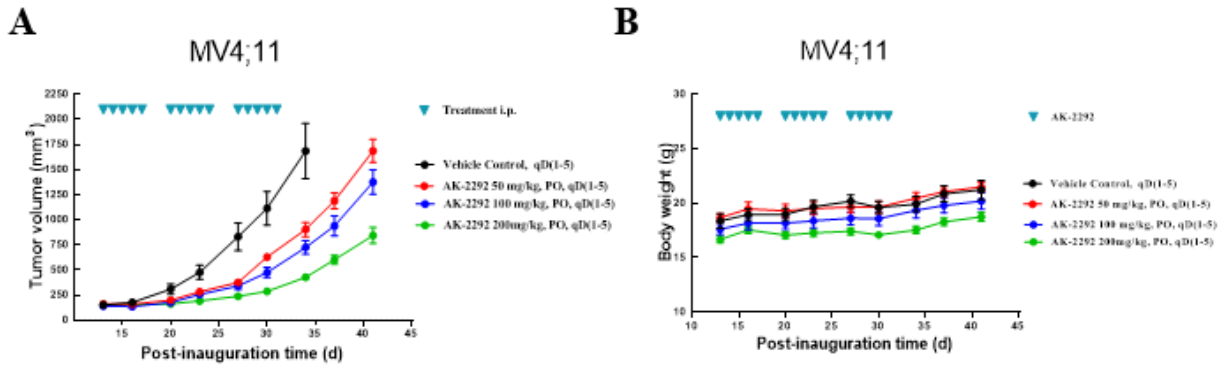

Figure 3-8 Figure 8. Antitumor Activity of AK2292 in the MV4;11 Xenograft Model in Mice.

Figure 8. Antitumor Activity of AK2292 in the MV4;11 Xenograft Model in Mice.

(A) MV4;11 Tumor-bearing SCID mice were treated under the indicated treatment schedules. Tumor volumes were measured every 2-3 days (mean ±SEM; n = 8). qD: daily, (B) SCID mice bearing MV4;11 tumor were treated under the indicated treatment schedules and the body weights of mice were measured every 2-3 days (mean ± SEM; n = 8)

We also tested AK2292 in the MV4;11 xenograft model in SCID female mice (figure 8). Our cell viability assay indicated that AK2292 likely induced cell cycle arrest instead of cell killing in MV4;11 cells. We observed a similar effect *in vivo*, not showing the tumor regression, but still significantly delaying MV4;11 tumor growth.

3.4 CHEMISTRY

Scheme 1. Synthesis of 5-(Difluoro(phosphono)methyl)benzo[b]thiophene-2-carboxylic acid (95)

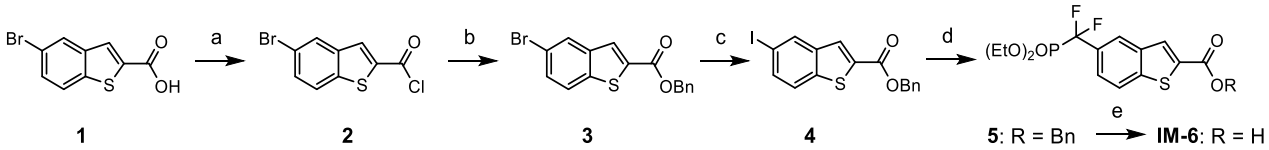

Figure 3-9 Scheme 1. Synthesis of 5-(Difluoro(phosphono)methyl)benzo[b]thiophene-2-carboxylic acid (95)

Reaction conditions: (a) Oxalyl Chloride, DMF, DCM, 0 °C to rt; (b) BnOH, TEA, DCM, rt; (c) CuI, KI, Dioxane, DMEDA, 110 °C, sealed; (d) BrCdCF2PO3Et2, CuI, DMF, rt; (e) Pd/C, H2, MeOH, rt

Scheme 2. Synthesis of AK256 – AK078

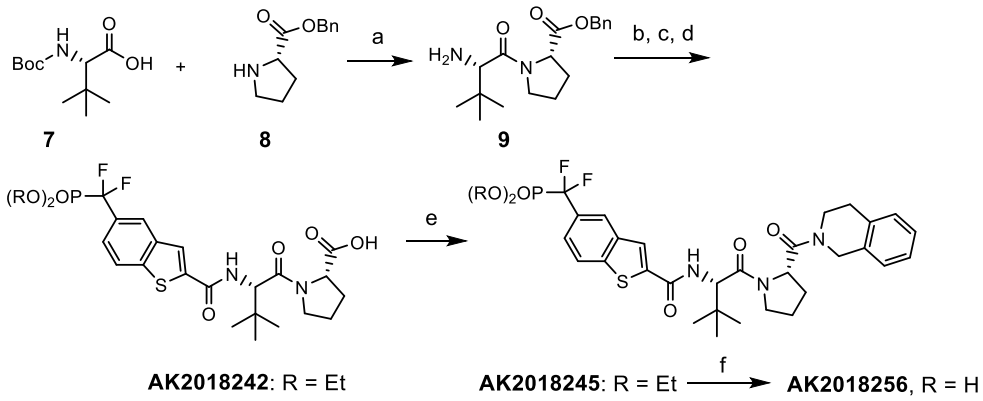

Figure 3-10 Scheme 2. Synthesis of AK256 – AK078

Reaction conditions: (a) HATU, DIPEA, DMF, rt; (b) TFA, DCM, rt; (c) HATU, TEA, DMF, rt; (d) Pd/C, H_2, EtOH, rt; (e) HATU, DIPEA, DMF, rt; (f) TMSI, BSTFA, DCM, 0 °C.

Scheme 3. Synthesis of AK2305 -

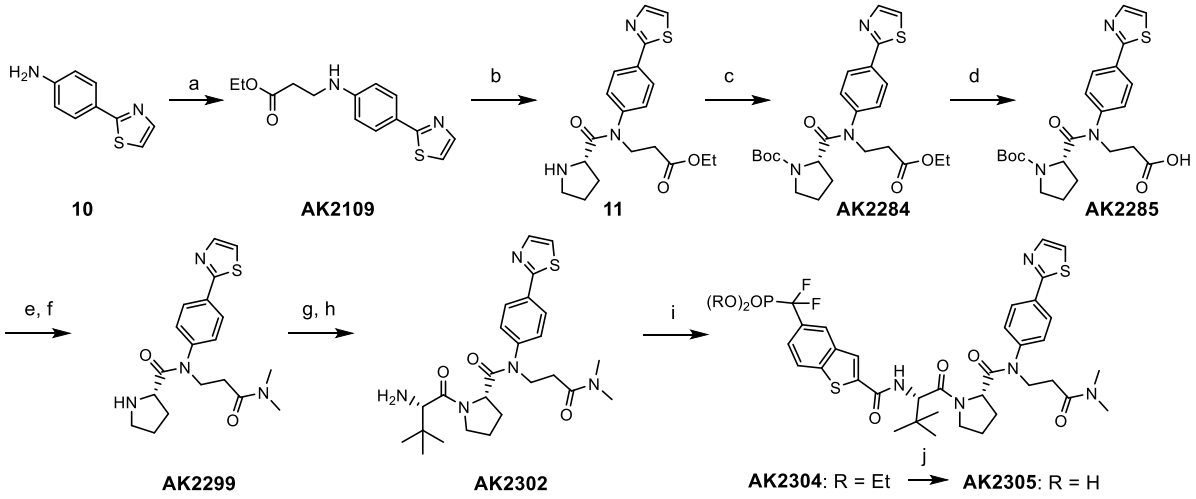

Figure 3-11 Scheme 3. Synthesis of AK2305

Reaction conditions: (a) Ethylacrylate, AcOH, 90 °C; (b) PCl_5, $CHCl_3$, 50 °C; (c) Boc2O, TEA, CH_3CN, rt; (d) LiOH, MeOH, water, rt; (e) HATU, DIPEA, DMF, rt; (f) TFA, DCM, rt; (g) HATU, DIPEA, DMF, rt; (h) TFA, DCM, rt; (i) HATU, DIPEA, DMF, rt; (j) TMSI, BSTFA, DCM, rt, 0 °C

Scheme 4. Synthesis of AK014

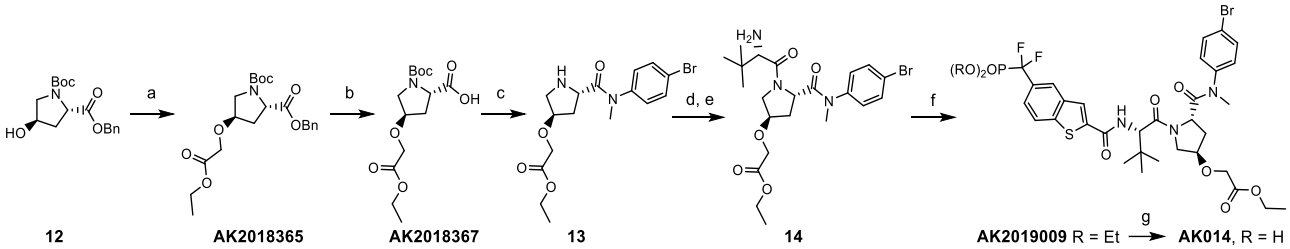

Figure 3-12 Scheme 4. Synthesis of AK014

Reaction conditions: (a) Ethylbromoacetate, NaH, TBAC, THF, rt; (b) Pd/C, H_2, EtOH, rt; (c) PCl_5, $CHCl_3$, 50 °C; (d) HATU, DIPEA, DMF, rt; (e) TFA, DCM, rt; (f) HATU, DIPEA, DMF, rt; (g) TMSI, BSTFA, DCM, 0 °C.

Scheme 5. Synthesis of AK2292 -

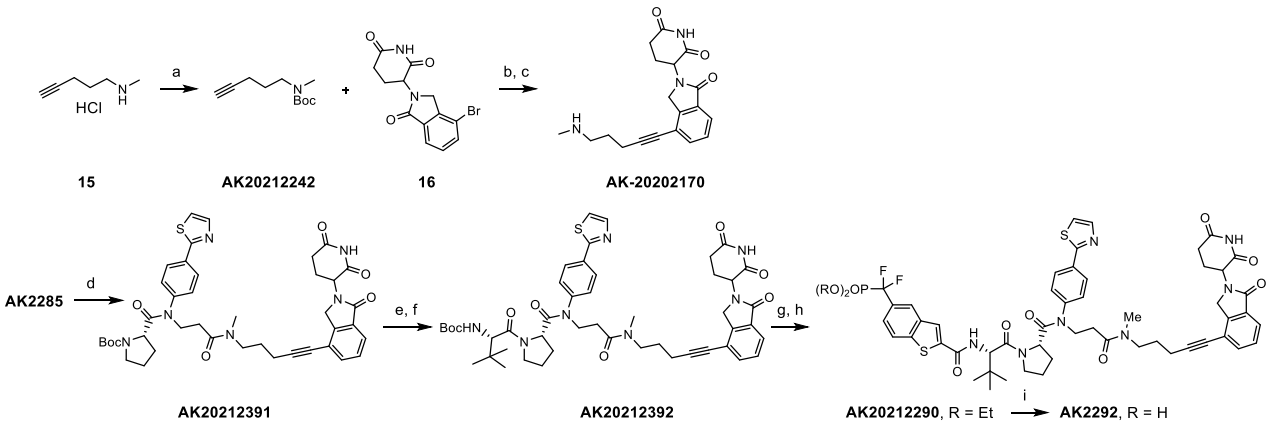

Figure 3-13 Scheme 5. Synthesis of AK2292 -

Reaction conditions: (a) Boc2O, TEA, CH_3CN, rt; (b) $PdCl2(PPh_3)_2$, CuI, TEA/DMF, 90 °C; (c) TFA, DCM, rt; (d) HATU, DIPEA, DMF, rt; (e) TFA, DCM, rt; (f) HATU, DIPEA, DMF, rt; (g) TFA, DCM, rt; (h) HATU, DIPEA, DMF, rt; (i) TMSI, BSTFA, DCM, rt, 0 °C

Scheme 6. Synthesis of AK026 –

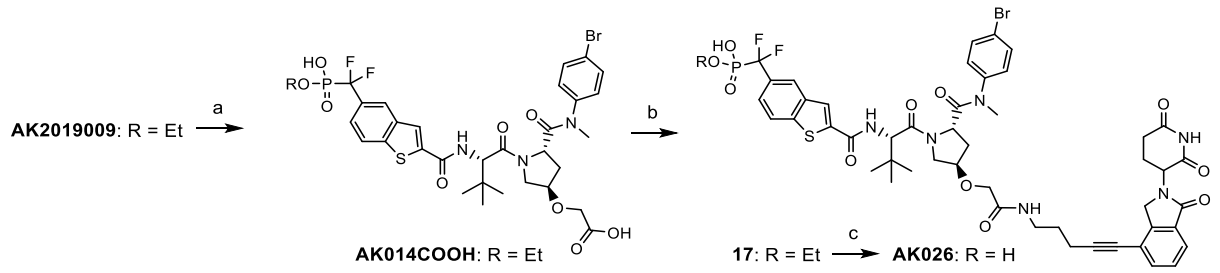

Figure 3-14 Scheme 6. Synthesis of AK026

Reaction conditions: (a) LiOH, MeOH, water, rt; (b) HATU, DIPEA, DMF, rt; (c) TMSI, BSTFA, DCM, 0 °C.

Scheme 7. Synthesis of AK2238

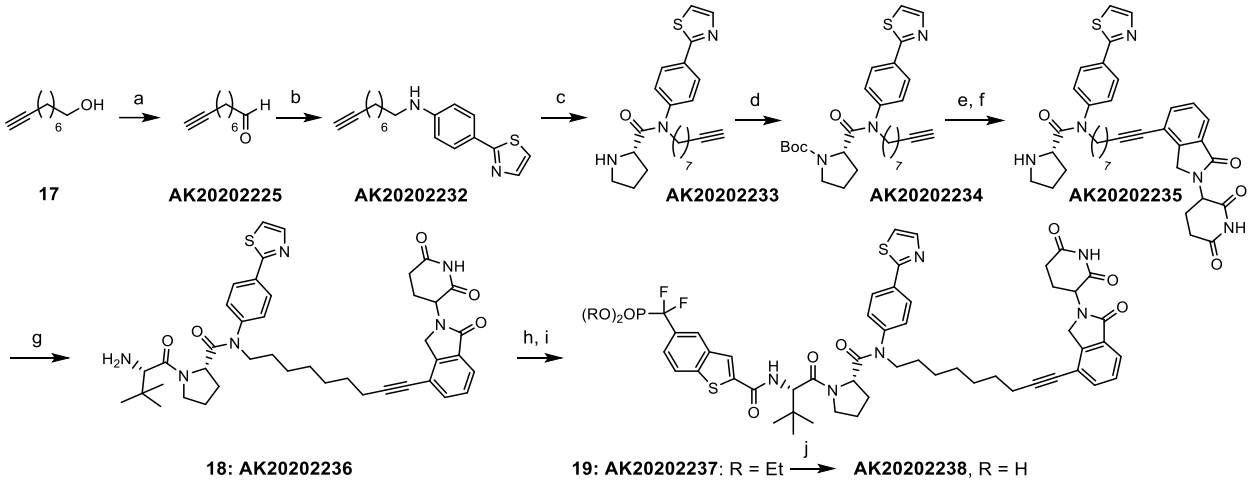

Figure 3-15 Scheme 7. Synthesis of AK2238

Reaction conditions: (a) IBX, DCM, rt; (b) $NaB(OAc)_3$, AcOH, DCM, rt; (c) PCl_5, $CHCl_3$, 50 °C; (d) Boc_2O, TEA, CH3CN, rt; (e) $PdCl_2(PPh_3)_2$, CuI, TEA/DMF, 90 °C; (f) TFA, DCM, rt; (g) HATU, DIPEA, DMF, rt; (h) TFA, DCM, rt; (i) HATU, DIPEA, DMF, rt; (j) TMSI, BSTFA, DCM, rt, 0 °C

Scheme 8. Synthesis of AK330

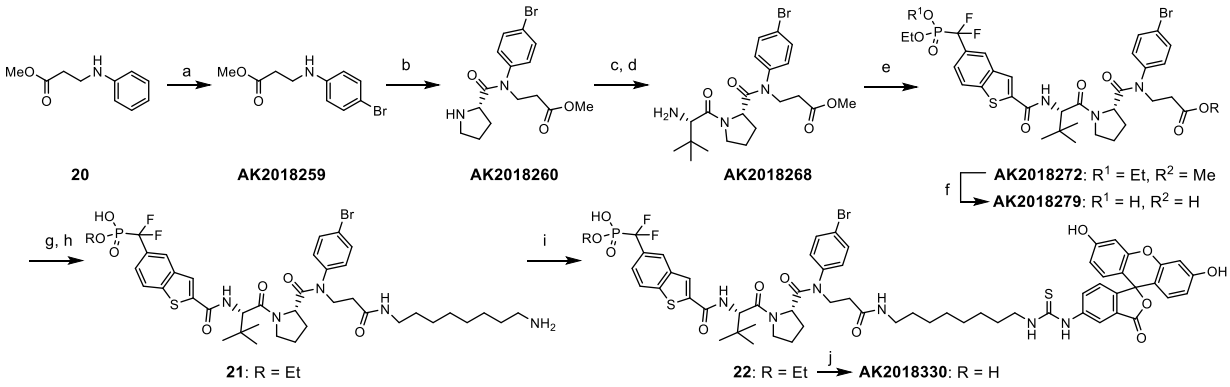

Figure 3-16 Scheme 8. Synthesis of AK330

Reaction conditions: (a) NBS, CH_3CN, rt; (b) PCl_5, $CHCl_3$, 50 °C; (c) HATU, DIPEA, DMF, rt; (d) TFA, DCM, rt; (e) HATU, DIPEA, DMF, rt; (f) LiOH, MeOH, water, rt; (g) HATU, DIPEA, DMF, rt; (h) TFA, DCM, rt; (i) DIPEA, DMF, rt; (j) TMSI, BSTFA, DCM, rt, 0 °C

Scheme 1 outlines the synthesis of the protected phosphoryrosine mimetic, 5-((diethoxyphosphoryl)difluoromethyl)benzo[b]thiophene-2-carboxylic acid **(IM-6**). Acid chloride **2** was generated from the responding carboxylic acid **1**, followed by the ester formation to yield **3**. Copper-catalyzed halogen exchange reaction yielded **4**. The α,α-difluoro derivative of **5** was synthesized as previously reported [90]. Finally, hydrogenation of **5** removed benzyl group to yield **IM-6**.

Scheme 2 outlines the synthesis of **AK-2018256**. The acid **AK-2018242** was synthesized by common amide couplings and deprotections. This acid was used as a key intermediate to synthesize analogues. **AK-2018242** was coupled with 1,2,3,4-tetrahydroisoquinoline and the resulting diethyl phosphate **AK-2018245** was treated with TMSI to yield **AK-2018256**. The same synthetic route was used to synthesize **AK-2452**, **AK-070**, **AK-073**, **AK-075**, **AK-063**, and **AK-078**.

Scheme 3 shows the synthesis of **AK-305**. 4-(thiazol-2-yl)aniline and ethylacrylate were heated in acetic acid to give a Michael adduct **AK-2109**. **AK-2109** was heated with excess amount of both Boc-proline and PCl_5 to give **11**. *N*-alkylanilines turned out to have relatively poor reactivities in amide coupling reactions and necessitated such uncommon coupling condition. From **11**, Boc protection and hydrolysis yielded the acid **AK-2285**. Multiple common amide couplings and deprotections generated the diethyl phosphate **AK-2304**. The removal of ethyl group from **AK-2304** by TMSI gave **AK-2305**.

Scheme 4 outlines the synthesis of **AK-014**. The hydroxyl group of *trans*-4-hydroxyproline was alkylated with ethybromoacetate under basic condition and benzyl group was removed by hydrogenation to yield **AK-2018367**. Excess amount of *N*-alkylaniline and PCL_5 were used to afford **13**. After multiple common amide couplings and deprotections gave the diethyl phosphate **AK-2019009**. The removal of ethyl group from AK-2019009 by TMSI generated **AK-014**.

Scheme 5 shows the synthesis of **AK-2292**. The linker amine was Boc protected and coupled with Cereblon ligand. After the removal of Boc, **AK-20202170** was obtained. **AK-2285** was coupled with **AK-20202170**, *N*-Boc-L-*tert*-leucine, and **IM-6** sequentially, followed by TMSI treatment to give **AK-2292**.

Scheme 6 explains the synthesis of **AK-026**. **AK-2019009** was exposed under hydrolysis condition to have carboxylic acid **AK-014COOH**. The resulting acid was coupled with Cereblon ligand via its linker amine to generate **AK-026**.

Scheme 7 outlines the synthesis of **AK-2338**. The alcohol was oxidized by Dess-martin periodinane and then exposed to hydroamination to make **AK-20202232**. Excess amount of Boc-L-proline and PCl_5 with heat generated **AK-20202233**. The resulting alkyne was coupled with Cereblon ligand under Sonogashira coupling, followed by Boc deprotection to generate **AK-20202235**. After sequential amide couplings with *N*-Boc-*tert*-leucine and **IM-6**, followed by TMSI treatment, yielded **AK-2238**.

Scheme 8 explains the synthesis of AK-2018330FL, a tracer for STAT5A/B and STAT6. Bromide was introduced at the para position of the aniline. The resulting aniline was mixed with excess amount of Boc-L-proline and PCl_5 to generate **AK-2018260**. Common amide couplings with *N*-Boc-*tert*-leucine and **IM-6** yielded the diethyl phosphate **AK2018272**. The acid **AK-**

2018279 was synthesized by hydrolysis. The acid was coupled with mono-Boc protected diamine and the resulting Boc amine was deprotected to yield **22**. The resulting amine and isothiocyanate fluorescein formed thiourea **22**. The ethyl group of **22** was removed by TMSI to yield **AK-2018330FL**.

3.5 CONCLUSION

In this study, we report noble STAT5/6 SH2 domain inhibitors and most importantly a series of potent, selective, efficacious STAT5A/B PROTAC degraders with AK-2292 being the best compound. Starting from our initial idea that McMurray group's STAT6 inhibitors may have binding to STAT5 due to their structural similarities especially in SH2 domain, we developed from a very weak STAT5 binder (Ki: > 10 uM) a set of STAT5/6 inhibitors with moderate binding affinity to STAT5 (Ki: 0.6-1.2 uM) and better binding affinity to STAT6 (Ki 0.1-0.6 uM). We faced tremendous difficulties in developing STAT5 selective inhibitors over STAT6, leading us to employing PROTAC technology to our non-selective STAT5/6 inhibitors.
Our newly reporting 3 co-crystal structures (PDBs) as well as previously reported (PDB) co-crystal structure gave us a basis of developing PROTAC degrader. AK-2292 as the best STAT5 degrader efficiently and selectively degrade STAT5 and importantly pSTATY694, an active form of STAT5, over other STAT family proteins, namely STAT1, STAT2, STAT3, STAT4, and STAT6. AK-2292 exerts growth-inhibitory activities in a set of AML cell lines, SKNO1, MV4;11, and Kasumi-3, all of which express pSTAT5Y694, but also showed no effect up to 15 uM in cell growth in a type of AML cells that do not express or only have very low level of pSTAT5Y694, indicating that pSTAT5Y694 level would be a good indicator of cellular response to AK-2292. AK-2292 also depletes STAT5 and pSTAT5Y694 in tumor tissues and significantly delayed tumor growth in MV4;11 tumor model without causing weight loss. Based on AK-

2292's excellent selectivity toward STAT5 over other STAT family proteins, and AK-2292's efficient STAT5 degradation in various cell types and in vivo, AK-2292 will serve as a great tool compound to study STAT5 biology and potentially offer a firm starting point to develop a new therapeutic to treat diseases where STAT5 plays a pivotal role.

3.6 EXPERIMENTAL SECTION

3.6.1 Chemistry General Information.

Unless otherwise noted, all purchased reagents were used as received without further purification. ^{1}H NMR and ^{13}C NMR spectra were recorded on a Bruker Advance 400 MHz spectrometer. ^{1}H NMR spectra were reported in parts per million (ppm) downfield from tetramethylsilane (TMS). All ^{13}C NMR spectra were reported in ppm and obtained with ^{1}H decoupling. In reported spectral data, the format (δ) chemical shift (multiplicity, J values in Hz, integration) was used with the following abbreviations: s = singlet, d = doublet, t = triplet, q = quartet, m = multiplet. Mass spectral (MS) analysis was carried out with a Waters UPLC mass spectrometer. Flash column chromatography was performed using silica gel (type H) from TM Chemicals, Inc. The final compounds were purified by C18 reverse phase preparative HPLC column with solvent A (0.1% TFA in H_2O) and solvent B (0.1% TFA in CH_3CN) as eluents. The purity of all the final compounds was confirmed to be >95% by UPLC−MS or UPLC.

3.6.2 Synthesis Procedures and Spectrum Data

5-(Difluoro(phosphono)methyl)benzo[b]thiophene-2-carboxylic acid (IM-6). To a 100 mL round bottom flask equipped with a magnetic stirring bar was added 5-bromobenzo[b]thiophene-2-carboxylic acid 1 (1.0 g, 3.9 mmol, 1.0 equiv) and anhydrous DCM (50 mL). The suspension was cooled with ice/water bath before adding oxalyl chloride (1.5 g,

11.7 mmol, 3.0 equiv) and DMF (0.3 mL). The solution was stirred at this temperature for 30 minutes and returned to room temperature. The suspension became a clear solution after 1.5 h. All of the solvent and excess oxalyl chloride was removed in vacuum. The residual crude product 2 was used directly for the next step without further purification.

To a 100 mL round bottom flask equipped with a magnetic stirring bar was added previous crude acyl chloride 2 and anhydrous DCM (50 mL). The solution was cooled in an ice water bath before adding benzyl alcohol (0.8 g, 0.8 mL, 7.8 mmol, 2.0 equiv) and triethylamine (1.2 g, 1.6 mL, 11.7 mmol, 3.0 equiv). The solution was returned to room temperature and stirred for 1 h before quenching with ammonium chloride aqueous solution. The reaction was extracted with DCM (50 mL x 3), dried with anhydrous sodium sulfate, filtered and concentrated under vacuum. The residual crude product was purified by flash column chromatography (PE:EA = 10:1) to afford the desired benzylic ester 3 as a white solid (1.1 g, 85% yield).

To a 50 mL sealed bottle equipped with a magnetic stirring bar was filled with argon before adding Benzyl 5-bromobenzo[b]thiophene-2-carboxylate 3 (1.0 g, 2.9 mmol, 1.0 equiv), copper(I) iodide (110 mg, 0.58 mmol, 0.2 equiv), potassium iodide (1.0 g, 5.8 mmol, 2.0 equiv), N,N'-Dimethylethane- 1,2-diamine (51 mg, 62 L, 0.58 mmol, 0.2 equiv) and anhydrous 1,4-dioxane (20 mL). The reaction system was changed to argon atmosphere another three times before reacting at 110 °C for 24 h. The reaction system was cooled to room temperature and quenched with ammonium chloride aqueous solution. The reaction mixture was extracted with EtOAc (50 mL x 3), washed with brine, dried with anhydrous sodium sulfate, then filtered and concentrated under vacuum. The residual crude product was purified by flash column chromatography (PE:EA = 10:1) to afford the mixture of desired iodide 4 and starting material 3

as a white solid (0.85 g, 4:3 = 3:1 monitored by LC-MS). This mixture can be used directly for the next step without further purification.

A 50 mL round bottom bottle equipped with a magnetic stirring bar was filled with argon before adding the previous mixture of 4 and 3 (0.85 g, 4:3 = 3:1, 2.1 mmol, 1.0 equiv), copper(I) iodide (0.8 g, 4.2 mmol, 2.0 equiv) and Cadmium reagent DMF solution A (13 mL, 0.33M, 4.2 mmol, 2.0 equiv). The reaction system was changed to argon atmosphere another three times before stirring at room temperature for 24 h. The reaction mixture was quenched with ammonium chloride aqueous solution, extracted with EtOAc (50 mL x 3), washed with brine for three times, dried with anhydrous sodium sulfate, filtered, and concentrated under vacuum. The residual crude product was purified by flash column chromatography (PE:EA = 1:1) to generate the desired phosphate 5 as a colorless oil (0.5 g, 70% yield).

A 50 mL round bottom bottle equipped with a magnetic stirring bar was filled with argon before adding benzyl 5-((diethoxyphosphoryl)difluoromethyl) benzo[b]thiophene-2-carboxylate 5 (130 mg, 0.28 mmol, 1.0 equiv), methanol (5 mL) and 10% Pd/C (150 mg). The reaction system was changed to hydrogen atmosphere three times before stirring at room temperature for 5 min (a longer reaction time can reduce the yield of this reaction). The reaction mixture was filtered to remove Pd/C and the solvent was removed under vacuum. The residual crude product was purified by HPLC (MeCN/H20 35%-100%, 65min, 60 mL/min, the product started coming out when MeCN was 46%) to afford the desired carboxylic acid **IM-6** as a white solid (43 mg, 42% yield). NMR (400 MHz, Methanol-i/4) δ 8.20 (s, 1H), 8.17 (s, 1H), 8.09 (d, = 8.4 Hz, 1H), 7.67 (d, = 8.4 Hz, 1H), 4.29-4.17 (m, 4H), 1.31 (td, = 7.1, 0.7 Hz, 6H). UPLC-MS calculated for $C_{14}H_{16}F_2O_5PS^+$ 365.03, found $[M + H]^+$ 365.24.

((2-(((S)-3,3-dimethyl-1-oxo-1-((S)-2-(1,2,3,4-tetrahydroisoquinoline-2-carbonyl)pyrrolidin-1-yl)butan-2-yl)carbamoyl)-1H-inden-5-yl)difluoromethyl)phosphonic acid (AK-256). To compound **7** (840 mg, 3.6 mmol) and **8** (740 mg, 3.6 mmol), CH_3CN (10 ml), triethylamine (0.74 ml, 1.5 equiv.) and HATU (1.5 g, 1.2 equiv.) were added. The mixture was stirred at room temperature for 30 min. The yellow solution was concentrated in vacuum and the crude was purified by flash column chromatography to yield Boc-protected **9**. Boc protection was removed by DCM/TFA at room temperature for 30 min. The volatile components were removed in vacuum to yield **9** as a TFA salt in 80% (1.2 g). To compound **9**, CH_3CN (10 ml), triethylamine (2 ml, 5 equiv.), benzothiophene head **IM-6** (1 g, 3.1 mmol, 1.1 equiv.), and HATU (1.3 g, 1.2 equiv.) were added. The mixture was stirred at room temperature for 30 min. The yellow solution was concentrated in vacuum and the crude was purified by flash column chromatography. The obtained compound was treated with 10% Pd/C and hydrogen in ethanol (10 ml) at room temperature for 1 h, followed by the filtration and concentration, to yield **AK2018242** in 75% (2 steps, 1.2 g). ^{1}H NMR (400 MHz, DMSO) δ 12.44 (s, 1H), 8.63 – 8.36 (m, 2H), 8.21 (d, *J* = 8.6 Hz, 1H), 8.11 (d, *J* = 1.7 Hz, 1H), 7.63 – 7.57 (m1H), 4.77 (d, *J* = 8.9 Hz, 1H), 4.30 – 4.25 (m, 1H), 4.18 – 4.05 (m, 4H), 4.00 – 3.85 (m, 1H), 3.73 – 3.66 (m, 1H), 2.25 – 2.11 (m, 1H), 2.01 – 1.76 (m, 3H), 1.25 – 1.15 (m, 6H), 1.08 (s, 9H). ESI−MS calculated for $C_{25}H_{33}F_2N_2O_7PS^+$ 574.58, found $[M + H]^+$ 575.51.

To **AK2018242** (20 mg, 0.035 mmol), CH_3CN (1 ml), DIPEA (20 µl, 3 equiv.), 1,2,3,4-tetrahydroisoquinoline (10 µg, 1.5 equiv.), and HATU (15 mg, 1.1 equiv.) were added. The mixture was stirred at room temperature for 30 min. The yellow solution was purified by HPLC to yield **AK2028245** in 85% (20 mg). ^{1}H NMR (400 MHz, DMSO) δ 8.53 – 8.50 (m, 1H), 8.44 – 8.32 (m, 1H), 8.21 (d, *J* = 8.6 Hz, 1H), 8.10 (s, 1H), 7.62 – 7.58 (m, 1H), 7.20 – 7.15 (m, 4H),

5.03 – 4.87 (m, 1H), 4.84 – 4.66 (m, 2H), 4.20 – 4.05 (m, 5H), 3.95 – 3.85 (m, 2H), 3.72 – 3.62 (m, 3H), 3.00 – 2.93 (m, 1H), 2.89 – 2.71 (m, 1H), 2.33 – 2.13 (m, 1H), 2.02 – 1.83 (m, 2H), 1.82 – 1.55 (m, 1H), 1.25 – 1.15 (m, 6H), 1.07 (s, 9H). ESI−MS calculated for $C_{34}H_{42}F_2N_3O_6PS^+$ 689.76, found $[M + H]^+$ 690.12.

To a round bottom flask were added **AK2028245** (15 mg, 0.02 mmol, 1 equiv.), DCM (2 ml) and $CF_3CON(TMS)_2$ (32 µl, 6 equiv.). The solution was cooled in an ice bath. To the ice cooled reaction mixture, 1M of TMS-I in DCM (0.1 ml, 5 equiv.) was added dropwise and the mixture was stirred for 10 min in an ice bath. The volatile components were removed under vacuum at below 5°C. The residue was dissolved in a mixed solvent of CH_3CN (3 ml) and water (1 ml). The resulting solution was purified by HPLC to yield **AK2018256** in 83% (11 mg). ^{1}H NMR (400 MHz, DMSO) δ 8.51 (d, *J* = 4.3 Hz, 1H), 8.34 – 8.24 (m, 1H), 8.11 (d, *J* = 8.5 Hz, 1H), 8.03 (s, 1H), 7.58 (d, *J* = 8.6 Hz, 1H), 7.19-7.21 (m, 3H), 4.98-4.92 (m, 1H), 4.84 – 4.63 (m, 2H), 4.51-4.97 (m, 1H), 3.98 – 3.79 (m, 2H), 3.73 – 3.61 (m, 2H), 3.00 – 2.89 (m, 1H), 2.88 – 2.67 (m, 1H), 2.31 – 2.07 (m, 1H), 2.06 – 1.81 (m, 2H), 1.73 – 1.67 (m, 1H), 1.07 (s, 9H). ESI−MS calculated for $C_{30}H_{34}F_2N_3O_6PS^+$ 633.65, found $[M + H]^+$ 634.25.

((2-(((S)-3,3-dimethyl-1-oxo-1-((S)-2-(phenylcarbamoyl)pyrrolidin-1-yl)butan-2-yl)carbamoyl)benzo[b]thiophen-5-yl)difluoromethyl)phosphonic acid (AK2452). AK2452 was synthesized by following a similar procedure used for **AK256**. ^{1}H NMR (400 MHz, DMSO) δ 10.03 (s, 1H), 8.53 (s, 1H), 8.35 (d, *J* = 8.7 Hz, 1H), 8.14 (d, *J* = 8.6 Hz, 1H), 8.05 (s, 1H), 7.64 – 7.52 (m, 3H), 7.38 – 7.24 (m, 2H), 7.11 – 6.96 (m, 1H), 4.77 (d, *J* = 8.7 Hz, 1H), 4.49 (dd, *J* = 8.1, 5.3 Hz, 1H), 3.90 – 3.85 (m, 1H), 3.76 – 3.70 (m, 1H), 2.23 – 2.16 (m, 1H), 2.06 – 2.00 (m, 1H), 1.98 – 1.82 (m, 2H), 1.09 (s, 9H). ESI−MS calculated for $C_{27}H_{30}F_2N_3O_6PS^+$ 593.58, found $[M + H]^+$ 594.12.

((2-(((S)-3,3-dimethyl-1-oxo-1-((S)-2-(2,3,4,5-tetrahydro-1H-benzo[d]azepine-3-carbonyl)pyrrolidin-1-yl)butan-2-yl)carbamoyl)-1H-inden-5-yl)difluoromethyl)phosphonic acid (AK-070) AK070 was synthesized by following a similar procedure used for **AK256**. ^{1}H NMR (400 MHz, DMSO) δ 8.50 (s, 1H), 8.31 (d, *J* = 8.9 Hz, 1H), 8.07 (d, *J* = 8.5 Hz, 1H), 8.01 (s, 1H), 7.65 – 7.50 (m, 1H), 7.25 – 7.02 (m, 4H), 4.94 (dd, *J* = 8.2, 6.4 Hz, 1H), 4.79 (d, *J* = 8.9 Hz, 1H), 3.95 – 3.88 (m, 3H), 3.69 – 3.59 (m, 2H), 3.20 – 3.10 (m, 2H), 2.90 – 2.76 (m, 3H), 2.24 – 2.15 (m, 1H), 2.06 – 1.94 (m, 1H), 1.92 – 1.77 (m, 1H), 1.69 – 1.65 (m, 1H), 1.09 (s, 9H). ESI−MS calculated for $C_{32}H_{38}F_2N_3O_6PS^+$ 647.67, found $[M + H]^+$: 648.40.

((2-(((S)-1-((S)-2-(benzyl(methyl)carbamoyl)pyrrolidin-1-yl)-3,3-dimethyl-1-oxobutan-2-yl)carbamoyl)benzo[b]thiophen-5-yl)difluoromethyl)phosphonic acid (AK-073) AK073 was synthesized by following a similar procedure used for **AK256**. ^{1}H NMR (400 MHz, DMSO) δ 8.55 (d, *J* = 2.0 Hz, 1H), 8.40 (d, *J* = 8.4 Hz, 1H), 8.09 (d, *J* = 8.6 Hz, 1H), 8.04 (s, 1H), 7.58 (d, *J* = 8.6 Hz, 1H), 7.40 – 7.21 (m, 5H), 4.87 – 4.81 (m, 3H), 4.27 – 4.23 (m, 1H), 3.93 – 3.88 (m, 1H), 3.72 – 3.64 (m, 1H), 3.01 (s, 3H), 2.26 – 2.20 (m, 1H), 2.15 – 1.99 (m, 1H), 1.97 – 1.84 (m, 1H), 1.77 – 1.73 (m, 1H), 1.10 (s, 9H). ESI−MS calculated for $C_{29}H_{34}F_2N_3O_6PS^+$ 621.67, found $[M + H]^+$ 622.17.

((2-(((S)-1-((S)-2-((4-bromobenzyl)(methyl)carbamoyl)pyrrolidin-1-yl)-3,3-dimethyl-1-oxobutan-2-yl)carbamoyl)benzo[b]thiophen-5-yl)difluoromethyl)phosphonic acid (AK075) AK075 was synthesized by following a similar procedure used for **AK256**. ^{1}H NMR (400 MHz, DMSO) δ 8.54 (d, *J* = 3.4 Hz, 1H), 8.43 – 8.34 (m, 1H), 8.11 (d, *J* = 8.5 Hz, 1H), 8.04 (s, 1H), 7.58 – 7.52 (m2H), 7.50 – 7.43 (m, 1H), 7.39 – 7.29 (m, 1H), 7.27 – 7.21 (m, 1H), 4.90 – 4.66 (m, 3H), 4.24 – 4.20 (m, 1H), 3.97 – 3.84 (m, 1H), 3.73 – 3.64 (m, 1H), 3.02 (s, 3H), 2.31 –

2.16 (m, 1H), 2.15 – 1.99 (m, 1H), 1.96 – 1.83 (m, 1H), 1.76 – 1.72 (m, 1H), 1.09 (s, 9H). ESI−MS calculated for $C_{29}H_{33}BrF_2N_3O_6PS^+$ 700.53, found $[M + H]^+$ 700.16, 701.98.

((2-(((S)-1-((S)-2-(6-azaspiro[3.4]octane-6-carbonyl)pyrrolidin-1-yl)-3,3-dimethyl-1-oxobutan-2-yl)carbamoyl)benzo[b]thiophen-5-yl)difluoromethyl)phosphonic acid (AK063)

AK063 was synthesized by following a similar procedure used for **AK256**. ^{1}H NMR (400 MHz, DMSO) δ 8.52 (d, *J* = 4.7 Hz, 1H), 8.35 – 8.29 (m, 1H), 8.08 (d, *J* = 8.6 Hz, 1H), 8.03 (s, 1H), 7.58 (d, *J* = 8.5 Hz, 1H), 4.75 (dd, *J* = 8.8, 2.0 Hz, 1H), 4.57 – 4.50 (m, 1H), 3.96 – 3.80 (m, 1H), 3.76 – 3.72 (m, 1H), 3.65 – 3.60 (m, 1H), 3.51 – 3.43 (m, 1H), 3.37 – 3.33 (m, 1H), 3.26 – 3.20 (m, 1H), 2.23 – 2.10 (m, 1H), 2.08 – 1.94 (m, 1H), 1.93 – 1.82 (m, 1H), 1.76 – 1.72 (m, 2H), 1.53 – 1.48 (m, 7H), 1.05 (s, 9H). ESI−MS calculated for $C_{28}H_{36}F_2N_3O_6PS^+$ 611.64, found $[M + H]^+$ 612.37.

((2-(((S)-1-((S)-2-(1,4-oxazepane-4-carbonyl)pyrrolidin-1-yl)-3,3-dimethyl-1-oxobutan-2-yl)carbamoyl)benzo[b]thiophen-5-yl)difluoromethyl)phosphonic acid (AK078)

AK078 was synthesized by following a similar procedure used for **AK256**. ^{1}H NMR (400 MHz, DMSO) δ 8.54 (s, 1H), 8.37 (dd, *J* = 8.9, 3.4 Hz, 1H), 8.12 (d, *J* = 8.5 Hz, 1H), 8.04 (s, 1H), 7.66 – 7.46 (m, 1H), 4.82 – 4.76 (m, 2H), 3.94 – 3.84 (m, 1H), 3.80 – 3.60 (m, 6H), 3.52 – 3.42 (m, 2H), 3.29 – 3.20 (m, 1H), 2.28 – 2.13 (m, 1H), 2.04 – 1.97 (m, 1H), 1.94 – 1.62 (m, 4H), 1.08 (s, 9H). ESI−MS calculated for $C_{26}H_{34}F_2N_3O_7PS^+$ 601.60, found $[M + H]^+$ 602.26.

((2-(((S)-1-((S)-2-((3-(dimethylamino)-3-oxopropyl)(4-(thiazol-2-yl)phenyl)carbamoyl)pyrrolidin-1-yl)-3,3-dimethyl-1-oxobutan-2-yl)carbamoyl)benzo[b]thiophen-5-yl)difluoromethyl)phosphonic acid (AK2305). To a round bottom flask equipped with a magnetic stirring bar was added 4-(thiazol-2-yl)aniline **10** (2.5 g, 14.2 mmol), acetic acid (8 ml), and ethylacrylate (1.3 ml, 0.9 equiv.). The suspension was stirred

at 90°C for 5 hours. The reaction mixture was cooled to room temperature and the solvent was removed on a rotary evaporator. The residual crude product was purified by flash column chromatography to yield **AK20202109** in 52% yield (2.0 g). ^{1}H NMR (400 MHz, DMSO) δ 7.79 (d, *J* = 3.4 Hz, 1H), 7.70 (d, *J* = 8.7 Hz, 2H), 7.56 (d, *J* = 3.4 Hz, 1H), 7.32 (s, 1H), 6.66 (d, *J* = 8.7 Hz, 2H), 4.08 (q, *J* = 7.1 Hz, 2H), 3.35 (t, *J* = 6.7 Hz, 2H), 2.59 (t, *J* = 6.7 Hz, 2H), 1.18 (t, *J* = 7.1 Hz, 3H). ^{13}C NMR (400 MHz, DMSO) δ 171.46, 168.52, 150.44, 142.03, 127.77, 120.35, 117.74, 112.06, 60.00, 38.43, 33.51, 14.07. ESI−MS calculated for $C_9H_8N_2S^+$ 276.35, found $[M + H]^+$ 276.89.

Boc-L-proline (5.8 g, 5 equiv.) was dissolved in $CHCl_3$ (50 ml). At room temperature, PCl_5 (5.6 g, 5 equiv.) was slowly added over a period of 10 min. After the addition, the mixture was stirred for 10 min at room temperature. To this mixture was added **AK20202109** (1.5 g, 5.4 mmol) and the mixture was stirred at 50°C for 20 min. The volatile components were removed on a rotary evaporator. The obtained crude oil was purified by reverse phase semi-preparative HPLC. The resulting colorless oil was dissolved in CH_3CN (20 ml). To the solution was added triethylamine (3 ml, 3.8 equiv.), followed by Boc_2O (1.75 g, 1.5 equiv.). The colorless mixture was stirred for 2 hours at room temperature. The volatile components were then removed by vacuum and the crude was purified by flash column chromatography to yield **AK20212284** in 39% (1.0 g, 2 steps yield). ^{1}H NMR (400 MHz, DMSO) δ 8.05 (d, *J* = 8.5 Hz, 2H), 7.94 (d, *J* = 3.3 Hz, 1H), 7.77 (d, *J* = 3.3 Hz, 1H), 7.58 – 7.08 (m, 2H), 4.12 (m, 1H), 4.10 – 3.75 (m, 4H), 3.43 – 3.23 (m, 2H), 2.55 (m, 2H), 1.86 (s, 3H), 1.70 (m, 1H), 1.42 (s, 9H), 1.14 (t, *J* = 7.1 Hz, 3H). ^{13}C NMR (400 MHz, DMSO) δ 171.34, 170.35, 165.75, 153.27, 143.64, 132.39, 128.88, 127.10, 120.49, 77.07, 59.61, 56.69, 46.48, 44.92, 32.39, 30.55, 29.63, 27.93, 22.42, 13.52. ESI−MS calculated for $C_{24}H_{31}N_3O_5S^+$ 473.59, found $[M + H]^+$ 374.06.

AK20212284 (450 mg, 0.95 mmol) was dissolved in MeOH (5 ml) and water (1 ml) and the mixture was placed in an ice bath. LiOH monohydrate (200 mg, 5 equiv.) was added to the mixture and then it was stirred for 30 min at room temperature. The mixture was placed in an ice bath again and neutralized by slowly adding TFA. The volatile components were removed on a rotary evaporator and the residue was purified by flash column chromatography to yield **AK20212285** in 73% (310 mg). ^{1}H NMR (400 MHz, DMSO) δ 12.00 (s, 1H), 8.05 (d, *J* = 8.0 Hz, 3H), 7.95 (d, *J* = 3.3 Hz, 1H), 7.78 (d, *J* = 3.3 Hz, 1H), 7.44 (s, 2H), 4.11 (m, 1H), 3.99 – 3.69 (m, 2H), 3.39 – 3.26 (m, 2H), 3.13 (s, 2H), 1.85 (m, 4H). ^{13}C NMR (400 MHz, DMSO) δ 171.78, 171.30, 165.79, 143.65, 132.34, 128.87, 127.10, 120.47, 78.39, 56.69, 46.50, 45.01, 32.31, 30.56, 29.38, 27.96, 23.04, 22.57. ESI−MS calculated for $C_{22}H_{77}N_3O_5S^+$ 445.53, found $[M + H]^+$ 346.20.

HATU (140 mg, 0.37 mmol, 1.1 equiv.) was added to a solution of **AK20212285** (150 mg, 0.33 mmol, 1 equiv.), dimethylamine (330 µl, 0.67 mmol, 2 equiv.) in 2M THF solution, and triethylamine (0.23 ml, 1.65 mmol, 5 equiv.) in CH_3CN (5 ml). The mixture was stirred at room temperature for 30 min. The yellow solution was concentrated in vacuum and the crude was purified by flash column chromatography to yield Boc-protected **AK20212299**. Boc protection was removed by DCM/TFA at room temperature for 30 min. The volatile components were removed in vacuum to yield **AK20212299** as a TFA salt in 80% (128 mg). ^{1}H NMR (400 MHz, $CDCl_3$) δ 8.11 – 8.03 (m, 2H), 7.75 – 7.71 (m, 1H), 7.59 (d, *J* = 3.2 Hz, 1H), 7.45 (d, *J* = 7.9 Hz, 2H), 4.42 – 4.38 (m, 1H), 4.28 – 4.24 (m, 1H), 3.89 (d, *J* = 6.6 Hz, 1H), 3.46 – 3.42 (m, 2H), 3.02 (s, 3H), 2.91 (s, 3H), 2.75 (d, *J* = 7.5 Hz, 1H), 2.69 – 2.50 (m, 1H), 2.02 – 1.96 (m, 1H), 1.93 – 1.85 (m, 3H). ESI−MS calculated for $C_{19}H_{24}N_4O_2S^+$ 372.49, found $[M + H]^+$ 372.99.

To **AK20212299** (128 mg, 0.26 mmol), CH_3CN (5 ml), triethylamine (0.18 ml, 2.5 mmol, 5 equiv.), Boc-L-*tert*-leucine (90 mg, 0.39 mmol, 1.5 equiv.), and HATU (118 mg, 0.31 mmol, 1.2 equiv.) were added. The mixture was stirred at room temperature for 30 min. The yellow solution was concentrated in vacuum and the crude was purified by flash column chromatography to yield Boc-protected **AK20212302**. Boc protection was removed by DCM/TFA at room temperature for 30 min. The volatile components were removed in vacuum to yield **AK20212302** as a TFA salt in 85% (107 mg). ^{1}H NMR (400 MHz, MeOD) δ 8.00 (d, *J* = 8.2 Hz, 2H), 7.90 (d, *J* = 3.3 Hz, 1H), 7.64 (d, *J* = 3.3 Hz, 1H), 7.57 (d, *J* = 8.1 Hz, 2H), 4.33 (t, *J* = 7.7 Hz, 1H), 3.96 – 3.90 (m, 3H), 3.75 – 3.68 (m=, 1H), 3.60 – 3.55 (m, 1H), 3.00 (s, 3H), 2.83 (s, 3H), 2.69 (t, *J* = 7.4 Hz, 2H), 2.10 – 1.80 (m, 3H), 1.80 – 1.60 (m, 1H), 1.13 (s, 9H). ESI−MS calculated for $C_{25}H_{35}N_5O_3S^+$ 485.65, found $[M + H]^+$ 486.21.

To **AK20212302** (107 mg, 0.22 mmol), CH_3CN (5 ml), triethylamine (0.15 ml, 1.1 mmol, 5 equiv.), benzothiophene head IM-6 (97 mg, 0.26 mmol, 1.2 equiv.), and HATU (100 mg, 0.26 mmol, 1.2 equiv.) were added. The mixture was stirred at room temperature for 30 min. The yellow solution was concentrated in vacuum and the crude was purified by flash column chromatography to yield **AK20212304** in 68% (147 mg). ^{1}H NMR (400 MHz, $CDCl_3$) δ 8.09 (s, 1H), 8.00 (d, *J* = 1.4 Hz, 1H), 7.98 (d, *J* = 1.5 Hz, 1H), 7.94 – 7.88 (m, 3H), 7.66 – 7.60 (m, 1H), 7.51 – 7.44 (m, 2H), 7.38 (d, *J* = 3.3 Hz, 1H), 7.24 (d, *J* = 9.4 Hz, 1H), 4.92 (d, *J* = 9.4 Hz, 1H), 4.35 (t, *J* = 7.6 Hz, 1H), 4.25 – 4.13 (m, 5H), 4.04 – 3.93 (m, 1H), 3.91 – 3.70 (m, 2H), 3.07 (s, 3H), 2.92 (s, 3H), 2.85 – 2.70 (m, 2H), 2.12 – 2.08 (m, 1H), 1.98 – 1.87 (m, 2H), 1.87 – 1.74 (m, 1H), 1.34 – 1.30 (m, 6H), 1.17 (s, 9H). ESI−MS calculated for $C_{39}H_{48}F_2N_5O_7PS_2^+$ 831.93, found $[M + H]^+$ 832.12.

To a round bottom flask were added **AK20212304** (150 mg, 0.17 mmol, 1 equiv.), DCM (2 ml) and $CF_3CON(TMS)_2$ (0.27 ml, 1.0 mmol, 6 equiv.). The solution was cooled in an ice bath. To the ice cooled reaction mixture, 1M of TMS-I in DCM (0.9 ml, 0.9 mmol, 5 equiv.) was added dropwise and the mixture was stirred for 10 min in an ice bath. The volatile components were removed under vacuum at below 5°C. The residue was dissolved in a mixed solvent of CH_3CN (3 ml) and water (1 ml). The resulting solution was purified by HPLC to yield **AK2305** in 80% (150 mg). ^{1}H NMR (400 MHz, DMSO) δ 8.54 (s, 1H), 8.43 (d, *J* = 9.0 Hz, 1H), 8.11 (m, 1H), 8.06 – 7.95 (m, 3H), 7.92 (m, *J* = 3.2 Hz, 1H), 7.79 (d, *J* = 3.2 Hz, 1H), 7.55 (m, 2H), 4.77 (d, *J* = 9.0 Hz, 1H), 4.19 (m, 1H), 3.93 – 3.70 (m, 3H), 3.70 – 3.57 (m, 1H), 2.94 (m, 4H), 2.77 (m, 4H), 2.66 – 2.53 (m, 2H), 2.06 – 1.92 (m, 1H), 1.85 (m, 3H), 1.10 (s, 9H). ESI−MS calculated for $C_{30}H_{40}F_2N_5O_7PS_2^+$ 775.82, found $[M + H]^+$ 775.89.

((4-((E)-4-(((S)-3,3-Dimethyl-1-oxo-1-((S)-2-(1,2,3,4-tetrahydroquinoline-1-carbonyl)pyrrolidin-1-yl)butan-2-yl)amino)-4-oxobut-2-en-2-yl)phenyl)difluoromethyl)phosphonic acid (AK-2335). Similar synthetic methods were previously reported [70]. ^{1}H NMR (400 MHz, DMSO) δ 10.34 (s, 1H), 8.05 (d, J = 9.1 Hz, 1H), 7.65 – 7.51 (m, 4H), 7.16 (m, 3H), 6.57 (s, 1H), 4.78 (m, 1H), 4.62 (d, J = 9.0 Hz, 1H), 4.05 – 3.76 (m, 2H), 3.76 – 3.61 (m, 1H), 3.46 (m, 1H), 2.75 (m, 2H), 2.47 (s, 3H), 2.28 – 1.98 (m, 3H), 1.89 (m, 5H), 1.00 (s, 9H). ^{13}C NMR (400 MHz, DMSO) δ 171.83, 169.11, 165.72, 158.54, 158.17, 147.67, 144.06, 139.15, 133.93, 128.63, 126.30, 126.24, 126.17, 125.87, 124.60, 121.30, 119.86, 117.83, 56.96, 56.23, 48.12, 35.07, 29.38, 26.50, 26.02, 24.98, 23.38, 16.52. ESI−MS calculated for $C_{31}H_{38}F_2N_3O_9PS^+$ 617.63, found $[M + H]^+$ 617.98.

((2-(((S)-3,3-Dimethyl-1-oxo-1-((S)-2-(1,2,3,4-tetrahydroquinoline-1-carbonyl)pyrrolidin-1-yl)butan-2-yl)carbamoyl)benzo[b]thiophen-5-

yl)difluoromethyl)phosphonic acid (AK2336). AK-2336 was synthesized by employing a similar procedure for **AK2305**. ^{1}H NMR (400 MHz, DMSO) δ 8.53 (s, 1H), 8.39 (d, *J* = 8.9 Hz, 1H), 8.12 (d, *J* = 8.5 Hz, 1H), 8.04 (s, 1H), 7.58 (m, 1H), 7.22 – 7.04 (m, 3H), 5.14 – 4.43 (m, 3H), 4.00 – 3.76 (m, 2H), 3.76 – 3.62 (m, 1H), 3.50 (m, 1H), 2.88 – 2.56 (m, 2H), 2.50 (s, 1H), 2.05 (m, 2H), 1.88 (m, 4H), 1.07 (s, 9H). ^{13}C NMR (400 MHz, DMSO) δ 171.74, 168.48, 161.49, 141.89, 140.38, 139.02, 138.76, 131.17, 130.95, 130.83, 130.61, 128.62, 126.11, 125.86, 125.22, 124.55, 123.71, 123.64, 122.93, 122.79, 57.42, 57.07, 48.19, 35.36, 29.34, 26.56, 26.01, 24.95, 23.39. ESI−MS calculated for $C_{30}H_{34}F_2N_3O_6PS^+$ 633.65, found $[M + H]^+$ 634.01.

((2-(((S)-3,3-Dimethyl-1-((S)-2-(methyl(phenyl)carbamoyl)pyrrolidin-1-yl)-1-oxobutan-2-yl)carbamoyl)benzo[b]thiophen-5-yl)difluoromethyl)phosphonic acid (AK2337). AK-2337 was synthesized by employing a similar procedure for **AK2305**. ^{1}H NMR (400 MHz, DMSO) δ 11.51 (s, 1H), 8.53 (s, 1H), 8.39 (d, *J* = 8.9 Hz, 1H), 8.19 – 7.94 (m, 2H), 7.62 – 7.54 (m, 1H), 7.46 – 7.32 (m, 4H), 4.76 (d, *J* = 8.9 Hz, 1H), 4.23 (s, 1H), 3.85 – 3.71 (m, 1H), 3.71 – 3.47 (m, 1H), 3.16 (s, 3H), 2.15 – 1.87 (m, 2H), 1.76 (d, *J* = 5.5 Hz, 3H), 1.09 (s, 9H). ^{13}C NMR (400 MHz, DMSO) δ 171.11, 168.45, 161.47, 143.39, 141.93, 140.46, 138.81, 129.67, 127.75, 127.61, 126.11, 125.97, 123.76, 122.83, 57.47, 57.11, 48.19, 37.18, 36.07, 35.42, 29.11, 26.63, 26.20, 24.79. ESI−MS calculated for $C_{28}H_{32}F_2N_3O_6PS^+$ 607.61, found $[M + H]^+$ 607.96.

((2-(((S)-1-((S)-2-((3-(dimethylamino)-3-oxopropyl)(phenyl)carbamoyl)pyrrolidin-1-yl)-3,3-dimethyl-1-oxobutan-2-yl)carbamoyl)benzo[b]thiophen-5-yl)difluoromethyl)phosphonic acid (AK2446). AK-2446 was synthesized by employing a similar procedure for **AK2305**. ^{1}H NMR (400 MHz, DMSO) δ 8.53 (s, 1H), 8.41 (d, *J* = 9.0 Hz, 1H), 8.14 – 8.02 (m, 2H), 7.60 – 7.55 (m, 1H), 7.43 (m, 4H), 7.37 – 3.33 (m, 1H), 4.76 (d, *J* =

9.0 Hz, 1H), 4.11 (t, *J* = 7.1 Hz, 1H), 3.79 – 3.75 (m, 3H), 3.70 – 3.58 (m, 1H), 2.93 (s, 3H), 2.76 (s, 3H), 2.60 – 2.51 (m, 2H), 2.02 – 1.87 (m, 1H), 1.84 – 1.69 (m, 3H), 1.09 (s, 9H). ESI−MS calculated for $C_{32}H_{39}F_2N_4O_7PS^+$ 692.72, found $[M + H]^+$ 693.13.

((2-(((S)-1-((S)-2-((4-chlorophenyl)(3-(dimethylamino)-3-oxopropyl)carbamoyl)pyrrolidin-1-yl)-3,3-dimethyl-1-oxobutan-2-yl)carbamoyl)benzo[b]thiophen-5-yl)difluoromethyl)phosphonic acid (AK2338). AK-2338 was synthesized by employing a similar procedure for **AK2305**. ^{1}H NMR (400 MHz, DMSO) δ 8.54 (s, 1H), 8.41 (d, *J* = 9.0 Hz, 1H), 8.12 (d, *J* = 8.4 Hz, 1H), 8.04 (s, 1H), 7.62 – 7.55 (m, 1H), 7.52 – 7.35 (m, 4H), 4.75 (d, *J* = 9.0 Hz, 1H), 4.15 – 4.05 (m, 1H), 3.84 – 3.69 (m, 3H), 3.69 – 3.61 (m, 1H), 2.93 (s, 3H), 2.77 (s, 3H), 2.60 – 2.52 (m, 2H), 2.02 – 1.90 (m, 1H), 1.89 – 1.67 (m, 3H), 1.08 (s, 9H). ESI−MS calculated for $C_{32}H_{38}ClF_2N_4O_7PS^+$ 727.16, found $[M + H]^+$ 727.08.

((2-(((S)-1-((S)-2-((4-bromophenyl)(3-(dimethylamino)-3-oxopropyl)carbamoyl)pyrrolidin-1-yl)-3,3-dimethyl-1-oxobutan-2-yl)carbamoyl)benzo[b]thiophen-5-yl)difluoromethyl)phosphonic acid (AK2339). AK-2339 was synthesized by employing a similar procedure for **AK2305**. ^{1}H NMR (400 MHz, DMSO) δ 8.54 (s, 1H), 8.41 (d, *J* = 8.9 Hz, 1H), 8.12 (d, *J* = 8.2 Hz, 1H), 8.04 (s, 1H), 7.66 – 7.54 (m, 3H), 7.44 – 7.32 (m, 2H), 4.75 (d, *J* = 9.0 Hz, 1H), 4.15 – 4.10 (m, 1H), 3.84 – 3.57 (m, 4H), 2.93 (s, 3H), 2.77 (s, 3H), 2.60 – 2.50 (m, 2H), 2.03 – 1.92 (m, 1H), 1.87 – 1.62 (m, 3H), 1.08 (s, 9H). ESI−MS calculated for $C_{32}H_{38}BrF_2N_4O_7PS^+$ 771.61, found $[M + H]^+$ 771.00, 772.93.

((2-(((S)-1-((S)-2-((3-bromophenyl)(3-(dimethylamino)-3-oxopropyl)carbamoyl)pyrrolidin-1-yl)-3,3-dimethyl-1-oxobutan-2-yl)carbamoyl)benzo[b]thiophen-5-yl)difluoromethyl)phosphonic acid (AK2367). AK-2367

was synthesized by employing a similar procedure for **AK2305**. ^{1}H NMR (400 MHz, DMSO) δ 8.55 (s, 1H), 8.48 (d, *J* = 9.0 Hz, 1H), 8.12 (d, *J* = 8.8 Hz, 1H), 8.04 (s, 1H), 7.69 – 7.65 (m, 1H), 7.62 – 7.55 (m, 2H), 7.47 – 7.38 (m, 2H), 4.77 (d, *J* = 9.0 Hz, 1H), 4.15 – 4.05 (m, 1H), 3.85 – 3.75 (m, 3H), 3.69 – 3.59 (m, 1H), 2.94 (s, 3H), 2.77 (s, 3H), 2.62 – 2.54 (m, 2H), 2.00 – 1.90 (m, 1H), 1.85 – 1.75 (m, 3H), 1.09 (s, 9H). ESI−MS calculated for $C_{32}H_{38}BrF_2N_4O_7PS^+$ 771.61, found $[M + H]^+$ 770.99, 772.13.

((2-(((S)-1-((S)-2-((3-(dimethylamino)-3-oxopropyl)(naphthalen-2-yl)carbamoyl)pyrrolidin-1-yl)-3,3-dimethyl-1-oxobutan-2-yl)carbamoyl)benzo[b]thiophen-5-yl)difluoromethyl)phosphonic acid (AK2342). AK-2342 was synthesized by employing a similar procedure for **AK2305**. ^{1}H NMR (400 MHz, DMSO) δ 8.53 (s, 1H), 8.43 (d, *J* = 9.0 Hz, 1H), 8.10 (d, *J* = 8.5 Hz, 1H), 8.04 (s, 1H), 7.99 (d, *J* = 8.7 Hz, 1H), 7.96 – 7.86 (m, 3H), 7.60 – 7.48 (m, 4H), 4.76 (d, *J* = 9.0 Hz, 1H), 4.18 – 4.12 (m, 1H), 3.90 – 3.84 (m, 2H), 3.79 – 3.70 (m, 1H), 3.68 – 3.57 (m, 1H), 2.94 (s, 3H), 2.76 (s, 3H), 2.70 – 2.60 (m, 2H), 2.01 – 1.90 (m, 1H), 1.88 – 1.82 (m, 2H), 1.77 – 1.66 (m, 1H), 1.11 (s, 9H). ESI−MS calculated for $C_{36}H_{41}F_2N_4O_7PS^+$ 742.78, found $[M + H]^+$ 743.15.

((2-(((S)-1-((S)-2-([1,1'-biphenyl]-4-yl(3-(dimethylamino)-3-oxopropyl)carbamoyl)pyrrolidin-1-yl)-3,3-dimethyl-1-oxobutan-2-yl)carbamoyl)benzo[b]thiophen-5-yl)difluoromethyl)phosphonic acid (AK2343). AK-2343 was synthesized by employing a similar procedure for **AK2305**. ^{1}H NMR (400 MHz, DMSO) δ 8.55 (s, 1H), 8.43 (d, *J* = 9.0 Hz, 1H), 8.13 – 8.08 (m, 1H), 8.04 (s, 1H), 7.73 (d, *J* = 8.5 Hz, 2H), 7.70 – 7.63 (m, 2H), 7.61 – 7.55 (m, 1H), 7.53 – 7.48 (m, 2H), 7.47 – 7.43 (m, 2H), 7.37 – 7.32 (m, 1H), 4.76 (d, *J* = 9.0 Hz, 1H), 4.21 (t, *J* = 7.1 Hz, 1H), 3.82 – 3.78 (m, 3H), 3.70 – 3.62 (m,

1H), 2.95 (s, 3H), 2.78 (s, 3H), 2.63 – 2.55 (m, 2H), 2.04 – 1.93 (m, 1H), 1.90 – 1.69 (m, 3H), 1.10 (s, 9H). ESI−MS calculated for $C_{38}H_{43}F_2N_4O_7PS^+$ 768.81, found $[M + H]^+$ 769.16.

((2-(((S)-1-((S)-2-((3-(dimethylamino)-3-oxopropyl)(3-(thiazol-2-yl)phenyl)carbamoyl)pyrrolidin-1-yl)-3,3-dimethyl-1-oxobutan-2-yl)carbamoyl)benzo[b]thiophen-5-yl)difluoromethyl)phosphonic acid (AK2368). AK-2368 was synthesized by employing a similar procedure for **AK2305**. ^{1}H NMR (400 MHz, DMSO) δ 8.52 (s, 1H), 8.43 (d, *J* = 8.9 Hz, 1H), 8.17 – 8.05 (m, 2H), 8.03 (s, 1H), 7.97 (d, *J* = 2.0 Hz, 1H), 7.95 – 7.89 (m, 2H), 7.78 (d, *J* = 3.3 Hz, 1H), 7.60 – 7.50 (m, 3H), 4.76 (d, *J* = 8.9 Hz, 1H), 4.17 (t, *J* = 7.2 Hz, 1H), 3.91 – 3.73 (m, 3H), 3.70 – 3.58 (m, 1H), 2.95 (s, 3H), 2.77 (s, 3H), 2.64 – 2.55 (m, 2H), 2.02 – 1.92 (m, 1H), 1.90 – 1.80 (m, 2H), 1.78 – 1.70 (m, 1H), 1.10 (s, 9H). ESI−MS calculated for $C_{35}H_{40}F_2N_5O_7PS^+$ 775.82, found $[M + H]^+$ 775.95.

((2-(((S)-1-((S)-2-(benzofuran-5-yl(3-(dimethylamino)-3-oxopropyl)carbamoyl)pyrrolidin-1-yl)-3,3-dimethyl-1-oxobutan-2-yl)carbamoyl)benzo[b]thiophen-5-yl)difluoromethyl)phosphonic acid (AK2340). AK-2340 was synthesized by employing a similar procedure for **AK2305**. ^{1}H NMR (400 MHz, DMSO) δ 8.54 (s, 1H), 8.42 (d, *J* = 9.0 Hz, 1H), 8.17 – 8.10 (m, 1H), 8.10 – 8.00 (m, 2H), 7.70 (d, *J* = 2.1 Hz, 1H), 7.65 (d, *J* = 8.7 Hz, 1H), 7.60 – 7.54 (m, 1H), 7.43 – 7.32 (m, 1H), 6.98 (s, 1H), 4.75 (d, *J* = 9.0 Hz, 1H), 4.15 – 4.10 (m, 1H), 3.90 – 3.70 (m, 3H), 3.69 – 3.55 (m, 1H), 2.94 (s, 3H), 2.76 (s, 3H), 2.66 – 2.54 (m, 2H), 2.00 – 1.90 (m, 1H), 1.86 – 1.65 (m, 3H), 1.10 (s, 9H). ESI−MS calculated for $C_{34}H_{39}F_2N_4O_8PS^+$ 732.74, found $[M + H]^+$ 733.11.

((2-(((S)-1-((S)-2-(Benzo[d]thiazol-5-yl(3-(dimethylamino)-3-oxopropyl)carbamoyl)pyrrolidin-1-yl)-3,3-dimethyl-1-oxobutan-2-yl)carbamoyl)benzo[b]thiophen-5-yl)difluoromethyl)phosphonic acid (AK2341). AK-2341

was synthesized by employing a similar procedure for **AK2305**. ^{1}H NMR (400 MHz, DMSO) δ 9.44 (s, 1H), 8.57 – 8.41 (m, 2H), 8.22 – 8.03 (m, 4H), 7.60 – 7.52 (m, 2H), 4.76 (d, *J* = 9.0 Hz, 1H), 4.15 (m, 1H), 3.98 – 3.46 (m, 5H), 2.97 (d, *J* = 14.2 Hz, 3H), 2.75 (d, *J* = 10.9 Hz, 3H), 2.63 (m, 2H), 2.03 – 1.66 (m, 5H), 1.11 (s, 9H). ^{13}C NMR (400 MHz, DMSO) δ 171.29, 168.50, 168.10, 161.45, 158.02, 153.68, 141.90, 140.47, 140.44, 139.90, 138.79, 134.02, 133.25, 126.11, 125.85, 123.36, 122.80, 57.42, 57.38, 48.19, 46.50, 36.70, 36.08, 35.45, 34.69, 30.77, 29.01, 26.62, 26.21, 24.85. ESI−MS calculated for $C_{33}H_{38}F_2N_5O_7PS^+$ 749.79, found $[M + H]^+$ 750.10.

((2-(((S)-1-cyclopropyl-2-((S)-2-((3-(dimethylamino)-3-oxopropyl)(4-(thiazol-2-yl)phenyl)carbamoyl)pyrrolidin-1-yl)-2-oxoethyl)carbamoyl)benzo[b]thiophen-5-yl)difluoromethyl)phosphonic acid (AK2415). AK-2415 was synthesized by employing a similar procedure for **AK2305**. ^{1}H NMR (400 MHz, DMSO) δ 9.02 (d, *J* = 7.4 Hz, 1H), 8.39 (s, 1H), 8.21 – 8.08 (m, 1H), 8.08 – 7.97 (m, 2H), 7.94 (d, *J* = 3.2 Hz, 1H), 7.81 (d, *J* = 3.2 Hz, 1H), 7.69 – 7.43 (m, 3H), 4.39 m, 1H), 4.20 (s, 1H), 3.90 (m, 1H), 3.80 – 3.50 (m, 3H), 2.94 (s, 3H), 2.77 (s, 3H), 2.62 – 2.51 (m, 2H), 2.13 – 1.93 (m, 1H), 1.85 (m, 3H), 1.29 (m, 1H), 0.73 – 0.40 (m, 3H), 0.41 – 0.17 (m, 1H). ESI−MS calculated for $C_{34}H_{36}F_2N_5O_7PS^+$ 759.78, found $[M + H]^+$ 760.11.

((2-(((S)-1-cyclohexyl-2-((S)-2-((3-(dimethylamino)-3-oxopropyl)(4-(thiazol-2-yl)phenyl)carbamoyl)pyrrolidin-1-yl)-2-oxoethyl)carbamoyl)benzo[b]thiophen-5-yl)difluoromethyl)phosphonic acid (AK2417). AK2417 was synthesized by employing a similar procedure for **AK2305**. ^{1}H NMR (400 MHz, DMSO) δ 8.87 (m, 1H), 8.38 (s, 1H), 8.11 (m, 1H), 8.06 – 7.95 (m, 3H), 7.93 (d, *J* = 3.2 Hz, 1H), 7.80 (d, *J* = 3.2 Hz, 1H), 7.54 (m, 3H), 4.52 (t, *J* = 8.8 Hz, 1H), 4.18 (t, *J* = 6.8 Hz, 1H), 3.99 – 3.79 (m, 2H), 3.74 (m, 1H), 3.63 (m,

1H), 2.95 (s, 3H), 2.77 (s, 3H), 2.56 (m, 2H), 2.11 – 1.79 (m, 6H), 1.68 (m, 4H), 1.20 (m, 3H), 1.03 (m, 2H). ESI−MS calculated for $C_{37}H_{42}F_2N_5O_7PS^+$ 801.86, found $[M + H]^+$ 802.15.

((2-(((S)-2-((S)-2-((3-(dimethylamino)-3-oxopropyl)(4-(thiazol-2-yl)phenyl)carbamoyl)pyrrolidin-1-yl)-2-oxo-1-phenylethyl)carbamoyl)benzo[b]thiophen-5-yl)difluoromethyl)phosphonic acid (AK2418). AK2418 was synthesized by employing a similar procedure for **AK2305**. ^{1}H NMR (400 MHz, DMSO) δ 9.26 (m, 2H), 8.43 (s, 1H), 8.13 (d, *J* = 8.6 Hz, 1H), 8.07 – 7.99 (m, 3H), 7.95 (d, *J* = 3.3 Hz, 1H), 7.82 (d, *J* = 3.2 Hz, 1H), 7.71 – 7.48 (m, 4H), 7.39 (m, 3H), 5.92 (d, *J* = 7.7 Hz, 1H), 4.27 (m, 1H), 3.93 (m, 1H), 3.82 – 3.52 (m, 2H), 3.11 (m, 1H), 2.94 (s, 3H), 2.77 (s, 3H), 2.56 (m, 2H), 2.07 – 1.62 (m, 4H). ESI−MS calculated for $C_{37}H_{36}F_2N_5O_7PS^+$ 795.81, found $[M + H]^+$ 796.11.

((2-(((S)-1-((S)-2-((3-(dimethylamino)-3-oxopropyl)(4-(thiazol-2-yl)phenyl)carbamoyl)pyrrolidin-1-yl)-3-(4-fluorophenyl)-1-oxopropan-2-yl)carbamoyl)benzo[b]thiophen-5-yl)difluoromethyl)phosphonic acid (AK2419). AK2419 was synthesized by employing a similar procedure for **AK2305**. ^{1}H NMR (400 MHz, DMSO) δ 9.07 (m, 1H), 8.28 (s, 1H), 8.22 – 7.98 (m, 4H), 7.92 (m, 1H), 7.81 (m, 1H), 7.56 (m, 3H), 7.42 (m, 2H), 7.15 – 7.02 (m, 2H), 4.85 (m, 1H), 4.22 (m, 1H), 4.01 – 3.83 (m, 1H), 3.82 – 3.56 (m, 3H), 2.95 (s, 3H), 2.77 (s, 3H), 2.55 (s, 3H), 2.03 (m, 1H), 1.86 (m, 3H). ESI−MS calculated for $C_{38}H_{37}F_3N_5O_7PS^+$ 827.83, found $[M + H]^+$ 828.04.

((2-(((S)-3-(4-bromophenyl)-1-((S)-2-((3-(dimethylamino)-3-oxopropyl)(4-(thiazol-2-yl)phenyl)carbamoyl)pyrrolidin-1-yl)-1-oxopropan-2-yl)carbamoyl)benzo[b]thiophen-5-yl)difluoromethyl)phosphonic acid (AK2420). AK2420 was synthesized by employing a similar procedure for **AK2305**. ^{1}H NMR (400 MHz, DMSO) δ 9.22 – 8.89 (m, 1H), 8.27 (s, 1H), 8.20 – 7.98 (m, 4H), 7.94 (d, *J* = 3.2 Hz, 1H), 7.81 (d, *J* = 3.2 Hz, 1H), 7.70 – 7.50 (m, 3H), 7.48

– 7.39 (m, 1H), 7.39 – 7.26 (m, 1H), 7.19 (d, *J* = 8.4 Hz, 1H), 6.93 (d, *J* = 8.4 Hz, 1H), 4.86 (m, 1H), 4.23 (m, 1H), 4.02 – 3.83 (m, 1H), 3.83 – 3.55 (m, 3H), 3.50 – 3.25 (m, 1H), 3.16 – 3.01 (m, 1H), 2.95 (s, 3H), 2.77 (s, 3H), 2.64 – 2.53 (m, 2H), 2.04 (m, 1H), 1.94 – 1.71 (m, 2H). ESI−MS calculated for $C_{38}H_{37}BrF_2N_5O_7PS^+$ 888.74, found $[M + H]^+$ 887.91, 889.87.

((2-(((S)-1-((S)-2-((3-(dimethylamino)-3-oxopropyl)(4-(thiazol-2-yl)phenyl)carbamoyl)pyrrolidin-1-yl)-1-oxo-3-(4-(trifluoromethyl)phenyl)propan-2-yl)carbamoyl)benzo[b]thiophen-5-yl)difluoromethyl)phosphonic acid (AK2421). AK2421 was synthesized by employing a similar procedure for **AK2305**. ^{1}H NMR (400 MHz, DMSO) δ 9.13 (d, *J* = 8.2 Hz, 1H), 8.27 (s, 1H), 8.23 – 7.96 (m, 5H), 7.95 – 7.91 (m, 1H), 7.82 (d, *J* = 3.2 Hz, 1H), 7.71 – 7.44 (m, 6H), 4.95 – 4.90 (m, 1H), 4.24 (t, *J* = 6.4 Hz, 1H), 3.99 – 3.86 (m, 1H), 3.82 – 3.60 (m, 3H), 3.25 – 3.06 (m, 2H), 2.94 (s, 3H), 2.77 (s, 3H), 2.60 – 2.53 (m, 2H), 2.06 – 2.02 (m, 1H), 1.94 – 1.74 (m, 3H). ESI−MS calculated for $C_{39}H_{37}F_5N_5O_7PS^+$ 877.84, found $[M + H]^+$ 878.15.

((2-(((S)-1-((S)-2-((3-(dimethylamino)-3-oxopropyl)(4-(thiazol-2-yl)phenyl)carbamoyl)pyrrolidin-1-yl)-1-oxo-4-phenylbutan-2-yl)carbamoyl)benzo[b]thiophen-5-yl)difluoromethyl)phosphonic acid (AK2422). AK2422 was synthesized by employing a similar procedure for **AK2305**. ^{1}H NMR (400 MHz, DMSO) δ 9.02 (d, *J* = 7.6 Hz, 1H), 8.36 (s, 1H), 8.13 (d, *J* = 8.5 Hz, 1H), 8.07 (s, 1H), 8.04 – 8.00 (m, 2H), 7.94 (d, *J* = 3.2 Hz, 1H), 7.81 (d, *J* = 3.2 Hz, 1H), 7.63 – 7.45 (m, 3H), 7.37 – 7.24 (m, 4H), 7.24 – 7.16 (m, 1H), 4.68 – 4.62 (m, 1H), 4.21 (t, *J* = 6.8 Hz, 1H), 3.94 – 3.81 (m, 1H), 3.81 – 3.67 (m, 1H), 3.63 – 3.59 (m, 1H), 3.53 – 3.27 (m, 2H), 2.91 (s, 3H), 2.77 – 2.73 (m, 4H), 2.58 – 2.53 (m, 2H), 2.14 – 1.91 (m, 3H), 1.81 – 1.75 (m, 3H). ESI−MS calculated for $C_{39}H_{40}F_2N_5O_7PS^+$ 823.87, found $[M + H]^+$ 824.06.

((2-(((S)-1-((2S,4R)-2-((4-bromophenyl)(methyl)carbamoyl)-4-(2-ethoxy-2-oxoethoxy)pyrrolidin-1-yl)-3,3-dimethyl-1-oxobutan-2-yl)carbamoyl)benzo[b]thiophen-5-yl)difluoromethyl)phosphonic acid (AK2019014). To a round bottom flask equipped with a magnetic stirring bar were added **12** (1 g, 3.1 mmol), THF (7 ml), and tetra-butylammonium chloride (100 mg, 0.1 equiv.). NaH (170 mg, 1.2 equiv., 60% in oil) was slowly added to the reaction mixture in ice bath. Then ethylbromoacetate (400 µl, 1.2 equiv.) was added and the mixture was stirred at room temperature for 2 hours. The reaction was quenched by slowly adding ice in ice bath. The reaction was neutralized by slowly adding TFA. The solvent was removed on a rotary evaporator. The residual crude product was purified by flash column chromatography to yield **AK2018365** in 39% yield (500 mg). ^{1}H NMR (400 MHz, DMSO) δ 7.46 – 7.22 (m, 5H), 5.15 (s, 2H), 4.26 – 4.22 (m, 1H), 4.18 – 4.05 (m, 4H), 3.55 – 3.38 (m, 3H), 2.00 – 1.94 (m, 2H), 1.26 (s, 9H), 1.19 (t, *J* = 7.1 Hz, 3H). ESI−MS calculated for $C_{21}H_{29}NO_7^+$ 407.46, found $[M + H]^+$ 408.81.

AK2018365 was treated with 10% Pd/C and hydrogen in ethanol (10 ml) at room temperature for 1 h, followed by the filtration and concentration, to yield **AK2018367** in quantitative yield (380 mg). ^{1}H NMR (400 MHz, DMSO) δ 4.22 – 4.00 (m, 5H), 3.54 – 3.09 (m, 3H), 2.42 – 2.24 (m, 1H), 2.01 – 1.86 (m, 1H), 1.34 (s, 9H), 1.20 (t, *J* = 7.1 Hz, 3H). ESI−MS calculated for $C_{14}H_{23}NO_7^+$ 317.34, found $[M + H]^+$ 318.25.

AK2018367 (100 mg, 0.31 mmol, 1 equiv.) was dissolved in $CHCl_3$ (3 ml). At room temperature, PCl_5 (20 mg, 3 equiv.) was added. After the addition, the mixture was stirred for 10 min at room temperature. To this mixture was added 4-bromo-*N*-methylaniline (300 mg, 5 equiv.) and the mixture was stirred at reflux for 4 hours. The volatile components were removed on a rotary evaporator. The obtained crude oil was purified by HPLC to yield **13**. The resulting

colorless oil **13** was dissolved in CH_3CN (5 ml). To the solution were added CH_3CN (5 ml), triethylamine (0.22 ml, 5 equiv.), Boc-L-*tert*-leucine (80 mg, 1.1 equiv.), and HATU (140 mg, 1.2 equiv.). The mixture was stirred at room temperature for 30 min. The yellow solution was concentrated in vacuum and the crude was purified by flash column chromatography to yield Boc-protected **14**. Boc protection was removed by DCM/TFA at room temperature for 30 min. The volatile components were removed in vacuum to yield **14** as a TFA salt. To **14**, CH_3CN (5 ml), triethylamine (0.22 ml, 5 equiv.), **IM-6** (130 mg, 1.1 equiv.), and HATU (130 mg, 1.1 equiv.) were added. The mixture was stirred at room temperature for 30 min. The yellow solution was concentrated in vacuum and the crude was purified by flash column chromatography to yield **AK2019009** in 40% (4 steps, 104 mg). ^{1}H NMR (400 MHz, DMSO) δ 8.53 (d, *J* = 0.8 Hz, 1H), 8.42 (d, *J* = 8.7 Hz, 1H), 8.20 (d, *J* = 8.6 Hz, 1H), 8.11 (d, *J* = 1.9 Hz, 1H), 7.72 – 7.56 (m, 3H), 7.36 (d, *J* = 8.2 Hz, 2H), 4.70 (d, *J* = 8.8 Hz, 1H), 4.23 – 4.05 (m, 9H), 3.40 – 3.30 (m, 3H), 3.15 (s, 3H), 2.30 – 2.20 (m, 1H), 1.70 – 1.60 (m, 1H), 1.36 – 1.14 (m, 9H), 1.09 (s, 9H). ESI−MS calculated for $C_{36}H_{45}BrF_2N_3O_9PS^+$ 844.70, found $[M + Na]^+$ 866.26, 868.26.

To a round bottom flask were added **AK2019009** (20 mg, 0.023 mmol, 1 equiv.), DCM (2 ml) and $CF_3CON(TMS)_2$ (40 µl, 6 equiv.). The solution was cooled in an ice bath. To the ice cooled reaction mixture, 1M of TMS-I in DCM (0.12 ml, 5 equiv.) was added dropwise and the mixture was stirred for 10 min in an ice bath. The volatile components were removed under vacuum at below 5°C. The residue was dissolved in a mixed solvent of CH_3CN (3 ml) and water (1 ml). The resulting solution was purified by HPLC to yield **AK2019014** in 80% (15 mg). ^{1}H NMR (400 MHz, DMSO) δ 8.50 (s, 1H), 8.33 (d, *J* = 8.8 Hz, 1H), 8.03 (s, 2H), 7.70 – 7.55 (m, 3H), 7.43 – 7.30 (m, 2H), 4.70 (d, *J* = 8.7 Hz, 1H), 4.25 – 4.00 (m, 7H), 3.15 (s, 3H), 2.36 – 2.10

(m, 2H), 1.70 – 1.63 (m, 2H), 1.08 (s, 9H). ESI−MS calculated for $C_{32}H_{37}BrF_2N_3O_9PS^+$ 788.59, found $[M + H]^+$ 788.18, 790.15.

((2-(((2S)-1-((2S)-2-((3-((5-(2-(2,6-Dioxopiperidin-3-yl)-1-oxoisoindolin-4-yl)pent-4-yn-1-yl)(methyl)amino)-3-oxopropyl)(4-(thiazol-2-yl)phenyl)carbamoyl)pyrrolidin-1-yl)-3,3-dimethyl-1-oxobutan-2-yl)carbamoyl)benzo[b]thiophen-5-yl)difluoromethyl)phosphonic acid (AK-2292) To a round bottom flask equipped with a magnetic stirring bar were added N-methylpent-4-yn-1-amine hydrochloride **15** (1 g, 7.5 mmol, 1 equiv.), CH_3CN (10 ml), triethylamine (3 ml, 22.5 mmol, 3 equiv.), and Boc_2O (2.45 g, 11.3 mmol, 1.5 eq). The mixture was stirred at room temperature for 1 h. The volatile components were removed in vacuum. The residue was purified by flash column chromatography to yield **AK20212242** in 90%. ^{1}H NMR (400 MHz, DMSO) δ 3.21 (s, *J* = 7.1 Hz, 3H), 2.76 (m, 3H), 2.13 (m, 2H), 1.62 (m, 2H), 1.39 (s, 9H). ^{13}C NMR (400 MHz, DMSO) δ 154.71, 83.80, 78.32, 71.22, 47.15, 33.79, 28.03, 26.42, 15.17. ESI−MS calculated for $C_{11}H_{19}NO_2^+$ 339.40, found $[M + H]^+$ 340.26.

Triethylamine (1.5 ml) was added to a mixture of **16** (323 mg, 1 mmol, 1 equiv.), **AK20212242** (300 mg, 1.5 mmol, 1.5 eq), CuI (40 mg, 0.2 mmol, 0.2 equiv.), and $Pd(PPh_3)_2Cl_2$ (70 mg, 0.1 mmol, 0.1 equiv.) in DMF (1.5 ml). The resulting mixture was purged and refilled with argon three times and stirred at 90°C for 1.5 hours under argon. The reaction mixture was cooled to room temperature. The mixture was filtered through celite and evaporated to remove most of the solvent. The residue was purified by HPLC to yield Boc-protected **AK20202170**. The Boc-protected **AK20202170** was dissolved in DCM (5 ml), and TFA (2 ml) was added to remove Boc protection. The mixture was stirred at room temperature for 10 min. Most of the volatile components were removed in vacuum and the residue was purified by HPLC. The

sample was dried by lyophilizer, yielding 270 mg of **AK20202170** (60%). ^{1}H NMR (400 MHz, DMSO) δ 11.00 (s, 1H), 8.73 (s, 2H), 7.73 (dd, *J* = 7.6, 1.1 Hz, 1H), 7.66 (dd, *J* = 7.6, 1.1 Hz, 1H), 7.53 (t, *J* = 7.6 Hz, 1H), 5.15 (dd, *J* = 13.3, 5.1 Hz, 1H), 4.48 (d, *J* = 17.7 Hz, 1H), 4.33 (d, *J* = 17.7 Hz, 1H), 3.81 (s, 3H), 2.93 (m, 1H), 2.42 (m, 1H), 2.03 (m, 1H), 1.89 (m, 2H). ^{13}C NMR (400 MHz, DMSO) δ 172.88, 170.99, 167.65, 143.86, 134.18, 132.00, 128.62, 122.87, 118.49, 94.53, 77.12, 51.65, 47.39, 46.93, 32.52, 31.21, 24.53, 22.42, 16.16. ESI−MS calculated for $C_{19}H_{21}N_3O_3^+$ 197.28, found $[M + H]^+$ 142.02.

HATU (280 mg, 0.74 mmol, 1.1 equiv.) was added to a solution of **AK20212285** (300 mg, 0.67 mmol, 1 equiv.), **AK20202170** (300mg, 0.67 mmol, 1 equiv.), and triethylamine (0.46 ml, 3.35 mmol, 5 equiv.) in CH_3CN (5 ml). The mixture was stirred at room temperature for 30 min. The yellow solution was concentrated in vacuum and the crude was purified by flash column chromatography to yield **AK20212391** in 74% (385 mg). ^{1}H NMR (400 MHz, DMSO) δ 10.76 (s, 1H), 8.03 (s, 2H), 7.93 (d, *J* = 3.3 Hz, 1H), 7.76 (d, *J* = 3.3 Hz, 1H), 7.69 (d, *J* = 7.6 Hz, 1H), 7.60 (d, *J* = 7.6 Hz, 1H), 7.53 – 7.43 (m, 2H), 5.10 (m, 1H), 4.48 (m, 1H), 4.36 (m, 1H), 4.10 (m, 1H), 3.87 (m, 2H), 3.46 – 3.27 (m, 4H), 3.11 (s, 3H), 2.98 – 2.79 (m, 4H), 2.62 (m, 3H), 2.46 (m, 2H), 2.05 (m, 1H), 1.78 (m, 5H), 1.41 (s, 9H). ^{13}C NMR (400 MHz, DMSO) δ 172.82, 171.56, 170.93, 170.00, 167.65, 153.70, 152.48, 150.94, 144.03, 133.85, 132.57, 131.92, 129.32, 128.53, 127.45, 122.59, 121.07, 120.71, 118.71, 95.74, 78.69, 78.49, 77.24, 74.25, 56.92, 51.57, 46.79, 45.77, 38.21, 35.71, 31.18, 28.21, 25.81, 22.82, 22.30, 16.39, 8.61. ESI−MS calculated for $C_{41}H_{46}N_6O_7S^+$ 766.91, found $[M + H]^+$ 767.19.

AK20212391 (380 mg, 0.5 mmol, 1 equiv.) was dissolved in DCM (5 ml), and TFA (2 ml) was added to remove Boc protection. The mixture was stirred at room temperature for 10 min. Most of the volatile components were removed in vacuum. To the residue, CH_3CN (5 ml),

triethylamine (0.35 ml, 2.5 mmol, 5 equiv.), Boc-L-*tert*-leucine (175 mg, 0.75 mmol, 1.5 equiv.), and HATU (230 mg, 0.6 mmol, 1.2 equiv.) were added. The mixture was stirred at room temperature for 30 min. The yellow solution was concentrated in vacuum and the crude was purified by flash column chromatography to yield **AK20212392** in 70% (354 mg). ^{1}H NMR (400 MHz, DMSO) δ 10.99 (m, 1H), 8.07 – 7.88 (m, 3H), 7.86 – 7.77 (m, 1H), 7.77 – 7.63 (m, 2H), 7.62 – 7.47 (m, 3H), 5.14 (m, 1H), 4.47 (m, 1H), 4.39 – 4.23 (m, 1H), 4.15 (m, 2H), 3.93 – 3.74 (m, 2H), 3.43 – 3.25 (m, 2H), 2.99 – 2.85 (m, 3H), 2.79 (m, 1H), 2.67 – 2.41 (m, 7H), 2.13 – 1.60 (m, 8H), 1.36 (s, 9H), 0.97 (s, 9H). ^{13}C NMR (400 MHz, DMSO) δ 172.84, 170.95, 169.95, 169.67, 169.29, 167.67, 166.10, 155.39, 144.01, 133.86, 132.45, 131.94, 129.22, 128.53, 127.28, 122.60, 120.94, 118.74, 95.76, 95.13, 78.04, 76.69, 76.53, 58.44, 57.29, 51.59, 48.00, 46.99, 45.93, 45.74, 35.10, 34.91, 31.21, 28.93, 28.11, 26.33, 25.88, 24.88, 22.33, 16.41, 8.59. ESI−MS calculated for $C_{47}H_{57}N_7O_8S^+$ 880.07, found $[M + H]^+$ 880.24.

AK20212392 (230 mg, 0.26 mmol, 1 equiv.) was dissolved in DCM (3 ml), and TFA (1.5 ml) was added to remove Boc protection. The mixture was stirred at room temperature for 10 min. Most of the volatile components were removed in vacuum. To the residue, CH_3CN (5 ml), triethylamine (0.18 ml, 1.3 mmol, 5 equiv.), benzothiophene head IM-6 (115 mg, 0.31 mmol, 1.2 equiv.), and HATU (118 mg, 0.31 mmol, 1.2 equiv.) were added. The mixture was stirred at room temperature for 30 min. The yellow solution was concentrated in vacuum and the crude was purified by flash column chromatography to yield **AK20212290** in 68% (200 mg). ^{1}H NMR (400 MHz, DMSO) δ 11.08 – 10.86 (m, 1H), 8.60 – 8.39 (m, 2H), 8.18 (m, 1H), 8.09 (s, 1H), 8.04 – 7.92 (m, 2H), 7.91 (m, 1H), 7.78 (d, *J* = 3.3 Hz, 1H), 7.74 – 7.64 (m, 1H), 7.63 – 7.40 (m, 5H), 5.15 (m, 1H), 4.75 (m, 1H), 4.48 (m, 1H), 4.33 (m, 1H), 4.23 – 4.00 (m, 5H), 3.87 – 3.73 (m, 3H), 3.46 – 3.35 (m, 2H), 2.99 – 2.83 (m, 3H), 2.72 – 2.53 (m, 3H), 2.47 (m, 3H),

2.44 (m, 2H), 2.04 – 1.93 (m, 2H), 1.89 – 1.57 (m, 5H), 1.22 (m, 6H), 1.09 (m, 9H). ^{13}C NMR (400 MHz, DMSO) δ 172.85, 170.97, 169.92, 168.44, 167.68, 167.64, 166.06, 161.36, 143.98, 142.63, 140.92, 138.90, 133.87, 132.48, 131.95, 129.15, 128.54, 127.31, 126.04, 123.40, 122.62, 120.94, 118.74, 118.62, 117.05, 95.76, 95.12, 76.72, 76.56, 64.76, 64.69, 57.46, 51.59, 48.19, 47.00, 45.96, 45.78, 35.42, 35.36, 34.89, 33.13, 31.22, 29.01, 26.57, 26.27, 25.87, 24.87, 22.33, 16.42, 16.20, 16.15, 8.62. ESI−MS calculated for $C_{56}H_{62}F_2N_7O_{10}PS_2^+$ 1126.24, found $[M + H]^+$ 1126.31.

To a round bottom flask were added **AK20212290** (200 mg, 0.17 mmol, 1 equiv.), DCM (2 ml) and $CF_3CON(TMS)_2$ (0.27 ml, 1.0 mmol, 6 equiv.). The solution was cooled in an ice bath. To the ice cooled reaction mixture, 1M of TMS-I in DCM (0.85 ml, 0.85 mmol, 5 equiv.) was added dropwise and the mixture was stirred for 10 min in an ice bath. The volatile components were removed under vacuum at below 5°C. The residue was dissolved in a mixed solvent of CH_3CN (3 ml) and water (1 ml). The resulting solution was purified by HPLC to yield **AK-2292** in 82% (150 mg). ^{1}H NMR (400 MHz, DMSO) δ 10.99 (s, 1H), 8.53 (m, 1H), 8.40 (m, 1H), 8.12 – 8.04 (m, 2H), 8.00 (m, 2H), 7.90 (m, 1H), 7.75 (m, 1H), 7.70 (m, 1H), 7.59 (m, 3H), 7.49 (m, 2H), 5.23 – 5.05 (m, 1H), 4.77 (m, 1H), 4.46 (m, 1H), 4.40 – 4.25 (m, 1H), 4.20 (m, 1H), 4.00 – 3.70 (m, 3H), 3.64 (m, 1H), 3.50 – 3.28 (m, 2H), 2.95 (m, 3H), 2.80 (m, 1H), 2.61 (m, 3H), 2.43 (m, 2H), 2.00 (m, 2H), 1.77 (m, 5H), 1.10 (s, 9H). ^{13}C NMR (400 MHz, DMSO) δ 172.97, 171.09, 170.08, 169.80, 168.63, 167.84, 166.22, 161.57, 159.11, 158.72, 158.34, 157.96, 144.03, 142.03, 140.54, 138.89, 133.97, 132.59, 132.12, 132.08, 129.26, 128.62, 127.45, 126.19, 123.84, 122.87, 121.01, 119.47, 118.89, 116.60, 113.74, 110.87, 95.86, 95.21, 76.68, 57.59, 51.74, 48.33, 47.14, 46.09, 35.54, 35.01, 34.98, 32.97, 31.35, 29.14, 26.68, 25.98, 25.00, 22.48, 16.54. ESI−MS calculated for $C_{52}H_{54}F_2N_7O_{10}PS_2^+$ 1070.13, found $[M + H]^+$ 1070.40.

((2-(((2S)-3,3-Dimethyl-1-((2S)-2-((3-(methyl(5-(2-(1-methyl-2,6-dioxopiperidin-3-yl)-1-oxoisoindolin-4-yl)pent-4-yn-1-yl)amino)-3-oxopropyl)(4-(thiazol-2-yl)phenyl)carbamoyl)pyrrolidin-1-yl)-1-oxobutan-2-yl)carbamoyl)benzo[b]thiophen-5-yl)difluoromethyl)phosphonic acid (AK2292ME). AK-2292ME was synthesized by employing a similar procedure for **AK-2292**. ^{1}H NMR (400 MHz, DMSO) δ 8.53 (s, 1H), 8.41 (m, 1H), 8.19 – 8.04 (m, 2H), 8.00 (m, 1H), 7.98 – 7.93 (m, 1H), 7.90 (m, 1H), 7.77 (m, 1H), 7.71 (m, 1H), 7.68 – 7.40 (m, 5H), 5.21 (m, 1H), 4.76 (m, 1H), 4.46 (m, 1H), 4.37 (m, 1H), 4.18 (m, 1H), 4.01 – 3.69 (m, 3H), 3.65 (m, 1H), 3.40 (m, 2H), 3.05 – 2.92 (m, 6H), 2.80 (m, 2H), 2.59 (m, 3H), 2.44 (m, 2H), 2.01 (m, 2H), 1.76 (m, 5H), 1.10 (s, 9H). ^{13}C NMR (400 MHz, DMSO) δ 171.91, 171.17, 171.06, 170.64, 169.98, 169.71, 168.53, 167.79, 166.13, 161.49, 159.02, 158.64, 158.26, 157.87, 144.01, 141.95, 140.46, 138.81, 133.94, 132.56, 132.03, 132.00, 129.18, 128.58, 127.39, 126.13, 123.76, 122.83, 120.98, 119.46, 118.82, 116.59, 113.72, 110.86, 95.78, 95.13, 76.65, 57.51, 52.14, 48.25, 47.04, 45.97, 35.47, 35.41, 34.90, 32.90, 31.44, 29.08, 26.62, 25.92, 24.94, 21.67, 16.47. ESI−MS calculated for $C_{53}H_{56}F_2N_7O_{10}PS^+$ 1087.16, found $[M + H]^+$ 1084.08.

((2-(((2S)-1-((2S)-2-((4-bromophenyl)(3-((4-(2-(2,6-dioxopiperidin-3-yl)-1-oxoisoindolin-4-yl)but-3-yn-1-yl)amino)-3-oxopropyl)carbamoyl)pyrrolidin-1-yl)-3,3-dimethyl-1-oxobutan-2-yl)carbamoyl)benzo[b]thiophen-5-yl)difluoromethyl)phosphonic acid (AK1930). AK1930 was synthesized by employing a similar procedure for **AK-2292**. ^{1}H NMR (400 MHz, DMSO) δ 11.00 (s, 1H), 8.48 (s, 1H), 8.33 (m, 1H), 8.17 (m, 1H), 8.02 (m, 1H), 7.75 – 7.46 (m, 7H), 7.34 (m, 2H), 5.14 (m, 1H), 4.74 (m, 1H), 4.45 (m, 2H), 4.31 (m, 1H), 4.08 (m, 1H), 3.77 (m, 2H), 2.89 (m, 2H), 2.60 – 2.53 (m, 3H), 2.36 – 2.22 (m, 2H), 2.12 – 1.88

(m, 3H), 1.75 (m, 4H), 1.07 (s, 9H). ESI−MS calculated for $C_{47}H_{48}BrF_2N_6O_{10}PS^+$ 1037.87, found $[M + H]^+$ 1037.00, 1039.43.

((2-(((2S)-1-((2S)-2-((4-bromophenyl)(3-((5-(2-(2,6-dioxopiperidin-3-yl)-1-oxoisoindolin-4-yl)pent-4-yn-1-yl)amino)-3-oxopropyl)carbamoyl)pyrrolidin-1-yl)-3,3-dimethyl-1-oxobutan-2-yl)carbamoyl)benzo[b]thiophen-5-yl)difluoromethyl)phosphonic acid (AK318). AK318 was synthesized by employing a similar procedure for **AK-2292**. ^{1}H NMR (400 MHz, DMSO) δ 10.98 (s, 1H), 8.49 (s, 1H), 8.32 (m, 1H), 8.02 (m, 2H), 7.95 (s, 1H), 7.72 – 7.47 (m, 5H), 7.35 (m, 2H), 5.14 (m, 2H), 4.74 (m, 2H), 4.46 (m, 2H), 4.31 (m, 2H), 4.10 (m, 2H), 3.76 (m, *J* = 8.5 Hz, 2H), 2.95 – 2.83 (m, 2H), 2.35 – 2.18 (m, 3H), 1.98 (m, 3H), 1.87 – 1.57 (m, 6H), 1.08 (s, 9H). ESI−MS calculated for $C_{48}H_{50}BrF_2N_6O_{10}PS^+$ 1051.89, found $[M + H]^+$ 1051.23.

((2-(((2S)-1-((2S)-2-((4-bromophenyl)(3-((6-(2-(2,6-dioxopiperidin-3-yl)-1-oxoisoindolin-4-yl)hex-5-yn-1-yl)amino)-3-oxopropyl)carbamoyl)pyrrolidin-1-yl)-3,3-dimethyl-1-oxobutan-2-yl)carbamoyl)benzo[b]thiophen-5-yl)difluoromethyl)phosphonic acid (AK2450). AK2450 was synthesized by employing a similar procedure for **AK-2292**. ^{1}H NMR (400 MHz, DMSO) δ 10.98 (s, 1H), 8.52 (s, 1H), 8.36 (d, *J* = 8.9 Hz, 1H), 8.12 (d, *J* = 8.4 Hz, 1H), 8.04 (s, 1H), 7.927.88 (m, 1H), 7.69 – 7.55 (m, 5H), 7.34 (d, *J* = 8.5 Hz, 2H), 5.14 (dd, *J* = 13.2, 5.2 Hz, 1H), 4.74 (d, *J* = 8.9 Hz, 1H), 4.47 – 4.42 (m, 1H), 4.33 – 4.28 (m, 1H), 4.09 (dd, *J* = 8.0, 5.8 Hz, 1H), 3.93 – 3.46 (m, 4H), 3.05 – 3.00 (m, 2H), 2.98 – 2.85 (m, 1H), 2.69 – 2.52 (m, 2H), 2.44 – 2.16 (m, 3H), 2.10 – 1.89 (m, 3H), 1.88 – 1.67 (m, 3H), 1.63 – 1.41 (m, 5H), 1.08 (s, 9H). ESI−MS calculated for $C_{49}H_{52}BrF_2N_6O_{10}PS^+$ 1065.92, found $[M + H]^+$ 1065.21, 1067.31.

((2-(((2S)-1-((2S)-2-((4-bromophenyl)(3-((7-(2-(2,6-dioxopiperidin-3-yl)-1-oxoisoindolin-4-yl)hept-6-yn-1-yl)amino)-3-oxopropyl)carbamoyl)pyrrolidin-1-yl)-3,3-dimethyl-1-oxobutan-2-yl)carbamoyl)benzo[b]thiophen-5-yl)difluoromethyl)phosphonic acid (AK317). AK317 was synthesized by employing a similar procedure for **AK-2292**. ^{1}H NMR (400 MHz, DMSO) δ 10.97 (s, 1H), 8.52 (s, 1H), 8.36 (m, 1H), 8.12 (m, 1H), 8.04 (s, 1H), 7.87 (m, 1H), 7.72 – 7.49 (m, 5H), 7.34 (m, 2H), 5.14 (m, 1H), 4.74 (d, *J* = 8.9 Hz, 1H), 4.44 (m, 2H), 4.31 (m, 1H), 4.09 (m, 1H), 3.86 – 3.75 (m, 2H), 3.64 (m, 2H), 2.95 – 2.79 (m, 2H), 2.36 – 2.15 (m, 3H), 2.07 – 1.91 (m, 3H), 1.76 (m, 3H), 1.56 (m, 3H), 1.39 (m, 4H), 1.08 (s, 9H). ESI−MS calculated for $C_{50}H_{54}BrF_2N_6O_{10}PS^+$ 1079.95, found $[M + H]^+$ 1079.01, 1081.13.

((2-(((2S)-1-((2S)-2-((4-bromophenyl)(3-((8-(2-(2,6-dioxopiperidin-3-yl)-1-oxoisoindolin-4-yl)oct-7-yn-1-yl)amino)-3-oxopropyl)carbamoyl)pyrrolidin-1-yl)-3,3-dimethyl-1-oxobutan-2-yl)carbamoyl)benzo[b]thiophen-5-yl)difluoromethyl)phosphonic acid (AK316). AK316 was synthesized by employing a similar procedure for **AK-2292**. ^{1}H NMR (400 MHz, DMSO) δ 10.98 (s, 1H), 8.52 (s, 1H), 8.36 (d, *J* = 8.9 Hz, 1H), 8.10 (d, *J* = 8.5 Hz, 1H), 8.04 (s, 1H), 7.86 – 7.82 (m, 1H), 7.69 – 7.51 (m, 5H), 7.39 – 7.32 (m, 2H), 5.13 (dd, *J* = 13.3, 5.1 Hz, 1H), 4.74 (d, *J* = 8.9 Hz, 1H), 4.44 (d, *J* = 17.7 Hz, 1H), 4.31 (d, *J* = 17.7 Hz, 1H), 4.11 – 4.08 (m, 1H), 3.87 – 3.64 (m, 4H), 2.95 – 2.85 (m, 4H), 2.36 – 2.14 (m, 3H), 2.07 – 1.90 (m, 3H), 1.85 – 1.70 (m, 3H), 1.60 – 1.50 (m, 3H), 1.47 – 1.22 (m, 7H), 1.08 (s, 9H). ESI−MS calculated for $C_{51}H_{56}BrF_2N_6O_{10}PS^+$ 1093.98, found $[M + H]^+$ 1093.02, 1095.15.

((2-(((2S)-1-((2S)-2-((4-bromophenyl)(3-(4-((2-(2,6-dioxopiperidin-3-yl)-1-oxoisoindolin-4-yl)amino)piperidin-1-yl)-3-oxopropyl)carbamoyl)pyrrolidin-1-yl)-3,3-dimethyl-1-oxobutan-2-yl)carbamoyl)benzo[b]thiophen-5-yl)difluoromethyl)phosphonic acid (AK1930). AK1931 was synthesized by employing a similar procedure for **AK-2292**. ^{1}H

NMR (400 MHz, DMSO) δ 11.01 (s, 1H), 8.07 – 8.02 (m, 2H), 7.70 – 7.55 (m, 3H), 7.43 – 7.38 (m, 2H), 7.30 – 7.26 (m, 2H), 7.02 – 6.80 (m, 3H), 5.36 – 3.32 (m, 1H), 5.12 (dd, *J* = 13.2, 5.3 Hz, 1H), 4.75 (d, *J* = 9.0 Hz, 1H), 4.25 – 4.1 (m, 5H), 3.90 – 3.70 (m, 4H), 3.68 – 3.55 (m, 4H), 2.93 – 2.89 (m, 2H), 2.37 – 2.22 (m, 2H), 2.05 – 1.70 (m, 9H), 1.08 (s, 9H). ESI−MS calculated for $C_{48}H_{53}BrF_2N_7O_{10}PS^+$ 1068.93, found $[M + H]^+$ 1068.23, 1070.19.

((2-(((2S)-1-((2S)-2-((4-bromophenyl)(3-(4-((2-(2,6-dioxopiperidin-3-yl)-1-oxoisoindolin-4-yl)ethynyl)piperidin-1-yl)-3-oxopropyl)carbamoyl)pyrrolidin-1-yl)-3,3-dimethyl-1-oxobutan-2-yl)carbamoyl)benzo[b]thiophen-5-yl)difluoromethyl)phosphonic acid (AK1929). AK1929 was synthesized by employing a similar procedure for **AK-2292**. ^{1}H NMR (400 MHz, DMSO) δ 11.00 (s, 1H), 8.48 (m, 1H), 8.37 (m, 1H), 8.02 (m, 2H), 7.74 – 7.52 (m, 6H), 7.40 (m, 2H), 5.13 (m, 1H), 4.75 (m, 1H), 4.52 – 4.38 (m, 2H), 4.32 (m, 2H), 4.10 (m, 1H), 3.76 (m, 4H), 2.97 (m, 2H), 2.13 – 1.91 (m, 5H), 1.81 (m, 5H), 1.57 (m, 4H), 1.08 (s, 9H). ESI−MS calculated for $C_{50}H_{52}BrF_2N_6O_{10}PS^+$ 1077.93, found $[M + H]^+$ 1077.24, 1077.15.

((2-(((2S)-1-((2S)-2-((4-bromophenyl)(3-((5-(2-(2,6-dioxopiperidin-3-yl)-1-oxoisoindolin-4-yl)pent-4-yn-1-yl)(methyl)amino)-3-oxopropyl)carbamoyl)pyrrolidin-1-yl)-3,3-dimethyl-1-oxobutan-2-yl)carbamoyl)benzo[b]thiophen-5-yl)difluoromethyl)phosphonic acid (AK2220). AK2220 was synthesized by employing a similar procedure for **AK-2292**. ^{1}H NMR (400 MHz, DMSO) δ 10.98 (s, 1H), 8.52 (m, 1H), 8.40 (m, 1H), 8.12 (m, 1H), 8.04 (m, 1H), 7.75 – 7.49 (m, 6H), 7.44 – 7.30 (m, 2H), 5.15 (m, 1H), 4.79 – 4.68 (m, 1H), 4.47 (m, 2H), 4.39 – 4.24 (m, 1H), 4.09 (m, 1H), 3.77 (m, 2H), 3.64 (m, 1H), 3.38 (m, 2H), 2.95 (s, 3H), 2.79 (m, 1H), 2.65 – 2.53 (m, 2H), 2.26 (m, 2H), 1.99 (m, 2H), 1.87 – 1.57 (m, 6H), 1.08 (s, 9H). ESI−MS calculated for $C_{49}H_{52}BrF_2N_6O_{10}PS^+$ 1065.92, found $[M + H]^+$ 1064.94, 1066.79.

((2-(((2S)-1-((2S)-2-((4-bromophenyl)(3-(3-(4-(2-(2,6-dioxopiperidin-3-yl)-1-oxoisoindolin-4-yl)but-3-yn-1-yl)azetidin-1-yl)-3-oxopropyl)carbamoyl)pyrrolidin-1-yl)-3,3-dimethyl-1-oxobutan-2-yl)carbamoyl)benzo[b]thiophen-5-yl)difluoromethyl)phosphonic acid (AK2221). AK2221 was synthesized by employing a similar procedure for **AK-2292**. ^{1}H NMR (400 MHz, DMSO) δ 10.99 (s, 1H), 8.52 (m, 1H), 8.37 (m, 1H), 8.14 – 7.99 (m, 2H), 7.72 – 7.51 (m, 6H), 7.37 (m, 2H), 5.22 – 5.09 (m, 1H), 4.73 (m, 1H), 4.45 (m, 2H), 4.31 (m, 1H), 4.21 – 4.04 (m, 2H), 3.90 (m, 2H), 3.64 (m, 2H), 3.00 – 2.84 (m, 2H), 2.73 – 2.53 (m, 4H), 2.28 (m, 2H), 2.10 – 1.93 (m, 3H), 1.91 – 1.65 (m, 5H), 1.07 (s, 9H). ESI−MS calculated for $C_{50}H_{52}BrF_2N_6O_{10}PS^+$ 1077.93, found $[M + H]^+$ 1076.97, 1078.83.

((2-(((2S)-1-((2S)-2-((4-bromophenyl)(3-(3-(3-(2-(2,6-dioxopiperidin-3-yl)-1-oxoisoindolin-4-yl)prop-2-yn-1-yl)azetidin-1-yl)-3-oxopropyl)carbamoyl)pyrrolidin-1-yl)-3,3-dimethyl-1-oxobutan-2-yl)carbamoyl)benzo[b]thiophen-5-yl)difluoromethyl)phosphonic acid (AK2222). AK2222 was synthesized by employing a similar procedure for **AK-2292**. ^{1}H NMR (400 MHz, DMSO) δ 11.00 (s, 1H), 8.52 (d, *J* = 7.0 Hz, 1H), 8.39 (d, *J* = 8.6 Hz, 1H), 8.15 – 8.00 (m, 2H), 7.73 – 7.53 (m, 6H), 7.38 – 7.32 (m, 2H), 5.15 – 5.10 (m, 1H), 4.74 (dd, *J* = 8.9, 5.2 Hz, 1H), 4.51 – 4.37 (m, 2H), 4.30 – 4.17 (m, 2H), 4.13 – 4.05 (m, 2H), 3.80 – 3.75 (m, 3H), 3.68 – 3.60 (m, 2H), 2.85 – 2.70 (m, 3H), 2.38 – 2.19 (m, 3H), 2.12 – 1.92 (m, 3H), 1.77 – 1.72 (m, 4H), 1.06 (s, 9H). ESI−MS calculated for $C_{49}H_{50}BrF_2N_6O_{10}PS^+$ 1063.91, found $[M + H]^+$ 1062.93, 1064.34.

((2-(((2S)-1-((2S)-2-((3-((5-(2-(2,6-dioxopiperidin-3-yl)-1-oxoisoindolin-4-yl)pent-4-yn-1-yl)amino)-3-oxopropyl)(phenyl)carbamoyl)pyrrolidin-1-yl)-3,3-dimethyl-1-oxobutan-2-yl)carbamoyl)benzo[b]thiophen-5-yl)difluoromethyl)phosphonic acid (AK1992). AK1992 was synthesized by employing a similar procedure for **AK-2292**. **AK1992** was synthesized by

employing a similar procedure for **AK-2292**. ^{1}H NMR (400 MHz, DMSO) δ 10.98 (s, 1H), 8.52 (s, 1H), 8.37 (d, *J* = 8.9 Hz, 1H), 8.13 – 7.96 (m, 3H), 7.65 – 7.33 (m, 9H), 5.16 (dd, *J* = 13.2, 5.3 Hz, 1H), 4.74 (d, *J* = 8.8 Hz, 1H), 4.57 – 4.38 (m, 2H), 4.31 (d, *J* = 17.8 Hz, 1H), 4.11 (t, *J* = 6.9 Hz, 1H), 3.97 – 3.44 (m, 5H), 2.98 – 2.79 (m, 1H), 2.65 – 2.53 (m, 1H), 2.39 – 2.14 (m, 3H), 2.09 – 1.86 (m, 3H), 1.87 – 1.49 (m, 6H), 1.09 (s, 9H). ESI−MS calculated for $C_{48}H_{51}F_2N_6O_{10}PS^+$ 973.00, found $[M + H]^+$ 972.95.

((2-(((2S)-1-((2S)-2-((3-((5-(2-(2,6-dioxopiperidin-3-yl)-1-oxoisoindolin-4-yl)pent-4-yn-1-yl)amino)-3-oxopropyl)(4-fluorophenyl)carbamoyl)pyrrolidin-1-yl)-3,3-dimethyl-1-oxobutan-2-yl)carbamoyl)benzo[b]thiophen-5-yl)difluoromethyl)phosphonic acid (AK1993). AK1993 was synthesized by employing a similar procedure for **AK-2292**. ^{1}H NMR (400 MHz, DMSO) δ 10.97 (s, 1H), 8.49 (s, 1H), 8.13 – 7.87 (m, 3H), 7.76 – 7.37 (m, 6H), 7.28 – 7.24 (m, 3H), 5.16 – 5.11 (m, 1H), 4.74 (d, *J* = 9.0 Hz, 1H), 4.46 (d, *J* = 18.3 Hz, 1H), 4.31 (d, *J* = 17.7 Hz, 1H), 4.09 – 4.06 (m, 1H), 3.87 – 3.54 (m, 4H), 3.17 – 3.13 (m, 3H), 3.01 – 2.77 (m, 2H), 2.37 – 2.16 (m, 3H), 2.05 – 2.00 (m, 3H), 1.83 – 1.53 (m, 5H), 1.08 (s, 9H). ESI−MS calculated for $C_{48}H_{50}F_3N_6O_{10}PS^+$ 990.99, found $[M + H]^+$ 991.10.

((2-(((2S)-1-((2S)-2-((4-chlorophenyl)(3-((5-(2-(2,6-dioxopiperidin-3-yl)-1-oxoisoindolin-4-yl)pent-4-yn-1-yl)amino)-3-oxopropyl)carbamoyl)pyrrolidin-1-yl)-3,3-dimethyl-1-oxobutan-2-yl)carbamoyl)benzo[b]thiophen-5-yl)difluoromethyl)phosphonic acid (AK1994). AK1994 was synthesized by employing a similar procedure for **AK-2292**. ^{1}H NMR (400 MHz, DMSO) δ 10.98 (s, 1H), 8.50 (s, 1H), 8.35 (d, *J* = 8.9 Hz, 1H), 8.08 – 7.94 (m, 2H), 7.76 – 7.37 (m, 9H), 5.14 (dd, *J* = 13.1, 5.3 Hz, 1H), 4.74 (d, *J* = 8.9 Hz, 1H), 4.46 (d, *J* = 17.9 Hz, 1H), 4.31 (d, *J* = 17.7 Hz, 1H), 4.11 – 4.07 (m, 1H), 3.86 – 3.70 (m, 3H), 3.66 – 3.62 (m, 2H), 3.18 – 3.14 (m, 2H), 2.93 – 2.87 (m, 1H), 2.37 – 2.19 (m, 3H), 2.02 – 1.97 (m, 3H),

1.87 – 1.51 (m, 6H), 1.08 (s, 9H). ESI−MS calculated for $C_{48}H_{50}ClF_2N_6O_{10}PS^+$ 1007.44, found $[M + H]^+$ 1006.85.

((2-(((2S)-1-((2S)-2-((4-chloro-3-fluorophenyl)(3-((5-(2-(2,6-dioxopiperidin-3-yl)-1-oxoisoindolin-4-yl)pent-4-yn-1-yl)amino)-3-oxopropyl)carbamoyl)pyrrolidin-1-yl)-3,3-dimethyl-1-oxobutan-2-yl)carbamoyl)benzo[b]thiophen-5-yl)difluoromethyl)phosphonic acid (AK1995). AK1995 was synthesized by employing a similar procedure for **AK-2292**. ^{1}H NMR (400 MHz, DMSO) δ 10.98 (s, 1H), 8.51 (s, 1H), 8.39 (d, *J* = 8.9 Hz, 1H), 8.16 – 7.99 (m, 2H), 7.96 – 7.93 (m, 1H), 7.76 – 7.42 (m, 7H), 5.14 (dd, *J* = 12.8, 5.2 Hz, 1H), 4.75 (d, *J* = 8.9 Hz, 1H), 4.46 (d, *J* = 18.0 Hz, 1H), 4.35 – 4.23 (m, 1H), 4.18 – 4.13 (m, 1H), 3.80 – 3.75 (m, 2H), 3.68 – 3.65 (m, 1H), 3.16 – 3.12 (m, 3H), 3.02 – 2.83 (m, 2H), 2.37 – 2.21 (m, 3H), 2.05 – 1.90 (m, 3H), 1.87 – 1.56 (m, 6H), 1.08 (s, 9H). ESI−MS calculated for $C_{48}H_{49}ClF_3N_6O_{10}PS^+$ 1025.43, found $[M + H]^+$ 1024.91.

((2-(((2S)-1-((2S)-2-((3-((5-(2-(2,6-dioxopiperidin-3-yl)-1-oxoisoindolin-4-yl)pent-4-yn-1-yl)amino)-3-oxopropyl)(4-iodophenyl)carbamoyl)pyrrolidin-1-yl)-3,3-dimethyl-1-oxobutan-2-yl)carbamoyl)benzo[b]thiophen-5-yl)difluoromethyl)phosphonic acid (AK1996). AK1996 was synthesized by employing a similar procedure for **AK-2292**. ^{1}H NMR (400 MHz, DMSO) δ 10.98 (s, 1H), 8.63 – 8.13 (m, 3H), 8.11 – 7.89 (m, 3H), 7.85 – 7.35 (m, 7H), 5.13 (dd, *J* = 13.2, 5.2 Hz, 1H), 4.81 – 4.68 (m, 1H), 4.46 (d, *J* = 17.8 Hz, 1H), 4.27 (d, *J* = 12.5 Hz, 1H), 4.11 – 4.07 (m, 1H), 3.8 – 3.5 (m, 4H), 3.16 – 3.11 (m, 2H), 2.36 – 2.14 (m, 4H), 2.02 – 1.98 (m, 3H), 1.85 – 1.50 (m, 7H), 1.08 (s, 9H). ESI−MS calculated for $C_{48}H_{50}F_2IN_6O_{10}PS^+$ 1098.90, found $[M + H]^+$ 1099.14.

((2-(((2S)-1-((2S)-2-((4-chlorophenyl)(2-((6-(2-(2,6-dioxopiperidin-3-yl)-1-oxoisoindolin-4-yl)hex-5-yn-1-yl)amino)-2-oxoethyl)carbamoyl)pyrrolidin-1-yl)-3,3-

dimethyl-1-oxobutan-2-yl)carbamoyl)benzo[b]thiophen-5-yl)difluoromethyl)phosphonic acid (AK2000). AK2000 was synthesized by employing a similar procedure for **AK-2292**. ^{1}H NMR (400 MHz, DMSO) δ 10.98 (s, 1H), 8.52 (s, 1H), 8.38 (d, *J* = 8.8 Hz, 1H), 8.13 (d, *J* = 8.5 Hz, 1H), 8.05 (s, 1H), 7.86 (s, 1H), 7.70 – 7.46 (m, 8H), 5.15 – 5.09 (m, 1H), 4.73 (d, *J* = 8.8 Hz, 1H), 4.44 (dd, *J* = 17.8, 3.0 Hz, 2H), 4.32 – 4.24 (m, 2H), 3.98 (d, *J* = 16.2 Hz, 1H), 3.80 – 3.76 (m, 1H), 3.66 – 6.62 (m, 1H), 3.19 – 3.10 (m, 2H), 2.96 – 2.87 (m, 1H), 2.02 – 1.97 (m, 4H), 1.87 – 1.67 (m, 4H), 1.66 – 1.38 (m, 5H), 1.07 (s, 9H). ESI−MS calculated for $C_{48}H_{50}ClF_2IN_6O_{10}PS^+$ 1007.44, found $[M + H]^+$ 1007.25.

((2-(((2S)-1-((2S)-2-((4-chloro-3-fluorophenyl)(3-((6-(2-(2,6-dioxopiperidin-3-yl)-1-oxoisoindolin-4-yl)hex-5-yn-1-yl)amino)-3-oxopropyl)carbamoyl)pyrrolidin-1-yl)-3,3-dimethyl-1-oxobutan-2-yl)carbamoyl)benzo[b]thiophen-5-yl)difluoromethyl)phosphonic acid (AK1998). AK1998 was synthesized by employing a similar procedure for **AK-2292**. ^{1}H NMR (400 MHz, DMSO) δ 10.98 (s, 1H), 8.51 (s, 1H), 8.39 (d, *J* = 9.0 Hz, 1H), 8.14 – 7.98 (m, 2H), 7.90 (d, *J* = 5.6 Hz, 1H), 7.76 – 7.40 (m, 7H), 7.29 (d, *J* = 8.5 Hz, 1H), 5.13 (dd, *J* = 13.3, 5.3 Hz, 1H), 4.75 (d, *J* = 8.9 Hz, 1H), 4.44 (d, *J* = 17.5 Hz, 1H), 4.30 (d, *J* = 17.7 Hz, 1H), 4.17 – 4.13 (m, 1H), 3.85 – 3.75 (m, 2H), 3.66 – 3.62 (m, 1H), 3.05 – 3.01 (m, 2H), 2.94 – 2.83 (m, 1H), 2.39 – 2.13 (m, 4H), 2.08 – 1.90 (m, 3H), 1.86 – 1.66 (m, 3H), 1.55 – 1.51 (m, 4H), 1.08 (s, 9H). ESI−MS calculated for $C_{48}H_{49}Cl_2F_2IN_6O_{10}PS^+$ 1039.46, found $[M + H]^+$ 1039.26.

((2-(((2S)-1-((2S)-2-((4-cyanophenyl)(3-((5-(2-(2,6-dioxopiperidin-3-yl)-1-oxoisoindolin-4-yl)pent-4-yn-1-yl)amino)-3-oxopropyl)carbamoyl)pyrrolidin-1-yl)-3,3-dimethyl-1-oxobutan-2-yl)carbamoyl)benzo[b]thiophen-5-yl)difluoromethyl)phosphonic acid (AK2094). AK2094 was synthesized by employing a similar procedure for **AK-2292**. ^{1}H NMR (400 MHz, DMSO) δ 10.98 (s, 1H), 8.52 (s, 1H), 8.38 (d, *J* = 8.8 Hz, 1H), 8.11 (d, *J* = 8.6

Hz, 1H), 8.04 (s, 1H), 7.99 – 7.83 (m, 3H), 7.75 – 7.46 (m, 6H), 5.16 – 5.11 (m, 1H), 4.74 (d, *J* = 8.9 Hz, 1H), 4.46 (d, *J* = 17.8 Hz, 1H), 4.31 (d, *J* = 17.8 Hz, 1H), 4.13 – 4.08 (m, 1H), 3.85 – 3.75 (m, 4H), 3.68 – 3.63 (m, 1H), 3.16 – 3.12 (m, 2H), 3.03 – 2.85 (m, 1H), 2.46 – 2.19 (m, 4H), 2.02 – 1.96 (m, 3H), 1.90 – 1.72 (m, 3H), 1.68 – 1.64 (m, 2H), 1.08 (s, 9H). ESI−MS calculated for $C_{49}H_{50}F_2N_7O_{10}PS^+$ 998.01, found $[M + H]^+$ 998.00.

((2-(((2S)-1-((2S)-2-((3-cyanophenyl)(3-((5-(2-(2,6-dioxopiperidin-3-yl)-1-oxoisoindolin-4-yl)pent-4-yn-1-yl)amino)-3-oxopropyl)carbamoyl)pyrrolidin-1-yl)-3,3-dimethyl-1-oxobutan-2-yl)carbamoyl)benzo[b]thiophen-5-yl)difluoromethyl)phosphonic acid (AK2095). AK2095 was synthesized by employing a similar procedure for **AK-2292**. ^{1}H NMR (400 MHz, DMSO) δ 10.97 (s, 1H), 8.52 (s, 1H), 8.43 (d, *J* = 9.0 Hz, 1H), 8.10 (d, *J* = 8.5 Hz, 1H), 8.04 (s, 1H), 7.96 (d, *J* = 6.0 Hz, 1H), 7.85 – 7.47 (m, 8H), 5.14 (dd, *J* = 13.2, 5.3 Hz, 1H), 4.76 (d, *J* = 8.9 Hz, 1H), 4.46 (d, *J* = 16.9 Hz, 1H), 4.33 – 4.29 (m, 1H), 4.08 – 4.04 (m, 1H), 3.78 – 3.74 (m, 4H), 3.68 – 3.62 (m, 1H), 2.97 – 2.81 (m, 2H), 2.42 – 2.16 (m, 4H), 2.02 – 1.96 (m, 3H), 1.79 – 1.75 (m, 3H), 1.68 – 1.64 (m, 2H), 1.08 (s, 9H). ESI−MS calculated for $C_{49}H_{50}F_2N_7O_{10}PS^+$ 998.01, found $[M + H]^+$ 998.16.

((2-(((2S)-1-((2S)-2-((3-((5-(2-(2,6-dioxopiperidin-3-yl)-1-oxoisoindolin-4-yl)pent-4-yn-1-yl)amino)-3-oxopropyl)(4-(trifluoromethyl)phenyl)carbamoyl)pyrrolidin-1-yl)-3,3-dimethyl-1-oxobutan-2-yl)carbamoyl)benzo[b]thiophen-5-yl)difluoromethyl)phosphonic acid (AK2096). AK2096 was synthesized by employing a similar procedure for **AK-2292**. ^{1}H NMR (400 MHz, DMSO) δ 10.98 (s, 1H), 8.50 (s, 1H), 8.36 – 8.35 (m, 1H), 8.06 – 8.05 (m, 1H), 7.98 – 7.95 (m, 1H), 7.81 (d, *J* = 8.2 Hz, 2H), 7.73 – 7.45 (m, 7H), 5.14 (dd, *J* = 13.3, 5.3 Hz, 1H), 4.75 (d, *J* = 9.0 Hz, 1H), 4.46 (d, *J* = 18.0 Hz, 1H), 4.32 – 4.28 (m, 1H), 4.11 – 4.08 (m, 1H), 3.79 – 7.75 (m, 3H), 3.67 – 3.63 (m, 1H), 3.16 – 3.12 (m, 3H), 2.92 – 2.88 (m, 2H), 2.40 –

2.22 (m, 2H), 2.02 – 2.96 (m, 3H), 1.79 – 1.76 (m, 3H), 1.69 – 1.54 (m, 2H), 1.09 (s, 9H). ESI−MS calculated for $C_{49}H_{50}F_5N_7O_{10}PS^+$ 1041.00, found $[M + H]^+$ 1040.99.

((2-(((2S)-1-((2S)-2-((3-((5-(2-(2,6-dioxopiperidin-3-yl)-1-oxoisoindolin-4-yl)pent-4-yn-1-yl)amino)-3-oxopropyl)(3-(trifluoromethyl)phenyl)carbamoyl)pyrrolidin-1-yl)-3,3-dimethyl-1-oxobutan-2-yl)carbamoyl)benzo[b]thiophen-5-yl)difluoromethyl)phosphonic acid (AK2097). AK2097 was synthesized by employing a similar procedure for **AK-2292**. ^{1}H NMR (400 MHz, DMSO) δ 10.98 (s, 1H), 8.50 (s, 1H), 8.38 (d, *J* = 8.9 Hz, 1H), 8.09 – 7.92 (m, 3H), 7.77 – 7.47 (m, 8H), 5.14 (dd, *J* = 13.2, 5.3 Hz, 1H), 4.75 (d, *J* = 9.0 Hz, 1H), 4.46 (d, *J* = 17.8 Hz, 1H), 4.30 (d, *J* = 17.7 Hz, 1H), 4.07 – 4.03 (m, 1H), 3.92 – 3.98 (m, 1H), 3.78 – 3.74 (m, 2H), 3.67 – 3.63 (m, 1H), 3.16 – 3.08 (m, 2H), 2.92 – 2.88 (m, 2H), 2.37 – 2.16 (m, 3H), 2.02 – 1.95 (m, 3H), 1.79 – 1.75 (m, 3H), 1.67 – 1.63 (m, 3H), 1.09 (s, 9H). ESI−MS calculated for $C_{49}H_{50}F_5N_7O_{10}PS^+$ 1041.00, found $[M + H]^+$ 1040.98.

((2-(((2S)-1-((2S)-2-((3-((5-(2-(2,6-dioxopiperidin-3-yl)-1-oxoisoindolin-4-yl)pent-4-yn-1-yl)amino)-3-oxopropyl)(p-tolyl)carbamoyl)pyrrolidin-1-yl)-3,3-dimethyl-1-oxobutan-2-yl)carbamoyl)benzo[b]thiophen-5-yl)difluoromethyl)phosphonic acid (AK2098). AK2098 was synthesized by employing a similar procedure for **AK-2292**. ^{1}H NMR (400 MHz, DMSO) δ 10.97 (s, 1H), 8.52 (s, 1H), 8.35 (d, *J* = 8.8 Hz, 1H), 8.11 (d, *J* = 8.5 Hz, 1H), 8.04 (s, 1H), 7.98 – 7.89 (m, 1H), 7.74 – 7.66 (m, 1H), 7.61 – 7.48 (m, 3H), 7.29 – 7.18 (m, 4H), 5.13 (dd, *J* = 13.2, 5.3 Hz, 1H), 4.73 (d, *J* = 8.9 Hz, 1H), 4.50 – 4.40 (m, 1H), 4.31 (d, *J* = 17.8 Hz, 1H), 4.13 – 4.08 (m, 1H), 3.80 – 3.65 (m, 5H), 2.92 – 2.88 (m, 1H), 2.39 – 2.10 (m, 8H), 2.06 – 1.87 (m, 3H), 1.81 – 1.52 (m, 6H), 1.08 (s, 9H). ESI−MS calculated for $C_{49}H_{53}F_2N_6O_{10}PS^+$ 987.03, found $[M + H]^+$ 987.07.

((2-(((2S)-1-((2S)-2-((4-(tert-butyl)phenyl)(3-((5-(2-(2,6-dioxopiperidin-3-yl)-1-oxoisoindolin-4-yl)pent-4-yn-1-yl)amino)-3-oxopropyl)carbamoyl)pyrrolidin-1-yl)-3,3-dimethyl-1-oxobutan-2-yl)carbamoyl)benzo[b]thiophen-5-yl)difluoromethyl)phosphonic acid (AK2099). AK2099 was synthesized by employing a similar procedure for **AK-2292**. ^{1}H NMR (400 MHz, DMSO) δ 10.97 (s, 1H), 8.51 (s, 1H), 8.33 (d, *J* = 8.8 Hz, 1H), 8.13 – 8.00 (m, 2H), 7.98 – 7.95 (m, 1H), 7.70 (d, *J* = 7.7 Hz, 1H), 7.65 – 7.46 (m, 3H), 7.44 – 7.40 (m, 2H), 7.29 (d, *J* = 8.3 Hz, 2H), 5.13 (dd, *J* = 13.1, 5.3 Hz, 1H), 4.73 (d, *J* = 9.0 Hz, 1H), 4.46 (d, *J* = 18.0 Hz, 1H), 4.31 (d, *J* = 17.9 Hz, 1H), 4.11 – 4.07 (m, 1H), 3.90 – 3.56 (m, 4H), 3.18 – 3.14 (m, 3H), 2.92 – 2.88 (m, 2H), 2.39 – 2.14 (m, 3H), 2.06 – 1.87 (m, 3H), 1.80 – 1.60 (m, 5H), 1.25 (s, 9H), 1.09 (s, 8H). ESI−MS calculated for $C_{52}H_{59}F_2N_6O_{10}PS^+$ 1029.11, found $[M + H]^+$ 1029.30.

((2-(((2S)-1-((2S)-2-((3-((5-(2-(2,6-dioxopiperidin-3-yl)-1-oxoisoindolin-4-yl)pent-4-yn-1-yl)amino)-3-oxopropyl)(4-(tetrahydro-2H-pyran-4-yl)phenyl)carbamoyl)pyrrolidin-1-yl)-3,3-dimethyl-1-oxobutan-2-yl)carbamoyl)benzo[b]thiophen-5-yl)difluoromethyl)phosphonic acid (AK2103). AK2103 was synthesized by employing a similar procedure for **AK-2292**. ^{1}H NMR (400 MHz, DMSO) δ 10.97 (s, 1H), 8.52 (s, 1H), 8.36 (d, *J* = 8.8 Hz, 1H), 8.11 (d, *J* = 8.5 Hz, 2H), 8.04 (s, 1H), 7.99 – 7.90 (m, 1H), 7.79 – 7.36 (m, 7H), 5.16 – 5.08 (m, 1H), 4.73 (d, *J* = 8.8 Hz, 1H), 4.48 – 4.44 (m, 2H), 4.33 – 4.29 (m, 1H), 4.11 – 4.07 (m, 1H), 3.42 – 3.35 (m, 3H), 3.67 – 3.63 (m, 2H), 3.39 – 3.32 (m, 2H), 3.18 – 3.14 (m, 2H), 2.93 – 2.85 (m, 1H), 2.78 – 2.70 (m, 1H), 2.39 – 2.19 (m, 3H), 2.10 – 1.87 (m, 4H), 1.85 – 1.52 (m, 11H), 1.08 (s, 9H). ESI−MS calculated for $C_{53}H_{59}F_2N_6O_{11}PS^+$ 1057.12, found $[M + H]^+$ 1057.33.

((2-(((2S)-1-((2S)-2-((3-((5-(2-(2,6-dioxopiperidin-3-yl)-1-oxoisoindolin-4-yl)pent-4-yn-1-yl)amino)-3-oxopropyl)(4-(methylsulfonyl)phenyl)carbamoyl)pyrrolidin-1-yl)-3,3-dimethyl-1-oxobutan-2-yl)carbamoyl)benzo[b]thiophen-5-yl)difluoromethyl)phosphonic acid (AK2145). AK2145 was synthesized by employing a similar procedure for **AK-2292**. ^{1}H NMR (400 MHz, DMSO) δ 10.97 (s, 1H), 8.52 (s, 1H), 8.37 (d, *J* = 8.8 Hz, 1H), 8.14 – 7.91 (m, 5H), 7.76 – 7.46 (m, 6H), 5.14 (dd, *J* = 13.1, 5.2 Hz, 1H), 4.73 (d, *J* = 8.8 Hz, 1H), 4.48 – 4.44 (m, 1H), 4.33 – 4.29 (m, 1H), 4.12 – 4.08 (m, 1H), 3.93 – 3.89 (m, 1H), 3.80 – 3.76 (m, 1H), 3.67 – 3.64 (m, 1H), 3.23 (s, 3H), 3.17 – 3.13 (m, 2H), 2.97 – 2.82 (m, 2H), 2.40 – 2.15 (m, 4H), 2.10 – 1.91 (m, 3H), 1.83 – 1.79 (m, 4H), 1.70 – 1.58 (m, 2H), 1.09 (s, 9H). ESI−MS calculated for $C_{49}H_{53}F_2N_6O_{12}PS_2^+$ 1051.08, found $[M + H]^+$ 1051.83.

((2-(((2S)-1-((2S)-2-((3-((5-(2-(2,6-dioxopiperidin-3-yl)-1-oxoisoindolin-4-yl)pent-4-yn-1-yl)amino)-3-oxopropyl)(4-(thiophen-2-yl)phenyl)carbamoyl)pyrrolidin-1-yl)-3,3-dimethyl-1-oxobutan-2-yl)carbamoyl)benzo[b]thiophen-5-yl)difluoromethyl)phosphonic acid (AK2100). AK2100 was synthesized by employing a similar procedure for **AK-2292**. ^{1}H NMR (400 MHz, DMSO) δ 10.97 (s, 1H), 8.52 (s, 1H), 8.36 (d, *J* = 8.9 Hz, 1H), 8.14 – 7.90 (m, 3H), 7.72 – 7.64 (m, 3H), 7.60 – 7.34 (m, 7H), 7.13 – 7.09 (m, 1H), 5.13 (dd, *J* = 13.1, 5.3 Hz, 1H), 4.74 (d, *J* = 8.9 Hz, 1H), 4.46 (d, *J* = 17.8 Hz, 1H), 4.31 (d, *J* = 17.8 Hz, 1H), 4.20 – 4.16 (m, 1H), 3.92 – 3.81 (m, 1H), 3.78 – 3.74 (m, 2H), 3.66 – 3.62 (m, 1H), 3.18 – 3.14 (m, 3H), 2.91 – 2.88 (m, 1H), 2.41 – 2.20 (m, 3H), 2.11 – 1.89 (m, 3H), 1.88 – 1.51 (m, 6H), 1.09 (s, 9H). ESI−MS calculated for $C_{52}H_{53}F_2N_6O_{10}PS_2^+$ 1055.12, found $[M + H]^+$ 1054.99.

((2-(((2S)-1-((2S)-2-((3-((5-(2-(2,6-dioxopiperidin-3-yl)-1-oxoisoindolin-4-yl)pent-4-yn-1-yl)amino)-3-oxopropyl)(4-(thiazol-2-yl)phenyl)carbamoyl)pyrrolidin-1-yl)-3,3-dimethyl-1-oxobutan-2-yl)carbamoyl)benzo[b]thiophen-5-yl)difluoromethyl)phosphonic

acid (AK2146). AK2146 was synthesized by employing a similar procedure for **AK-2292**. ^{1}H NMR (400 MHz, DMSO) δ 10.97 (s, 1H), 8.52 (s, 1H), 8.37 (m, 2H), 8.11 (m, 2H), 8.05 – 7.96 (m, 3H), 7.91 (m, 1H), 7.78 (m, 1H), 7.69 (m, 1H), 7.62 – 7.54 (m, 2H), 7.50 (m, 2H), 5.13 (m, 1H), 4.75 (m, 1H), 4.45 (m, 2H), 4.30 (m, 2H), 4.18 (m, 1H), 3.77 (m, 4H), 3.15 (m, 2H), 2.92 – 2.86 (m, 1H), 1.98 (m, 3H), 1.81 (m, 4H), 1.66 (m, 3H), 1.09 (s, 9H). ESI−MS calculated for $C_{51}H_{52}F_2N_7O_{10}PS_2^+$ 1056.11, found $[M + H]^+$ 1056.88.

((2-(((2S)-1-((2S)-2-(benzo[b]thiophen-5-yl(3-((5-(2-(2,6-dioxopiperidin-3-yl)-1-oxoisoindolin-4-yl)pent-4-yn-1-yl)amino)-3-oxopropyl)carbamoyl)pyrrolidin-1-yl)-3,3-dimethyl-1-oxobutan-2-yl)carbamoyl)benzo[b]thiophen-5-yl)difluoromethyl)phosphonic acid (AK2102). AK2102 was synthesized by employing a similar procedure for **AK-2292**. ^{1}H NMR (400 MHz, DMSO) δ 10.97 (s, 1H), 8.50 (s, 1H), 8.36 (d, *J* = 9.1 Hz, 1H), 8.11 – 7.99 (m, 3H), 7.95 (d, *J* = 6.0 Hz, 1H), 7.88 (d, *J* = 8.8 Hz, 1H), 7.84 – 7.80 (m, 1H), 7.72 – 7.68 (m, 1H), 7.64 – 7.54 (m, 2H), 7.53 – 7.34 (m, 3H), 5.13 (dd, *J* = 13.2, 5.2 Hz, 1H), 4.74 (d, *J* = 8.9 Hz, 1H), 4.45 (dd, *J* = 17.9, 2.5 Hz, 2H), 4.32 – 4.28 (m, 1H), 4.15 – 4.11 (m, 1H), 3.96 – 3.85 (m, 1H), 3.77 – 3.74 (m, 2H), 3.65 – 3.60 (m, 1H), 3.17 – 3.11 (m, 2H), 2.92 – 2.88 (m, 1H), 2.35 – 2.30 (m, 3H), 2.04 – 1.89 (m, 3H), 1.86 – 1.74 (m, 2H), 1.74 – 1.53 (m, 4H), 1.10 (s, 9H). ESI−MS calculated for $C_{50}H_{51}F_2N_6O_{10}PS_2^+$ 1029.08, found $[M + H]^+$ 1029.26.

((2-(((2S)-1-((2S)-2-(benzo[b]thiophen-4-yl(3-((5-(2-(2,6-dioxopiperidin-3-yl)-1-oxoisoindolin-4-yl)pent-4-yn-1-yl)amino)-3-oxopropyl)carbamoyl)pyrrolidin-1-yl)-3,3-dimethyl-1-oxobutan-2-yl)carbamoyl)benzo[b]thiophen-5-yl)difluoromethyl)phosphonic acid (AK2215). AK2215 was synthesized by employing a similar procedure for **AK-2292**. ^{1}H NMR (400 MHz, DMSO) δ 10.97 (s, 1H), 9.42 (d, *J* = 1.0 Hz, 1H), 8.51 (s, 1H), 8.39 (d, *J* = 8.9 Hz, 1H), 8.20 (t, *J* = 2.3 Hz, 1H), 8.16 – 8.07 (m, 2H), 8.03 (s, 1H), 7.99 – 7.90 (m, 1H), 7.71 –

7.66 (m, 2H), 7.63 – 7.54 (m, 3H), 7.53 – 7.44 (m, 1H), 5.13 (dd, *J* = 13.1, 5.3 Hz, 1H), 4.74 (d, *J* = 8.9 Hz, 1H), 4.50 – 4.39 (m, 2H), 4.30 – 4.26 (m, 1H), 4.14 – 4.10 (m, 1H), 3.97 – 3.92 (m, 1H), 3.80 – 3.75 (m, 2H), 3.66 – .61 (m, 1H), 3.15 – 3.10 (m, 2H), 2.91 – 2.86 (m, 2H), 2.42 – 2.23 (m, 3H), 2.09 – 1.92 (m, 3H), 1.89 – 1.74 (m, 3H), 1.72 – 1.48 (m, 3H), 1.10 (s, 9H). ESI−MS calculated for $C_{50}H_{51}F_2N_6O_{10}PS_2^+$ 1029.08, found $[M + H]^+$ 1030.00.

((2-(((2S)-1-((2S)-2-(benzo[d]thiazol-6-yl(3-((5-(2-(2,6-dioxopiperidin-3-yl)-1-oxoisoindolin-4-yl)pent-4-yn-1-yl)amino)-3-oxopropyl)carbamoyl)pyrrolidin-1-yl)-3,3-dimethyl-1-oxobutan-2-yl)carbamoyl)benzo[b]thiophen-5-yl)difluoromethyl)phosphonic acid (AK2217). AK2217 was synthesized by employing a similar procedure for **AK-2292**. ^{1}H NMR (400 MHz, DMSO) δ 10.97 (s, 1H), 8.50 (s, 1H), 8.17 – 7.91 (m, 5H), 7.70 – 7.39 (m, 7H), 5.13 (dd, *J* = 13.3, 5.3 Hz, 1H), 4.75 (d, *J* = 9.0 Hz, 1H), 4.45 (dd, *J* = 17.7, 5.8 Hz, 2H), 4.35 – 4.25 (m, 2H), 4.16 – 4.12 (m, 2H), 3.94 – 3.90 (m, 2H), 3.14 – 3.10 (m, 3H), 2.92 – 2.88 (m, 1H), 2.36 – 2.18 (m, 2H), 2.09 – 1.80 (m, 4H), 1.76 – 1.45 (m, 5H), 1.12 (s, 9H). ESI−MS calculated for $C_{49}H_{50}F_2N_7O_{10}PS_2^+$ 1030.07, found $[M + H]^+$ 1029.02.

((2-(((2S)-1-((2S)-2-(benzofuran-5-yl(3-((5-(2-(2,6-dioxopiperidin-3-yl)-1-oxoisoindolin-4-yl)pent-4-yn-1-yl)amino)-3-oxopropyl)carbamoyl)pyrrolidin-1-yl)-3,3-dimethyl-1-oxobutan-2-yl)carbamoyl)benzo[b]thiophen-5-yl)difluoromethyl)phosphonic acid (AK2216). AK2216 was synthesized by employing a similar procedure for **AK-2292**. ^{1}H NMR (400 MHz, DMSO) δ 10.97 (s, 1H), 8.52 (s, 1H), 8.37 (d, *J* = 9.0 Hz, 1H), 8.14 – 8.07 (m, 1H), 8.03 (d, *J* = 1.8 Hz, 2H), 7.98 – 7.91 (m, 1H), 7.73 – 7.42 (m, 7H), 7.32 (d, *J* = 8.6 Hz, 1H), 5.13 (dd, *J* = 13.1, 5.4 Hz, 1H), 4.74 (d, *J* = 9.0 Hz, 1H), 4.45 (d, *J* = 17.6 Hz, 1H), 4.30 (d, *J* = 17.8 Hz, 1H), 4.13 – 4.09 (m, 1H), 3.91 – 3.86 (m, 1H), 3.77 – 3.70 (m, 2H), 3.65 – 3.60 (m, 1H), 3.16 – 3.11 (m, 2H), 2.93 – 2.88 (m, 1H), 2.38 – 2.22 (m, 3H), 2.01 – 1.96 (m, 3H), 1.85 –

1.49 (m, 6H), 1.10 (s, 9H). ESI−MS calculated for $C_{50}H_{51}F_2N_6O_{11}PS^+$ 1013.02, found $[M + H]^+$ 1013.03.

((2-(((2S)-1-((2S)-2-((3-((5-(2-(2,6-dioxopiperidin-3-yl)-1-oxoisoindolin-4-yl)pent-4-yn-1-yl)amino)-3-oxopropyl)(naphthalen-2-yl)carbamoyl)pyrrolidin-1-yl)-3,3-dimethyl-1-oxobutan-2-yl)carbamoyl)benzo[b]thiophen-5-yl)difluoromethyl)phosphonic acid (AK2147). AK2147 was synthesized by employing a similar procedure for **AK-2292**. ^{1}H NMR (400 MHz, DMSO) δ 10.97 (s, 1H), 8.51 (s, 1H), 8.38 (d, *J* = 9.0 Hz, 1H), 8.10 (dd, *J* = 9.2, 5.2 Hz, 1H), 8.03 (s, 1H), 8.00 – 7.85 (m, 5H), 7.72 – 7.65 (m, 1H), 7.63 – 7.48 (m, 6H), 5.12 (dd, *J* = 13.3, 5.3 Hz, 1H), 4.74 (d, *J* = 9.0 Hz, 1H), 4.44 (dd, *J* = 17.9, 4.1 Hz, 2H), 4.29 (d, *J* = 17.8 Hz, 1H), 4.17 – 4.12 (m, 1H), 3.99 – 3.92 (m, 1H), 3.76 – 3.70 (m, 3H), 3.66 – 3.60 (m, 1H), 2.92 – 2.87 (m, 2H), 2.40 – 2.17 (m, 3H), 2.03 – 1.76 (m, 5H), 1.76 – 1.54 (m, 4H), 1.10 (s, 9H). ESI−MS calculated for $C_{52}H_{53}F_2N_6O_{10}PS^+$ 1023.06, found $[M + H]^+$ 1023.00.

((2-(((2S)-1-((2S)-2-(chroman-6-yl(3-((5-(2-(2,6-dioxopiperidin-3-yl)-1-oxoisoindolin-4-yl)pent-4-yn-1-yl)amino)-3-oxopropyl)carbamoyl)pyrrolidin-1-yl)-3,3-dimethyl-1-oxobutan-2-yl)carbamoyl)benzo[b]thiophen-5-yl)difluoromethyl)phosphonic acid (AK2224). AK2224 was synthesized by employing a similar procedure for **AK-2292**. ^{1}H NMR (400 MHz, DMSO) δ 10.97 (s, 1H), 8.53 (s, 1H), 8.38 (d, *J* = 8.9 Hz, 1H), 8.12 (d, *J* = 8.7 Hz, 2H), 8.04 (s, 1H), 7.96 (d, *J* = 2.2 Hz, 1H), 7.81 – 7.39 (m, 6H), 5.14 (dd, *J* = 13.1, 5.4 Hz, 1H), 4.74 (d, *J* = 8.9 Hz, 1H), 4.51 – 4.41 (m, 2H), 4.31 (d, *J* = 17.9 Hz, 1H), 4.18 – 4.05 (m, 4H), 3.79 – 3.74 (m, 1H), 3.65 – 3.60 (m, 1H), 3.21 – 3.09 (m, 2H), 2.75 – 2.67 (m, 2H), 2.39 – 2.18 (m, 4H), 2.07 – 1.49 (m, 12H), 1.08 (s, 9H). ESI−MS calculated for $C_{51}H_{55}F_2N_6O_{11}PS^+$ 1029.06, found $[M + H]^+$ 1029.11.

((2-(((2S)-1-((2S)-2-((3-((5-(2-(2,6-dioxopiperidin-3-yl)-1-oxoisoindolin-4-yl)pent-4-yn-1-yl)(methyl)amino)-3-oxopropyl)(4-(thiazol-2-yl)phenyl)carbamoyl)pyrrolidin-1-yl)-1-oxo-4-phenylbutan-2-yl)carbamoyl)benzo[b]thiophen-5-yl)difluoromethyl)phosphonic acid (AK2435). AK2435 was synthesized by employing a similar procedure for **AK-2292**. ^{1}H NMR (400 MHz, DMSO) δ 10.98 (d, *J* = 5.4 Hz, 1H), 9.02 (d, *J* = 7.7 Hz, 1H), 8.35 (d, *J* = 3.6 Hz, 1H), 8.19 – 7.85 (m, 6H), 7.81 – 7.78 (m, 1H), 7.71 – 7.39 (m, 7H), 7.37 – 7.22 (m, 4H), 5.13 (dd, *J* = 11.2, 6.7 Hz, 1H), 4.67 – 4.63 (m, 1H), 4.53 – 4.39 (m, 1H), 4.33 – 4.28 (m, 1H), 4.21 – 4.18 (m, 1H), 4.03 – 3.64 (m, 3H), 3.62 – 3.58 (m, 1H), 3.47 – 3.33 (m, 3H), 2.95 – 2.90 (m, 3H), 2.78 (s, 3H), 2.44 – 2.40 (m, 2H), 2.12 – 1.88 (m, 5H), 1.87 – 1.51 (m, 6H). ESI−MS calculated for $C_{56}H_{54}F_2N_7O_{10}PS_2^+$ 1118.18, found $[M + H]^+$ 1118.29.

((2-(((2S)-1-((2S)-2-(benzo[d]thiazol-5-yl(3-((5-(2-(2,6-dioxopiperidin-3-yl)-1-oxoisoindolin-4-yl)pent-4-yn-1-yl)amino)-3-oxopropyl)carbamoyl)pyrrolidin-1-yl)-3,3-dimethyl-1-oxobutan-2-yl)carbamoyl)benzo[b]thiophen-5-yl)difluoromethyl)phosphonic acid (AK2223). AK2223 was synthesized by employing a similar procedure for **AK-2292**. ^{1}H NMR (400 MHz, DMSO) δ 10.97 (s, 1H), 9.43 (d, *J* = 2.4 Hz, 1H), 8.52 (d, *J* = 2.4 Hz, 1H), 8.41 (m, 1H), 8.23 (d, *J* = 8.4 Hz, 1H), 8.15 – 7.93 (m, 4H), 7.78 – 7.41 (m, 6H), 5.19 – 5.06 (m, 1H), 4.75 (m, 1H), 4.45 (m, 2H), 4.30 (m, 2H), 4.20 – 4.10 (m, 2H), 3.20 – 3.10 (m, 3H), 2.95 – 2.85 (s, 3H), 2.00 – 1.90 (m, 3H), 1.85 – 1.60 (m, 7H), 1.10 (s, 9H). ESI−MS calculated for $C_{49}H_{50}F_2N_7O_{10}PS_2^+$ 1030.07, found $[M + H]^+$ 1030.07.

((2-(((2S)-1-((2S)-2-(benzo[d]thiazol-5-yl(3-((5-(2-(2,6-dioxopiperidin-3-yl)-1-oxoisoindolin-4-yl)pent-4-yn-1-yl)(methyl)amino)-3-oxopropyl)carbamoyl)pyrrolidin-1-yl)-3,3-dimethyl-1-oxobutan-2-yl)carbamoyl)benzo[b]thiophen-5-yl)difluoromethyl)phosphonic acid (AK2437). AK2437 was synthesized by employing a

similar procedure for **AK-2292**. ^{1}H NMR (400 MHz, DMSO) δ 10.98 (s, 1H), 9.43 (s, 1H), 8.53 (m, 1H), 8.44 (d, *J* = 8.3 Hz, 1H), 8.25 – 8.16 (m, 2H), 8.11 (d, *J* = 8.6 Hz, 1H), 8.03 (s, 1H), 7.75 – 7.65 (m, 2H), 7.58 – 7.49 (m, 3H), 5.18 – 5.05 (m, 1H), 4.75 (m, 1H), 4.53 – 4.43 (m, 1H), 4.36 – 4.29 (m, 1H), 4.13 (m, 1H), 3.85 (m, 2H), 3.78 – 3.72 (m, 1H), 3.65 (d, *J* = 8.1 Hz, 1H), 3.47 – 3.32 (m, 3H), 3.03 – 2.91 (m, 3H), 2.80 – 2.61 (m, 4H), 1.22 – 1.95 (d, *J* = 5.4 Hz, 3H), 1.87 – 1.60 (m, 6H), 1.10 (s, 9H). ESI−MS calculated for $C_{50}H_{52}F_2N_7O_{10}PS_2^+$ 1044.10, found $[M + H]^+$ 1044.32.

((2-(((2S)-1-((2S)-2-(benzofuran-5-yl(3-((5-(2-(2,6-dioxopiperidin-3-yl)-1-oxoisoindolin-4-yl)pent-4-yn-1-yl)(methyl)amino)-3-oxopropyl)carbamoyl)pyrrolidin-1-yl)-3,3-dimethyl-1-oxobutan-2-yl)carbamoyl)benzo[b]thiophen-5-yl)difluoromethyl)phosphonic acid (AK2436). AK2436 was synthesized by employing a similar procedure for **AK-2292**. ^{1}H NMR (400 MHz, DMSO) δ 10.98 (d, *J* = 4.5 Hz, 1H), 8.52 (d, *J* = 5.0 Hz, 1H), 8.45 – 8.34 (m, 1H), 8.13 – 8.10 (m, 1H), 8.05 – 8.02 (m, 1H), 7.71 – 7.47 (m, 7H), 6.99 – 6.93 (m, 1H), 5.18 – 5.10 (m, 1H), 4.74 (d, *J* = 8.9 Hz, 1H), 4.53 – 4.42 (m, 1H), 4.38 – 4.27 (m, 1H), 4.13 – 4.09 (m, 1H), 3.79 – 3.75 (m, 2H), 3.65 – 3.60 (m, 1H), 3.47 – 3.34 (m, 3H), 2.97 (s, 3H), 2.65 – 2.55 (m, 3H), 2.46 – 2.40 (m, 2H), 2.00 – 1.95 (m, 3H), 1.83 – 1.79 (m, 2H), 1.75 – 1.65 (m, 3H), 1.10 (s, 9H). ESI−MS calculated for $C_{51}H_{53}F_2N_6O_{11}PS^+$ 1027.05, found $[M + H]^+$ 1027.33.

((2-(((2S)-1-((2S)-2-((3-((5-(2-(2,6-dioxopiperidin-3-yl)-1-oxoisoindolin-4-yl)pent-4-yn-1-yl)(methyl)amino)-3-oxopropyl)(naphthalen-2-yl)carbamoyl)pyrrolidin-1-yl)-3,3-dimethyl-1-oxobutan-2-yl)carbamoyl)benzo[b]thiophen-5-yl)difluoromethyl)phosphonic acid (AK2291). AK2291 was synthesized by employing a similar procedure for **AK-2292**. ^{1}H NMR (400 MHz, DMSO) δ 10.98 (s, 1H), 8.52 (d, *J* = 5.0 Hz, 1H), 8.42 (d, *J* = 8.5 Hz, 1H),

8.10 (d, *J* = 8.4 Hz, 1H), 8.03 (s, 1H), 8.00 – 7.84 (m, 4H), 7.72 – 7.66 (m, 1H), 7.64 – 7.46 (m, 7H), 5.19 – 5.08 (m, 1H), 4.77 – 4.72 (m, 1H), 4.50 – 4.41 (m, 1H), 4.34 – 4.30 (m, 1H), 4.16 – 4.10 (m, 1H), 3.98 – 3.72 (m, 4H), 3.66 – 3.62 (m, 1H), 3.48 – 3.32 (m, 3H), 2.97 (s, 3H), 2.43 – 2.38 (m, 2H), 2.07 – 1.50 (m, 10H), 1.10 (s, 9H). ESI−MS calculated for $C_{53}H_{55}F_2N_6O_{10}PS^+$ 1037.09, found $[M + H]^+$ 1037.40.

((2-(((2S)-1-((2S)-2-(benzo[b]thiophen-5-yl(3-((5-(2-(2,6-dioxopiperidin-3-yl)-1-oxoisoindolin-4-yl)pent-4-yn-1-yl)(methyl)amino)-3-oxopropyl)carbamoyl)pyrrolidin-1-yl)-3,3-dimethyl-1-oxobutan-2-yl)carbamoyl)benzo[b]thiophen-5-yl)difluoromethyl)phosphonic acid (AK-2438). AK-2438 was synthesized by employing a similar procedure for **AK-2292**. ^{1}H NMR (400 MHz, DMSO) δ 10.98 (s, 1H), 8.52 (d, *J* = 5.0 Hz, 1H), 8.41 (d, *J* = 8.4 Hz, 1H), 8.11 (d, *J* = 8.6 Hz, 1H), 8.09 – 8.00 (m, 2H), 7.93 – 7.90 (m, 1H), 7.82 (dd, *J* = 5.4, 1.4 Hz, 2H), 7.70 (dd, *J* = 7.7, 3.1 Hz, 1H), 7.63 – 7.55 (m, 2H), 7.53 – 7.48 (m, 1H), 7.45 – 7.40 (m, 2H), 5.20 – 5.10 (m, 1H), 4.78 – 4.72 (m, 1H), 4.52 – 4.45 (m, 2H), 4.37 – 4.28 (m, 1H), 4.17 – 4.07 (m, 1H), 3.85 – 3.82 (m, 1H), 3.78 – 3.71 (m, 2H), 3.68 – 3.61 (m, 1H), 3.44 – 3.33 (m, 2H), 3.04 – 2.85 (m, 4H), 2.42 – 2.12 (m, 3H), 2.00 – 1.92 (m, 3H), 1.86 – 1.77 (m, 2H), 1.78 – 1.68 (m, 4H), 1.10 (s, 9H). ESI−MS calculated for $C_{51}H_{53}F_2N_6O_{10}PS_2^+$ 1043.11, found $[M + H]^+$ 1043.32.

((2-(((2S)-1-((2S,4R)-2-((4-bromophenyl)(methyl)carbamoyl)-4-(2-((5-(2-(2,6-dioxopiperidin-3-yl)-1-oxoisoindolin-4-yl)pent-4-yn-1-yl)amino)-2-oxoethoxy)pyrrolidin-1-yl)-3,3-dimethyl-1-oxobutan-2-yl)carbamoyl)benzo[b]thiophen-5-yl)difluoromethyl)phosphonic acid (AK2019026). AK2019009 (285 mg, 0.33 mmol) was dissolved in MeOH (5 ml) and water (1 ml) and the mixture was placed in an ice bath. LiOH monohydrate (90 mg, 6 equiv.) was added to the mixture and then it was stirred for 3 hours at

room temperature. The mixture was placed in an ice bath again and neutralized by slowly adding TFA. The volatile components were removed on a rotary evaporator and the residue was purified by flash column chromatography to yield **AK2019014-COOH** in 70% (182 mg). ^{1}H NMR (400 MHz, DMSO) δ 8.51 (s, 1H), 8.37 (d, *J* = 8.8 Hz, 1H), 8.13 (d, *J* = 8.6 Hz, 1H), 8.06 (s, 1H), 7.75 – 7.55 (m, 3H), 7.36 (d, *J* = 8.2 Hz, 2H), 4.70 (d, *J* = 8.8 Hz, 1H), 4.34 – 3.84 (m, 7H), 3.40 (t, *J* = 9.1 Hz, 1H), 3.12 (s3H), 2.32 – 2.25 (m, 1H), 1.70 – 1.65 (m, 1H), 1.18 (t, *J* = 7.1 Hz, 3H), 1.09 (s, 9H). ESI−MS calculated for $C_{32}H_{37}BrF_2N_3O_9PS^+$ 1087.16, found $[M + H]^+$ 1084.08.

To **AK2019014-COOH** (10 mg, 0.012 mmol), CH_3CN (2 ml), DIPEA (10 µl, 5 equiv.), amine (6 mg, 1.2 equiv.), and HATU (5 mg, 1.1 equiv.) were added. The mixture was stirred at room temperature for 30 min. The yellow solution was concentrated in vacuum and the crude was purified by HPLC to yield **17** in 80% (11 mg). To a round bottom flask were added **17** (11 mg, 0.01 mmol, 1 equiv.), DCM (2 ml) and $CF_3CON(TMS)_2$ (15 µl, 6 equiv.). The solution was cooled in an ice bath. To the ice cooled reaction mixture, 1M of TMS-I in DCM (50 µl, 5 equiv.) was added dropwise and the mixture was stirred for 10 min in an ice bath. The volatile components were removed under vacuum at below 5°C. The residue was dissolved in a mixed solvent of CH_3CN (3 ml) and water (1 ml). The resulting solution was purified by HPLC to yield **AK2019026** in 85% (9 mg). ^{1}H NMR (400 MHz, DMSO) δ 10.98 (s, 1H), 8.48 (s, 1H), 8.31 (d, *J* = 8.7 Hz, 1H), 8.08 (s, 1H), 8.02 – 7.97 (m, 2H), 7.75 – 7.56 (m, 5H), 7.54 – 7.50 (m, 1H), 7.37 (s, 1H), 5.16 – 5.12 (m, 1H), 4.71 (d, *J* = 8.7 Hz, 1H), 4.50 – 4.43 (m, 1H), 4.35 – 4.30 (m, 2H), 4.13 – 4.08 (m, 1H), 3.91 (s, 3H), 2.99 – 2.87 (m, 2H), 2.35 – 2.30 (m, 1H), 2.27 – 2.09 (m, 2H), 2.08 – 1.93 (m, 2H), 1.80 – 1.76 (m, 3H), 1.08 (s, 9H). ESI−MS calculated for $C_{48}H_{50}BrF_2N_6O_{11}PS^+$ 1067.89, found $[M + H]^+$ 1067.12, 1069.13.

((2-(((2S)-1-((2S,4R)-2-((4-bromophenyl)(methyl)carbamoyl)-4-(2-((7-(2-(2,6-dioxopiperidin-3-yl)-1-oxoisoindolin-4-yl)hept-6-yn-1-yl)amino)-2-oxoethoxy)pyrrolidin-1-yl)-3,3-dimethyl-1-oxobutan-2-yl)carbamoyl)benzo[b]thiophen-5-yl)difluoromethyl)phosphonic acid (AK2019027). AK2019027 was synthesized by employing a similar procedure for **AK2019026**. ^{1}H NMR (400 MHz, DMSO) δ 10.98 (s, 1H), 8.48 (s, 1H), 8.31 (d, *J* = 8.8 Hz, 1H), 8.06 – 7.94 (m, 3H), 7.73 – 7.60 (m, 5H), 7.53 (d, *J* = 7.6 Hz, 1H), 7.37 (s, 1H), 5.16 – 5.11 (m, 1H), 4.71 (d, *J* = 8.9 Hz, 1H), 4.45 (d, *J* = 17.8 Hz, 2H), 4.34 (s, 2H), 4.10 (s, 2H), 3.92 (s, 3H), 3.75 – 3.70 (m, 2H), 3.18 – 3.12 (m, 3H), 2.97 – 2.84 (m, 3H), 2.35 – 2.30 (m, 1H), 2.21 – 1.96 (m, 4H), 1.65 – 1.43 (m, 6H), 1.08 (s, 9H). ESI−MS calculated for $C_{50}H_{54}BrF_2N_6O_{11}PS^+$ 1095.95, found $[M + H]^+$ 1095.20, 1096.85.

((2-(((2S)-1-((2S,4R)-2-((4-bromophenyl)(methyl)carbamoyl)-4-(2-((8-(2-(2,6-dioxopiperidin-3-yl)-1-oxoisoindolin-4-yl)oct-7-yn-1-yl)amino)-2-oxoethoxy)pyrrolidin-1-yl)-3,3-dimethyl-1-oxobutan-2-yl)carbamoyl)benzo[b]thiophen-5-yl)difluoromethyl)phosphonic acid (AK2019028). AK2019028 was synthesized by employing a similar procedure for **AK2019026**. ^{1}H NMR (400 MHz, DMSO) δ 10.99 (s, 1H), 8.48 (s, 1H), 8.31 (d, *J* = 8.5 Hz, 1H), 8.00 (d, *J* = 18.0 Hz, 3H), 7.75 – 7.56 (m, 5H), 7.54 – 7.49 (m, 1H), 7.37 (d, *J* = 8.4 Hz, 1H), 5.13 (dd, *J* = 13.3, 5.1 Hz, 1H), 4.70 (d, *J* = 8.7 Hz, 1H), 4.47 – 4.43 (m, 2H), 4.33 – 4.29 (m, 2H), 4.12 – 4.08 (m, 1H), 3.89 (s, 3H), 3.75 – 3.71 (m, 2H), 3.17 – 3.13 (m, 3H), 3.08 – 3.02 (m, 1H), 2.97 – 2.85 (m, 2H), 2.17 – 2.12 (m, 2H), 2.08 – 1.97 (m, 2H), 1.86 – 1.80 (m, 2H), 1.63 – 1.33 (m, 8H), 1.08 (s, 9H). ESI−MS calculated for $C_{51}H_{56}BrF_2N_6O_{11}PS^+$ 1109.97, found $[M + H]^+$ 1110.56, 1111.47.

((2-(((2S)-1-((2S,4R)-2-((4-bromophenyl)(methyl)carbamoyl)-4-(2-((10-(2-(2,6-dioxopiperidin-3-yl)-1-oxoisoindolin-4-yl)dec-9-yn-1-yl)amino)-2-oxoethoxy)pyrrolidin-1-

yl)-3,3-dimethyl-1-oxobutan-2-yl)carbamoyl)benzo[b]thiophen-5-yl)difluoromethyl)phosphonic acid (AK2019029). AK2019029 was synthesized by employing a similar procedure for **AK2019026**. ^{1}H NMR (400 MHz, DMSO) δ 10.99 (s, 1H), 8.48 (s, 1H), 8.32 (d, *J* = 8.8 Hz, 1H), 8.08 – 7.93 (m, 3H), 7.75 – 7.58 (m, 5H), 7.53 – 7.78 (m, 1H), 7.40 – 7.36 (m, 1H), 5.14 (dd, *J* = 13.3, 5.1 Hz, 1H), 4.71 (d, *J* = 8.7 Hz, 1H), 4.44 (d, *J* = 17.6 Hz, 1H), 4.30 (d, *J* = 17.6 Hz, 2H), 4.12 – 4.05 (m, 2H), 3.91 (s, 3H), 3.75 – 3.70 (m, *J* = 12.4 Hz, 1H), 3.16 (s, 3H), 3.06 – 3.00 (m, 1H), 2.96 – 2.87 (m, 2H), 2.15 – 2.08 (m, 2H), 2.07 – 1.97 (m, 2H), 1.890 – 1.85(m, 2H), 1.60 – 1.55 (m, 3H), 1.45 – 1.40 (m, 4H), 1.35 – 1.25 (m, 5H), 1.08 (s, 9H). ESI−MS calculated for $C_{53}H_{60}BrF_2N_6O_{11}PS^+$ 1138.03, found $[M + H]^+$ 1138.97.

((2-(((2S)-1-((2S,4R)-2-((4-bromophenyl)(methyl)carbamoyl)-4-(2-((11-(2-(2,6-dioxopiperidin-3-yl)-1-oxoisoindolin-4-yl)undec-10-yn-1-yl)amino)-2-oxoethoxy)pyrrolidin-1-yl)-3,3-dimethyl-1-oxobutan-2-yl)carbamoyl)benzo[b]thiophen-5-yl)difluoromethyl)phosphonic acid (AK2019030). AK2019030 was synthesized by employing a similar procedure for **AK2019026**. ^{1}H NMR (400 MHz, DMSO) δ 10.99 (s, 1H), 8.49 (s, 1H), 8.32 (d, *J* = 8.9 Hz, 1H), 8.10 – 7.85 (m, 3H), 7.75 – 7.54 (m, 5H), 7.54 – 7.48 (m, 1H), 7.37 (d, *J* = 7.8 Hz, 1H), 5.14 (dd, *J* = 13.3, 5.1 Hz, 1H), 4.70 (d, *J* = 8.7 Hz, 1H), 4.44 (d, *J* = 17.7 Hz, 1H), 4.32 – 4.28 (m, 2H), 4.12 – 4.08 (m, 2H), 3.89 (s, 3H), 3.76 – 3.70 (m, 1H), 3.18 – 3.12 (m, 4H), 2.98 – 2.84 (m, 2H), 2.15 – 2.10 (m, 2H), 2.08 – 1.97 (m, 2H), 1.90 – 1.86 (m, 2H), 1.60 – 1.53 (m, 3H), 1.45 – 1.40 (m, 4H), 1.30 – 1.20 (m, 7H), 1.08 (s, 9H). ESI−MS calculated for $C_{54}H_{64}BrF_2N_6O_{11}PS^+$ 1152.06, found $[M + H]^+$ 1153.17.

((2-(((2S)-1-((2S)-2-((9-(2-(2,6-dioxopiperidin-3-yl)-1-oxoisoindolin-4-yl)non-8-yn-1-yl)(4-(thiazol-2-yl)phenyl)carbamoyl)pyrrolidin-1-yl)-3,3-dimethyl-1-oxobutan-2-yl)carbamoyl)benzo[b]thiophen-5-yl)difluoromethyl)phosphonic acid (AK2238). To **17** (1 g,

7.13 mmol) in DCM (20 ml), Dess-martin periodinane (3 g, 1 equiv.) was added. The mixture was stirred at room temperature for 30 min. White precipitates were formed. Celite was added to the reaction mixture and the mixture was concentrated in vacuum. Then, after the purification by flash column chromatography, **AK-20202225** was obtained as colorless oil in 70% yield (700 mg). ^{1}H NMR (400 MHz, DMSO) δ 9.66 (s, 1H), 2.76 – 2.69 (m, 1H), 2.24 – 2.05 (m, 4H), 1.52 – 1.21 (m, 8H). ESI−MS calculated for $C_9H_{14}O^+$ 138.21, found $[M + H]^+$ 139.31.

To **AK-20202225** (200 mg, 1.4 mmol) in DCM (5 ml), 4-(thiazol-2-yl)aniline (1 equiv.), NaB(OAc)3 (2 equiv.), and AcOH (1 equiv.) were added and the mixture was stirred for 30 minutes at room temperature. Water and ethanol were added to the mixture and the mixture was concentrated in vacuum. The purification by HPLC gave **AK-20202232** in 92% (400 mg). ^{1}H NMR (400 MHz, DMSO) δ 7.75 (d, *J* = 3.3 Hz, 1H), 7.70 – 7.61 (m, 2H), 7.53 (d, *J* = 3.3 Hz, 1H), 6.64 (d, *J* = 8.8 Hz, 2H), 3.06 (t, *J* = 7.0 Hz, 2H), 2.73 (t, *J* = 2.7 Hz, 1H), 2.15 (td, *J* = 6.9, 2.7 Hz, 2H), 1.55 (t, *J* = 6.9 Hz, 2H), 1.48 – 1.10 (m, 8H). ESI−MS calculated for $C_{18}H_{22}N_2S^+$ 298.45, found $[M + H]^+$ 299.01.

Boc-L-proline (1.8 g, 5 equiv.) was dissolved in $CHCl_3$ (20 ml). At room temperature, PCl_5 (1.7 g, 5 equiv.) was slowly added over a period of 10 min. After the addition, the mixture was stirred for 10 min at room temperature. To this mixture was added **AK-20202232** (400 mg, 1.3 mmol) and the mixture was stirred at 50°C for 20 min. The volatile components were removed on a rotary evaporator. The obtained crude oil was purified by reverse phase semi-preparative HPLC to give **AK-20202233** as TFA salt in 60% (420 mg). ^{1}H NMR (400 MHz, DMSO) δ 8.10 (d, *J* = 8.5 Hz, 2H), 7.99 (d, *J* = 3.2 Hz, 1H), 7.87 (d, *J* = 3.2 Hz, 1H), 7.53 (d, *J* = 8.5 Hz, 2H), 4.06 (t, *J* = 7.6 Hz, 1H), 3.86 – 3.80 (m, 1H), 3.66 – 3.58 (m, 1H), 3.23 – 3.18 (m, 2H), 3.13 – 3.02 (m, 1H), 2.15 – 2.07 (m, 2H), 1.98 – 1.93 (m, 1H), 1.87 – 1.61 (m, 4H), 1.57 –

1.37 (m, 4H), 1.35 – 1.20 (d, *J* = 18.1 Hz, 5H). ESI−MS calculated for $C_{23}H_{29}N_3OS^+$ 395.57, found $[M + H]^+$ 396.25.

AK-20202233 (420 mg, 0.82 mmol) was dissolved in CH_3CN (8 ml). To the solution was added triethylamine (350 µl, 3 equiv.), followed by Boc_2O (260 mg, 1.5 equiv.). The colorless mixture was stirred for 2 hours at room temperature. The volatile components were then removed by vacuum and the crude was purified by flash column chromatography to yield **AK-20202234** in 56% (230 mg). ^{1}H NMR (400 MHz, DMSO) δ 8.08 (d, *J* = 8.5 Hz, 2H), 7.98 – 7.94 (m, 1H), 7.86 – 7.82 (m, 1H), 7.41 (d, *J* = 8.5 Hz, 2H), 4.04 (dd, *J* = 7.3, 5.1 Hz, 1H), 3.86 – 3.72 (m, 1H), 3.72 – 3.62 (m, 1H), 3.61 – 3.46 (m, 1H), 3.38 – 3.34 (m, 1H), 2.71 – 2.69 (m, 1H), 2.14 – 2.10 (m, 2H), 1.91 – 1.71 (m, 3H), 1.66 – 1.62 (m, 1H), 1.45 – 1.39 (m, 13H), 1.30 – 1.08 (m, 6H).). ESI−MS calculated for $C_{28}H_{37}N_3O_3S^+$ 495.68, found $[M + H]^+$ 396.10.

Triethylamine (1.5 ml) was added to a mixture of **16** (323 mg, 1 mmol, 1 equiv.), **AK20202234** (230 mg, 0.46 mmol, 1 equiv.), CuI (35 mg, 0.4 equiv.), and $Pd(PPh_3)_2Cl_2$ (65 mg, 0.2 equiv.) in DMF (1.5 ml). The resulting mixture was purged and refilled with argon three times and stirred at 90°C for 1.5 hours under argon. The reaction mixture was cooled to room temperature. The mixture was filtered through celite and evaporated to remove most of the solvent. The residue was purified by HPLC to yield Boc-protected **AK-20202235**. The Boc-protected **AK-20202235** was dissolved in DCM (5 ml), and TFA (5 ml) was added to remove Boc protection. The mixture was stirred at room temperature for 10 min. Most of the volatile components were removed in vacuum and the residue was purified by HPLC to yield **AK-20202235** as TFA salt in 43% (150 mg). ^{1}H NMR (400 MHz, DMSO) δ 10.98 (s, 1H), 8.19 – 8.04 (m, 2H), 8.56 – 8.49 (m, 1H), 8.11 – 8.04 (m, 1H), 7.98 (d, *J* = 3.2 Hz, 1H), 7.87 (d, *J* = 3.2 Hz, 1H), 7.70 (d, *J* = 7.6 Hz, 1H), 7.61 (d, *J* = 7.6 Hz, 1H), 7.55 – 7.36 (m, 3H), 5.18 – 5.12 (m,

1H), 4.43 (d, *J* = 17.6 Hz, 1H), 4.29 (d, *J* = 17.7 Hz, 1H), 4.08 – 4.04 (m, 1H), 3.90 – 3.71 (m, 2H), 3.65 – 3.58 (m, 1H), 3.23 – 3.17 (m, 2H), 3.11 – 3.07 (m, 1H), 2.95 – 2.78 (m, 1H), 2.45 – 2.36 (m, 2H), 2.11 – 1.90 (m, 2H), 1.86 – 1.62 (m, 4H), 1.60 – 0.95 (m, 10H). ESI−MS calculated for $C_{36}H_{39}N_5O_4S^+$ 637.80, found $[M + H]^+$ 638.25.

To **AK-20202235** (75 mg, 0.1 mmol, 1 equiv.), CH_3CN (5 ml), triethylamine (70 µl, 5 equiv.), Boc-L-*tert*-leucine (45 mg, 2 equiv.), and HATU (80 mg, 2 equiv.) were added. The mixture was stirred at room temperature for 30 min. The yellow solution was concentrated in vacuum and the crude was purified by flash column chromatography to yield Boc-protected **AK-20202236**. Boc protection was removed by DCM/TFA at room temperature for 30 min. The volatile components were removed in vacuum to yield **AK-20202236** as a TFA salt in 57% (50 mg).

To **AK-20202236** (25 mg, 0.03 mmol), DMF (3 ml), triethylamine (70 µl), benzothiophene head IM-6 (13 mg, 1.2 equiv.), and HATU (15 mg, 1.2 equiv.) were added. The mixture was stirred at room temperature for 30 min. The yellow solution was purified by HPLC to yield **AK20212237** in 93% (30 mg)

To a round bottom flask were added **AK-20202237** (30 mg, 0.027 mmol, 1 equiv.), DCM (2 ml) and $CF_3CON(TMS)_2$ (45 µl, 6 equiv.). The solution was cooled in an ice bath. To the ice cooled reaction mixture, 1M of TMS-I in DCM (0.14 ml, 5 equiv.) was added dropwise and the mixture was stirred for 10 min in an ice bath. The volatile components were removed under vacuum at below 5°C. The residue was dissolved in a mixed solvent of CH_3CN (3 ml) and water (1 ml). The resulting solution was purified by HPLC to yield **AK-20212238** in 83% (23 mg). ^{1}H NMR (400 MHz, DMSO) δ 10.99 (s, 1H), 8.53 (s, 1H), 8.41 (d, *J* = 9.0 Hz, 1H), 8.11 (d, *J* = 8.5 Hz, 1H), 8.06 – 7.97 (m, 3H), 7.92 (d, *J* = 3.2 Hz, 1H), 7.79 (d, *J* = 3.2 Hz, 1H), 7.70 – 7.48 (m,

6H), 5.14 (m, 1H), 4.75 (m, 1H), 4.51 – 4.36 (m, 2H), 4.30 (m, 1H), 4.20 (m, 1H), 3.94 – 3.72 (m, 2H), 3.64 (m, 1H), 3.48 (m, 1H), 2.90 (m, 1H), 2.59 (m, 1H), 2.26 (m, 1H), 2.09 – 1.92 (m, 2H), 1.86 (m, 1H), 1.81 – 1.64 (m, 2H), 1.70 – 1.50 (m, 2H), 1.40 – 1.25 (m, 8H), 1.08 (s, 9H). ESI−MS calculated for $C_{52}H_{55}F_2N_6O_9PS_2^+$ 1041.14, found $[M + H]^+$ 1041.33.

((2-(((S)-1-((S)-2-((4-bromophenyl)(3-((8-(3-(3',6'-dihydroxy-3-oxo-3H-spiro[isobenzofuran-1,9'-xanthen]-5-yl)thioureido)octyl)amino)-3-oxopropyl)carbamoyl)pyrrolidin-1-yl)-3,3-dimethyl-1-oxobutan-2-yl)carbamoyl)benzo[b]thiophen-5-yl)difluoromethyl)phosphonic acid (AK2018330). To a round bottom flask were added **20** (520 mg, 2.9 mmol, 1 equiv.), CH_3CN (5 ml) and NBS (520 mg, 1 equiv.). The solution was stirred at room temperature for 10 min. The volatile components were removed under vacuum. To the residue were added water and ethylacetate and normal workup was performed. After the volatile components were removed under vacuum, **AK2018259** was obtained as white solid in 80% (598 mg). ^{1}H NMR (400 MHz, DMSO) δ 7.19 (d, *J* = 8.8 Hz, 2H), 6.52 (d, *J* = 8.9 Hz, 2H), 5.86 (t, *J* = 5.8 Hz, 1H), 3.60 (s, 3H), 3.28 – 3.23 (m, 2H), 2.56 (t, *J* = 6.7 Hz, 2H). ESI−MS calculated for $C_{10}H_{12}BrNO_2^+$ 258.12, found $[M + H]^+$ 258.21, 260.12.

Boc-L-proline (1.6 g, 5 equiv.) was dissolved in $CHCl_3$ (10 ml). At room temperature, PCl_5 (1.5 g, 5 equiv.) was slowly added over a period of 10 min. After the addition, the mixture was stirred for 10 min at room temperature. To this mixture was added **AK2018259** (390 mg, 1.5 mmol) and the mixture was stirred at 50°C for 20 min. The volatile components were removed on a rotary evaporator. The obtained crude oil was purified by HPLC to yield **AK2018260** as TFA salt in 60% (420 mg). ^{1}H NMR (400 MHz, DMSO) δ 7.81 – 7.68 (m, 2H), 7.41 – 7.35 (m, 2H), 4.02 – 3.78 (m, 3H), 3.53 (s, 3H), 3.22 – 3.13 (m, 1H), 3.08 – 3.02 (m, 1H), 2.56 – 2.53 (m, 1H), 2.45 –

2.40 (m, 1H), 1.80 – 1.70 (m, 5H). ESI−MS calculated for $C_{15}H_{19}BrN_2O_3^+$ 355.23, found $[M + H]^+$ 355.17, 357.17.

To **AK2018260** TFA salt (230 mg, 0.49 mmol), CH_3CN (5 ml), triethylamine (0.45 ml, 5 equiv.), Boc-L-*tert*-leucine (170 mg, 1.5 equiv.), and HATU (230 mg, 1.2 equiv.) were added. The mixture was stirred at room temperature for 30 min. The yellow solution was concentrated in vacuum and the crude was purified by flash column chromatography to yield Boc-protected **AK2018268**. Boc protection was removed by DCM/TFA at room temperature for 30 min. The volatile components were removed in vacuum to yield **AK2018268** as a TFA salt in 85% (240 mg). ^{1}H NMR (400 MHz, DMSO) δ 7.98 (s, 2H), 7.80 – 7.59 (m, 2H), 7.48 – 7.26 (m, 2H), 4.09 – 4.03 (m, 1H), 4.00 – 3.88 (m, 1H), 3.80 – 3.60 (m, 5H), 3.57 – 3.37 (m, 2H), 2.45 – 2.40 (m, 2H), 2.02 – 1.47 (m, 4H), 1.05 (s, 9H). ESI−MS calculated for $C_{21}H_{30}BrN_3O_4^+$ 468.39, found $[M + H]^+$ 468.32, 470.31.

To **AK2018268** TFA salt (110 mg, 0.19 mmol), CH_3CN (5 ml), triethylamine (0.13 ml, 5 equiv.), IM-6 (70 mg, 1.1 equiv.), and HATU (75 mg, 1.1 equiv.) were added. The mixture was stirred at room temperature for 30 min. The yellow solution was concentrated in vacuum and the crude was purified by flash column chromatography to yield **AK2018272** in 75% (116 mg). ^{1}H NMR (400 MHz, DMSO) δ 8.54 (s, 1H), 8.47 (dd, *J* = 9.0, 2.1 Hz, 1H), 8.19 (d, *J* = 8.5 Hz, 1H), 8.10 (s, 1H), 7.75 – 7.57 (m, 3H), 7.37 (dd, *J* = 8.6, 2.2 Hz, 2H), 4.75 (d, *J* = 8.9 Hz, 1H), 4.29 – 4.06 (m, 6H), 3.91 – 3.71 (m, 3H), 3.66 – 3.62 (m, 1H), 3.52 (s,32H), 2.46 – 2.33 (m, 1H), 2.00 – 1.95 (m, 1H), 1.91 – 1.62 (m, 3H), 1.25 – 1.20 (m, 6H), 1.08 (s, 9H). ESI−MS calculated for $C_{35}H_{43}BrF_2N_3O_8PS^+$ 814.68, found $[M + H]^+$ 814.19, 816.16.

AK2018272 (150 mg, 0.18 mmol) was dissolved in MeOH (5 ml) and water (1 ml) and the mixture was placed in an ice bath. LiOH monohydrate (60 mg, 8 equiv.) was added to the

mixture and then it was stirred for 1 h at room temperature. The mixture was placed in an ice bath again and neutralized by slowly adding TFA. The volatile components were removed on a rotary evaporator and the residue was purified by flash column chromatography to yield **AK2018279** in 70% (100 mg). ^{1}H NMR (400 MHz, DMSO) δ 8.52 (s, 1H), 8.42 (d, *J* = 8.9 Hz, 1H), 8.12 (d, *J* = 8.5 Hz, 1H), 8.05 (s, 1H), 7.76 – 7.55 (m, 3H), 7.44 – 7.30 (m, 2H), 4.75 (d, *J* = 9.0 Hz, 1H), 4.09 (t, *J* = 7.1 Hz, 1H), 4.02 – 3.97 (m, 2H), 3.78 (t, *J* = 7.4 Hz, 3H), 3.66 – 3.62 (m, 1H), 2.46 – 2.35 (m, 2H), 1.99 – 1.95 (m, 1H), 1.89 – 1.67 (m, 3H), 1.18 (t, *J* = 7.1 Hz, 3H), 1.08 (s, 9H). ESI−MS calculated for $C_{32}H_{37}BrF_2N_3O_8PS^+$ 772.60, found $[M + H]^+$ 771.32, 773.53.

To **AK2018279** (20 mg, 0.026 mmol), DMF (2 ml), DIPEA (30 µl, 6 equiv.), 1-Boc-1,8-diaminooctane (10 mg, 1.5 equiv.), and HATU (12 mg, 1.1 equiv.) were added. The mixture was stirred at room temperature for 30 min. The yellow solution was purified by HPLC to yield Boc-protected **19**. Boc protection was removed by DCM/TFA at room temperature for 30 min. The volatile components were removed in vacuum to yield **21** as a TFA salt in 80% (20 mg). **21** (10 mg), DMF (1 ml), fluorescein 5-isothiocyanate (5 mg), and DIPEA (10 µl) were mixed at room temperature for 30 min. The mixture was purified by HPLC to yield **20** in 75% (10 mg). To a round bottom flask were added **22** (10 mg, 8 µmol, 1 equiv.), DCM (2 ml), and $CF_3CON(TMS)_2$ (12 µl, 6 equiv.). The solution was cooled in an ice bath. To the ice cooled reaction mixture, 1M of TMS-I in DCM (40 µl, 5 equiv.) was added dropwise and the mixture was stirred for 10 min in an ice bath. The volatile components were removed under vacuum at below 5°C. The residue was dissolved in a mixed solvent of CH_3CN (3 ml) and water (1 ml). The resulting solution was purified by HPLC to yield **AK2018330** in 83% (8 mg). ^{1}H NMR (400 MHz, DMSO-d_6) δ 10.11 (s, 2H), 8.49 – 8.45 (m, 2H), 8.16 – 8.12 (m, 2H), 7.95 (s, 1H), 7.83 – 7.73 (m, 2H), 7.65 – 7.58

(m, 2H), 7.38 – 7.30 (m, 2H), 6.65 – 6.49 (m, 9H), 4.75 (s, 1H), 4.11 – 4.03 (m, 2H), 3.78 – 3.60 (d, *J* = 50.5 Hz, 6H), 2.98 – 2.92 (m, 2H), 2.40 – 2.30 (m, 2H), 1.99 – 1.87 (m, 2H), 1.80 – 1.70 (m, 2H), 1.50 – 0.93 (m, 21H). ESI−MS calculated for $C_{59}H_{62}BrF_2N_6O_{12}PS_2^+$ 1260.17, found $[M + H]^+$ 630.31.

3.6.3 Cell Lines and Cell Culture

BDCM (cat. no. CRL-2740), KASUMI-3 (cat. no. CRL-2725), and MV4;11 (cat. no. CRL-9591) cells were purchased from American Type Culture Collection (ATCC). HL-60 (cat. no. ACC 3), MOLM-13 (cat. no. ACC 554), OCI-AML2 (cat. no. ACC 99), OCI-M2 (cat. no. ACC 619), RS4;11 (cat. no. ACC 508), and SKNO-1 (cat. no. ACC 690) cells were purchased from German Collection of Microorganisms and Cell Culture GmbH (DSMZ). BDCM (ATCC CRL-2740) cells were cultured in RPMI 1640 medium (cat. no. 22400-089, Thermo Fisher Scientific) supplemented with 10% (vol/vol) heat-inactivated fetal bovine serum (FBS, cat. no. S11150H, Atlanta Biologicals, Flowery Branch, GA, USA), 100 U/ml penicillin and 100 µg/ml streptomycin (penicillin-streptomycin, cat. no. 15140122, Thermo Fisher Scientific). SKNO-1 (DSMZ ACC 690) cells were cultured in RPMI 1640 medium supplemented with 10% (vol/vol) heat-inactivated FBS, 100 U/ml penicillin,100 µg/ml streptomycin and 10 ng/ml granulocyte-macrophage colony-stimulating factor (GM-CSF, cat. no. 78015.1, Thermo Fisher Scientific). KASUMI-3 (ATCC CRL-2725) and MOLM-13 (DSMZ ACC 554) cells were cultured in RPMI 1640 medium supplemented with 20% (vol/vol) heat-inactivated FBS, 100 U/ml penicillin,100 µg/ml streptomycin. MV4;11 (ATCC CRL-9591) cells were cultured in Iscove's Modified Dulbecco's Medium (IMDM, cat. no. 12440061, Thermo Fisher Scientific) supplemented with 10% (vol/vol) heat-inactivated FBS, 100 U/ml penicillin and 100 µg/ml streptomycin. HL-60 (DSMZ ACC 3) and OCI-M2 (DSMZ ACC 619) were cultured in IMDM supplemented with

20% (vol/vol) heat-inactivated FBS, 100 U/ml penicillin and 100 µg/ml streptomycin. OCI-AML2 (DSMZ ACC 99) and RS4;11 (DSMZ ACC 508) cells were cultured in Minimum Essential Medium (MEM α, cat. no. 12571063 Thermo Fisher Scientific) supplemented with 10% (vol/vol) heat-inactivated FBS, 100 U/ml penicillin and 100 µg/ml streptomycin. All the cell lines were maintained in a humidified incubator at 37 º and 5% CO_2.

3.6.4 Mice

All the *in vivo* studies were performed under an animal protocol (PRO00007499) approved by the Institutional Animal Care & Use Committee of the University of Michigan, in accordance with the recommendations in the Guide for the Care and Use of Laboratory Animals of the National Institutes of Health.

For PK, PD and efficacy studies, NOD/SCID female mice were injected subcutaneously with 1×10^6 MV4;11cells in 5 mg/ml Matrigel (Corning) for tumor growth. When the tumors reached an average volume of 150 mm^3, mice were tumor size-matched and randomly assigned to different experimental groups for experiments. For PK and PD studies, mice were treated as described in the Results. At the indicated time-points, mice were euthanized and blood and tissue samples were collected for analyses. The PK analysis was performed by the University of Michigan Pharmacokinetics Core.

For toxicity studies in CD-1 female mice, mice were treated with AK2292 or vehicle control (10% PEG400 + 90% PBS) as described in the Results. Mouse body weights were measured 2–3 times per week. At the end of experiments, mice were euthanized and blood and main organs were collected for analyses. The toxicity studies, including hematology, chemistry and histology

analyses, were performed by the University of Michigan Unit for Laboratory Animal Medicine *In Vivo* Animal Core.

For efficacy studies, drugs or vehicle control (10% PEG400 + 90% PBS) were given at the dose schedules as indicated in the Figures. Tumor sizes and animal weights were measured 2–3 times per week. Tumor volume (mm^3) = (length×$width^2$)/2. Tumor growth inhibition (TGI) was calculated as TGI (%) = $(V_c-V_t)/(V_c-V_o) \times 100$, where V_c and V_t are the medians of the control and treated groups at the end of the study respectively, and V_o at the start.

3.6.5 STAT5A Expression and Purification

The gene for human STAT5a corresponding to residues 136 – 705 was cloned, expressed and purified as previously described [37]. Briefly, Stat5a was expressed as a N-terminal 6x-His-MBP-TEV fusion protein in *Escherichia coli* Rosetta 2 (DE3) cells. Transformed cells were grown at 37 °C in Terrific Broth, induced overnight at 20 °C by addition of 0.4 mM isopropyl β-d-1-thiogalactopyranoside then pelleted by centrifugation. The harvested pellet was frozen at -80 °C.

Protein was purified from a thawed pellet resuspended in lysis buffer containing 25 mM HEPES pH 7.5, 150 mM NaCl, 10 mM $MgCl_2$, 10 µg/mL aprotinin, 1 µg/mL leupeptin, 0.1% □-mercaptoethanol, and ~200 U Benzonase Nuclease (Millipore-Sigma) and lysed by sonication. Lysate was cleared by centrifugation then incubated with Ni-NTA Agarose (QIAGEN) for 1 hour at 4 °C. Resin was washed with lysis buffer containing 10 mM imidazole followed by a high salt wash (25 mM HEPES pH 7.5 and 1 M NaCl). Protein was eluted in buffer containing 25 mM HEPES pH 7.5, 150 mM NaCl, and 300 mM imidazole. Eluate was dialyzed into buffer containing 25 mM HEPES pH 7.0, 150 mM NaCl, and 0.1% □-mercaptoethanol and cleaved with Tobacco Etch Virus protease overnight at 4 °C. Cleaved STAT5a was treated with

additional Ni-NTA resin to remove additional His-tagged MBP and further purified on a 5 mL HiTrap Heparin HP (GE Healthcare) column followed by size exclusion chromatography on a HiLoad 16/60 Superdex 200 column (GE Healthcare) in buffer containing 20 mM HEPES 7.0, 200 mM NaCl, and 5 mM DTT.

3.6.6 STAT5A:inhibitor Crystallization and Structure Determination

AK2339, AK2340 or AK2341 was added to concentrated STAT5A (7.25 mg/mL in 20 mM HEPES 7.0, 200 mM NaCl, and 5 mM DTT) in a 3:1 molar ratio and incubated at 4 °C for 2 hours. The Stat5A-inhibitor complexes were crystallized via sitting drop vapor diffusion at 20 °C in a 2:1 protein to well drop ratio. Stat5A-AK2339 crystals grew in well solution containing 1.1 M sodium malonate pH 7.0, 0.1 M HEPES pH 7.0, and 0.5% Jeffamine pH 7.0. Stat5A-AK2340 and Stat5A-AK2341 crystals grew in well solution containing 1.1 M ammonium tartrate pH 7.0. Crystals were cryoprotected in well solution with 20% glycerol and flash-cooled in liquid nitrogen prior to data collection. Diffraction data (Figure S3-A) were collected on Advanced Photon Source LS-CAT beamline 21-ID-F and processed in HKL2000 [79].

The structures of were solved by molecular replacement in Phaser[2] using a Stat5A structure previously solved in the lab as a search model. The Stat5A-inhibitor crystals grew in the R32 space group with 1 molecule in the asymmetric unit. Electron density corresponding to the inhibitors was observed in the phosphotyrosine binding site of Stat5A after molecular replacement. Iterative model-building and refinement were performed in COOT [80] and BUSTER [81], respectively. Ligand restraints were generated in Grade [82].

3.6.7 Cell Viability Assay

The stock solutions of AK2292 and other compounds in DMSO were diluted accordingly with cell culture medium. The prepared compound solution was added to 96-well Microplates (Corning cat 3610) in triplicate and serial 1/3 delusion was performed. Wells in one column were left with no compounds as control wells. The volume of each well at this point was set to 50 ul. Cell culture medium containing approximately 100,000 cells per ml was prepared in a reagent reservoir and 50 ul of the prepared cell containing medium was added to each well to seed approximately 5,000 cells per well. After 3-4 days in an incubator at 37 °C and 5% CO2, the cell viability was measured by CellTiter-Glo (CTG) Luminescent Cell Viability Assay. 50 μl of CTG reagent (Promega cat G7573) was added to each well and the plate was gently vortexed for 5 minutes. The luminescence was recorded using plate reader (). The average cell viability values were calculated by setting the average luminescence value in control wells as 100%.

3.6.8 Immunoblotting

About 1 million cells per each data point were treated with AK2292 and other compounds at indicated concentrations and durations. Untreated and treated cells in cell culture medium were transferred into tubes, followed by centrifuge at 3,000 rpm and 4 ºC for 6 minutes. Supernatants were removed from tubes and radioimmunoprecipitation assay (RIPA) lysis buffer supplemented with 1% protease inhibitor cocktail (cat) and phosphatase inhibitor (cat) were added to tubes containing the remaining cell pellets. The tubes were then left on ice for 30 minutes and put in a -80 ºC freezer. Afterwards they were thawed out in 37 ºC water, centrifuged at 14,000 rpm for 15 minutes and the cell lysates transferred to new tubes. The concentration of total proteins in each tube was calculated using the Pierce BCA protein Assay kit (cat). Based on the calculated protein concentration, cell lysates containing approximately the same amount of proteins were transferred to new tubes, then distilled water and 4X Protein Sample Loading Buffer for Western

Blots (LI-COR) supplemented with 20% of mercaptoethanol were added on ice. The cell lysates were then reduced and denatured at 95 ºC for 5 minutes. From the tubes containing cell lysates an equal amount of protein samples (20-40 µg) was sucked and loaded into precast 8%, 10%, 4%-12%, or 4%-20% Tris-glycine gels (cat) filled with Tris-glycine SDS running buffer. After the proteins were resolved, they were transferred onto Immobile-FL PVDF Membrane (Millipore Sigma cat), using Mini Trans-Blot Electrophoretic Transfer Cell (Bio-Rad 1703930). The membranes were blocked with Intercept Blocking Buffer (LI-COR cat) in LI-COR Western Blot boxes for 1 hour at room temperature. The membranes were washed with 1X Tris-buffered saline-Tween-20 (TBST, 1X solution was made from 20X TBST solution, ThermoFisher Scientific cat) for 5 minutes 4 times. The membranes were incubated overnight at 4C in Intercept Blocking Buffer supplemented with primary antibodies (normally antibody:bugger 1:1000) and Tween-20. The membranes were washed with TBST for 5 minutes 4 times and were incubated with Intercept Blocking Buffer supplemented with IRDye 800CE Secondary Antibodies, IRDye 680RD Secondary Antibodies (LI-COR biosciences cat), Tween-20, and 10% SDS solution, for 1 hour at room temperature. The membranes were then washed with TBST for 5 minutes 4 times and rinsed with deionized water before drying and scanning with Odyssey Dlx Amazing System (LI-COR). The immunoblots were finally quantified by the software (LI-COR).

3.7 Supporting Information

3.7.1 Figure S1.

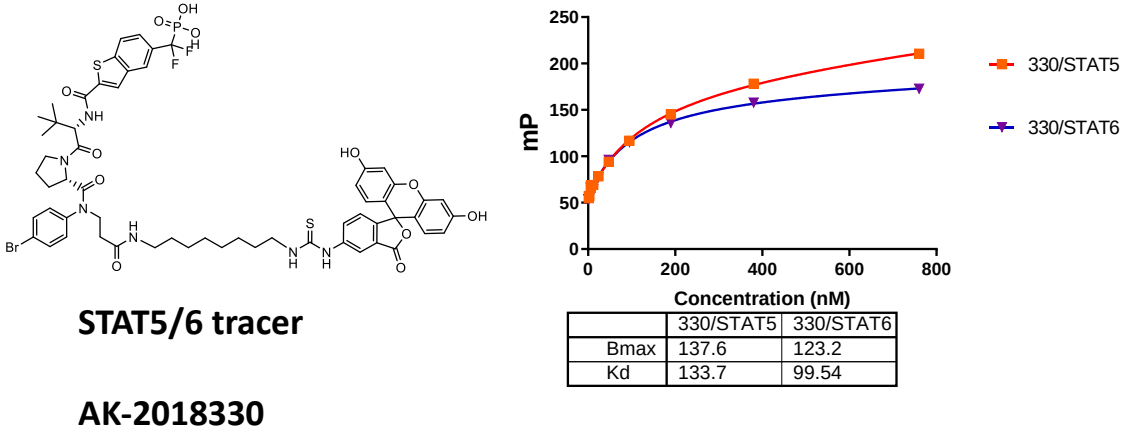

	330/STAT5	330/STAT6
Bmax	137.6	123.2
Kd	133.7	99.54

Figure 3-17 Figure S1. The structure of STAT5/6 tracer, AK-2018330 and its Kd values for STAT5 and STAT6.

Figure S1. The structure of STAT5/6 tracer, AK-2018330 and its Kd values for STAT5 and STAT6.

3.7.2 Figure S2.

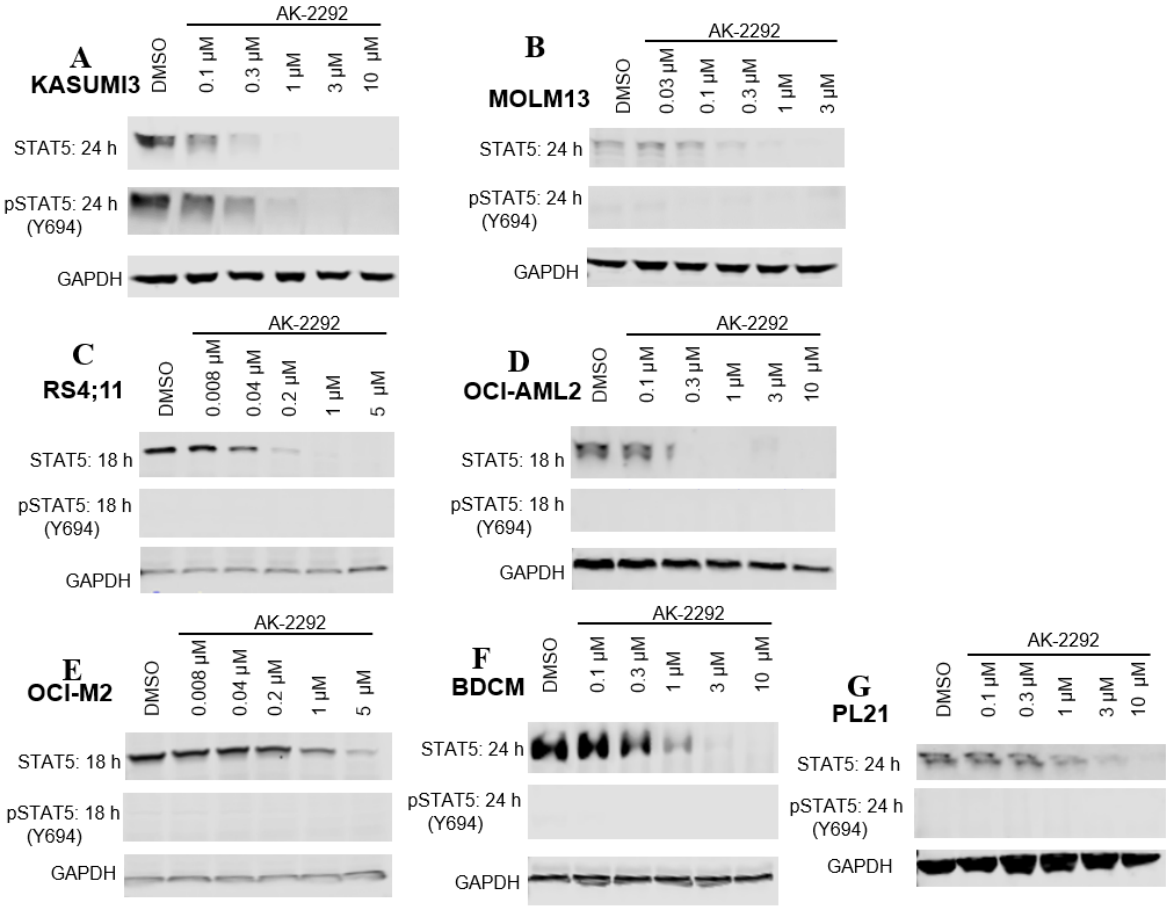

Figure 3-18 Figure S2.

Figure S2. (A) Western blotting analysis of Kasumi-3 treated with AK-2292., (B) Western blotting analysis of Molm-13 treated with AK-2292., (C) Western blotting analysis of RS4;11 treated with AK-2292., (D) Western blotting analysis of OCI-AML2 treated with AK-2292., (E) Western blotting analysis of OCI-M2 treated with AK-2292., (F) Western blotting analysis of BDCM treated with AK-2292., (G) Western blotting analysis of PL-21 treated with AK-2292.

3.7.3 Table S3. Crystallography Data Collection and Refinement Statistics

Table 8 Table S3. Crystallography Data Collection and Refinement Statistics

Data Collection	**Stat5a:AK2339**	**Stat5a:AK2340**	**Stat5a:AK2341**
PDBID	7UC6	7UC7	7UBT
Space Group	R32	R32	R32
Unit Cell (Å)	237.7 237.7 122.8 90 90 120	238.9 238.9 113.30 90 90 120	234.9 234.9 112.9 90 90 120
Wavelength (Å)	0.9787	0.9787	0.9787
Resolution (Å)[1]	3.1	3.1	2.25
Rsym[2]	0.13 (1.40)	0.076 (1.58)	0.098 (1.834)
$\langle I/\sigma I \rangle$[3]	21.7 (2.1)	35.9 (1.9)	29.9 (2.0)
Completeness (%)[4]	100 (100)	99.9 (100)	100 (100)
Redundancy	11.4 (11.5)	11.4 (11.6)	11.2 (10.3)
Refinement			
Resolution (Å)	3.1	3.1	2.35
R-Factor [5]	0.194	0.224	0.199
R-Free [6]	0.243	0.283	0.225
Protein atoms	4397	4408	4403
Ligands	1	1	1
Water Molecules	91	73	439
Unique Reflections	19118	18512	49238
R.m.s.d.[7]			
Bonds	0.009	0.008	0.008
Angles	1.06	0.98	1.02
MolProbity Score[8]	2.16	2.43	1.98
Clash Score[8]	5.36	4.43	2.71
RSCC[9]	0.88	0.91	0.95
RSR[9]	0.30	0.27	0.12

[1]Statistics for highest resolution bin of reflections in parentheses.

[2]$R_{sym} = \Sigma_h \Sigma_j | I_{hj} - \langle I_h \rangle | / \Sigma_h \Sigma_j I_{hj}$, where I_{hj} is the intensity of observation j of reflection h and $\langle I_h \rangle$ is the mean intensity for multiply recorded reflections.

[3]Intensity signal-to-noise ratio.

[4]Completeness of the unique diffraction data.

[5]R-factor = $\Sigma_h | IF_oI - IF_cI | / \Sigma_h |F_o|$, where F_o and F_c are the observed and calculated structure factor amplitudes for reflection h.

[6]R_{free} is calculated against a 5% random sampling of the reflections that were removed before structure refinement.

[7]Root mean square deviation of bond lengths and bond angles.

[8]Chen et al. (2010) MolProbity: all-atom structure validation for macromolecular crystallography. Acta Crystallographica D66:12-21.

[9]wwPDB Validation Server.

Table S3. Crystallography Data Collection and Refinement Statistics.

3.7.4 Figure S3:

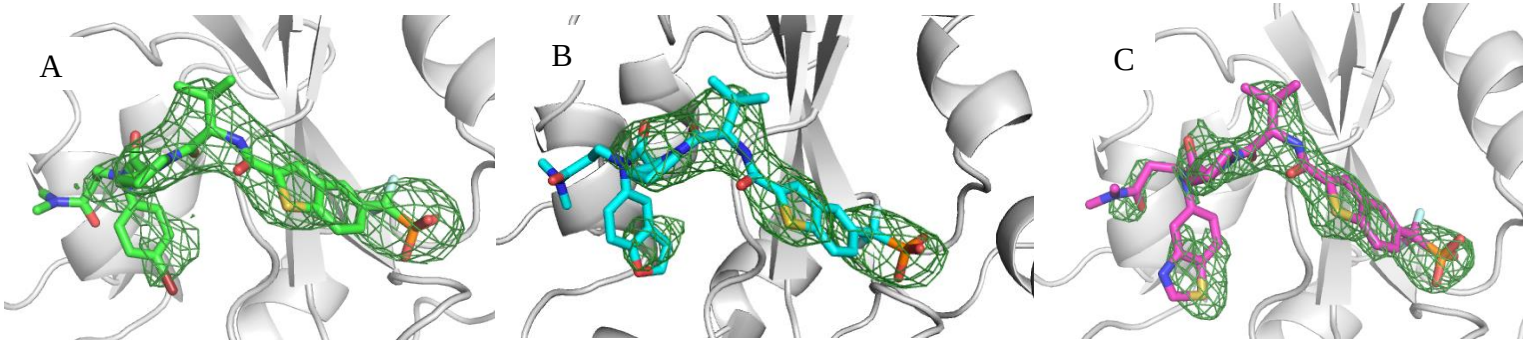

Figure 3-19 Figure S3: Maps showing the unbiased difference electron density (Fo-Fc) for the inhibitors from the initial refinement

Figure S3: Maps showing the unbiased difference electron density (Fo-Fc) for the inhibitors from the initial refinement (A) AK2339 (B) AK2340 and (C) AK2341. The maps are contoured at 3σ.

Chapter 4 General Discussion and Future Directions

4.1 Achievements and implications in this dissertation

1) Because of the absence of STAT5 inhibitors with sufficient binding affinity to STAT5 we developed at the beginning of this dissertation project, our own a set of unique STAT5 inhibitors.
2) We developed first-in-class selective and efficacious STAT5 PROTAC degraders.
3) We solved the first co-crystal structures of complexes of STAT5 with inhibitors as well as a STAT5 degrader in a complex with STAT5A.
4) We demonstrated that excellent selectivity can be achieved with PROTAC technology, even though corresponding inhibitors preferably bind off-target proteins rather than target proteins of interest.
5) We offer to the community AK-2292, an excellent tool compound with an exceptional selectivity toward STAT5 to facilitate STAT5 related research.

4.2 Further improvement of the potency of AK-2292 both *in vitro* and *in vivo*

4.2.1 Binding affinities of inhibitors

The current corresponding inhibitor used in our best STAT5 degrader, AK-2292, has only moderate binding affinity to STAT5 (K_i value = 1.2 μM). The SH2 domains of STAT5 protein and nearby sites are very shallow pockets, making development of a high affinity inhibitor particularly challenging. However, based on the detailed interactions observed in the co-crystals whose structure we solved, further modifications of the C-terminal moiety of inhibitors may improve the binding affinity. In Chapter 2, we described our attempts to make intensive

modifications at the C-terminus of STAT5 inhibitors, and discovered that the thiazole group is the best group in this position. In fact, π- π interactions as well as hydrophilic interactions are observed between the C-terminal thiazole group and surrounding hydrophobic and hydrophilic residues of the STAT5 protein surface. Further exploration investigating other heteroaromatic ring systems at the C-terminus may yield inhibitors with better binding affinities.

4.2.2 Linker optimization

In PROTAC molecule development, linker lengths and linker compositions are major factors affecting degradation potency, and presumably result from the contribution of better ternary complexes among proteins of interest, degraders and E3 ligases. In this dissertation work, optimal linker length and composition were established. Linear linkers were found to contribute to the activity more significantly than rigid linkers. Furthermore, the amide group at the tethering site appears to be very important in retaining the binding affinity to STAT5. Subtle tweaks to the linker of our STAT5 degraders made huge, mostly negative differences in the degradation efficiency. Further detailed tuning in the linker however may yield beneficial outcomes in the formation of better ternary complexes and improved binding affinity.

4.2.3 E3 ligase ligand optimization

It is clear that the E3 ligase ligand moiety plays an important role in the degradation efficiency. In this dissertation, I focused on a lenalidomide type E3 ligase ligand as the ligand for cereblon/cullin 4A. The linker moiety is tethered at position 4 in the aromatic ring system. But other positions such as position 5, 6 or 7 may also be candidates if their synthesis is feasible. We also developed a new class of E3 ligase ligand, called TX-11, which may improve the degradation efficiency and will be investigated. In such investigations, it is important to

remember that the optimal linker length and the linker composition may change drastically depending on the tethering positions at the aromatic ring of E3 ligase ligand. This is because the optimal formation of the ternary complex among STAT5, degraders and E3 ligase will differ as the tethering sites change.

4.2.4 PK property optimization

Pharmacokinetic (PK) properties can dramatically impact the overall efficacy of STAT5B degraders. Despite rules of thumb regarding improvement of PK properties, it may be difficult to determine how to improve the PK properties of relatively inevitably large molecules such as AK-2292. However, if the PK properties of AK-2292, for example its clearance are improved, a dramatic improvement in efficacy may be possible.

4.3 Further selectivity study over STAT6

AK-305, as the parent structure of AK-2292, showed high affinity to STAT5A and STAT5B with Ki values 1.2 and 0.6 μM, that is similar as AK-2292. It is fair to question Why AK-305 did not affect the activity of STAT5 in cells? To see the effect on pSTAT5 and pSTAT6, we tested AK-2292 and AK-305 at up to 100 μM in L1236 and HDLM2 (data not shown). We chose L1236 and HDLM2 cells because L1236 and HDLM2 express STAT5/pSTAT5 and STAT6/pSTAT6 and they are probably good representative cells to study the impact of AK-305 and AK-2292 on especially pSTAT6 level. AK-2292 induced STAT5/pSTAT5 degradation in L1236 and HDLM2. The effect of AK-305 on pSTAT5 level in L1236 seems very limited even at very high concentrations. Moreover, AK-305 and AK-2292 showed no effect in the level of pSTAT6 in both L1236 and HDLM2 cells.

We also tested the cell permeability of AK-2292 and AK-305 and Caco-2 study showed that both compounds have very low cell permeabilities as low as 0.06 x 10^{-6} cm/s, compared to control compounds such as atenolol and propranolol with cell permeabilities 0.43 x 10^{-6} cm/s and 27.66 x 10^{-6} cm/s respectively.

Furthermore, we performed a reporter gene assay, showing no or minimal effect of AK-2292 and AK-305 on representative STAT6 target genes.

Taken together, even though AK-2292 and AK-305 can bind STAT6 with Ki values around 1 μM or below, both compounds cannot inhibit the phosphorylation of STAT6 due to their low cell permeability. However, the catalytic nature of AK-2292 as a STAT5 PROTAC degrader enable AK-2292 to deplete STAT5A/B despite its low cell permeability.

4.4 Why STAT6 is not degraded by AK-2292?

We have developed a selective STAT6 degrader, AK-1690 by using the similar strategy we used for STAT5 degrader development. Our selective STAT6 degrader AK-1690 binds to STAT5 as well as STAT6, but it only degrades STAT6, leaving STAT5 level intact. AK-1690 has a different linking site to tether Cereblon ligand and that switched the degradation selectivity, suggestive of AK-2292's productive ternary complex with STAT5 and Cereblon but not with STAT6, and vise versa with STAT6 degrader AK-1690. We still cannot definitively explain the reason of AK-2292's degradation specificity to STAT5 over STAT6, but a ternary complex formation efficiency plays a key factor of selectivity and the tethering site eventually switched the degradation selectivity from STAT5 (AK-2292) to STAT6 (AK-1690).

4.5 Proteins impacted by AK-2292 and their association with STAT5

We performed multiple unbiased proteomics analyses using different cell types and different conditions. Smoothelin (SMTN) showed up once, but in none of other unbiased proteomics analyses. Also, based on our RNAseq analyses with KU812 and NCO2 cell lines, several hallmark pathways have been downregulated. Among them, p53 pathway, for example, is also downregulated. We have not found many publications indicating the association of SMTN, but at least two literatures appeared [91, 92], suggesting p53 induces SMTN. We speculate that because of the downregulation of p53 pathway, SMTN gene could also be downregulated. Regarding FAM18B2, we did not find any literature that strongly suggests any relation to STAT5 biology and its target genes. FAM18B2 seems very under studied. We close-looked at the abundance of FAM18B2 and SMTN in KU812 cells treated by AK-2292 at 1 μM for 24 h and at 10 μM for 8 h, and also looked at PBMCs treated by AK-2292 at 5 μM for 18 h, but the protein levels of both proteins were not affected at all. Taken together, SMTN and FAM18B2 have a very limited impact from STATA/B depletion by AK-2292. Based on our data, it is safe to say that AK-2292 is selective over all other STAT family members and >6,000 other proteins.

4.6 Genes impacted by AK-2292 and their association with STAT5

RNA-seq analysis showed marked downregulation of OSM, PIM1, CISH, SOCS1 and SOCS3, all indicating AK2292's selective downregulation of STAT5A and STAT5B [93]. Oncostatin M (OSM), a profibrogenic and angiogenic modulator, has been reported as a STAT5 dependent mediator [76]. PIM1, an oncogenic serine/threonine kinase, is a STAT5 target gene [73, 94, 95]. SOCS1, SOCS3 and CISH are members of the suppressor of cytokine signaling (SOCS) family of proteins that form a part of a negative feedback circuit in which STAT5A and STAT5B are negatively regulated by these proteins [75, 96-99]. The downregulation of the

related genes is consistent with the downregulated hallmark pathways. The downregulation of Myc targets hallmark pathways [74, 100, 101] and estrogen response related hallmark pathways [102] possibly as a result of PIM1 downregulation and STAT5A/STAT5B depletion. STAT5A/STAT5B depletion and SOCS1 downregulation probably contribute to the downregulation of the p53 related pathway [103-105]. The STAT5A/STAT5B depletion is likely attributable to the downregulation of IL6 JAK/STAT3 signaling hallmark pathway [106] and TNFA signaling *via* the NF-κB hallmark pathway since STAT5A/B and NFkB are in a negative feedback circuit [107]. Taken together, our western blotting, proteomics and RNA-seq analysis strongly support the conclusion that AK2292 is a selective STAT5A/STAT5B PROTAC degrader.

We looked all the down-regulated and up-regulated genes. We found 34 genes down-regulated ≥2-fold and 5 genes up-regulated ≥2-fold in KU812 cells treated with 1 μM for 8 h. In NCO2 cells treated with 1 μM for 8 h, total 29 genes were downregulated ≥2-fold and no genes were upregulated ≥2-fold. Because AK-2292 binds to STAT6 well to the similar extent to STAT5, STAT6 target genes would appear as down-regulated genes. However, none of representative STAT6 target genes were found down-regulated in our RNA-seq analyses [108, 109]. As reviewed by Goenka et al., if AK-2292 inhibited STAT6 functions, at least some of representative STAT6 target genes would have appeared such as GATA3, BATF, II24, MAF, GFI1, FIZZ, ARG1, CCL11, ALOX15, TL-ALPHA, AGT, CY1, CY3, ITGB3, HLA-DP, SELP, and FIG 1. However, none of them showed up in our RNA-seq analyses, indicating AK-2292's selectivity to STAT5.

4.7 Cell types to be tested

In our CellTiter-Glo assay, AK2292 showed growth-inhibitory activities in CML cells, and in a subset of AML cells [9]. Other cell types such as PTCL [10] and TALL [21] with their high expression levels of STAT5 are also expected to react to STAT5 depletion by AK-2292. Our investigation of basal protein levels in sensitive and insensitive cells indicated that $pSTAT5^{Y694}$ level is a key indicator predicting cellular responses of CML cells. Tested CML cells with BCR-ABL and $pSTAT5^{Y694}$ showed complete responses to AK2292.

Similar phenomena were observed in AML cells. Overall, the spectrum of responses of AML cells to AK2292 was found to be significantly limited. Although it has been reported that AML cells with FLT3 mutation are sensitive to the inhibition of STAT5 phosphorylation [29], we found that most of the AML cells tested, including MOLM-13, PL21 and THP-1 have very low levels of $pSTAT5^{Y694}$ and failed to respond to AK2292 at concentrations up to 15 μM, even though AK2292 efficiently and completely depleted STAT5A/STAT5B and $pSTAT5^{Y694}$ at much lower, but detectable basal levels. In contrast, AML cells such as MV4;11, SKNO1 and Kasumi-3 which have higher STAT5 and $pSTAT5^{Y694}$ basal levels, do respond to protein depletion induced by AK-2292. The basal level expression of $pSTAT5^{Y694}$ in AML cells is also a good indicator of cellular responses to AK-2292, as observed in CML cells.

With respect to other cell types, it has been reported that PTCL cells have high STAT5A/STAT5B and $pSTAT5^{Y694}$ levels and representative PTCL cells such as T8ML-1, Mac1 and Mac2a all have very high expression of STAT5A/STAT5B and $pSTAT5^{Y694}$. Given this high level of expression, PTCL cells are expected to respond to AK-2292 [10]. In a further example, T cell derived ALL, such as TALL-104, has also been predicted to be sensitive to STAT5A/STAT5B depletion [21].

The results from our cellular protein analysis and cell viability assay, suggest that the expression of $pSTAT5^{Y694}$, but apparently not the whole STAT5A/STAT5B, could be a good indicator of cellular response to AK2292. It should be noted that some of cell lines require cytokines in their cell culture media. Examples include GM-CSF for SKNO1 cells and IL-2 for T8ML-1 and TALL-104 cells. These cytokines are known to induce the phosphorylation of STAT5 and may contribute to the dependence of such cells on $pSTAT5^{Y694}$ [110]. To further expand the spectrum of sensitive cell lines in any of these diseases, it is of interest to look into the basal expression levels of $pSTAT5^{Y694}$.

4.8 Toxicity

We performed toxicity studies to assess the potential toxicity induced by STAT5A/STAT5B depletion by AK2292. BALB/c mice tolerated daily dosing of AK-2292 at 200 mg/kg for 2 weeks and experienced minimal weight loss (<10%). We examined liver toxicity and blood chemistry, but all the observed parameters failed to show any significant difference compared to the control group. Our multiple tumor xenograft models also tolerated a 200 mg/kg daily dosing schedule for 2 to 3 weeks. In addition to observing weight change or completing an analysis of the blood chemistry, it would be also important to look into the impact of STAT5 depletion on the immune system because STAT5 plays pivotal roles in the immune system, especially in T-cell development [4, 111-113] and NK cell development [114].

4.9 Future directions

In this dissertation, I have reported the first-in-class STAT5 PROTAC degrader, AK-2292. This compound will serve as an excellent tool with which to study STAT5 related biology

in vitro and *in vivo*. Importantly, this first successful STAT5 targeting provides a firm starting point of STAT5 targeted therapy to treat diseases in which STAT5 plays an important role.

An initial strategy would be to improve the *in vivo* potency of AK-2292. In our *in vivo* study with multiple tumor xenograft mouse models, AK-2292 required a dose of at least 50 mg/kg to attain any tumor growth inhibitory effect and 100 mg/kg to gain a significant therapeutic effect. These dosing amounts of drugs are not ideal and by modifying the structures of inhibitor, linker, and E3 ligase ligand, further boosting of the *in vivo* potency is certainly possible.

The second future strategy would be to investigate the effect of STAT5 depletion in other types of hematologic malignancies. CML and AML cells were used in this proof-of-concept work, but other types of cells, such as PTCL [10] and TALL [21], both of are which derived from T-cells and have been reported to have high STAT5 expression, should respond to STAT5 depletion induced by AK-2292. Previous publications have demonstrated that STAT5 plays an important role in T-cell development [10, 115], suggesting that the inhibition of STAT5 functions would be beneficial in treatment of T cell-derived hematologic malignancies.

A third future strategy would be to investigate either the single depletion of STAT5 or the dual depletion of STAT5 and STAT3 in solid tumors since publications have suggested that solid tumors such as epithelial ovarian cancer are associated with aberrant activation of STAT5 and STAT3 [25, 116, 117]. It would be interesting to see the effect on epithelial ovarian cancer cells [118] and other types of solid tumors of the STAT5 degrader of AK-2292, alone or in combination with the STAT3 degrader developed by our lab.

The fourth strategy would be to answer some of the STAT5 related biology questions with AK-2292 as a tool compound. For example, the role played by STAT5 in cancer energy

metabolism has been reviewed [119], and the association of STAT5 and reactive oxygen species has also been reviewed [120]. An intensive evaluation of STAT5 as a therapeutic target in terms of toxicity would be worthwhile since STAT5 plays important roles in the immune system, especially in the development of T-cells [4, 111-113] and NK cells [114].

I leave these suggestions to any researchers who are interested in the biology of STAT5 or the development of STAT5 targeted therapy or investigation of the mechanism of STAT5 related diseases.

Bibliography

1. Wang, Z. and K.D. Bunting, *STAT5 in hematopoietic stem cell biology and transplantation.* JAKSTAT, 2013. **2**(4): p. e27159.
2. Vainchenker, W. and S.N. Constantinescu, *JAK/STAT signaling in hematological malignancies.* Oncogene, 2013. **32**(21): p. 2601-13.
3. Able, A.A., J.A. Burrell, and J.M. Stephens, *STAT5-Interacting Proteins: A Synopsis of Proteins that Regulate STAT5 Activity.* Biology (Basel), 2017. **6**(1).
4. Rani, A. and J.J. Murphy, *STAT5 in Cancer and Immunity.* J Interferon Cytokine Res, 2016. **36**(4): p. 226-37.
5. Ferbeyre, G. and R. Moriggl, *The role of Stat5 transcription factors as tumor suppressors or oncogenes.* Biochim Biophys Acta, 2011. **1815**(1): p. 104-14.
6. Hoelbl, A., et al., *Stat5 is indispensable for the maintenance of bcr/abl-positive leukaemia.* EMBO Mol Med, 2010. **2**(3): p. 98-110.
7. Walz, C., et al., *Essential role for Stat5a/b in myeloproliferative neoplasms induced by BCR-ABL1 and JAK2(V617F) in mice.* Blood, 2012. **119**(15): p. 3550-60.
8. Yan, D., R.E. Hutchison, and G. Mohi, *Critical requirement for Stat5 in a mouse model of polycythemia vera.* Blood, 2012. **119**(15): p. 3539-49.
9. Yoshimoto, G., et al., *FLT3-ITD up-regulates MCL-1 to promote survival of stem cells in acute myeloid leukemia via FLT3-ITD-specific STAT5 activation.* Blood, 2009. **114**(24): p. 5034-43.
10. Maurer, B., et al., *High activation of STAT5A drives peripheral T-cell lymphoma and leukemia.* Haematologica, 2020. **105**(2): p. 435-447.
11. Halim, C.E., et al., *Involvement of STAT5 in Oncogenesis.* Biomedicines, 2020. **8**(9).
12. Wingelhofer, B., et al., *Implications of STAT3 and STAT5 signaling on gene regulation and chromatin remodeling in hematopoietic cancer.* Leukemia, 2018. **32**(8): p. 1713-1726.
13. Warsch, W., C. Walz, and V. Sexl, *JAK of all trades: JAK2-STAT5 as novel therapeutic targets in BCR-ABL1+ chronic myeloid leukemia.* Blood, 2013. **122**(13): p. 2167-75.
14. Malin, S., S. McManus, and M. Busslinger, *STAT5 in B cell development and leukemia.* Curr Opin Immunol, 2010. **22**(2): p. 168-76.
15. Yu, H. and R. Jove, *The STATs of cancer--new molecular targets come of age.* Nat Rev Cancer, 2004. **4**(2): p. 97-105.
16. Taketani, T., et al., *FLT3 mutations in the activation loop of tyrosine kinase domain are frequently found in infant ALL with MLL rearrangements and pediatric ALL with hyperdiploidy.* Blood, 2004. **103**(3): p. 1085-1088.
17. Quentmeier, H., et al., *FLT3 mutations in acute myeloid leukemia cell lines.* Leukemia, 2003. **17**(1): p. 120-4.
18. McMahon, C.M. and S.M. Luger, *Relapsed T Cell ALL: Current Approaches and New Directions.* Curr Hematol Malig Rep, 2019. **14**(2): p. 83-93.

19. Ribeiro, D., et al., *STAT5 is essential for IL-7-mediated viability, growth, and proliferation of T-cell acute lymphoblastic leukemia cells.* Blood Adv, 2018. **2**(17): p. 2199-2213.
20. Minieri, V., et al., *Targeting STAT5 or STAT5-Regulated Pathways Suppresses Leukemogenesis of Ph+ Acute Lymphoblastic Leukemia.* Cancer Res, 2018. **78**(20): p. 5793-5807.
21. Vanden Bempt, M., et al., *Cooperative Enhancer Activation by TLX1 and STAT5 Drives Development of NUP214-ABL1/TLX1-Positive T Cell Acute Lymphoblastic Leukemia.* Cancer Cell, 2018. **34**(2): p. 271-285 e7.
22. Peng, B., P. Lloyd, and H. Schran, *Clinical pharmacokinetics of imatinib.* Clin Pharmacokinet, 2005. **44**(9): p. 879-94.
23. Casetti, L., et al., *Differential contributions of STAT5A and STAT5B to stress protection and tyrosine kinase inhibitor resistance of chronic myeloid leukemia stem/progenitor cells.* Cancer Res, 2013. **73**(7): p. 2052-8.
24. Ye, D., et al., *STAT5 signaling is required for the efficient induction and maintenance of CML in mice.* Blood, 2006. **107**(12): p. 4917-25.
25. Orlova, A., et al., *Direct Targeting Options for STAT3 and STAT5 in Cancer.* Cancers (Basel), 2019. **11**(12).
26. Page, B.D., et al., *Small molecule STAT5-SH2 domain inhibitors exhibit potent antileukemia activity.* J Med Chem, 2012. **55**(3): p. 1047-55.
27. Cumaraswamy, A.A., et al., *Nanomolar-Potency Small Molecule Inhibitor of STAT5 Protein.* ACS Med Chem Lett, 2014. **5**(11): p. 1202-1206.
28. Liao, Z., et al., *Structure-Based Screen Identifies a Potent Small Molecule Inhibitor of Stat5a/b with Therapeutic Potential for Prostate Cancer and Chronic Myeloid Leukemia.* Mol Cancer Ther, 2015. **14**(8): p. 1777-93.
29. Wingelhofer, B., et al., *Pharmacologic inhibition of STAT5 in acute myeloid leukemia.* Leukemia, 2018. **32**(5): p. 1135-1146.
30. Elumalai, N., et al., *Nanomolar inhibitors of the transcription factor STAT5b with high selectivity over STAT5a.* Angew Chem Int Ed Engl, 2015. **54**(16): p. 4758-63.
31. Becker, S., B. Groner, and C.W. Muller, *Three-dimensional structure of the Stat3beta homodimer bound to DNA.* Nature, 1998. **394**(6689): p. 145-51.
32. Chen, X., et al., *Crystal structure of a tyrosine phosphorylated STAT-1 dimer bound to DNA.* Cell, 1998. **93**(5): p. 827-39.
33. Levy, D.E. and J.E. Darnell, Jr., *Stats: transcriptional control and biological impact.* Nat Rev Mol Cell Biol, 2002. **3**(9): p. 651-62.
34. Muller, J., et al., *Discovery of chromone-based inhibitors of the transcription factor STAT5.* Chembiochem, 2008. **9**(5): p. 723-7.
35. Natarajan, K., et al., *Stafia-1: a STAT5a-Selective Inhibitor Developed via Docking-Based Screening of in Silico O-Phosphorylated Fragments.* Chemistry, 2020. **26**(1): p. 148-154.
36. Chen, J., et al., *Structure-Based Design of Conformationally Constrained, Cell-Permeable STAT3 Inhibitors.* ACS Med Chem Lett, 2010. **1**(2): p. 85-89.
37. Bai, L., et al., *A Potent and Selective Small-Molecule Degrader of STAT3 Achieves Complete Tumor Regression In Vivo.* Cancer Cell, 2019. **36**(5): p. 498-511 e17.

38. Zhou, H., et al., *Structure-Based Discovery of SD-36 as a Potent, Selective, and Efficacious PROTAC Degrader of STAT3 Protein.* J Med Chem, 2019. **62**(24): p. 11280-11300.
39. Lai, A.C. and C.M. Crews, *Induced protein degradation: an emerging drug discovery paradigm.* Nat Rev Drug Discov, 2017. **16**(2): p. 101-114.
40. Neklesa, T.K., J.D. Winkler, and C.M. Crews, *Targeted protein degradation by PROTACs.* Pharmacol Ther, 2017. **174**: p. 138-144.
41. Nabet, B., et al., *The dTAG system for immediate and target-specific protein degradation.* Nat Chem Biol, 2018. **14**(5): p. 431-441.
42. Pettersson, M. and C.M. Crews, *PROteolysis TArgeting Chimeras (PROTACs) - Past, present and future.* Drug Discov Today Technol, 2019. **31**: p. 15-27.
43. Nalawansha, D.A. and C.M. Crews, *PROTACs: An Emerging Therapeutic Modality in Precision Medicine.* Cell Chem Biol, 2020. **27**(8): p. 998-1014.
44. Salami, J. and C.M. Crews, *Waste disposal-An attractive strategy for cancer therapy.* Science, 2017. **355**(6330): p. 1163-1167.
45. Wells, J.A. and C.L. McClendon, *Reaching for high-hanging fruit in drug discovery at protein-protein interfaces.* Nature, 2007. **450**(7172): p. 1001-1009.
46. Sakamoto, K.M., et al., *Protacs: Chimeric molecules that target proteins to the Skp1-Cullin-F box complex for ubiquitination and degradation.* Proceedings of the National Academy of Sciences of the United States of America, 2001. **98**(15): p. 8554-8559.
47. Sakamoto, K.M., et al., *Development of Protacs to target cancer-promoting proteins for ubiquitination and degradation.* Mol Cell Proteomics, 2003. **2**(12): p. 1350-8.
48. Schneekloth, J.S., Jr., et al., *Chemical genetic control of protein levels: selective in vivo targeted degradation.* J Am Chem Soc, 2004. **126**(12): p. 3748-54.
49. Schneekloth, A.R., et al., *Targeted intracellular protein degradation induced by a small molecule: En route to chemical proteomics.* Bioorg Med Chem Lett, 2008. **18**(22): p. 5904-8.
50. Itoh, Y., et al., *Protein Knockdown Using Methyl Bestatin-Ligand Hybrid Molecules: Design and Synthesis of Inducers of Ubiquitination-Mediated Degradation of Cellular Retinoic Acid-Binding Proteins.* Journal of the American Chemical Society, 2010. **132**(16): p. 5820-5826.
51. Demizu, Y., et al., *Development of BCR-ABL degradation inducers via the conjugation of an imatinib derivative and a cIAP1 ligand.* Bioorg Med Chem Lett, 2016. **26**(20): p. 4865-4869.
52. Naito, M., et al., *Degradation of oncogenic proteins by SNIPER compounds.* Cancer Science, 2018. **109**: p. 562-562.
53. Ito, T., et al., *Identification of a primary target of thalidomide teratogenicity.* Science, 2010. **327**(5971): p. 1345-50.
54. Lu, J., et al., *Hijacking the E3 Ubiquitin Ligase Cereblon to Efficiently Target BRD4.* Chem Biol, 2015. **22**(6): p. 755-63.
55. Winter, G.E., et al., *Phthalimide conjugation as a strategy for in vivo target protein degradation.* Science, 2015. **348**(6241): p. 1376-1381.
56. Bekes, M., D.R. Langley, and C.M. Crews, *PROTAC targeted protein degraders: the past is prologue.* Nat Rev Drug Discov, 2022. **21**(3): p. 181-200.
57. Alabi, S.B. and C.M. Crews, *Major advances in targeted protein degradation: PROTACs, LYTACs, and MADTACs.* J Biol Chem, 2021. **296**: p. 100647.

58. Kim, J.H. and A.R. Scialli, *Thalidomide: the tragedy of birth defects and the effective treatment of disease.* Toxicol Sci, 2011. **122**(1): p. 1-6.
59. Banik, S.M., et al., *Lysosome-targeting chimaeras for degradation of extracellular proteins.* Nature, 2020. **584**(7820): p. 291-297.
60. Nedelsky, N.B., P.K. Todd, and J.P. Taylor, *Autophagy and the ubiquitin-proteasome system: collaborators in neuroprotection.* Biochim Biophys Acta, 2008. **1782**(12): p. 691-9.
61. Takahashi, D., et al., *AUTACs: Cargo-Specific Degraders Using Selective Autophagy.* Mol Cell, 2019. **76**(5): p. 797-810 e10.
62. Li, Z., et al., *ATTEC: a potential new approach to target proteinopathies.* Autophagy, 2020. **16**(1): p. 185-187.
63. Jabbour, E. and H. Kantarjian, *Chronic myeloid leukemia: 2020 update on diagnosis, therapy and monitoring.* Am J Hematol, 2020. **95**(6): p. 691-709.
64. Nieborowska-Skorska, M., et al., *Signal transducer and activator of transcription (STAT)5 activation by BCR/ABL is dependent on intact Src homology (SH)3 and SH2 domains of BCR/ABL and is required for leukemogenesis.* J Exp Med, 1999. **189**(8): p. 1229-42.
65. Carlesso, N., D.A. Frank, and J.D. Griffin, *Tyrosyl phosphorylation and DNA binding activity of signal transducers and activators of transcription (STAT) proteins in hematopoietic cell lines transformed by Bcr/Abl.* J Exp Med, 1996. **183**(3): p. 811-20.
66. Ilaria, R.L., Jr. and R.A. Van Etten, *P210 and P190(BCR/ABL) induce the tyrosine phosphorylation and DNA binding activity of multiple specific STAT family members.* J Biol Chem, 1996. **271**(49): p. 31704-10.
67. Shuai, K., et al., *Constitutive activation of STAT5 by the BCR-ABL oncogene in chronic myelogenous leukemia.* Oncogene, 1996. **13**(2): p. 247-54.
68. Hantschel, O., et al., *BCR-ABL uncouples canonical JAK2-STAT5 signaling in chronic myeloid leukemia.* Nat Chem Biol, 2012. **8**(3): p. 285-93.
69. Zhou, H., et al., *SD-91 as A Potent and Selective STAT3 Degrader Capable of Achieving Complete and Long-Lasting Tumor Regression.* ACS Med Chem Lett, 2021. **12**(6): p. 996-1004.
70. Mandal, P.K., et al., *Targeting the Src Homology 2 (SH2) Domain of Signal Transducer and Activator of Transcription 6 (STAT6) with Cell-Permeable, Phosphatase-Stable Phosphopeptide Mimics Potently Inhibits Tyr641 Phosphorylation and Transcriptional Activity.* J Med Chem, 2015. **58**(22): p. 8970-84.
71. Knight, J.M., et al., *Small molecule targeting of the STAT5/6 Src homology 2 (SH2) domains to inhibit allergic airway disease.* J Biol Chem, 2018. **293**(26): p. 10026-10040.
72. Wang, S., et al., *SMALL MOLECULE DEGRADERS OF STAT3*, T.R.O.T.U.O. MICHIGAN, Editor. 2020: US.
73. Peltola, K.J., et al., *Pim-1 kinase inhibits STAT5-dependent transcription via its interactions with SOCS1 and SOCS3.* Blood, 2004. **103**(10): p. 3744-50.
74. Lord, J.D., et al., *The IL-2 receptor promotes lymphocyte proliferation and induction of the c-myc, bcl-2, and bcl-x genes through the trans-activation domain of Stat5.* J Immunol, 2000. **164**(5): p. 2533-41.
75. Matsumoto, A., et al., *CIS, a cytokine inducible SH2 protein, is a target of the JAK-STAT5 pathway and modulates STAT5 activation.* Blood, 1997. **89**(9): p. 3148-54.

76. Hoermann, G., et al., *Identification of oncostatin M as a STAT5-dependent mediator of bone marrow remodeling in KIT D816V-positive systemic mastocytosis.* Am J Pathol, 2011. **178**(5): p. 2344-56.
77. *Molecular Operating Environment (MOE), 2020.09 Chemical Computing Group ULC, 1010 Sherbooke St. West, Suite #910, Montreal, QC, Canada, H3A 2R7*. 2020.
78. Gianti, E. and R.J. Zauhar, *An SH2 domain model of STAT5 in complex with phospho-peptides define "STAT5 Binding Signatures".* Journal of Computer-Aided Molecular Design, 2015. **29**(5): p. 451-470.
79. Otwinowski, Z. and W. Minor, *Processing of X-ray diffraction data collected in oscillation mode.* Methods Enzymol, 1997. **276**: p. 307-26.
80. Emsley, P., et al., *Features and development of Coot.* Acta Crystallogr D Biol Crystallogr, 2010. **66**(Pt 4): p. 486-501.
81. Bricogne, G., et al., *BUSTER*. 2017, Global Phasing Ltd.: Cambridge, United Kingdom.
82. Smart, O.S., et al., *GRADE*. 2017, Global Phasing Ltd.: Cambridge, United Kingdom.
83. Nikolovska-Coleska, Z., et al., *Development and optimization of a binding assay for the XIAP BIR3 domain using fluorescence polarization.* Anal Biochem, 2004. **332**(2): p. 261-73.
84. Reich, M., et al., *GenePattern 2.0.* Nat Genet, 2006. **38**(5): p. 500-1.
85. Subramanian, A., et al., *Gene set enrichment analysis: a knowledge-based approach for interpreting genome-wide expression profiles.* Proc Natl Acad Sci U S A, 2005. **102**(43): p. 15545-50.
86. Liberzon, A., et al., *Molecular signatures database (MSigDB) 3.0.* Bioinformatics, 2011. **27**(12): p. 1739-40.
87. Liberzon, A., et al., *The Molecular Signatures Database (MSigDB) hallmark gene set collection.* Cell Syst, 2015. **1**(6): p. 417-425.
88. McAlister, G.C., et al., *MultiNotch MS3 enables accurate, sensitive, and multiplexed detection of differential expression across cancer cell line proteomes.* Anal Chem, 2014. **86**(14): p. 7150-8.
89. Morlacchi, P., P.K. Mandal, and J.S. McMurray, *Synthesis and in Vitro Evaluation of a Peptidomimetic Inhibitor Targeting the Src Homology 2 (SH2) Domain of STAT6.* ACS Med Chem Lett, 2014. **5**(1): p. 69-72.
90. Mandal, P.K., et al., *Potent and selective phosphopeptide mimetic prodrugs targeted to the Src homology 2 (SH2) domain of signal transducer and activator of transcription 3.* J Med Chem, 2011. **54**(10): p. 3549-63.
91. Kannan, K., et al., *DNA microarrays identification of primary and secondary target genes regulated by p53.* Oncogene, 2001. **20**(18): p. 2225-2234.
92. Chen, X., et al., *Isolation and characterization of fourteen novel putative and nine known target genes of the p53 family.* Cancer biology & therapy, 2003. **2**(1): p. 56-63.
93. Nosaka, T., et al., *STAT5 as a molecular regulator of proliferation, differentiation and apoptosis in hematopoietic cells.* EMBO J, 1999. **18**(17): p. 4754-65.
94. Natarajan, K., et al., *Pim-1 kinase phosphorylates and stabilizes 130 kDa FLT3 and promotes aberrant STAT5 signaling in acute myeloid leukemia with FLT3 internal tandem duplication.* PLoS One, 2013. **8**(9): p. e74653.
95. Tursynbay, Y., et al., *Pim-1 kinase as cancer drug target: An update.* Biomed Rep, 2016. **4**(2): p. 140-146.

96. Ghazawi, F.M., et al., *Suppressor of cytokine signaling (SOCS) proteins are induced by IL-7 and target surface CD127 protein for degradation in human CD8 T cells.* Cell Immunol, 2016. **306-307**: p. 41-52.
97. Palmer, D.C., et al., *Cish actively silences TCR signaling in CD8+ T cells to maintain tumor tolerance.* J Exp Med, 2015. **212**(12): p. 2095-113.
98. Yoshimura, A., et al., *Negative Regulation of Cytokine Signaling in Immunity.* Cold Spring Harb Perspect Biol, 2018. **10**(7).
99. Krebs, D.L. and D.J. Hilton, *SOCS proteins: negative regulators of cytokine signaling.* Stem Cells, 2001. **19**(5): p. 378-87.
100. Pinz, S., S. Unser, and A. Rascle, *Signal transducer and activator of transcription STAT5 is recruited to c-Myc super-enhancer.* BMC Mol Biol, 2016. **17**: p. 10.
101. Wang, J., et al., *Pim1 kinase synergizes with c-MYC to induce advanced prostate carcinoma.* Oncogene, 2010. **29**(17): p. 2477-87.
102. Malinen, M., et al., *Proto-oncogene PIM-1 is a novel estrogen receptor target associating with high grade breast tumors.* Mol Cell Endocrinol, 2013. **365**(2): p. 270-6.
103. Girardot, M., et al., *Persistent STAT5 activation in myeloid neoplasms recruits p53 into gene regulation.* Oncogene, 2015. **34**(10): p. 1323-32.
104. Ren, Z., et al., *Phosphorylated STAT5 regulates p53 expression via BRCA1/BARD1-NPM1 and MDM2.* Cell Death Dis, 2016. **7**(12): p. e2560.
105. Mallette, F.A., et al., *SOCS1, a novel interaction partner of p53 controlling oncogene-induced senescence.* Aging (Albany NY), 2010. **2**(7): p. 445-52.
106. Tormo, A.J., et al., *IL-6 activates STAT5 in T cells.* Cytokine, 2012. **60**(2): p. 575-82.
107. Geymayer, S. and W. Doppler, *Activation of NF-kappaB p50/p65 is regulated in the developing mammary gland and inhibits STAT5-mediated beta-casein gene expression.* FASEB J, 2000. **14**(9): p. 1159-70.
108. Goenka, S. and M.H. Kaplan, *Transcriptional regulation by STAT6.* Immunologic research, 2011. **50**(1): p. 87-96.
109. Chen, Z., et al., *Identification of novel IL-4/Stat6-regulated genes in T lymphocytes.* The Journal of Immunology, 2003. **171**(7): p. 3627-3635.
110. Tan, S.H. and M.T. Nevalainen, *Signal transducer and activator of transcription 5A/B in prostate and breast cancers.* Endocr Relat Cancer, 2008. **15**(2): p. 367-90.
111. Heltemes-Harris, L.M., et al., *The role of STAT5 in the development, function, and transformation of B and T lymphocytes.* Ann N Y Acad Sci, 2011. **1217**: p. 18-31.
112. Owen, D.L. and M.A. Farrar, *STAT5 and CD4 (+) T Cell Immunity.* F1000Res, 2017. **6**: p. 32.
113. Zhou, J., et al., *The ubiquitin ligase MDM2 sustains STAT5 stability to control T cell-mediated antitumor immunity.* Nat Immunol, 2021. **22**(4): p. 460-470.
114. Gotthardt, D., et al., *STAT5 Is a Key Regulator in NK Cells and Acts as a Molecular Switch from Tumor Surveillance to Tumor Promotion.* Cancer Discov, 2016. **6**(4): p. 414-29.
115. de Araujo, E.D., et al., *Structural and functional consequences of the STAT5B(N642H) driver mutation.* Nat Commun, 2019. **10**(1): p. 2517.
116. Gleixner, K.V., et al., *Combined targeting of STAT3 and STAT5: a novel approach to overcome drug resistance in chronic myeloid leukemia.* Haematologica, 2017. **102**(9): p. 1519-1529.

117. de Araujo, E.D., et al., *Targeting STAT3 and STAT5 in Cancer*. Cancers (Basel), 2020. **12**(8).
118. Wu, C.J., et al., *Activation of STAT3 and STAT5 Signaling in Epithelial Ovarian Cancer Progression: Mechanism and Therapeutic Opportunity*. Cancers (Basel), 2019. **12**(1).
119. Valle-Mendiola, A. and I. Soto-Cruz, *Energy Metabolism in Cancer: The Roles of STAT3 and STAT5 in the Regulation of Metabolism-Related Genes.* Cancers (Basel), 2020. **12**(1).
120. Mi, T., Z. Wang, and K.D. Bunting, *The Cooperative Relationship between STAT5 and Reactive Oxygen Species in Leukemia: Mechanism and Therapeutic Potential.* Cancers (Basel), 2018. **10**(10).